

Spectral Modelling of Coastal Waves over Spatial Inhomogeneity

Akrish, G.

DOI

[10.4233/uuid:caa3cf7f-d438-40ea-9c31-0033f8c38b1f](https://doi.org/10.4233/uuid:caa3cf7f-d438-40ea-9c31-0033f8c38b1f)

Publication date

2023

Document Version

Final published version

Citation (APA)

Akrish, G. (2023). *Spectral Modelling of Coastal Waves over Spatial Inhomogeneity*. [Dissertation (TU Delft), Delft University of Technology]. <https://doi.org/10.4233/uuid:caa3cf7f-d438-40ea-9c31-0033f8c38b1f>

Important note

To cite this publication, please use the final published version (if applicable).
Please check the document version above.

Copyright

Other than for strictly personal use, it is not permitted to download, forward or distribute the text or part of it, without the consent of the author(s) and/or copyright holder(s), unless the work is under an open content license such as Creative Commons.

Takedown policy

Please contact us and provide details if you believe this document breaches copyrights.
We will remove access to the work immediately and investigate your claim.

SPECTRAL MODELLING OF COASTAL WAVES OVER SPATIAL INHOMOGENEITY

SPECTRAL MODELLING OF COASTAL WAVES OVER SPATIAL INHOMOGENEITY

Dissertation

for the purpose of obtaining the degree of doctor
at Delft University of Technology,
by the authority of Rector Magnificus prof.dr.ir. T.H.J.J. van der Hagen,
chair of the Board for Doctorates,
to be defended publicly on
Monday 15 May 2023 at 10:00 o'clock

by

Gal AKRISH

Master of Science in Civil Engineering,
Technion – Israel Institute of Technology,
born in Tveria, Israel.

This dissertation has been approved by the promotor.

Composition of the doctoral committee:

Rector Magnificus,	chairperson
Prof. dr. ir. A.J.H.M. Reniers	Delft University of Technology, promotor
Dr. ir. M. Zijlema	Delft University of Technology, copromotor

Independent members:

Prof. dr. ir. M.R.A. van Gent	Delft University of Technology
Prof. dr. ir. P. Troch	Ghent University, Belgium
Prof. dr. ir. M. Verlaan	Delft University of Technology
Dr. ir. Y. Toledo	Tel Aviv University, Israel
Dr. ir. P.B. Smit	Sofar Ocean Technologies, USA



Keywords: Spectral modelling, Statistical wave modelling, Quadratic modelling, Coastal waves, Wave interference, Wave nonlinearity, Wigner distribution, Weyl rule of association

Printed by: Ridderprint.

Cover: Surface ripples over a shallow depth at De Slufter, Texel on the 7th of January 2023, photo by Gal Akrish.

Copyright © 2023 by Gal Akrish

ISBN 978-94-6366-691-6

An electronic version of this dissertation is available at
<http://repository.tudelft.nl/>.

CONTENTS

Abstract	ix
Samenvatting	xi
1 Introduction	1
1.1 Ocean waves: qualitative description and impacts	1
1.2 Wave modelling.	2
1.2.1 Large and small scale modelling approaches.	2
1.2.2 Spectral modelling of waves in the open ocean	4
1.2.3 Spectral modelling of coastal waves	5
1.2.4 Spectral modelling over spatial inhomogeneity	5
1.2.5 Spectral modelling of shallow water nonlinearity	8
1.3 Objectives and outline	10
2 Weyl rule of association for water waves applications	13
2.1 Introduction	14
2.2 The equivalence between Weyl and DtN operators	15
2.2.1 The mild-slope DtN operator	15
2.2.2 Weyl operator and its asymptotic form.	18
2.3 A Schrödinger-type model for linear waves over variable bathymetry.	20
2.4 The Wigner-Weyl formalism	22
2.4.1 The traditional formulation of the energy balance equation	23
2.4.2 A formal derivation of the energy balance equation and its general- ization	25
2.5 Discussion	25
2.5.1 Fully nonlinear formulation through Weyl rule of association	26
2.5.2 Weakly nonlinear wave modelling	27
2.6 Conclusions.	29
Appendices	31
2.A Weyl calculus	31
2.A.1 Asymptotic operational form	31
2.A.2 Operator composition	32
2.B The relation with the classical mild-slope equation	33
3 Modelling statistical wave interferences over shear currents	37
3.1 Introduction	38
3.2 Stochastic model for waves over current and bathymetry	39
3.2.1 The action variable and its evolution equation.	40
3.2.2 Second-order statistics.	41
3.2.3 Evolution equation for the Wigner distribution	43

3.2.4	Numerical implementation	45
3.2.5	Setup and overview of the considered numerical simulations	45
3.3	Model verification.	47
3.4	Discussion	49
3.4.1	The evolution of the cross-correlation terms.	50
3.4.2	The validity of the QCM	55
3.5	Conclusions.	56
	Appendices	59
3.A	The Weyl operator and its asymptotic form	59
3.B	On the evolution equation of the action variable	61
3.C	From Wigner distribution to local energy	63
3.D	The evolution equation for the Wigner distribution.	65
3.E	On the numerical model	67
4	Spectral forecasting of coastal waves using quadratic models	69
4.1	Introduction	71
4.2	Model analysis over finite depth	73
4.2.1	Second-order bound waves	74
4.2.2	Amplitude dispersion	76
4.2.3	Modulational instability	79
4.3	QuadWave1D: A fully dispersive quadratic model in one dimension	88
4.3.1	General properties for the quadratic interaction coefficients.	88
4.3.2	A parametric derivation of improved fully dispersive quadratic coefficients	89
4.4	Model verification.	95
4.4.1	Monochromatic wave evolution	96
4.4.2	Evolution of bichromatic groups and irregular waves over a slope	100
4.5	Discussion and concluding remarks	108
	Appendices	111
4.A	Different formulations for the quadratic model	111
4.A.1	Dispersion relation.	114
4.A.2	Quadratic coefficients	115
4.A.3	Shoaling term	116
4.B	Cubic interaction coefficients of the quadratic formulation.	118
4.C	Spatial modulational growth of narrow-banded wave fields.	120
4.C.1	Stability condition	120
4.C.2	Spatial modulational growth.	122
4.C.3	Benjamin-Feir Index (BFI)	123
5	Conclusions and outlook	125
5.1	Conclusions.	125
5.2	Outlook.	128

Acknowledgements	131
Bibliography	143
List of Publications	145
Curriculum Vitae	147

ABSTRACT

Spectral wave models are widely used for wave prediction over large spatio-temporal scales. Over global scales, spectral models (e.g. WAM and WAVEWATCH III) are used regularly by environmental modelling centers, such as the European Centre for Medium-Range Weather Forecasts (ECMWF) and the American National Center for Environmental Prediction (NCEP), in order to support human activity at sea. Along the coasts, practitioners rely on spectral models which are designated to the coastal environment (e.g. SWAN and TOMAWAC) for applications such as coastal hazard assessment, future coastal development, planning of defense strategies for coastal safety, evacuation planning of coastal communities and so forth.

An important property that characterizes the spectral approach and enables its applicability for large scales is efficiency. This property is achieved owing to the simple wave description that underlies its formulation. Specifically, the spectral approach represents ocean wave fields as quasi-Gaussian, quasi-homogeneous and quasi-stationary processes. These convenient statistical properties provide a full statistical description of wave fields based on the energy spectrum alone, and therefore, allow to describe the waves in the ocean in a complete statistical sense through the solution of a single transformation equation - the energy balance equation.

The validity of this statistical modelling framework is based on the weak (in the mean) wave forcing and the dispersion effects. These two agents provide reasonable justifications that the deviation from the assumed statistical properties (i.e. Gaussianity, homogeneity and stationarity) is kept negligible in the course of wave evolution. While these arguments are reasonable in the open ocean (where dispersive effects are strong and wave processes are characterized by large scales), they become somewhat loose for the coastal environment (where wave dispersion weakens and wave processes develop rapidly). Evidently, processes like medium-induced wave interferences and energy exchanges due to shallow water nonlinearity are not properly represented under this statistical framework.

This study is set forward with the aim of advancing the spectral modelling capabilities in coastal waters by allowing the development of inhomogeneous and non-Gaussian statistics. To this end, the effort of this work is directed to three different parts, concerning three principle issues. The first part considers the formal connection between the classical deterministic formulation (e.g. the Euler equations) and the statistical formulation given by the so-called Wigner-Weyl formulation (a statistical framework that includes the information of wave interferences and reduces to the energy balance equation when interference effects are negligible). The second parts aims to generalize the Wigner-Weyl formulation (which presently accounts for wave-bottom interactions) to allow for the interaction of waves and ambient currents. Finally, the third part is devoted to the investigation of the quadratic modelling approach which defines the starting point for the present phase-averaged formulation of shallow water nonlinearity.

The objective of the first part of this study is achieved by showing the equivalence between a formal definition of the Dirichlet-to-Neumann operator of waves over variable bathymetry and the Weyl operator of the dispersion relation. This equivalence opens the door to a formal use of Weyl calculus, based on which the Wigner-Weyl formulation is formally derived. This result establishes the desired formal link between the deterministic formulation for water waves and the statistical formulation given by the Wigner-Weyl formulation, which includes the energy balance equation as a statistically well-defined limiting case. In the second part of this study, the Wigner-Weyl formulation for water waves is extended to account for wave-current interactions. The outcome is a generalized action balance model that is able to predict the evolution of the wave statistics over variable media, while preserving statistical contributions due to wave interferences. Comparisons with results of the SWAN model and the REF/DIF 1 model through several examples verify model performance and demonstrate that retention of interference contributions is essential for accurate prediction of wave statistics in shear-current-induced focal zones. Finally, the third part of this study explores the predictive capabilities of the quadratic approach. This is performed by analyzing the nonlinear properties of six different quadratic formulations, three of which are of the Boussinesq type and the other three are referred to as fully dispersive formulations. It is found that while the Boussinesq formulations predict reliably the nonlinear development of coastal waves, the predictions by the fully dispersive formulations tend to be affected by false developments of modulational instability. As a result, the predicted fields by the fully dispersive formulations are characterized by unexpectedly strong modulations of the sea-swell part and associated unexpected infragravity response. Additionally, this part of the study also presents an attempt to push the limits of the predictive capabilities of the quadratic approach. The outcome is the model QuadWave1D: a fully dispersive quadratic model for coastal wave prediction in one dimension. Based on a wide set of examples (including monochromatic, bichromatic and irregular wave conditions), it is found that the new formulation presents superior forecasting capabilities of both the sea-swell components and the infragravity field.

In summary, the overall effort of this study provides an additional step toward the broader goal of efficient and accurate spectral modelling capabilities of coastal waves. This step includes strengthening the theoretical foundations of the spectral approach, improving the spectral description of wave transformation over spatial inhomogeneity and helping to minimize the errors associated with the spectral formulation of shallow water nonlinearity. Ultimately, this study also points on and prepares the background to additional required model developments.

SAMENVATTING

Spectrale golfmodellen worden veelal toegepast voor de voorspelling van windgolven over grote ruimtelijke en temporele schalen. Op mondiale schaal worden deze modellen (bijv. WAM en WAVEWATCH III) frequent gebruikt door gerenommeerde klimaat instituten, zoals het European Centre for Medium-Range Weather Forecasts (ECMWF) en het American National Center for Environmental Prediction (NCEP), ten behoeve van de ondersteuning van menselijke activiteiten op zee. Ook worden de spectrale modellen ingezet door ze toe te passen op de kustomgeving (bijv. SWAN en TOMAWAC), zoals kustrisicobeoordeling, toekomstige kustontwikkeling, planning van verdedigingsstrategieën voor kustveiligheid, evacuatieplanning van kustgemeenschappen, enzovoort.

Een belangrijke eigenschap van de spectrale benadering is efficiëntie. Dit maakt de toepasbaarheid op grote schaal mogelijk. Deze eigenschap wordt bereikt dankzij de eenvoudige golfbeschrijving die ten grondslag ligt aan de formulering ervan. In dit verband worden oceaangolfvelden als quasi-Gaussiaanse, quasi-homogene en quasi-stationaire processen beschouwd. Deze prettige statistische eigenschappen bieden een volledige statistische beschrijving van golfvelden op basis van slechts het energiespectrum, en maken het daarom mogelijk om de golven op de oceaan op een volledige statistische wijze te beschrijven door de oplossing van een enkelvoudige vergelijking - de energiebalansvergelijking.

De validiteit van deze statistische modelleringsaanpak is gebaseerd op de zwakke (gemiddelde) golf-forcering en de dispersie effecten. Deze twee aspecten bieden een voldoende rechtvaardiging in de zin dat de afwijking van de veronderstelde statistische eigenschappen (d.w.z. Gaussianiteit, homogeniteit en stationariteit) verwaarloosbaar wordt gehouden in het verloop van de golfevolutie. Hoewel deze argumenten aanneemelijk zijn voor wat betreft golven op de open oceaan (waar de dispersie effecten sterk zijn en de golfprocessen worden gekenmerkt door grote ruimtelijke schalen), worden ze enigszins discutabel met betrekking tot golven dichtbij de kust (waar de golfdispersie inmiddels is afgezwakt en de golfprocessen zich snel ontwikkelen). Het is evident dat de processen zoals bodem-geïnduceerde golfinterferenties en energie-uitwisselingen als gevolg van niet-lineariteit in ondiep water niet goed worden weergegeven in dit statistische referentiekader.

De onderhavige studie is opgezet met als doel de mogelijkheden voor spectrale modellering in kustwateren te verbeteren door de ontwikkeling van inhomogene en niet-Gaussiaanse statistieken mogelijk te maken. Daartoe is het streven van dit werk gericht op drie verschillende onderdelen die betrekking hebben op drie principiële kwesties. Het eerste deel betreft het formele verband tussen de klassieke deterministische formulering (zoals bijv. de Euler vergelijkingen) en de statistische formulering die wordt gegeven door de zogenaamde Wigner-Weyl formulering (een statistisch referentiekader dat de informatie over golfinterferenties omvat en reduceert tot de energiebalansvergelijking wanneer interferentie-effecten zijn te verwaarlozen). Het tweede deel heeft tot

doel de Wigner-Weyl formulering (die thans de golfbodeminteracties duidt) te generaliseren om de interactie van golven met de omgevingsstroom mogelijk te maken. Ten slotte is het derde deel gewijd aan het onderzoek van de kwadratische modelleringsbenadering die het startpunt fungeert voor de huidige fasegemiddelde formulering van niet-lineariteit in ondiep water.

Het doel van het eerste deel van deze studie wordt gerealiseerd door de gelijkwaardigheid tussen een formele definitie van de Dirichlet-to-Neumann operator van golven over variabele bodem en de Weyl operator van de dispersierelatie aan te tonen. Deze gelijkwaardigheid opent de deur naar een formeel gebruik van Weyl calculus, waarvan de Wigner-Weyl formulering formeel is afgeleid. Dit resultaat legt de gewenste formele link tussen de deterministische formulering voor watergolven en de statistische formulering gegeven door de Wigner-Weyl formulering, die de energiebalansvergelijking als een statistisch goed gedefinieerd grensgeval omvat. In het tweede deel van deze studie wordt de Wigner-Weyl formulering voor watergolven uitgebreid om rekening te houden met golf-stroominteracties. Het resultaat is een gegeneraliseerd actiebalansmodel dat in staat is om de evolutie van de golfstatistieken over variabele media te beschrijven, met behoud van statistische bijdragen als gevolg van golfinterferenties. Vergelijkingen met de resultaten van het SWAN model en het REF/DIF 1 model door middel van verschillende voorbeelden verifiëren de modelprestaties en tonen aan dat het behoud van interferentiebijdragen essentieel is voor nauwkeurige voorspelling van golfstatistieken in door stromingspatronen geïnduceerde focale zones. Ten slotte onderzoekt het derde deel van deze studie de voorspellende mogelijkheden van de kwadratische benadering. Dit wordt uitgevoerd door de niet-lineaire eigenschappen van zes verschillende kwadratische formuleringen te analyseren, waarvan er drie van het Boussinesq-type zijn en de andere drie volledig dispersieve formuleringen worden genoemd. Hoewel de Boussinesq formuleringen de niet-lineaire ontwikkeling van kustgolven betrouwbaar voorspellen, hebben de voorspellingen van de volledig dispersieve formuleringen de neiging beïnvloed te worden door de foutieve ontwikkelingen van de modulatie-instabiliteit. Dientengevolge worden de voorspelde golfvelden door de volledig dispersieve formuleringen gekenmerkt door onverhoeds sterke modulaties van de wind golven en de bijbehorende infragravity respons. Daarnaast presenteert dit deel van de studie ook een poging om de grenzen van de voorspellende mogelijkheden van de kwadratische benadering te verleggen. Het resultaat is het model QuadWave1D: een volledig dispersief kwadratisch model voor kustgolfvoorspelling in één dimensie. Op basis van een groot aantal voorbeelden (waaronder monochromatische, bichromatische en onregelmatige golfcondities) is gebleken dat de nieuwe formulering superieure voorspellingsmogelijkheden biedt voor zowel de wind golf componenten als het infragravity veld.

Samengevat, het algehele onderzoek van deze studie biedt een nieuwe stap in de richting van het bredere doel van efficiënte en nauwkeurige spectrale modelleringsmogelijkheden van kustgolven. Deze stap omvat het versterken van de theoretische basis van de spectrale benadering, het verbeteren van de spectrale beschrijving van golftransformatie over ruimtelijke inhomogeniteit en het helpen minimaliseren van de fouten die samenhangen met de spectrale formulering van niet-lineariteit in ondiep water. Tot slot biedt deze studie de basis voor vervolgonderzoek naar aanvullende vereiste modelontwikkelingen.

1

INTRODUCTION

1.1. OCEAN WAVES: QUALITATIVE DESCRIPTION AND IMPACTS

The energy of ocean surface waves is obtained by the action of the wind and transported through the ocean basins to the coasts. Wave evolution away from the generation area is characterized by frequency and direction dispersion. These processes disintegrate the generated fields into their regular long crested components (see, e.g., the detailed description by Holthuijsen, 2007, section 6.4.2). Therefore, if other wave processes are negligible, wave fields closer to shore become narrow-banded and are characterized by lower wave heights. More generally though, deep ocean waves evolve due to a combination of several physical processes. In addition to wave dispersion, the waves also interact nonlinearly and slowly exchange energy through resonant interactions of wave quartets (Phillips, 1960, Longuet-Higgins, 1962, Hasselmann, 1962). Non-conservative processes (wind generation and dissipation due to, e.g., wave breaking) apply as well and significantly contribute to the development of wave fields (see Komen et al., 1994 and references therein).

For certain conditions at sea, the combination of the different wave processes may lead to severe wave fields (e.g. Onorato et al., 2001, Kharif and Pelinovsky, 2003, Janssen, 2003, Onorato et al., 2009, Fedele et al., 2016, Toffoli et al., 2017). Extreme wave fields may also develop due to spatial inhomogeneities of the oceanic medium (induced by ambient currents and bottom topography) which may scatter and focus the waves through a process called refraction (see, e.g., the reviews on the spatial focusing mechanism given by Kharif and Pelinovsky, 2003 and Dysthe et al., 2008). Violent sea states have already caused many disasters and led to many casualties, and are continuously threatening deep water human activities (e.g. Nikolkina and Didenkulova, 2011).

Over coastal waters, wave fields evolve more rapidly due to medium inhomogeneities of smaller scales (e.g., submerged shoals and channels and small scale eddies and jets). In addition, as waves penetrating further towards the shore and propagating over shallower waters, their energy focuses due to the process known as shoaling. The waves become higher and nonlinear and start to interact and exchange energy through near-resonant interactions of wave triads (e.g. Mei and Ünlüata, 1972, Bryant, 1973). This

process transforms the typical quasi-sinusoidal appearance of the surface elevation into a skewed and asymmetric saw-tooth like shape. The associated spectral transformation shows significant development of higher harmonics (e.g. Elgar and Guza, 1985, Herbers and Burton, 1997). The combination of wave shoaling and nonlinearity also results in the development of the field's modulations and the associated infragravity response (e.g. Battjes et al., 2004). Ultimately, the waves break leading to substantial dissipation of the primary and the higher harmonics and to weaker modulations and associated weaker coupling with the infragravity components (e.g. Janssen et al., 2003). Breaking waves induce wave setup (e.g. Longuet-Higgins and Stewart, 1964), alongshore currents (e.g. Bowen, 1969, Longuet-Higgins, 1970, Reniers and Battjes, 1997, Ruessink et al., 2001), return flow (e.g. Dyhr-Nielsen and Sørensen, 1970, Stive and De Vriend, 1994) and associated sediment transport processes (e.g. Fredsoe and Deigaard, 1992, Van Rijn, 1993). In addition, the associated decoupling between the field's modulations and the infragravity components generates freely propagating wave energy at the infragravity band that penetrates into the surfzone and significantly contributes to shoreline processes such as wave run-up and overtopping on dikes and dunes (e.g. Van Gent, 2001), dune erosion and sediment transport (e.g. Roelvink and Stive, 1989, Roelvink et al., 2009), and harbour oscillations (e.g. Bowers, 1977). These wave impacts may lead to significant consequences for the coastal environment and coastal communities. For example, sediment transport and coastal erosion jeopardize the integrity and utility of coastal infrastructures, such as, coastal defence structures, foundations of buildings along the shore, etc. (e.g. Ruggiero et al., 2001). Furthermore, wave setup, run-up and overtopping contribute to the threat of flooding, thereby endangering the lives and property of coastal residents (see, e.g., Hoeke et al., 2013, Roeber and Bricker, 2015, Chen, 2016).

In conclusion, the above discussion clearly emphasizes the importance of predicting the evolution of ocean waves offshore and in the coastal environment in order to avoid, mitigate, protect against and design with respect to their associated impacts. Wave prediction is commonly based on numerical models which are discussed next.

1.2. WAVE MODELLING

1.2.1. LARGE AND SMALL SCALE MODELLING APPROACHES

There are many different wave models aiming to predict the evolution of waves and their impacts. Roughly speaking, wave models can be classified according to their designated applications which determine the governing spatio-temporal scales and the wave processes to be described. For example, the problem of wave-induced pressure on coastal or marine structures requires a modelling approach that can resolve the detailed wave-structure interactions, which involve complex and rapid wave processes such as wave breaking. While for the determination of shipping routes, the required wave information is much less detailed, but should be provided over much larger spatio-temporal scales and should take into account, e.g., contribution due to wave generation by wind.

Models intended for detailed wave description are referred to here as small-scale models, while models intended for wave forecasting over larger spatio-temporal scales are referred to as large-scale models. Small-scale modelling typically refers to different approximations of the primitive governing equations (i.e., the Navier-Stokes equations).

Common models in this class are, e.g., the Boussinesq models (well-known Boussinesq formulations are the classical weakly-nonlinear formulation of Peregrine, 1967, and the advanced fully-nonlinear formulation of Wei et al., 1995), the Serre–Green Naghdi models (see, e.g., Bonneton et al., 2011) and other detailed modelling approaches such as the non-hydrostatic (e.g. Zijlema et al., 2011) or the particle-based (e.g. Dalrymple and Rogers, 2006) approaches. On the other hand, large-scale modelling usually refers to spectral models which are formulated based on the assumption that the fluid flow can be represented by a superposition of progressive sinusoidal wave components. This modelling approach includes phase-averaged models (e.g. global-scale models such as WAM model, WAMDI Group, 1988 and WAVEWATCH model, Tolman, 1991, and regional-scale models such as SWAN model, Booij et al., 1999 and TOMAWAC model, Benoit et al., 1996) and may also refer to phase-resolving models (e.g. Freilich and Guza, 1984 and Madsen and Sørensen, 1993), which compared to the phase-averaged approach, are limited to smaller scales.

Naturally, the different modelling strategies are complimentary. A small-scale model that predicts detailed wave processes is usually nested in a large scale model. The latter provides the boundary conditions for the former. This complementarity also manifests itself in terms of computational efficiency. That is, large-scale models are usually efficient enough to provide wave prediction over large domains in a reasonable amount of time. While small-scale models are computationally expensive, and therefore limited to small-scale domains. Nevertheless, the overlap regions between the different modelling approaches (i.e., large-scale and small-scale approaches) tend to expand. There are two reasons for that, one is the availability of advanced computational capabilities that allow efficient complicated operations, and the second is the need to predict relatively rapid wave processes over relatively large scales. The former allows to employ accurate small-scale models over larger domains, whereas the latter motivates further developments of large-scale models to accurately and efficiently predict rapid wave processes.

Typical regions where this "model approach competition" arises are coastal regions which on one hand are commonly defined by large domains and on the other hand are characterized by relatively rapid wave processes (e.g. triad wave interactions, wave diffraction etc.). Therefore, the obvious demand for wave data over coastal regions of large scales (e.g. for applications concern coastal management and coastal safety) pose a challenge for small-scale models to meet the required efficiency and a challenge for large scale models to meet the required accuracy.

Presently, advanced computational resources which enable the use of small-scale models for coastal application over large domains are usually not available in practice, i.e., to organizations such as consultancy firms and governmental agencies. Furthermore, over relatively large scales, wind generation becomes an important factor and presently cannot be accounted for by the small-scale approaches. Finally, aspects such as large-scale model validations and model coupling to other prediction tools (e.g., surface circulation and transport models) are not developed enough for small-scale models. As a result, practitioners usually rely on wave data obtained using large-scale models for coastal hazard assessment, future coastal development, planning of defense strategies for coastal safety, evacuation planning of coastal communities, etc. Obviously, it is desired that these type of applications would rely on reliable wave information. This clearly

calls to inspect and further develop the predication capabilities of large-scale models.

1.2.2. SPECTRAL MODELLING OF WAVES IN THE OPEN OCEAN

Large-scale wave forecasting commonly relies on phase-averaged spectral models (e.g. the WAM model, WAMDI Group, 1988 and the WAVEWATCH III model, Tolman, 1991). For example, these models are used regularly by environmental modelling centers, e.g. the European Centre for Medium-Range Weather Forecasts (ECMWF) and the American National Center for Environmental Prediction (NCEP) in order to support human activity at sea. The main basic assumption underlying the development of the phase-averaged approach is that waves at sea are subjected to weak (in the mean) conservative (e.g. refraction and resonant wave-wave interactions, Phillips, 1960) and non-conservative (e.g. wind generation, Miles, 1957 and white-capping dissipation, Hasselmann, 1974) forcing. The weak forcing assumption allows to describe the evolution of ocean waves through a quasi-linear approach. Specifically, under the weak forcing assumption, wave fields at sea can be seen as multiple scale processes. At the leading order, wave fields are described through a superposition of many wave components which originated from different well-separated oceanic regions, and therefore, may regarded as statistically independent (Komen et al., 1994). These wave components are characterized by rapid phase variations (governed by the wave period and length) and by slow variation of energy density. The slow evolving energy spectrum is governed by the weak forcing and is solved at a higher order through the well-known energy balance equation (e.g. Komen et al., 1994 and Holthuijsen, 2007), written schematically as

$$\partial_t E = P + S \quad (1.1)$$

where $E(\mathbf{x}, \mathbf{k}, t)$ is the spectrum of the energy density given as a function of the physical space \mathbf{x} , the wavenumber space, \mathbf{k} and time t . The implicit terms on the right-hand-side of (1.1), i.e. P and S , represent the propagation terms (corresponding to the spatial and spectral energy radiation) and the source terms (due to processes such as wind generation, white-capping dissipation and resonant quadruplet interactions). Statistically, this quasi-linear description (representing wave fields at sea as a superposition of many slowly varying and statistically independent wave components) allows to treat ocean wave fields as quasi-Gaussian, quasi-homogeneous and quasi-stationary processes (Komen et al., 1994). These convenient statistical properties provide a full statistical description of wave fields based on the energy spectrum alone (e.g., Goodman, 1985). Moreover, the weakness of the forcing and the strong dispersion that characterizes deep ocean waves provide reasonable justifications to assume that the deviation from these statistical properties is kept negligible in the course of wave evolution (e.g. Hasselmann, 1962, Benney and Saffman, 1966, Newell, 1968, Komen et al., 1994). Therefore, the remarkable consequence of the weak (in the mean) forcing assumption is that it allows to describe the waves in the ocean in a complete statistical sense (which to any person observing the sea surface would seem impossible) through the solution of a single transformation equation - the energy balance equation (1.1).

To summarize, phase-averaged spectral models essentially solve the energy balance equation (1.1) (subjected to input forcing data, e.g. wind field) using a resolution that corresponds to the slow evolution scale of the waves (e.g. typical spatial resolution over

oceanic basins can be $O(10 - 100)$ km). This explains the capabilities of this modelling approach to predict the parameters of ocean waves over large-scales within a reasonable computing time.

1.2.3. SPECTRAL MODELLING OF COASTAL WAVES

The success of the phase-averaged approach in the open ocean (e.g. Janssen et al., 1997) has motivated its application to large-scale coastal water domains as well. As a result, phase-averaged models, such as, the SWAN model (Booij et al., 1999) and the TOMAWAC model (Benoit et al., 1996) were developed, and nowadays, are routinely used for coastal applications (e.g. Wu et al., 2020). These models essentially solve the same single energy balance equation, (1.1), which was developed for wave forecasting over global scales. Yet, some modifications are implemented. At first, finite depth effects are taken into account (e.g. Tolman, 1991). Second, important shallow water processes (e.g. near-resonant triad interactions, Eldeberky, 1996, and depth-induced breaking, Eldeberky and Battjes, 1996) are included using designated source terms in S (see (1.1)).

These modifications build upon the same statistical assumptions that coastal wave fields can be regarded as quasi-Gaussian, quasi-homogeneous and quasi-stationary random processes (e.g. Holthuijsen, 2007). However, as waves penetrate into shallower waters, the mean forcing becomes stronger (e.g., triad interactions dominate quartet interactions), and accordingly, waves evolve faster. Additionally, over shallower waters the dispersion effect weakens. As a result, the arguments that provided the justification for the preservation of the assumed statistical properties (i.e. weakly forced and strongly dispersed wave fields) become weaker in shallower waters, thus raising a question mark regarding the validity of the energy balance equation used in coastal phase-averaged models and its capability to provide a complete statistical description of coastal wave fields.

Two assumed properties clearly become questionable over coastal waters. The first is the quasi-homogeneity, which to the leading order, disregards possible coherent structures induced by simple linear interference effects. However, these fundamental effects often emerge over coastal waters where wave fields evolve rapidly due to medium inhomogeneities (bathymetry and ambient current patterns) of smaller scales (e.g. O'Reilly and Guza, 1991). The second property that becomes questionable over coastal waters is the quasi-Gaussianity. This property is questionable since over shallower coastal waters, wave triads are nearly resonant, and thus, develop strong correlations over relatively small scales. Additionally, over shallower water, the dispersion effect, which serves as a relaxation factor towards Gaussian statistics, becomes relatively weak. Therefore, it would be plausible to assume that coastal waves which evolve over relatively shallow water depths are strictly non-Gaussian (e.g. Benney and Saffman, 1966). To summarize, it is clearly emphasised that the extension of the phase-averaged approach to coastal waters requires further model development to account for the generation and transportation of statistical inhomogeneous and non-Gaussian contributions.

1.2.4. SPECTRAL MODELLING OVER SPATIAL INHOMOGENEITY

To leading order, statistical inhomogeneity of wave fields is induced by variations in the medium (due to slowly varying currents and bathymetry). The quasi-homogeneous as-

assumption taken by the present phase-averaged formulations states that over relatively small-scales, wave fields can be represented as a superposition of statistically independent plane waves. Weak inhomogeneity is introduced over larger scales through slow variations of the spectral energy density. This weak inhomogeneity is represented through the propagation term, P , in (1.1) which is given explicitly by

$$\partial_t E = -\nabla_{\mathbf{x}} \cdot (\mathbf{C}_x E) - \nabla_{\mathbf{k}} \cdot (\mathbf{C}_k E) \quad (1.2)$$

and is composed of two energy flux terms (written on the right-hand-side of (1.2)), describing the transport of energy over the spatial and the spectral domains with flux velocities \mathbf{C}_x and \mathbf{C}_k , respectively.

The formulation in (1.2) is based on the well-known result of the Wentzel–Kramers–Brillouin (WKB) approximation (e.g. Mei, 1989), which provides a phase-averaged (slowly varying) description of individual wave components over slowly varying media. However, in contrast to the WKB representation, which follows the slow evolution of each wave component separately, the expression given by (1.2) shows a fully Eulerian representation (often referred to as the phase space representation) based on the independent spatial and spectral variables \mathbf{x} and \mathbf{k} .

The relation between the two representations is obtained in the limit $N \rightarrow \infty$, where N is the number of wave components. This relation was argued by Hasselmann (1963) based on the wave-particle analogy (also refer to Komen et al., 1994). Specifically, over large-scales (zooming out to the resolution where the typical spatial step of $O(10 - 100)$ km would seem like an infinitesimal surface point), Hasselmann (1963) proposed that wave fields can be seen as a superposition of large number of non-interacting wave packets whose dimension is much smaller than the characteristic scale of medium variations. The elegant result of this representation is that the large-scale dynamics of these wave packets is completely analogous to the dynamics of a non-colliding system of classical particles, where the position, wavenumber and frequency play the role of the generalized coordinates, momenta and Hamiltonian, respectively. Consequently, Liouville's theorem becomes applicable to statistically describe the density of such wave packets. This result and the linearity of the dispersion relation allows to describe the evolution of the energy density, E , through the so-called collisionless Boltzmann equation (see additional details in Komen et al., 1994) which shows exactly the same structure of (1.2). Alternatively, (1.2) can be derived directly, based on the following explicit relation between the energy density, E , and the individual energy components, E_j , of the N wave packets:

$$E(\mathbf{x}, \mathbf{k}, t) d\mathbf{x} d\mathbf{k} = \sum_j E_j \Delta(\mathbf{x}, \mathbf{x}_j, \mathbf{k}, \mathbf{k}_j) \quad (1.3)$$

where the function Δ is equal 1 if the phase space location of wave packet j is found within the volume $dV = d\mathbf{x} d\mathbf{k}$ centered at (\mathbf{x}, \mathbf{k}) , and is equal 0 otherwise. Taking the time derivative of both sides of (1.3) and using the canonical equations governing the phase space (i.e., the mutual spatial and spectral space) trajectories of the wave packets (e.g., Dingemans, 1997) eventually leads to the phase-averaged formulation in (1.2) (see details in, e.g., Willebrand, 1975, Hertzog et al., 2002 and Muraschko et al., 2015). However, the particle-like representation underlying the above derivation alternatives of (1.2) ignores the wave-like behaviour of the wave packets (note however that Dewar,

1970 suggested a derivation starting with a similar representation of many slowly varying wave components but without invoking a "number density like" relation, e.g. (1.3), which principally could have allowed him to preserve wave-like effects). Consequently, the contributions of wave interference, which are statistically obtained by the cross correlations of different wave components, are inherently neglected by the existing phase-averaged models (e.g. WAM, WAVEWATCH III, SWAN).

Relying on the typical resolution implemented for ocean wave forecasting, the disregard of interference contributions by the present phase-averaged approach seems reasonable, since the relatively small-scale dimensions characterizing these contributions are simply not resolvable (and accordingly not necessarily relevant for applications relying on global wave forecasting). However, if one is interested to capture the variation in wave statistics over finer scales (e.g. for coastal applications), then interference contributions may result in a significant signature (e.g., the emergence of lateral oscillations of the significant wave height behind a submerged shoal, demonstrated experimentally by Vincent and Briggs, 1989 and numerically using generalized phase-averaged models by Janssen et al., 2008, Smit and Janssen, 2013 and Smit et al., 2015a).

Statistically, the importance of the cross correlations is determined by the ratio between the second-order correlation and medium variation scales (e.g., Smit and Janssen, 2013). In the open ocean, where medium inhomogeneity is typically $O(100)$ km and the wave spectrum is relatively broad, this measure would rarely indicate a significant value and the particle-like representation of the wave components is therefore justified. However, for conditions where the medium is characterized by variations of relatively small-scales (i.e. $O(1 - 10)$ km) and the wave field is rather narrow-banded, the second-order statistics may be significantly affected by medium-induced interference patterns, leading to non-negligible cross-correlation contributions. Such conditions are rather typical over coastal waters, and thus, call for fundamental modifications of the phase-averaged approach (i.e., (1.2)) for the forecasting of coastal waves over spatial inhomogeneity. Principally, in order to include cross-correlation contributions, it is required to develop an evolution equation for the complete second-order statistics. Namely, besides the energy related terms (the variance or auto-correlation terms), the generation and transportation of the interference related terms (the cross-correlation terms) should be accounted as well.

A generalized statistical framework that accounts for inhomogeneity induced by statistical wave interferences is provided by the Wigner-Weyl formalism (Moyal, 1949). The associated Wigner-Weyl kinetic equation transports the Wigner distribution (a generalized energy density definition, e.g. Hlawatsch and Flandrin, 1997) of wave fields which includes cross-correlation information that are ignored in E by definition (i.e. (1.3)). As such, this generalized kinetic equation describes the evolution of the complete second-order statistics, and accordingly, reduces to the energy balance equation, (1.2), when cross-correlation contributions are negligible (see Smit and Janssen, 2013). The Wigner-Weyl kinetic equation was implemented in other fields of physics (e.g. Leaf, 1968, Bremer, 1973, Besieris and Tappert, 1976, McDonald and Kaufman, 1985, Zhu and Dodin, 2021) and recently proposed by Smit and Janssen (2013) for water waves to describe the statistics of wave fields over relatively small-scale bathymetric variations. The Wigner-Weyl formulation developed by Smit and Janssen (2013) (and later modified for imple-

mentation in existing phase-averaged models by Smit et al., 2015a) was successfully verified against laboratory experiments and field observations. These verification examples emphasize the added value gained by the Wigner-Weyl formulation. Namely, its ability to capture statistical wave interferences over bathymetric structures of relatively small-scales (e.g. Smit et al., 2015a). The success of the Wigner-Weyl formulation to describe the statistics of waves over bathymetry encourages its further development. Specifically, two issues are left open. One relates to the theoretical foundations of the Wigner-Weyl formulation and the other to its implementation. The required theoretical development stems from the fact that the formulation developed by Smit and Janssen (2013) and Smit et al. (2015a) is based on an assumed deterministic equation (i.e. Eq. (3) in Smit and Janssen, 2013) which was only verified for specific conditions (i.e. constant depth and slowly evolving monochromatic wave over mild sloping bathymetry) but not derived rigorously. If available, such a derivation would provide a formal link between the deterministic formulation (e.g. Euler equations) and the stochastic formulation of the Wigner-Weyl formalism, which includes (1.2) as a statistically well-defined limiting case. The second issue that should be resolved is the generalization of the development achieved by Smit and Janssen (2013) and Smit et al. (2015a) to account for wave-current interactions. In addition to the Doppler shift, this generalization should also include the adiabatic effect of the current on the waves' amplitudes (Longuet-Higgins and Stewart, 1961, Bretherton and Garrett, 1968). The latter is commonly taken into account implicitly using the so-called action density (defined as the energy density divided by the intrinsic frequency), which is conserved also in the presence of slowly varying currents (Bretherton and Garrett, 1968). Therefore, if successful, the extension of the Wigner-Weyl formulation to allow for wave-current interactions should result in a generalized action balance equation that is able to predict the evolution of wave statistics over variable media while preserving inhomogeneous contributions induced by wave interferences.

1.2.5. SPECTRAL MODELLING OF SHALLOW WATER NONLINEARITY

The adjustment of the phase-resolving approach for coastal waters also requires to cope with non-Gaussian statistical contributions. Non-Gaussianity arises due to the rapid development of high-order correlations triggered by shallow water nonlinearity and the associated near resonant interaction of wave triads (e.g. Benney and Saffman, 1966, Herbers and Burton, 1997). Phase-averaged models for shallow water nonlinearity are formulated based on a quadratic model (a deterministic system which is governed by quadratic nonlinearity) and a statistical truncation assumption. Principally, these ingredients involve unrelated errors, and therefore, require separated investigation. Given a quadratic model, the evolution equations of the statistical moments of a wave field can be formulated. The quadratic term generates a hierarchical dependency between the moments, therefore leading to an infinite set of equations which requires a truncation assumption. This expresses the famous closure problem of turbulence theory (e.g. Orszag, 1970). The common truncation strategy is the so-called fourth-cumulant discard, which result in a coupled set of two equations for the second-order spectrum and third-order bispectrum (e.g. Herbers and Burton, 1997, Eldeberky and Madsen, 1999).

The neglect of the fourth-cumulant is justified based on the expectation of a weak deviation from Gaussian statistics (e.g. see discussion by Herbers and Burton, 1997).

However, when nonlinearity intensifies, this assumption leads to over-predicted bispectral values (e.g. see discussions by Holloway and Hendershott, 1977 and Janssen, 2006). This observation has motivated the development of heuristic closure strategies which limit the significant deviation from Gaussian statistics (e.g. Holloway and Hendershott, 1977, Herbers et al., 2003, Janssen, 2006). The existing solutions to the closure problem emphasize the challenge it poses, and the need for its further research and development. Furthermore, numerical solution of the coupling between the spectrum and bispectrum over relatively large-scales is too demanding in terms of computation time, and therefore, motivated further simplifications for practical use (e.g. Eldeberky, 1996, Agnon and Sheremet, 1997, Becq-Girard et al., 1999, Toledo and Agnon, 2012, Salmon et al., 2016, Vrecica and Toledo, 2016).

A separate problem is the formulation of the starting point quadratic model. The errors associated with the quadratic model originate from several sources. The most dominant one is the neglect of the high-order nonlinear terms (third-order and higher). Thus, the description of wave nonlinearity essentially collapses into a single quadratic term. This raises concerns with regard to the ability of the quadratic approach to produce reliable predictions especially for waves in shallow waters subject to strong nonlinearity. Nevertheless, since the pioneering study of Freilich and Guza (1984), efforts have been mainly devoted to the improvement of the linear properties (e.g. Madsen and Sørensen, 1993, Agnon et al., 1993, Kaihatu and Kirby, 1995, Eldeberky and Madsen, 1999, Bredmose et al., 2005). There is no doubt that these developments have improved the linear characteristics of the quadratic modelling (i.e., dispersion and shoaling), however doubts arise concerning the improvement in the prediction of the nonlinear evolution. This doubt stems from the fact that the improvement of the linear properties of the quadratic model is accompanied by a change in the quadratic coefficients, and therefore, also by a change in the truncation error obtained due to the modelling reduction associated with the formulation of the quadratic model.

An example that clearly highlights the effect of improving the linear dispersion relation on the nonlinear model properties is given by the Whitham equation. The Whitham equation was proposed by Whitham (1967) as a generalized Korteweg–de Vries (KdV) equation that incorporates the full linear dispersion relation. Such a generalization is expected to provide a more faithful description of wave field evolution which may also be composed of shorter wave components. However, it is now known that this generalization is accompanied by a dramatic change in the characteristics of the modulational instability occurring in shallower water than expected (e.g., Van Groesen, 1998, Hur and Johnson, 2015). Thus, Whitham's generalization turns the modulationally stable KdV equation into a modulationally unstable Whitham equation, which together with improved dispersion, will also predict faulty focusing/defocusing recurrence of narrow-banded fields over regions of relatively shallow waters. This erroneous effect may not only lead to false energy exchanges and thus incorrect evolution of the peak frequency components, but may also contaminate the associated development of the infragravity components as a result of incorrect modulations of the wave field. This example clearly emphasizes the need to investigate the existing quadratic formulations (which present different approximations of the dispersion relation) and to search for a formulation that adequately describes both the linear and nonlinear wave evolution. Such an

investigation may help to minimize the errors associated with the development of the phase-averaged formulation for shallow water nonlinearity.

1.3. OBJECTIVES AND OUTLINE

The introduction above describes a clear need to modify the phase-averaged formulation (i.e. 1.1), which was originally designed for oceanic applications, in order to meet the conditions and desired resolutions that characterize the coastal environment. Specifically, inhomogeneous and non-Gaussian contributions must be included to adequately represent wave statistics over regional coastal scales. To this general end, the following objectives are defined:

(i) The first objective is to formally derive the starting point equation used by Smit and Janssen (2013) for the development of the Wigner-Weyl formulation for water waves. The significance of such a derivation is that it would allow for the establishment of a formal link between the deterministic modelling approach (e.g. the Euler equations) and the presently used stochastic modelling approach (i.e. the energy balance equation given in (1.2)) and its generalization (i.e. the Wigner-Weyl formulation obtained by Smit and Janssen, 2013). This theoretical development is pursued in Chapter 2 and is based on the Weyl's operational calculus which provides the key to the derivation of the starting point equation and to the direct connection to the Wigner-Weyl kinetic equation.

(ii) The second objective concerns the generalization of the phase-averaged formulation of Smit and Janssen, 2013 to account for wave-current interactions. The formulation achieved by Smit and Janssen (2013) accounts for bathymetry-induced statistical contributions due to wave interferences, which are ignored by presently used phase-averaged formulations (e.g. the SWAN model). However, the inhomogeneity that characterizes the coastal environment also involves ambient current patterns which should be taken into account for a more complete description of the wave statistics. Apart from the usual Doppler shift, the problem of wave-current interaction also involve the adiabatic effect of the current on the waves' amplitudes (Longuet-Higgins and Stewart, 1961, Bretherton and Garrett, 1968). Thus, if successful, this part of the study should result in a generalized action balance equation that is able to predict the evolution of wave statistics over variable media (due to varying currents and bathymetry), while preserving inhomogeneous contributions induced by wave interferences. This model development is considered in Chapter 3.

(iii) The third objective of this study relates to the ambitious goal of obtaining an adequate (accurate and efficient) statistical description of shallow water nonlinearity. In principle, such a development involves two separated steps. The first concerns the derivation of a well-behaved quadratic model. While the second is dedicated to the development of a statistical closure. This part of the study considers the first step. Specifically, it is aimed to gain a detailed picture of the nonlinear properties of the quadratic modelling approach (i.e., second-order bound solutions, amplitude dispersion and stability characteristics). In addition, it is aimed to gain insight into the prediction capabilities of different quadratic formulations to spectrally describe the nonlinear evolution of coastal wave fields, including the development of the sea-swell components (i.e., the primary harmonics and the secondary super-harmonics) and the generation and evolution of the infragravity components (i.e., the secondary sub-harmonics). Finally, this part of

the study also attempts to push the limit of the predictive capabilities of the quadratic approach through a heuristic formulation of a new quadratic model which combines accurate linear and nonlinear properties achieved by searching for the optimal quadratic coefficients under the constraint of full linear dispersion. Successful results of this investigation would minimize the overall error associated with the statistical formulation of shallow water nonlinearity and may also be used as an independent tool for efficient and accurate prediction of coastal wave evolution. The investigation and results of this part of the study are detailed in Chapter 4.

Finally, concluding remarks and future perspectives close this study in Chapter 5.

2

WEYL RULE OF ASSOCIATION FOR WATER WAVES APPLICATIONS

Weyl rule of association, proposed by Hermann Weyl for quantum mechanics applications (Weyl, 1931), can be used to associate between the dispersion relation of water waves and a non-local pseudo-differential operator. The central result of this study is that this operator correctly approximates the Dirichlet-to-Neumann operator derived for linear waves over a slowly varying bathymetry. This opens the door to a formal use of Weyl's operational calculus, and consequently, allowing straightforward derivations and generalizations of water waves' models (e.g., linear mild-slope, Boussinesq-type, Whitham-type, etc.) over mild slopes. Most significantly, the formulation through Weyl rule of association allows to derive a general linear kinetic equation for which the widely used energy balance equation (the central equation of forecasting models such as SWAN and WAVEWATCH) serves as a special case. As a consequence, Weyl rule of association leads to the establishment of a formal link between the deterministic Euler equations and the stochastic energy balance equation and its generalization.

2.1. INTRODUCTION

Wave dynamics in coastal waters are characterized by a rich set of phenomena (e.g., shoaling, refraction, breaking etc.) that are triggered due to nonlinear wave-wave interactions and through the interaction of waves with variable bottom topography and ambient currents. The prediction of these complex dynamics is challenging and highly important to coastal communities and municipalities and to engineers, as it forces nearshore circulation (e.g., Longuet-Higgins, 1970, Bowen, 1969, Ruessink et al., 2001, Reniers and Battjes, 1997) and sediment transport processes (e.g. Van Rijn, 1993, Fredsoe and Deigaard, 1992), as well as controlling shipping operations and associated downtime, and coastal safety through beach and dune erosion and potential inundation (e.g., Vellinga, 1982, Roelvink et al., 2009).

Wave prediction in regional domains is commonly based on deterministic models, which are computationally feasible through a dimensional reduction. Traditionally, the vertical dimension is reduced using Boussinesq or the mild-slope approach (Dingemans, 1997). However, these approaches impose constraints on the dispersive behaviour or on the spectral width of the incident wave field. A continuous effort to derive deterministic models in terms of the horizontal dimensions only, which do not impose such constraints, led to the development of non-local formulations based on the so-called Dirichlet-to-Neumann (DtN) operator (Watson and West, 1975, Milder, 1990, Craig and Sulem, 1993). The DtN operator assigns to the Dirichlet information on the free surface the Neumann information which incorporates the necessary interior information of the fluid motion. In this way, the original problem is reduced to the free surface only, while preserving the full linear dispersion relation. Initially, this fully dispersive approach was developed for wave propagation in deep water or over constant depth (e.g., Watson and West, 1975, West et al., 1987, Dommermuth and Yue, 1987, Craig and Sulem, 1993, Batsman et al., 2001), and subsequently generalized to capture bottom variations (e.g., Liu and Yue, 1998, Smith, 1998, Craig et al., 2005, Guyenne and Nicholls, 2008, Gouin et al., 2016). The development reported so far, concerning the DtN approach over bathymetry, typically confined to the assumption of small bottom perturbations which may display rapid variations. Frequently though, bottom slopes in coastal areas are mild and bottom amplitudes may reach the order of the water depth. Therefore, such formulations experience difficulties to adequately predict the parameters of a wave field (e.g., the significant wave height) that evolves from deeper to shallower waters.

Over long time and large spatial scales, the forecasting of wave statistics is inevitably addressed through phase-averaged spectral models (e.g. WAM model, WAMDI Group, 1988, WAVEWATCH model, Tolman, 1991, SWAN model, Booij et al., 1999), which are based on the so-called energy balance equation. The theoretical foundation of the energy balance equation relies on the traditional analogy between statistically independent wave packets and non-colliding particles (Hasselmann, 1963). This statistical framework supports the usual assumption of Gaussianity, but it is limited to quasi-homogeneous wave fields. However, specifically in coastal regions, through the interaction with bottom topography and ambient currents, waves are rapidly scattered and can form focal zones which give rise to wave interferences (e.g., Vincent and Briggs, 1989). This results in a significant deviation from the quasi-homogeneous state (e.g., Smit and Janssen, 2013, Akrish et al., 2020). The contribution of wave interferences is statistically represented by

cross-correlations which cannot be developed through the presently used energy balance equation. Therefore, the statistical description obtained based on the traditional theory is incomplete as it is limited to cases where statistical wave interferences show negligible contribution.

This study shows that Weyl rule of association can provide a key component to overcome the above described difficulties that arise in both deterministic and stochastic wave modelling. Weyl rule of association, introduced by Hermann Weyl for quantum mechanics applications (Weyl, 1931), associates between a "phase-space" symbol (a function dependent on the spatial space, \mathbf{x} , and wavenumber space, \mathbf{k}) and a non-local pseudo-differential operator. For water waves applications, the linear dispersion relation can serve as the "phase-space" symbol. The principle result of this study is that the corresponding operator correctly approximates the DtN operator derived for linear waves over a slowly varying bathymetry. The equivalence of these two operators is discussed in Section 2.2. Based on this equivalence and using Weyl's operational calculus (e.g., Cohen, 2012), the evolution of linear waves over slowly varying depth can be described through a compact Schrödinger-like equation as demonstrated in Section 2.3. This allows a formal use of the so-called Wigner-Weyl formalism, and therefore, provides a formal derivation of the energy balance equation and its generalization for the statistical modelling of inhomogeneous wave fields. This statistical framework is detailed in Section 2.4. Finally, Weyl rule of association can also be useful for modelling of finite-amplitude waves. In particular, it is shown that based on the Weyl operator, the usual expansion of the nonlinear DtN operator (e.g., see review by Schäffer, 2008) is consistently generalized to mild slope conditions. Such a generalization allows model formulation of any order of nonlinearity that is valid for slowly varying bathymetries. This framework of model derivation is discussed in Section 2.5. Concluding remarks are drawn in Section 2.6.

2.2. THE EQUIVALENCE BETWEEN WEYL AND DTN OPERATORS OVER MILD SLOPES

The aim of this section is to show the equivalence between a formal definition of the DtN operator and the Weyl operator over mild slopes. In fact, this is the principle result of this study, through which, the attractive properties of the Weyl operator become formally applicable for different implementations of wave modelling.

2.2.1. THE MILD-SLOPE DTN OPERATOR

The DtN operator was developed for applications in water waves in order to reduce the complexity of the originally three-dimensional flow problem to a two-dimensional problem that is formulated on the free surface only (Watson and West, 1975). In order to show the equivalence with the Weyl operator, this subsection aims to derive the leading contributions of the linear DtN operator for mild slopes.

Under the framework of the potential theory, which considers the flow to be incompressible, inviscid and irrotational, the water wave problem is formulated as a Laplace problem in terms of the velocity potential Φ in a three dimensional domain \mathcal{D} . However, it is well known that the interior solution, Φ , of the Laplace problem is fully determined

by the flow values given on the boundaries, and therefore, the original problem can be potentially reduced to a two-dimensional one. In an influential paper Zakharov (1968) showed that it is possible to formulate the potential problem for water waves in terms of the two canonical surface variables, ϕ and η . The former denote the surface potential and the latter is the elevation function. Through the assumption of small surface fluctuations of $O(\epsilon)$ (relative to the typical wave length of the fluctuations in deep/intermediate water or to the water depth in shallow water) and by ignoring surface-tension effect, Zakharov's formulation can be written as

$$\mathcal{H} = \int \left(\frac{1}{2} g \eta^2 + \frac{1}{2} \phi W_0 \right) dx \quad (2.1)$$

where \mathcal{H} is the Hamiltonian (the sum of potential and kinetic energy), g is the gravitational acceleration and W_0 is the free surface vertical velocity defined as $W_0 = (\partial_z \Phi)_0$. Additionally, z denotes the vertical coordinate and $\mathbf{x} = (x, y)$ denote the horizontal coordinates. Finally, the subscript $(\)_0$ represents terms that are evaluated on $z = 0$.

The linear Zakharov's formulation (2.1) leaves the vertical velocity W_0 as the only non-free surface component, as it is defined through Φ . Therefore, in order to obtain self-contained free-surface equations (provided by the canonical equation $\partial_t \eta = \delta_\phi \mathcal{H}$ and $\partial_t \phi = -\delta_\eta \mathcal{H}$), it is required to relate between W_0 and the free-surface variables. Such a relation can be obtained through the constraint posed by the following Laplace problem:

$$\begin{cases} \Delta \Phi = 0, & \text{in } \mathcal{D}, \\ \Phi = \phi, & \text{on } z = 0, \\ \partial_z \Phi + \nabla_{\mathbf{x}} h \cdot \nabla_{\mathbf{x}} \Phi = 0, & \text{on } z = -h \end{cases} \quad (2.2)$$

where $\nabla_{\mathbf{x}}$ is defined as $\nabla_{\mathbf{x}} = (\partial_x, \partial_y)$ (while ∇ stands for $\nabla = (\partial_x, \partial_y, \partial_z)$), $\Delta \equiv \nabla \cdot \nabla$ and h is the still water depth. Therefore, given a solution, Φ , of the Laplace problem (2.2), one can formulate the following relation:

$$W_0 = \mathcal{G}_0 \phi \quad (2.3)$$

This relation introduces the so-called DtN operator, \mathcal{G}_0 , that maps between the Dirichlet value ϕ and the Neumann value W_0 . Consequently, if an explicit solution Φ is found, the corresponding DtN map (2.3) leads to the desired dimensional reduction of the potential problem for linear water waves.

A general and explicit solution form of the linear Laplace problem (2.2) is achieved through the Boussinesq approach. This amounts to the expansion of the velocity potential Φ around some arbitrary level z_a , allowing to express its solution using only two unknowns functions. If the level around which the expansion is performed is $z_a = 0$, then the two unknowns are the surface potential ϕ and the vertical velocity W_0 , and thus, the general solution receives the following form (see Agnon et al., 1999 for further details):

$$\Phi = \mathcal{C}(z|D_{\mathbf{x}}|)\phi + \mathcal{S}(z|D_{\mathbf{x}}|)|D_{\mathbf{x}}|^{-1}W_0 \quad (2.4)$$

where $D_{\mathbf{x}}$ is defined as $D_{\mathbf{x}} \equiv -i\nabla_{\mathbf{x}}$. Note that the above formulation differs from the formulation of Agnon et al. (1999) in terms of notation only. Here \mathcal{C} and \mathcal{S} indicate the

pseudo-differential operators $\cosh(z|D_{\mathbf{x}}|)$ and $\sinh(z|D_{\mathbf{x}}|)$ (these types of operators can be interpreted, for example, through their power series). In addition, the operator $|D_{\mathbf{x}}|$ is defined here as $|D_{\mathbf{x}}| = (-\Delta_{\mathbf{x}})^{1/2}$ (e.g., Milewski, 1998), where $\Delta_{\mathbf{x}} \equiv \nabla_{\mathbf{x}} \cdot \nabla_{\mathbf{x}}$. The equivalence between the formulation using functions of $(z\nabla_{\mathbf{x}})$ (e.g., Agnon et al., 1999) and the formulation using functions of $(z|D_{\mathbf{x}}|)$ (e.g., Milewski, 1998) is understood due to the functional symmetry of the operators involved (e.g., $\cosh(z|D_{\mathbf{x}}|) \equiv \cos(z\nabla_{\mathbf{x}})$). The advantage of using $|D_{\mathbf{x}}|$ relies on its direct correspondence with the wavenumber magnitude $|\mathbf{k}| = (k_x^2 + k_y^2)^{1/2}$, where $\mathbf{k} = (k_x, k_y)$ defines the wavenumber space. Also note that these types of solution forms were already proposed by earlier studies (e.g., Sen, 1927, Miles, 1985).

Ultimately, the desired DtN relation between ϕ and W_0 , (2.3), is obtained through the bottom boundary condition of the considered Laplace problem (2.2). Accordingly, the expression for Φ , (2.4), is substituted into the bottom boundary condition (specified in (2.2)) which results in

$$\mathcal{C}W_0 = \mathcal{S}|D_{\mathbf{x}}|\phi + D_{\mathbf{x}}h \cdot \left(\mathcal{C}D_{\mathbf{x}}\phi - \mathcal{S}|D_{\mathbf{x}}|^{-1}D_{\mathbf{x}}W_0 \right) \quad (2.5)$$

Note that through the substitution of $z = -h$ (as is required by the bottom boundary condition), the above expression does not depend on the vertical coordinates, z (the operators \mathcal{C} and \mathcal{S} are now functions of $h|D_{\mathbf{x}}|$). In order to proceed, it should be recalled that the aim here is to derive the leading contributions of the DtN relation for mild slopes. To this end, W_0 is written asymptotically as,

$$W_0 = W_0^{(0)} + W_0^{(1)} + \dots \quad (2.6)$$

where, the superscript ${}^{(m)}$ represents contribution of $O(\beta^m)$, and β stands for the ratio between the characteristic wave length and the characteristic variation length of h , which for mild slopes, is assumed to be small. By substituting the expansion in (2.6) into the expression in (2.5) one obtains

$$\mathcal{C}\left(W_0^{(0)} + W_0^{(1)} + \dots\right) = \mathcal{S}|D_{\mathbf{x}}|\phi + D_{\mathbf{x}}h \cdot \left(\mathcal{C}D_{\mathbf{x}}\phi - \mathcal{S}|D_{\mathbf{x}}|^{-1}D_{\mathbf{x}}\left(W_0^{(0)} + \dots\right) \right) \quad (2.7)$$

The contribution of the DtN relation at each order is consistently extracted by a careful consideration of the operator compositions $(\mathcal{C}^{-1}\mathcal{C})$ and $(\mathcal{C}^{-1}\mathcal{S})$. Such compositions arise as a result of isolating the contribution of W_0 at each order on the left-hand-side of (2.7). Since these operators (namely, \mathcal{C} , \mathcal{S} and \mathcal{C}^{-1}) are of the "Standard" type (operators that are ordered such that all the factors $D_{\mathbf{x}}$ are placed to right of the \mathbf{x} factors, see details in Appendix 2.A), their composition can be expressed explicitly using (2.63) (e.g., $\cosh^{-1}(|\mathbf{k}|h)$ and $\cosh(|\mathbf{k}|h)$ would represent the symbols U and L in (2.63) in order to calculate the symbol of the composition $(\mathcal{C}^{-1}\mathcal{C})$, for which the operational form is obtained by associating back from \mathbf{k} to $D_{\mathbf{x}}$). Following (2.63), $O(1)$ contribution of the composition $(\mathcal{C}^{-1}\mathcal{C})$ is simply the unit operator associated to 1, while $O(1)$ contribution of the composition $(\mathcal{C}^{-1}\mathcal{S})$ is \mathcal{T} , where $\mathcal{T} \equiv \tanh(h|D_{\mathbf{x}}|)$. In addition, (2.63) specifies that $O(\beta)$ contributions of these compositions can be written as

$$\begin{cases} (\mathcal{C}^{-1}\mathcal{C})_{O(\beta)} = -h(D_{\mathbf{x}}h) \cdot \mathcal{T}^2 D_{\mathbf{x}} \\ (\mathcal{C}^{-1}\mathcal{S})_{O(\beta)} = -h(D_{\mathbf{x}}h) \cdot \mathcal{T} D_{\mathbf{x}} \end{cases} \quad (2.8)$$

Following (2.7) and based on the above observations, the expression obtained for $W_0^{(0)}$ is given by,

$$W_0^{(0)} = \mathcal{T} |D_x| \phi \quad (2.9)$$

whereas the expression for $W_0^{(1)}$ is provided by

$$W_0^{(1)} = (\mathcal{C}^{-1} \mathcal{S})_{O(\beta)} |D_x| \phi - (\mathcal{C}^{-1} \mathcal{C})_{O(\beta)} W_0^{(0)} + (D_x h) \cdot \left(D_x \phi - \mathcal{T} |D_x|^{-1} D_x W_0^{(0)} \right) \quad (2.10)$$

The expression for $W_0^{(1)}$ can be written more explicitly by substituting the expressions for the $O(\beta)$ contributions of the operator compositions, (2.8), and the expression for $W_0^{(0)}$, (2.9), into (2.10). Finally, summing the contributions due to $W_0^{(0)}$ and $W_0^{(1)}$ leads to the following formal mild-slope derivation of the DtN operator \mathcal{G}_0 :

$$\mathcal{G}_0 = \mathcal{T} |D_x| + (D_x h) \cdot (1 - \mathcal{T}^2)(1 - h\mathcal{T}|D_x|)D_x \quad (2.11)$$

Next, it is aimed to show that the Weyl operator reduces, up to $O(\beta)$, to the same expression for \mathcal{G}_0 .

2.2.2. WEYL OPERATOR AND ITS ASYMPTOTIC FORM

The definition of the Weyl operator is based on the Weyl rule of association, namely, the association between a "phase-space" symbol (a function which is defined in (\mathbf{x}, \mathbf{k}) space) and a pseudo-differential operator. For the considered linear Laplace problem (2.2) and under the mild-slope assumption, the symbol $G(\mathbf{x}, \mathbf{k}) = \sigma^2/g$ naturally arises as the "phase-space" symbol (as is implied by the usual WKB analysis, e.g., Dingemans, 1997; also refer to Van Groesen and Molenaar, 2007), where σ is defined through the linear dispersion relation, $\sigma(\mathbf{x}, \mathbf{k}) = \sqrt{|\mathbf{k}|g \tanh(|\mathbf{k}|h)}$. Given a "phase-space" symbol, the corresponding operator in the physical space can be defined through the association between \mathbf{k} and D_x . However, because \mathbf{x} and D_x do not commute, one must follow an association rule. Hermann Weyl (Weyl, 1931) suggested a rule of association that is defined through the following Fourier transform of $G(\mathbf{x}, \mathbf{k})$ (see, e.g., Cohen, 2012):

$$G(\mathbf{x}, \mathbf{k}) = \int \hat{G}(\mathbf{q}, \mathbf{p}) \exp(i\mathbf{q} \cdot \mathbf{x} + i\mathbf{p} \cdot \mathbf{k}) d\mathbf{q} d\mathbf{p} \quad (2.12)$$

The Weyl operator is then defined by substituting the operator D_x instead of \mathbf{k} , which provides the following expression:

$$\mathcal{G}_w(\mathbf{x}, D_x) = \int \hat{G}(\mathbf{q}, \mathbf{p}) \exp(i\mathbf{q} \cdot \mathbf{x} + i\mathbf{p} \cdot D_x) d\mathbf{q} d\mathbf{p} \quad (2.13)$$

and which can be simplified using the Baker–Campbell–Hausdorff formula and through the fact that the commutator, $[i\mathbf{q} \cdot \mathbf{x}, i\mathbf{p} \cdot D_x] = -i\mathbf{q} \cdot \mathbf{p}$, is constant, to obtain

$$\mathcal{G}_w(\mathbf{x}, D_x) = \int \hat{G}(\mathbf{q}, \mathbf{p}) \exp\left(\frac{i}{2}\mathbf{q} \cdot \mathbf{p}\right) \exp(i\mathbf{q} \cdot \mathbf{x}) \exp(i\mathbf{p} \cdot D_x) d\mathbf{q} d\mathbf{p} \quad (2.14)$$

where the subscript $()_w$ of the operator indicates that it is a Weyl operator. In order to show the equivalence between the Weyl operator $\mathcal{G}_w(\mathbf{x}, D_x)$ and the formal DtN operator up to $O(\beta)$, an explicit asymptotic form of the Weyl operator is required. This explicit asymptotic form is formally derived in Appendix 2.A and is given by (2.56). As an alternative of the formal derivation, the asymptotic form can be also observed directly from (2.14). Where by associating between D_x and \mathbf{k} , the corresponding symbol that is obtained is expressed as follows:

$$R(\mathbf{x}, \mathbf{k}) = \int \hat{G}(\mathbf{q}, \mathbf{p}) \exp\left(\frac{i}{2} \mathbf{q} \cdot \mathbf{p}\right) \exp(i \mathbf{q} \cdot \mathbf{x} + i \mathbf{p} \cdot \mathbf{k}) d\mathbf{q} d\mathbf{p} \quad (2.15)$$

Here the association is unique, since the order of the factors \mathbf{x} and D_x is explicitly given in (2.14) such that all the factors D_x are placed to right of the \mathbf{x} factors. Therefore, the asymptotic form of the operator can be obtained by writing the symbol $R(\mathbf{x}, \mathbf{k})$ asymptotically and then associate back to the operator representation, preserving the rule that all the factors D_x should be placed to right of the \mathbf{x} factors. The asymptotic form of $R(\mathbf{x}, \mathbf{k})$ is directly obtained in terms of the original symbol $G(\mathbf{x}, \mathbf{k})$ from the expression written in (2.15) as

$$R(\mathbf{x}, \mathbf{k}) = \exp\left(\frac{i}{2} D_x \cdot D_k\right) G(\mathbf{x}, \mathbf{k}) \quad (2.16)$$

which exactly represents the operation of the first exponent in (2.56). Whereas the back association is defined by the second exponent in (2.56). Neglecting $O(\beta^2)$ contributions, the approximation of $R(\mathbf{x}, \mathbf{k})$ reads

$$R(\mathbf{x}, \mathbf{k}) \sim \left(1 + \frac{i}{2} D_x \cdot D_k\right) G(\mathbf{x}, \mathbf{k}) \quad (2.17)$$

which after some algebra simplifies to

$$R(\mathbf{x}, \mathbf{k}) \sim T|\mathbf{k}| + (D_x h) \cdot (1 - T^2)(1 - hT|\mathbf{k}|)\mathbf{k} \quad (2.18)$$

where $T = \tanh(h|\mathbf{k}|)$ and recall that $G(\mathbf{x}, \mathbf{k}) = \sigma^2/g$, which means that $G(\mathbf{x}, \mathbf{k}) = T|\mathbf{k}|$. Ultimately, the association back to the operator representation recovers the formal mild-slope definition of the DtN, (2.11), and therefore, shows the equivalence between Weyl and DtN operators over mild slopes.

Note that the expression in (2.18) could be written using a more recognizable form using the relation $\nabla_{\mathbf{k}} G = 2CC_g \mathbf{k}/g$, where C and C_g are the phase and group velocity, defined as $C = \sigma/|\mathbf{k}|$ and $C_g = \partial_{|\mathbf{k}|} \sigma$. Then, one can write the approximation for the symbol $R(\mathbf{x}, \mathbf{k})$ as follows:

$$R(\mathbf{x}, \mathbf{k}) \sim \frac{1}{g} \left(\sigma^2 + D_x (CC_g) \cdot \mathbf{k} \right) \quad (2.19)$$

which seems to relate to the classical mild-slope operator (Berkhoff, 1972). Appendix 2.B presents a closer look on the relation between the Weyl operator and the classical mild-slope operator and confirms that the former indeed reduces to the latter for quasi-periodic wave fields.

The equivalence between Weyl and DtN operators is the principle results of this study since it opens the door to the formal use of the Weyl operator and Weyl calculus for application in deterministic and stochastic modelling of water waves. Most significantly, this result establishes the connection between Euler equations (and the associated linear wave theory) and the widely used energy balance equation.

2.3. A SCHRÖDINGER-TYPE MODEL FOR LINEAR WAVES OVER VARIABLE BATHYMETRY

The energy balance equation can be formally derived starting with the following Schrödinger equation:

$$\partial_t \zeta = -i \Sigma(\mathbf{x}, D_x) \zeta \quad (2.20)$$

where Σ is the Weyl operator that is associated with the dispersion relation σ and ζ is a complex variable which should be directly related to the energy density of the wave field. Specifically, the complex variable ζ should satisfy the following:

$$\rho \langle |\zeta|^2 \rangle = m_0 + O(\beta) \quad (2.21)$$

where the angular parentheses, $\langle \dots \rangle$, should be read as ensemble average, the variable m_0 provides a leading order measure (in β) of the mean energy density and ρ is the water mass density. The specific definitions required for Σ and ζ provide a direct path to the formulation of the energy balance equation as recently shown by Smit and Janssen (2013). However, formal derivation of (2.20) is unavailable. This derivation is made possible based on Weyl's operational calculus. The starting point is the linearized Hamiltonian given by (2.1). Then, the linear DtN map, (2.3), is employed to reduce the dimension of the problem,

$$W_0 = \mathcal{G}_w \phi \quad (2.22)$$

where instead of \mathcal{G}_0 , the equivalent Weyl operator, \mathcal{G}_w , is now being used. Finally, the evolution equations for η and ϕ are obtained through the canonical equations, $\partial_t \eta = \delta_\phi \mathcal{H}$ and $\partial_t \phi = -\delta_\eta \mathcal{H}$ as

$$\partial_t \begin{bmatrix} \eta \\ \phi \end{bmatrix} = \mathbf{A} \begin{bmatrix} \eta \\ \phi \end{bmatrix} \quad (2.23)$$

where the matrix \mathbf{A} is defined as

$$\mathbf{A} = \begin{bmatrix} 0 & \mathcal{G}_w \\ -g & 0 \end{bmatrix} \quad (2.24)$$

In order to derive the Schrödinger equation, (2.20), based on the above linear system, it is required that the matrix \mathbf{A} is diagonalizable. Namely, \mathbf{A} is required to satisfy the following expression:

$$\mathbf{A} = \mathbf{P}\mathbf{\Lambda}\mathbf{P}^{-1} \quad (2.25)$$

It is further required that the diagonal matrix $\mathbf{\Lambda}$ is composed of the Weyl operator Σ and its complex conjugate on the main diagonal. Additionally, \mathbf{P} is required to define the following transformation:

$$\begin{bmatrix} \zeta \\ \zeta^* \end{bmatrix} = \mathbf{P}^{-1} \begin{bmatrix} \eta \\ \phi \end{bmatrix} \quad (2.26)$$

such that the eigenvectors appearing along its columns provide the necessary relation between the complex variable ζ (or ζ^* where $()^*$ denotes complex conjugate) and the energy density.

The required result for $\mathbf{\Lambda}$ is obtained through the convenient formulas of operator composition (2.65). In a certain sense, these formulas allow one to manipulate operators as if they are simple functions. The "eigenvalues" of \mathbf{A} , which are found on the main diagonal of $\mathbf{\Lambda}$ and indicated by $\lambda_{1,2}$, can be obtained by setting the determinant $|\mathbf{A} - \lambda_{1,2}\mathbf{I}|$ to zero. This results in the following equation:

$$\lambda_{1,2} + \Sigma^2 = O(\beta^2) \quad (2.27)$$

By neglecting $O(\beta^2)$ terms, the desired results that $\lambda_1 = -i\Sigma$ and $\lambda_2 = i\Sigma^*$ are obtained. The corresponding definition of \mathbf{P}^{-1} can be written as

$$\mathbf{P}^{-1} = \frac{1}{\sqrt{2g}} \begin{bmatrix} g & i\Sigma \\ g & -i\Sigma \end{bmatrix} \quad (2.28)$$

This leads to the following definition for ζ :

$$\zeta = \frac{1}{\sqrt{2g}} (g\eta + i\Sigma\phi) \quad (2.29)$$

which by substituting in the required relation, (2.21), reads,

$$\rho\langle |\zeta|^2 \rangle = \left\langle \frac{1}{2}\rho g\eta^2 \right\rangle + \left\langle \frac{1}{2g}\rho(\Sigma\phi)^2 \right\rangle \quad (2.30)$$

This expression indeed equals to the leading order ($O(\beta^0)$) contribution of m_0 (see detailed explanation in Akrish et al., 2020, Appendix B), which consists of the mean potential energy density (the first term on the right-hand-side of (2.30)) and the mean kinetic energy density (the second term on the right-hand-side of (2.30)). This completes the verification that the system consisting of the Schrödinger equation, (2.20) and its complex conjugate is equivalent to the system given by (2.23)-(2.24). As a consequence, the Schrödinger equation, (2.20), is now made formally available as a mild-slope equation for linear water waves which can be conveniently used for the derivation of the energy balance equation.

2.4. THE WIGNER-WEYL FORMALISM AS A STATISTICAL FRAMEWORK FOR WATER WAVES

The energy balance equation is the central equation underlying the widely used operational forecasting wave models (e.g. WAM model (WAMDI Group, 1988), WAVEWATCH model (Tolman, 1991) and SWAN model (Booij et al., 1999)). This important equation can be written in the following form:

$$\partial_t E = \{\sigma, E\} \quad (2.31)$$

where E represents the spectrum of the energy density and the brackets $\{\}$ are the so-called Poisson brackets which define the following operation:

$$\{\sigma, E\} \equiv \sigma \left(\overleftarrow{\nabla}_x \cdot \overleftarrow{\nabla}_k - \overleftarrow{\nabla}_k \cdot \overleftarrow{\nabla}_x \right) E \quad (2.32)$$

where the arrows indicate the function on which the differential operator should operate, i.e., σ or E . The existing theoretical justification for the energy balance equation is based on the heuristic analogy between wave packets and classical particles (Hasselmann, 1963). This derivation approach of the energy balance equation is referred here as the traditional formulation.

The main aim of this section is to present an alternative formal derivation of the energy balance equation that is obtained directly from Euler equations. This is achieved using the newly derived Schrödinger formulation, (2.20). In fact, based on (2.20), the energy balance equation is formally obtained as a special case of the more general kinetic equation provided by the Wigner-Weyl formalism. The Wigner-Weyl kinetic equation can be written as

$$\partial_t \mathcal{W} = \{\{\sigma, \mathcal{W}\}\} \quad (2.33)$$

where \mathcal{W} is the Wigner distribution of the complex variable ζ (see detailed definitions for \mathcal{W} in Akrish et al., 2020). The Wigner distribution defines a generalized energy density, as it incorporates also cross-correlation values that are ignored in E by definition. In addition, the brackets $\{\{\}\}$ are now the so-called Moyal brackets (Moyal, 1949) defined as

$$\{\{\sigma, \mathcal{W}\}\} \equiv 2\sigma \sin \left(\overleftarrow{\nabla}_x \cdot \overleftarrow{\nabla}_k / 2 - \overleftarrow{\nabla}_k \cdot \overleftarrow{\nabla}_x / 2 \right) \mathcal{W} \quad (2.34)$$

Following the asymptotic relation $\sin(x) \sim x$ that applies for small values of x , one can immediately see that $\{\{\}\} \sim \{\}$ when the products $\left(\sigma \overleftarrow{\nabla}_x \cdot \overleftarrow{\nabla}_k \mathcal{W} \right)$ and $\left(\sigma \overleftarrow{\nabla}_k \cdot \overleftarrow{\nabla}_x \mathcal{W} \right)$ are small. Additionally, in such scenarios, cross-correlations that may develop due to variations in the medium are negligible and \mathcal{W} becomes asymptotically equal to E which ultimately leads to the reduction from (2.33) to (2.31) (also refer to Smit and Janssen, 2013 for further details). Consequently, beyond the fact that the Wigner-Weyl formalism based on the Schrödinger equation (2.20) provides a formal alternative to the existing traditional formulation, it also generalizes the statistical description of wave fields. In order to understand the limitation involved in the traditional formulation, and thus, the added value that is taken into account by the Wigner-Weyl formalism, the traditional formulation is briefly introduced and qualitatively examined through an idealized example.

2.4.1. THE TRADITIONAL FORMULATION OF THE ENERGY BALANCE EQUATION

The traditional formulation of the energy balance equation is based on the fundamental theorem of statistical mechanics known as Liouville's theorem. The applicability of Liouville's theorem is obtained through the analogy between classical particles and wave packets (Hasselmann, 1963). The basic assumption leading to this analogy is the representation of the wave field as a superposition of large number of statistically independent wave packets whose dimension is much smaller than the characteristic scale of the medium variation. The elegant result of such representation is that the position, \mathbf{x}_j , and the wavenumber, \mathbf{k}_j , of each packet (indicated by the subscript j) are governed by the following canonical equations (e.g., Dingemans, 1997)

$$\frac{d\mathbf{x}_j}{dt} = \nabla_{\mathbf{k}_j} \sigma_j, \quad \frac{d\mathbf{k}_j}{dt} = -\nabla_{\mathbf{x}_j} \sigma_j \quad (2.35)$$

where $\sigma_j = \sigma(\mathbf{x}_j, \mathbf{k}_j)$. Therefore, the wave packets effectively evolve as a non-colliding system of particles, where \mathbf{x}_j , \mathbf{k}_j and σ play the role of the generalized coordinates, momenta and the Hamiltonian. As a result, Liouville's theorem becomes applicable to describe statistically the wave packet system through the number density of wave packets in phase space, $n(\mathbf{x}, \mathbf{k}, t)$. Since σ does not involve coupling of different wave packets (as a result of the linearity of the problem), n is conserved along trajectories in phase space, namely, it is governed by the so-called collisionless Boltzmann equation,

$$\partial_t n = \{\sigma, n\} \quad (2.36)$$

which shows exactly the same structure of the energy balance equation. Thus, using the constraint that each packet has the same total wave-energy, the number density n becomes proportional to the energy density E (see Komen et al., 1994 for further details), which completes the traditional derivation of the energy balance equation (2.31).

Based on the usual assumptions of quasi-homogeneity and Gaussianity, the traditional particle-picture actually leads to a complete statistical description of the wave field. Since under these assumptions the probability-density-function of any ensemble of temporal-spatial elevation points of the water surface is recovered by the knowledge of E (assuming zero-mean field). However, there are situations where the representation of the wave field through a superposition of statistically independent wave packets results in an incomplete description. Such situations can be demonstrated through the following representative example. The example considers a rather narrow wave spectrum (as may often be the case for coastal wave fields which were generated far offshore) entering a domain that consists of two homogeneous regions separated by a scattering region. This example is illustrated in Fig. 2.1, where the scattering region (referred to as 'the scatterer') is represented by a submerged shoal. The particle picture for this example is illustrated by calculating the phase space trajectories of the wave packets using (2.35). The solution is obtained here assuming some fixed number of packets with equal initial wavenumber, \mathbf{k}_0 , that represents the carrier wavenumber of the spectrum. The projection of the phase space trajectories on the considered domain results in the wave-rays picture which qualitatively reflects on the packet density, and consequently, also on the spatial structure of E . Considering now the correlation function around point A . Since

the incoming spectrum is assumed to be relatively narrow, the corresponding correlation function around point A may extend over an area (occupied by the dotted-dashed circle in Fig. 2.1) such that correlation emerges between the incoming and the scattered wave fields. This should then give rise to cross-correlations between different wave packets, which were assumed to be statistically independent. As recently demonstrated (e.g. Smit and Janssen, 2013, Akriş et al., 2020), cross-correlation contributions in such cases lead to the development of prominent interference structures which significantly change the wave statistics. Therefore, as a result of the assumption that different wave packets are statistically independent, these contributions cannot be predicted by the traditional formulation. On the other hand, for wider spectra (corresponding to smaller correlation scales) interference patterns become effectively smoother following their superposition. Under these conditions, cross-correlation contributions become negligible and prediction due to the traditional formulation through the energy balance equation is expected to agree with the generalized kinetic equation of the Wigner-Weyl formalism. Ultimately, it remains to be seen how statistical interference patterns are taken into account by the Wigner-Weyl kinetic equation. To this end, this generalized equation is briefly derived and examined.

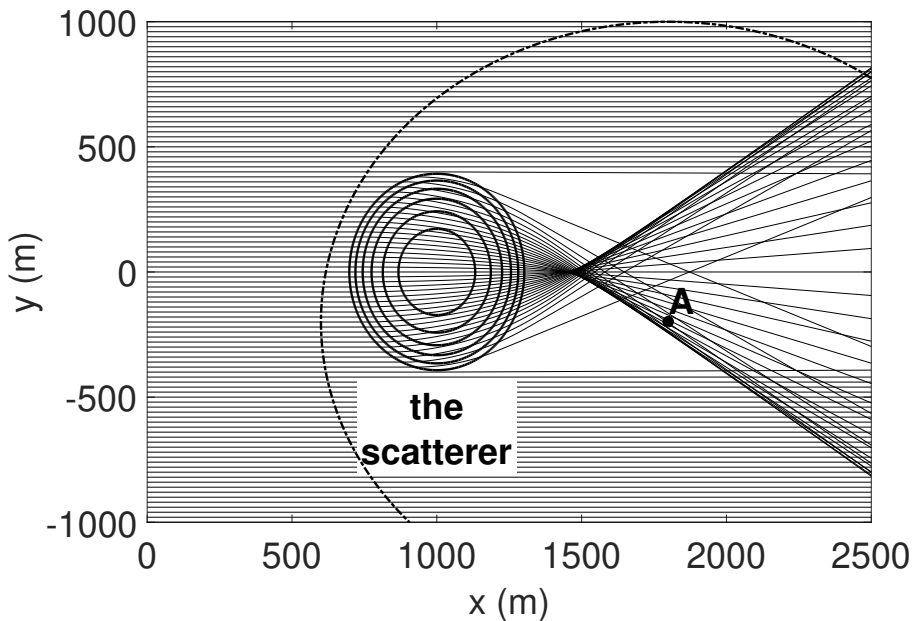


Figure 2.1: Normally incident wave-rays due to k_0 over a submerged shoal. The rays are indicated by solid curved lines. The shoal topography is illustrated by the solid elliptical lines at the center of the figure. Finally, the dashed circle line describe the effective support of the field's correlation function around point A .

2.4.2. A FORMAL DERIVATION OF THE ENERGY BALANCE EQUATION AND ITS GENERALIZATION

The formal derivation of the Schrödinger equation, (2.20), allows direct and formal derivation of the Wigner-Weyl kinetic equation, (2.33). The detailed derivation, starting with (2.20), is provided by numerous studies in other fields of physics (e.g., Moyal, 1949, Leaf, 1968, Bremmer, 1973, Besieris and Tappert, 1976, McDonald and Kaufman, 1985, Zhu and Dodin, 2021). In the context of water waves, the derivation is given by Smit and Janssen (2013). Concisely, the Wigner-Weyl kinetic equation is derived directly by considering the time derivative of the correlation function $\Gamma(\mathbf{x}_1, \mathbf{x}_2, t) = \langle \zeta(\mathbf{x}_1, t) \zeta^*(\mathbf{x}_2, t) \rangle$. Then, using the Schrödinger equation, (2.20), and the following definition of the Wigner distribution:

$$\mathcal{W}(\mathbf{x}, \mathbf{k}, t) = \int \Gamma(\mathbf{x} + \mathbf{x}'/2, \mathbf{x} - \mathbf{x}'/2, t) \exp(-i\mathbf{k} \cdot \mathbf{x}') d\mathbf{x}' \quad (2.37)$$

one arrives (also due to the properties of the Weyl operator Σ) at the correct expression for the Wigner-Weyl kinetic equation, (2.33).

Returning now to the example above which emphasizes the importance of the cross-correlations when considering a wave field with relatively narrow spectrum. As illustrated in Fig. 2.1, it may often be the case that the correlation function of such fields bridges across scattering regions, and therefore, the corresponding Wigner distribution is affected by interference patterns (obtained by the contribution of cross-correlations). As discussed by Smit and Janssen (2013), in such scenarios, the product $(\sigma \overleftarrow{\nabla}_x \cdot \overrightarrow{\nabla}_k \mathcal{W})$ of the Moyal brackets, $\{\{\}\}$, as appear in (2.34) is not small. Thus, the interpretation of $\{\{\}\}$ through Taylor expansion is no longer valid (this also implies that the conventional energy balance equation, (2.31), loses validity). Alternatively, the operation of $\{\{\}\}$ can be partially defined using a Fourier integral, leading to an integro-differential form, which remains valid also for cases in which the correlation length is larger than the characteristic scale of medium variation, but retains the assumption of weak spatial variability of the field statistics as implied by the Taylor interpretation of the second product of $\{\{\}\}$. This new interpretation of the Moyal brackets, $\{\{\}\}$, leads to a generalized energy balance equation that can be written in the following form (see Smit et al., 2015a):

$$\partial_t \mathcal{W} = \{\sigma, \mathcal{W}\} + S_{QC} \quad (2.38)$$

where S_{QC} is a scattering term that forces the generation of statistical wave interferences induced by variable bathymetry, and the subscript QC stands for 'quasicoherent' approximation (Smit and Janssen, 2013). The role of S_{QC} is demonstrated numerically through several representative examples of wave-bottom interactions (Smit and Janssen, 2013, Smit et al., 2015a) and has recently been generalized and demonstrated for cases of wave-current interactions (Akrish et al., 2020).

2.5. DISCUSSION

The application of the Weyl rule of association for water waves is not limited to the linear regime. In fact, in the following discussion it is shown that the Weyl operator, (2.14), naturally serves as a building block in the usual asymptotic representation of the nonlinear

DtN (see e.g., the review by Schäffer, 2008). The asymptotic expansion of the nonlinear DtN through the Weyl operator allows a model construction with any degree of nonlinearity that is consistently formulated for mild slopes. Examples are provided for the weak-nonlinear regime. In particular, a fully dispersive and weakly nonlinear model is derived using the symbol G that corresponds to the full linear dispersion relation. Finally, based on this generalized weakly nonlinear model, formulations of known scaling regimes (e.g., the classical Boussinesq scaling) are consistently derived.

2.5.1. FULLY NONLINEAR FORMULATION THROUGH WEYL RULE OF ASSOCIATION

The nonlinear formulation is also derived in a convenient manner through Zakharov's Hamiltonian framework, which by ignoring surface-tension effect, but preserving nonlinear contributions, can be written as

$$\mathcal{H} = \frac{1}{2} \int \left(g\eta^2 + \phi[(1 + \nabla_x \eta \cdot \nabla_x \eta)W - \nabla_x \eta \cdot \nabla_x \phi] \right) dx \quad (2.39)$$

To reduce the dimension of the problem it is again required to relate between W and the surface variables, ϕ and η . However, this time, the relation is implicit since it is required on the unknown level $z = \eta$. The usual approach to cope with this difficulty is to project the mapping to the constant level $z = 0$ through a suitable asymptotic expansion (Dommermuth and Yue, 1987). In this way W is evaluated asymptotically using the surface variables only, which then completes the desired dimension reduction. This asymptotic procedure is concisely summarized as follows. The starting point is the assumption of finite, though small, fluctuations of the free surface, allowing to express the velocity potential, Φ , as

$$\Phi = \sum_{m=1}^M \Phi^{(m)} \quad (2.40)$$

where, the superscript (m) represents contribution of $O(\epsilon^m)$ and M indicates the highest order of nonlinearity that is considered. Additionally, the value of each $\Phi^{(m)}$ on $z = \eta$ can be approximated as a Taylor expansion around $z = 0$. Ultimately, these asymptotic expansions can be combined to form an approximation for the surface potential as (Dommermuth and Yue, 1987),

$$\phi = \sum_{m=1}^M \sum_{j=0}^{(M-m)} \frac{\eta^j}{j!} (\partial_z^j \Phi^{(m)})_{z=0} \quad (2.41)$$

Effectively, (2.40) and (2.41) allow to replace the original Laplace problem that is subjected to the nonlinear surface condition $(\Phi)_{z=\eta} = \phi$ with M Laplace problems, such as given by (2.2), that are subjected to the linear condition $(\Phi^{(m)})_{z=0} = \Phi_0^{(m)}$, where $\Phi_0^{(m)}$ is given by

$$\begin{cases} \Phi_0^{(m)} = \phi, & m = 1 \\ \Phi_0^{(m)} = -\sum_{j=1}^{m-1} \frac{\eta^j}{j!} (\partial_z^j \Phi^{(m-j)})_{z=0}, & m \neq 1 \end{cases} \quad (2.42)$$

The advantage gained by breaking down the original Laplace problem into M Laplace problems with linear surface condition is that for the latter, the solution is already provided by (2.4) (by merely replacing the surface variables ϕ and W_0 with $\Phi_0^{(m)}$ and $W_0^{(m)}$, where $W_0^{(m)} = (\partial_z \Phi^{(m)})_{z=0}$). Accordingly, the linear DtN map in terms of the Weyl operator, (2.22),

$$W_0^{(m)} = \mathcal{G}_w \Phi_0^{(m)} \quad (2.43)$$

is applicable as well. Ultimately, base on these results, the approximation of W at each order m , which is written as

$$W^{(m)} = \sum_{j=0}^{m-1} \frac{\eta^j}{j!} (\partial_z^{j+1} \Phi^{(m-j)})_{z=0}, \quad (2.44)$$

is formally extended to mild slopes, leading to a consistent generalization of the nonlinear DtN formulation. To demonstrate this result, the contribution of the first three terms, $W^{(1)}$, $W^{(2)}$ and $W^{(3)}$ are considered. These are calculated based on the asymptotic expansions (2.44) and (2.42) and based on the solution of the linearized Laplace system (2.4) and the linear DtN map (2.43). The outcome is given as follows:

$$\begin{cases} W^{(1)} = \mathcal{G}_w \phi \\ W^{(2)} = \left(\eta D_x^2 - \mathcal{G}_w \eta \mathcal{G}_w \right) \phi \\ W^{(3)} = \left(\frac{1}{2} \eta^2 D_x^2 \mathcal{G}_w - \eta D_x^2 \eta \mathcal{G}_w - \frac{1}{2} \mathcal{G}_w \eta^2 D_x^2 + \mathcal{G}_w \eta \mathcal{G}_w \eta \mathcal{G}_w \right) \phi \end{cases} \quad (2.45)$$

The expressions above agree with the ones reported by Bateman et al. (2001) (Eqs. 22a-c) and those reported by Schäffer (2008) (Eqs 3.13-3.15, with a minor difference shown by the power of " G_0 " of the second term on right hand side of Eq. 3.15, which based on the present calculation, should be "1" instead of "2"). Here though, through the definition of the Weyl operator, these expression are now valid for mild slopes.

2.5.2. WEAKLY NONLINEAR WAVE MODELLING

By consistently substituting the approximation of W into the Hamiltonian (2.39), the governing equations for η and ϕ are derived through the following canonical equations: $\partial_t \eta = \delta_\phi \mathcal{H}$ and $\partial_t \phi = -\delta_\eta \mathcal{H}$. In principle, this formulation allows model derivation of any desired order of nonlinearity. However, for practical application the first leading orders are usually sufficient. Here, the discussion focuses on wave modelling over coastal waters, for which, if dissipation is absent, the first two orders already capture the dominant physical processes. To this end, only the first two terms of the expansion for W are required. Upon a consistent substitution in (2.39), the following second-order governing equations are derived:

$$\begin{cases} \partial_t \eta = \mathcal{G}_w \phi - \mathcal{G}_w (\eta \mathcal{G}_w \phi) + D_x \cdot (\eta D_x \phi) \\ \partial_t \phi = -g \eta + \frac{1}{2} [(\mathcal{G}_w \phi)^2 + |D_x \phi|^2] \end{cases} \quad (2.46)$$

These equations allow weakly nonlinear and fully dispersive modelling of water waves over mild slopes. Such modelling capabilities provide generalization to typical formulations for coastal areas, which usually rely on the assumption of weak dispersion.

As demonstrated for the linear mild-slope model (see Appendix 2.B), also here, the relation of the present formulation with well-known classical formulations is derived through appropriate approximations of the dispersion relation applied to the symbol G . Here though, the approximations of the dispersion relation are not related to the spectrum width, but to the characteristics of the wave components, which assumed to be fairly long, and therefore, characterized by rather small values of the so-called depth parameter $\mu = |\mathbf{k}|h$. Additionally, when nonlinearity is included, it is also necessary to determine the relation between μ and ϵ . This parametric relation gives rise to a whole range of model definitions (also refer to the discussion by Madsen and Schäffer, 1998), starting from fully nonlinear and weakly dispersive (Serre-type) formulations, ranging over Boussinesq-type of formulations (which may arbitrarily defined and include formulations corresponding to the classical regime $\epsilon = O(\mu^2)$) and heading towards Whitham-type of formulations which combine full linear dispersion with weak nonlinearity described by the classical Boussinesq terms. This range defines infinitely many model formulations with different degrees of dispersion and nonlinearity. Under the limit of weak nonlinearity, the derivation of other model formulations starting from the fully dispersive model, (2.46), is demonstrated for two special and well-known examples. The first example is the well-known classical Boussinesq formulation of Peregrine (1967), constructed through the assumption that $\epsilon = O(\mu^2)$. The second example discusses the derivation of the so-called Whitham system, which is derived by assuming a regime implied by the so-called Whitham equation (Whitham, 1967) and formally defined by Moldabayev et al. (2015).

For the first example, through the assumption that $\epsilon = O(\mu^2)$, Weyl operators which operate on nonlinear terms are neglected altogether, while the Weyl operation on the linear term in the first equation of (2.46) is approximated through the following approximation of G :

$$G \sim h|\mathbf{k}|^2 \left(1 - \frac{(|\mathbf{k}|h)^2}{3} \right) \quad (2.47)$$

which through (2.17) leads to the following R symbol:

$$R \sim h|\mathbf{k}|^2 - \frac{1}{3}h^3|\mathbf{k}|^4 + (D_x h) \cdot \mathbf{k} - 2h^2(D_x h) \cdot \mathbf{k}|\mathbf{k}|^2 \quad (2.48)$$

Then, by associating back from \mathbf{k} to D_x , one obtains the following system:

$$\begin{cases} \partial_t \eta = D_x \cdot (h D_x \phi) - 2h^2 D_x h \cdot D_x |D_x|^2 \phi - \frac{1}{3} h^3 |D_x|^4 \phi + D_x \cdot (\eta D_x \phi) \\ \partial_t \phi = -g\eta + \frac{1}{2} |D_x \phi|^2 \end{cases} \quad (2.49)$$

By neglecting $O(\beta^2)$ terms, this system becomes equivalent to the classical Boussinesq system (written in terms of the horizontal velocity at the still water level) introduced by Peregrine (1967) (see Eqs. 16-17 in Peregrine's paper). For the second example, the derivation is rather straightforward. Since, as a result of its underlying scaling (see Moldabayev et al. (2015)), the Whitham system is described by the nonlinear classical Boussinesq terms and fully dispersive linear terms. Consequently, the Whitham system re-

quires no further derivation other than neglecting the nonlinear terms in (2.46) that involve Weyl operators. This results in the following set of equations:

$$\begin{cases} \partial_t \eta = \mathcal{G}_w \phi + D_{\mathbf{x}} \cdot (\eta D_{\mathbf{x}} \phi) \\ \partial_t \phi = -g\eta + \frac{1}{2} |D_{\mathbf{x}} \phi|^2 \end{cases} \quad (2.50)$$

which are found to be equivalent to those reported by Moldabayev et al. (2015), Eqs. 16-17, if the lateral dimension (with respect to y) and bottom variability are ignored. So far, bottom variations for Whitham systems were formulated using the expansion devised by Craig et al. (2005) (e.g., Aceves-Sánchez et al., 2013, Vargas-Magana and Panayotaros, 2016), which allows rapid, but small bottom variations (see also recent work by Carter et al., 2021 which compares this expansion with the non-reduced implicit expression of the topographic operator proposed by Craig et al., 2005). Consequently, (2.50) provides an alternative version of the Whitham system suited for wave prediction over two-dimensional mildly sloped bathymetries, and allows bottom variations of $O(h)$.

In summary, this discussion shows that Weyl rule of association provides a simple tool allowing a consistent model derivation of any order of nonlinearity and dispersivity over mild slopes. The starting point is the nonlinear DtN expansion which to a desired order M can be written in terms of the Weyl operator (as demonstrated by (2.45)). Then, a decision upon a relation between ϵ and μ determines the required approximation of \mathcal{G}_w for each order of nonlinearity (as demonstrated by the two examples above), which is calculated by the corresponding approximation of the symbols G and R .

2.6. CONCLUSIONS

The principle result of this study is the equivalence between a formal definition of the linear Dirichlet-to-Neumann operator for mild slopes and the Weyl operator that is associated with the linear dispersion relation of water waves. This allows formal use of the Weyl operator and the Weyl operational calculus for deterministic and stochastic applications in water waves. Within the framework of linear wave theory, the formulation of a wave field over bathymetry using the Weyl operator provides a generalized mild-slope model which does not impose a limit on the spectral width and reduces to the classical time-dependent mild-slope model as a special case (Smith and Sprinks, 1975). It is shown that this generalized linear formulation based on the Weyl operator can be rewritten as a Schrödinger-type model in terms of the complex variable ζ that is intimately related to the energy density of the wave field. This model form allows a formal derivation of the Wigner-Weyl kinetic equation for water waves, which provides a general statistical description of linear wave fields in variable media, and reduces to the well-known energy balance equation as a special case. In fact, this result provides a formal link between Euler equations and the widely used energy balance equation. As such, Weyl rule of association leads to the establishment of a formal theoretical foundation of this important transport equation, and thus, provides an alternative foundation to the traditional formulation based on the heuristic wave-particle analogy. Finally, the application of Weyl rule of association for waves of finite amplitudes is discussed as well. It is shown that the Weyl operator serves as a simple tool to derive and generalize mild-slope models of any order of nonlinearity and dispersivity. As an example, the formulation through Weyl rule

of association for the classical Boussinesq scaling leads to the well-known formulation of Peregrine (1967). Additionally, for the Whitham scaling, the formulation through Weyl rule of association provides a formal mild-slope version of the Whitham system.

2**ACKNOWLEDGEMENTS**

This work is part of the research programme Earth and Life Sciences (ALW) with project number ALWOP.167, which is (partly) financed by the Dutch Research Council (NWO).

APPENDICES

2.A. WEYL CALCULUS

This appendix summarizes the main tools required to work with the Weyl operator and its generalizations. The derivations here follow closely after the book by Leon Cohen, "The Weyl operator and its generalization" (Cohen, 2012). The starting point of this appendix is the definition of the association between the phase-space symbol $G(\mathbf{x}, \mathbf{k})$ and the pseudo-differential operator $\mathcal{G}(\mathbf{x}, D_x)$. Such an association is not uniquely defined because \mathbf{x} and D_x do not commute. However, the infinitely different possible associations can be analyzed in a unified manner through a generalization of Weyl's definition (Cohen, 2012). The generalized Weyl operator is defined as

$$\mathcal{G}_g(\mathbf{x}, D_x) = \int \hat{G}(\mathbf{q}, \mathbf{p}) \mathcal{K}(\mathbf{q}, \mathbf{p}) \exp(i\mathbf{q} \cdot \mathbf{x} + i\mathbf{p} \cdot D_x) d\mathbf{q} d\mathbf{p} \quad (2.51)$$

where $\hat{G}(\mathbf{q}, \mathbf{p})$ is the Fourier transform of $G(\mathbf{x}, \mathbf{k})$, the subscript 0_g of the operator indicates that it is a generalized operator and the kernel $\mathcal{K}(\mathbf{q}, \mathbf{p})$ defines different rules of associations. Using the Baker–Campbell–Hausdorff formula and utilizing the fact that the commutator, $[i\mathbf{q} \cdot \mathbf{x}, i\mathbf{p} \cdot D_x] = -i\mathbf{q} \cdot \mathbf{p}$, is a constant, the operator definition can be simplified as follows:

$$\mathcal{G}_g(\mathbf{x}, D_x) = \int \hat{G}(\mathbf{q}, \mathbf{p}) \mathcal{K}(\mathbf{q}, \mathbf{p}) \exp\left(\frac{i}{2} \mathbf{q} \cdot \mathbf{p}\right) \exp(i\mathbf{q} \cdot \mathbf{x}) \exp(i\mathbf{p} \cdot D_x) d\mathbf{q} d\mathbf{p} \quad (2.52)$$

The generalization expressed in the generalized operator definition amounts to the inclusion of the kernel $\mathcal{K}(\mathbf{q}, \mathbf{p})$, as can be understood by substituting $\mathcal{K}(\mathbf{q}, \mathbf{p}) = 1$, for which the original definition of the Weyl association is recovered. For the purposes of this study, besides the Weyl rule of association, the definition of the so-called Standard rule of association, for which $\mathcal{K}(\mathbf{q}, \mathbf{p}) = \exp(-i\mathbf{q} \cdot \mathbf{p}/2)$, is needed as well. Therefore, it will be easier to summarize the following definitions using the generalized operator definition.

2.A.1. ASYMPTOTIC OPERATIONAL FORM

The asymptotic operational form that follows from the operator definition (2.52) is required in order to present its operation explicitly and to extract its leading order contributions. The derivation of the asymptotic operational form depends on a Taylor expansion of the dispersion relation, and therefore (at least conceptually), should be defined around $\mathbf{k} \neq 0$, since derivatives of the dispersion relation at $\mathbf{k} = 0$ are singular. The starting point of the derivation expresses the Fourier function $\hat{G}(\mathbf{q}, \mathbf{p})$ in term of its inverse Fourier transform around \mathbf{k} as,

$$\hat{G}(\mathbf{q}, \mathbf{p}) = \int \exp(i\bar{\mathbf{k}} \cdot D_{\mathbf{k}}) \hat{G}(\mathbf{q}, \mathbf{k}) \exp(-i\mathbf{p} \cdot (\bar{\mathbf{k}} + \mathbf{k})) d\bar{\mathbf{k}} \quad (2.53)$$

where the expansion $\exp(i\bar{\mathbf{k}} \cdot D_{\mathbf{k}})\hat{G}(\mathbf{q}, \mathbf{k})$ essentially represents the shifted function $\hat{G}(\mathbf{q}, \bar{\mathbf{k}} + \mathbf{k})$. By substituting the relation (2.53) into (2.52) the following operational form is obtained:

$$\mathcal{G}_g(\mathbf{x}, D_{\mathbf{x}}) = \int \exp(i\bar{\mathbf{k}} \cdot D_{\mathbf{k}})\hat{G}(\mathbf{q}, \mathbf{k}) \exp(-i\mathbf{p} \cdot \bar{\mathbf{k}})\mathcal{K}(\mathbf{q}, \mathbf{p}) \exp(\frac{i}{2}\mathbf{q} \cdot \mathbf{p}) \exp(i\mathbf{q} \cdot \mathbf{x}) \exp(i\mathbf{p} \cdot (D_{\mathbf{x}} - \mathbf{k})) d\bar{\mathbf{k}} d\mathbf{q} d\mathbf{p} \quad (2.54)$$

which, after Fourier transform with respect to $\bar{\mathbf{k}}$, reduces to,

$$\mathcal{G}_g(\mathbf{x}, D_{\mathbf{x}}) = \int \delta(\mathbf{p}) \left[\hat{G}(\mathbf{q}, \mathbf{k}) \exp(i\mathbf{q} \cdot \mathbf{x}) \exp(i\bar{D}_{\mathbf{k}} \cdot \bar{D}_{\mathbf{p}})\mathcal{K}(\mathbf{q}, \mathbf{p}) \exp[i\mathbf{p} \cdot (D_{\mathbf{x}} - \mathbf{k} + \frac{\mathbf{q}}{2})] \right] d\mathbf{q} d\mathbf{p} \quad (2.55)$$

and eventually, leading to the following asymptotic form for the Weyl operator by setting $\mathcal{K}(\mathbf{q}, \mathbf{p}) = 1$:

$$\mathcal{G}_w(\mathbf{x}, D_{\mathbf{x}}) = \left[G(\mathbf{x}, \mathbf{k}) \exp(\frac{i}{2}\overleftarrow{D}_{\mathbf{x}} \cdot \overleftarrow{D}_{\mathbf{k}}) \exp[i\overleftarrow{D}_{\mathbf{k}} \cdot (D_{\mathbf{x}} - \mathbf{k})] \right] \quad (2.56)$$

or to the asymptotic form for the Standard operator by setting $\mathcal{K}(\mathbf{q}, \mathbf{p}) = \exp(-i\mathbf{q} \cdot \mathbf{p}/2)$:

$$\mathcal{G}_s(\mathbf{x}, D_{\mathbf{x}}) = \left[G(\mathbf{x}, \mathbf{k}) \exp[i\overleftarrow{D}_{\mathbf{k}} \cdot (D_{\mathbf{x}} - \mathbf{k})] \right] \quad (2.57)$$

where the arrows indicate the function on which the differential operator should operate, and the subscripts $(\leftarrow)_w$ and $(\leftarrow)_s$ indicate on a Weyl or a Standard operator, respectively. These expressions can be interpreted as a combination of two steps. First, define the symbol that corresponds to the operator for which all the factors $D_{\mathbf{x}}$ are placed to right of the \mathbf{x} factors, such that the former does not operate on the latter. Secondly, replace all the \mathbf{k} factors with $D_{\mathbf{x}}$. Note that the Standard rule already defines the original symbol such that the factors $D_{\mathbf{x}}$ are placed to right of the \mathbf{x} , and therefore, the first step is not included in its asymptotic form (2.57).

2.A.2. OPERATOR COMPOSITION

Operator composition is defined symbolically as follows:

$$\mathcal{A}_g(\mathbf{x}, D_{\mathbf{x}}) = (\mathcal{U}_g \circ \mathcal{L}_g)(\mathbf{x}, D_{\mathbf{x}}) \quad (2.58)$$

where \mathcal{A}_g , \mathcal{U}_g and \mathcal{L}_g are some generalized operators. A general formula of the above generalized composition can be derived by substituting in (2.58) the definition of the generalized operator (2.52) for \mathcal{U}_g and \mathcal{L}_g and by using the Baker–Campbell–Hausdorff formula. This cumbersome derivation is detailed in Cohen (2012). Here only the end result is given, written in terms of the corresponding symbols as

$$A(\mathbf{x}, \mathbf{k}) = U(\mathbf{x}, \mathbf{k}) \mathcal{J} \exp(-i\overleftarrow{D}_{\mathbf{x}} \cdot \overleftarrow{D}_{\mathbf{k}}/2 + i\overleftarrow{D}_{\mathbf{k}} \cdot \overleftarrow{D}_{\mathbf{x}}/2) L(\mathbf{x}, \mathbf{k}) \quad (2.59)$$

where \mathcal{J} is defined in terms of the kernel \mathcal{K} (see also Cohen, 2012) as

$$\mathcal{J} = \frac{\mathcal{K}(\overleftarrow{D}_x, \overleftarrow{D}_k) \mathcal{K}(\overrightarrow{D}_x, \overrightarrow{D}_k)}{\mathcal{K}(\overleftarrow{D}_x + \overrightarrow{D}_x, \overleftarrow{D}_k + \overrightarrow{D}_k)} \quad (2.60)$$

This result leads to the formulas for operator compositions (in terms of the corresponding symbols) of two Weyl operators,

$$A(\mathbf{x}, \mathbf{k}) = U(\mathbf{x}, \mathbf{k}) \exp(-i\overleftarrow{D}_x \cdot \overrightarrow{D}_k/2 + i\overleftarrow{D}_k \cdot \overrightarrow{D}_x/2) L(\mathbf{x}, \mathbf{k}) \quad (2.61)$$

or two Standard operators,

$$A(\mathbf{x}, \mathbf{k}) = U(\mathbf{x}, \mathbf{k}) \exp(i\overleftarrow{D}_k \cdot \overrightarrow{D}_x) L(\mathbf{x}, \mathbf{k}) \quad (2.62)$$

The above formulas together with the tools that were summarized in this appendix allow to significantly simplify necessary operator manipulations. In particular, under the mild-slope assumption for which $O(\beta^2)$ terms are neglected, these tools allow to define and interpret the operation of operators in a straightforward manner. In the following, several examples of operator compositions which arise in the main text are considered. The first is the mild-slope composition of two Standard operators. For this case, the formula in (2.62) provides the following approximation for $A(\mathbf{x}, \mathbf{k})$:

$$A(\mathbf{x}, \mathbf{k}) \sim U(\mathbf{x}, \mathbf{k}) (1 + i\overleftarrow{D}_k \cdot \overrightarrow{D}_x) L(\mathbf{x}, \mathbf{k}) \quad (2.63)$$

for which an approximation for $\mathcal{A}_s(\mathbf{x}, D_x)$ is obtained by associating between \mathbf{k} and D_x , recalling that all the factors D_x should be placed to right of the \mathbf{x} factors. The second example is the mild-slope composition of two Weyl operators. The composition formula for Weyl operators, (2.61), generates the following approximation for $A(\mathbf{x}, \mathbf{k})$:

$$A(\mathbf{x}, \mathbf{k}) \sim U(\mathbf{x}, \mathbf{k}) (1 - i\overleftarrow{D}_x \cdot \overrightarrow{D}_k/2 + i\overleftarrow{D}_k \cdot \overrightarrow{D}_x/2) L(\mathbf{x}, \mathbf{k}) \quad (2.64)$$

This approximation reveals the following useful mild-slope results:

$$\left\{ \begin{array}{l} (\mathcal{L}_w \circ \mathcal{L}_w)(\mathbf{x}, D_x) \leftrightarrow L^2(\mathbf{x}, \mathbf{k}) \\ (\mathcal{L}_w^{-1} \circ \mathcal{L}_w)(\mathbf{x}, D_x) \leftrightarrow 1 \end{array} \right. \quad (2.65)$$

where \leftrightarrow means "associated with" and $\mathcal{L}_w^{-1}(\mathbf{x}, D_x)$ is the Weyl operator that is associated with the symbol $L^{-1}(\mathbf{x}, \mathbf{k})$.

2.B. THE RELATION WITH THE CLASSICAL MILD-SLOPE EQUATION

The formulation of linear water waves over bathymetry, as given by (2.23)-(2.24), provides a convenient starting-point for the derivation of the Schrödinger-type model discussed in Section 2.3. Here however, it is aimed to demonstrate the relation of this linear formulation with the classical mild-slope equation, for which, a convenient starting point is the following combined form:

$$\partial_t^2 \phi + g\mathcal{G}_w \phi = 0 \quad (2.66)$$

This combined form is derived by time differentiating the second equation in the system (2.23) and substituting the first equation accordingly. This combined formulation is reduced to the classical mild-slope equation (Smith and Sprinks, 1975) provided that the following relation holds:

$$g\mathcal{G}_w\phi \sim \left[D_x \cdot (CC_g D_x) + (\sigma_0^2 - |\mathbf{k}_0|^2 CC_g) \right] \phi \quad (2.67)$$

where σ_0^2 , C_0 and $C_{g,0}$ are defined as $\sigma_0^2 = gG(\mathbf{x}, \mathbf{k}_0)$, $C_0 = \sigma/|\mathbf{k}_0|$ and $C_{g,0} = \partial_{|\mathbf{k}_0|}\sigma$, respectively.

The asymptotic equivalence written above can be understood through the fundamental assumption underlying the derivation of the classical mild-slope equation, that is, the assumption of quasi-periodic motion in time at any spatial point. Equivalently, this assumption means that the spectrum of the field is narrowly supported in the direction of $|\mathbf{k}|$ around $|\mathbf{k}_0|$. In order to see how this fundamental assumption leads to the asymptotic relation, (2.67), it may be useful to demonstrate the effective operation of a pseudo-differential operator operating on a function with narrow-banded spectrum. To this end, consider a narrow-banded wave field propagating over a constant depth. In such a case, the linear DtN relation (2.22) can be written as a simple function multiplication in wavenumber space as,

$$\mathcal{G}_w(D_x)\phi(\mathbf{x}) = \int G(\mathbf{k})\hat{\phi}(\mathbf{k})\exp(i\mathbf{k}\cdot\mathbf{x})d\mathbf{k} \quad (2.68)$$

where the Fourier transform $\hat{\phi}$ is assumed to be narrowly supported around \mathbf{k}_0 , say between $[\mathbf{k}_0 - \Delta\mathbf{k}, \mathbf{k}_0 + \Delta\mathbf{k}]$. Using the change of variable $\bar{\mathbf{k}} = \mathbf{k} - \mathbf{k}_0$, the operation of \mathcal{G}_w is effectively given by

$$\mathcal{G}_w(D_x)\phi(\mathbf{x}) = \exp(i\mathbf{k}_0\cdot\mathbf{x}) \int_{-\Delta\mathbf{k}}^{\Delta\mathbf{k}} G(\mathbf{k}_0 + \bar{\mathbf{k}})\hat{A}(\bar{\mathbf{k}})\exp(i\bar{\mathbf{k}}\cdot\mathbf{x})d\bar{\mathbf{k}} + c.c. \quad (2.69)$$

where $\hat{A}(\bar{\mathbf{k}}) = \hat{\phi}(\mathbf{k}_0 + \bar{\mathbf{k}})$ is the Fourier transform of the slowly varying complex amplitude $A(\mathbf{x})$ and *c.c.* stands for complex conjugate. This representation clearly shows that for a function with narrow spectrum the operation of \mathcal{G}_w requires only limited information of G around \mathbf{k}_0 . Consequently, G can be efficiently expanded around \mathbf{k}_0 , leading to the following representation:

$$\mathcal{G}_w(D_x)\phi(\mathbf{x}) = \exp(i\mathbf{k}_0\cdot\mathbf{x}) \left[G \exp(i\overleftarrow{D}_k \cdot \overleftarrow{D}_x) A \right]_{\mathbf{k}=\mathbf{k}_0} \quad (2.70)$$

where the arrows indicate the function on which the differential operator should operate, i.e., G or A . To summarize, this example demonstrates the interpretation of a pseudo-differential operation (e.g., \mathcal{G}_w) on a narrow-banded function. Where in the limit given by $\hat{\phi} = A\delta(\mathbf{k} - \mathbf{k}_0)$ (for which A is a constant) the operation becomes a multiplication by $G(\mathbf{k}_0)$, while for a narrow spectrum of finite width, this operation can be approximated as a polynomial in D_x , as described by (2.70).

These observations point out the expansion of G around \mathbf{k}_0 as the key to derive the approximation (2.67) that relates the Weyl operator with the operator of the classical mild-slope equation. However, in order to obtain a valuable model, the expansion of G should admit some constraints. Most important, the approximated operator should

be self adjoint and should allow wave propagation in all directions (recall that the fundamental assumption of the classical mild-slope equation does not prioritize any direction of propagation). This means that the expansion of G should preserve the symmetry characterizes the original G , and therefore, requires a symmetrical expansion, namely an expansion in terms of $|\mathbf{k}|$. Additionally, it is also beneficial to preserve the symmetrical structure of G , which means that the approximation should only consist of terms such as $|\mathbf{k}|^n$ where n is even number. This requirement avoids terms like $|D_x|$ which are difficult to interpret. Accordingly, an appropriate expansion is given as follows (Radder, 1999):

$$G(\mathbf{x}, \mathbf{k}) \sim \frac{1}{g} \left[\sigma_0^2 + C_0 C_{g,0} (|\mathbf{k}|^2 - |\mathbf{k}_0|^2) \right] \quad (2.71)$$

where $C_0 C_{g,0} / g = (\partial_{|\mathbf{k}|^2} G)_{\mathbf{k}=\mathbf{k}_0}$ and recall that $\sigma_0^2 / g = G(\mathbf{x}, \mathbf{k}_0)$. The Weyl operator of this approximation is obtained by calculating first the corresponding $R(\mathbf{x}, \mathbf{k})$ symbol using (2.17), which reads,

$$R(\mathbf{x}, \mathbf{k}) \sim \frac{1}{g} \left[\sigma_0^2 - |\mathbf{k}_0|^2 C_0 C_{g,0} + C_0 C_{g,0} |\mathbf{k}|^2 + (D_x C_0 C_{g,0}) \cdot \mathbf{k} \right] \quad (2.72)$$

then, by the subsequent back association from \mathbf{k} to D_x , the classical mild-slope operator, as given by (2.67), is derived. This result shows that the Weyl operator of the full symbol G is equivalent to the classical mild-slope operator for quasi-periodic wave fields, and implies that the Weyl formulation as given by either of the formulations, namely (2.23) or (2.66), provides a generalized mild-slope model for wave fields of arbitrary spectral width.

3

MODELLING STATISTICAL WAVE INTERFERENCES OVER SHEAR CURRENTS

Wave forecasting in ocean and coastal waters commonly relies on spectral models based on the spectral action balance equation. These models assume that different wave components are statistically independent and as a consequence cannot resolve wave interference due to statistical correlation between crossing waves, as may be found in, for instance, a focal zone. This study proposes a statistical model for the evolution of wave fields over non-uniform currents and bathymetry that retains the information on the correlation between different wave components. To this end, the quasi-coherent model (Smit and Janssen, 2013) is extended to allow for wave-current interactions. The outcome is a generalized action balance model that predicts the evolution of the wave statistics over variable media, while preserving the effect of wave interferences. Two classical examples of wave-current interaction are considered to demonstrate the statistical contribution of wave interferences: 1) swell field propagation over a jet-like current, and 2) the interaction of swell waves with a vortex-ring. In both examples cross-correlation terms lead to development of prominent interference structures, that significantly change the wave statistics. Comparison with results of the SWAN model demonstrates that retention of cross-correlation terms is essential for accurate prediction of wave statistics in a shear-current induced focal zones.

This chapter has been published as: Akrish, G., Smit, P., Zijlema, M., & Reniers, A. (2020). Modelling statistical wave interferences over shear currents. *J. Fluid Mech.*, 891.

3.1. INTRODUCTION

Wind-generated waves play an important role in the dynamics of oceanic and coastal waters. In the upper ocean, surface waves can force large scale circulations (e.g., Craik and Leibovich, 1976), whereas nearshore, they can drive alongshore currents (e.g., Longuet-Higgins, 1970, Bowen, 1969, Ruessink et al., 2001, Reniers and Battjes, 1997), return flow (e.g., Dyhr-Nielsen and Sørensen, 1970, Stive and De Vriend, 1994) and associated sediment transport processes (e.g., Van Rijn, 1993, Fredsoe and Deigaard, 1992). Furthermore, waves control shipping operations and associated downtime as well as coastal safety through beach and dune erosion and potential inundation (e.g., Vellinga, 1982, Roelvink et al., 2009).

The common approach of predicting statistical parameters of wind waves is via operational (phase-averaged) wave models (e.g. WAM model, WAMDI Group, 1988, WAVE-WATCH model, Tolman, 1991, SWAN model, Booij et al., 1999). These models solve numerically the so-called spectral action balance equation that can be written in the following form:

$$\partial_t N + \nabla_{\mathbf{x}} \cdot (\mathbf{C}_x N) + \nabla_{\mathbf{k}} \cdot (\mathbf{C}_k N) = S \quad (3.1)$$

where N represents the spectrum of the action density, being equal to the spectrum of the energy density, E , divided by the intrinsic frequency, σ . The propagation part, on the left hand side, describes the kinematical behavior of the field as it propagates through slowly varying current, \mathbf{U} , and bathymetry, with propagation velocities \mathbf{C}_k and \mathbf{C}_x over wavenumber space, $\mathbf{k} = (k_1, k_2)$, and physical space, $\mathbf{x} = (x_1, x_2)$, respectively. On the right hand side, the equation is forced by source terms, S , to account for processes of wave generation (by wind), dissipation (e.g., due to whitecapping) and wave-wave interactions.

The statistical assumptions underlying the derivation of (3.1) are that the wave field can be regarded as Gaussian and quasi-homogeneous. The former suggests that the field is completely defined by its correlation function (assuming a zero-mean field), while the latter proposes that the correlation between any two distinct wave components equals zero. Based on these assumptions, variation of the field's statistics is governed completely by variations of the waves' variances (which are represented by N), as indeed described by (3.1).

In most circumstances at sea, the parameters of the wave field (e.g. wave amplitudes) are evolving slowly over spatial scales of $O(10\text{km} - 100\text{km})$ due to the action of wind, slow medium changes and weak nonlinearity. Under these conditions, the assumption of quasi-homogeneity is easily met, and (3.1) remains valid. However, there might be situations where the field encounters medium variability over much smaller scales ($O(100\text{m} - 1\text{km})$). Such situations can occur quite frequently in coastal regions, where currents and bathymetry can vary rapidly (e.g., Chen et al., 1999, Ardhuin et al., 2003). Furthermore, following recent studies (e.g., Poje et al., 2014, McWilliams, 2016), they may also occur in the open ocean over small-scale currents (e.g., submesoscale currents). Physically, in these situations, waves are rapidly scattered into multiple directions, and consequently, can form focal zones which give rise to wave interferences. A well-known examples of such wave-media interactions are given by the evolution of waves over a submerge shoal

(e.g., Vincent and Briggs, 1989) or over a vortex-ring (e.g., Yoon and Liu, 1989). Statistically, the interference effects that arise in such cases are described by cross-correlations between different wave components of the scattered field and may result in significant and rapid variations of the wave statistics (Janssen et al., 2008, Smit and Janssen, 2013, Smit et al., 2015a). The quasi-homogeneous assumption excludes the contribution of the cross-correlation terms, and therefore, (3.1) cannot describe the effect of wave interferences arising in interactions between waves and rapidly varying media.

The ability to account for the effect of wave interferences in these situations is important, since they can alter dramatically the spatial distributions of wave parameters (e.g., the significant wave height), which serve as input for numerous applications in the coastal zones. In addition, through the interaction of waves with small-scale ocean currents, generated interference structures may also introduce leading-order statistical contributions for applications in the open ocean. For example, they may contribute to changes driven by waves of submesoscale currents (McWilliams, 2018), or the interpretation of noise obtained (due to the presence of waves) in measurements of the sea surface, revealing the evolution of small-scale circulations (e.g., Ardhuin et al., 2017), and they may also enhance and alter the spatial distribution of extreme elevations in energetic focal regions (e.g., Metzger et al., 2014, Fedele et al., 2016).

In order to take into account the statistical effect of wave interference, Smit and Janssen (2013) and Smit et al. (2015a) have recently developed an evolution equation that allows for the generation and evolution of correlations between different wave components when interacting over small scale bathymetry changes. This newly developed stochastic model is called the quasi-coherent model (QCM). The main aim of the present study is to extend the capabilities of the QCM so it can handle the interaction between waves and ambient currents. The derivation of the extended QCM is detailed in 3.2. The model is verified in 3.3 through the problem of interaction between swell field and a jet-like current (e.g., Janssen and Herbers, 2009). Then, the model is used to study the statistical mechanism for the generation of wave interferences in Section 3.4, through the classical problem of interaction between swell waves and a vortex-ring (e.g., Yoon and Liu, 1989). Finally, conclusions are drawn in Section 3.5.

3.2. STOCHASTIC MODEL FOR LINEAR WAVES OVER VARYING CURRENT AND BATHYMETRY

Generally speaking, stochastic wave models are derived based on deterministic equations that physically describe the evolution of wave fields. This approach of deriving a stochastic formulation is also adopted here. Therefore, the derivation starts with a physical description of the wave field which is effectively represented by the so-called action variable. Subsection 3.2.1 introduces the definition of the action variable and its governing equation. As discussed in Subsection 3.2.2, the second-order statistics of the wave field, including the statistics of wave interferences, is fully described through the correlation function or the spectral distribution function of the action variable. These starting points are used in Subsection 3.2.3 to formulate a stochastic model that takes into account the generation and transportation of wave interference contributions. Finally, the numerical implementation of the model and an overview of the considered simulations

are described in Subsection 3.2.4 and Subsection 3.2.5, respectively.

3.2.1. THE ACTION VARIABLE AND ITS EVOLUTION EQUATION

The formulation starts by considering the evolution of a random linear wave field through a variable medium that can be represented by its surface potential and surface elevation, $\phi(\mathbf{x}, t)$ and $\eta(\mathbf{x}, t)$. It is assumed that the medium changes slowly so that the ratio, $\epsilon = L/L_m$, between the characteristic wave length, L , and the characteristic length scale of medium variation, L_m , is small ($\epsilon \ll 1$). Accordingly, the field can locally be approximated as a summation of plane waves with slowly varying phase and amplitude, which to the leading order in ϵ , obey to the following general dispersion relation (e.g., Dingemans, 1997):

$$\omega = \mathbf{U} \cdot \mathbf{k} + \sigma \quad (3.2)$$

Variations in the medium are introduced by the ambient current, $\mathbf{U}(\mathbf{x})$ and by the water depth, $h(\mathbf{x})$. Using the medium information and the definition of the intrinsic frequency, $\sigma(\mathbf{x}, \mathbf{k}) = \sqrt{|\mathbf{k}|g \tanh(|\mathbf{k}|h)}$, the value of the absolute frequency, ω , is obtained through (3.2), where, $|\mathbf{k}|$ stands for the magnitude of the local wavenumber, defined as $|\mathbf{k}| = \sqrt{k_1^2 + k_2^2}$, and g is the gravitational acceleration. Finally, from the statistical point of view, the field is assumed to be zero-mean, Gaussian and quasi-stationary.

Under this statistical and physical framework, it will be convenient to use the so-called action variable (e.g., Besieris and Tappert, 1976; Krasitskii, 1994), ψ , which is defined as,

$$\psi = \frac{1}{\sqrt{2g}} [g \mathcal{A}^{-1} \eta + i \mathcal{A} \phi] \quad (3.3)$$

where $\mathcal{A}(\mathbf{x}, -i\nabla_{\mathbf{x}})$ is a pseudo-differential operator that is associated with the symbol $a(\mathbf{x}, \mathbf{k}) = \sqrt{\sigma(\mathbf{x}, \mathbf{k})}$ (see detailed definition of this operator in Appendix A).

The convenience of working with the action variable, ψ , becomes significant in the formulation of the second-order statistics of the field. As, through its definition, (3.3), second-order statistical functions of ψ (e.g., the correlation function) are inherently related to the definition of the wave action (Bretherton and Garrett, 1968). As a consequence, the action variable, ψ , is intimately related to the mean action density and the mean energy density through the following expressions:

$$\rho \langle |\psi|^2 \rangle = m_0 / \Sigma + O(\epsilon) \quad (3.4)$$

$$\rho \langle |\mathcal{A}\psi|^2 \rangle = m_0 + O(\epsilon) \quad (3.5)$$

where, ρ is the water mass density, and the angular parentheses, $\langle \dots \rangle$, should be read as ensemble average. The variable m_0 provides a leading order estimation (in ϵ) of the mean energy density (also known as the zero order moment of the spectral energy density) and it is defined as follows:

$$m_0 = \rho \left\langle \frac{1}{2} g \eta_0^2 + \frac{1}{2g} (\Sigma \phi)_0^2 \right\rangle \quad (3.6)$$

where now (in (3.4) and (3.6)) $\Sigma(\mathbf{x}, -i\nabla_{\mathbf{x}})$ represents a pseudo-differential operator that is associated with the intrinsic frequency, $\sigma(\mathbf{x}, \mathbf{k})$, and the subscript 0 indicates on $O(1)$ terms (refer to Appendix A for the definition of $\Sigma(\mathbf{x}, -i\nabla_{\mathbf{x}})$ and its leading order operation, e.g., $(\Sigma\phi)_0$). Further details explaining why the expression in (3.6) defines the leading order estimation of the mean energy density are given in Appendix B.

An additional motivation for the definition of ψ , (3.3), is that, under the physical assumptions made here, the governing equation of the wave field, can be written as (Besieris and Tappert, 1976, Besieris, 1985)

$$\partial_t \psi = -i\Omega(\mathbf{x}, -i\nabla_{\mathbf{x}})\psi \quad (3.7)$$

where, $\Omega(\mathbf{x}, -i\nabla_{\mathbf{x}})$ is a pseudo-differential operator that is associated with the dispersion relation, $\omega(\mathbf{x}, \mathbf{k})$ (see Appendix A). This equation form is convenient since it can be transformed directly into an evolution equation of the correlation function, which under the assumption of Gaussian statistics, provides a complete statistical description of the wave field. A verification of this equation for homogeneous and weakly inhomogeneous media is described in Appendix B. For homogeneous media, (3.7) exactly describes the evolution of the considered linear field. For weakly inhomogeneous media, the governing equation, (3.7), reduces for each wave component to the local dispersion relation, (3.2) (or the eikonal equation, which governs the evolution of the wavenumber) at the leading order, and the well-known transport equation for the mean action density, $\langle |\psi|^2 \rangle$ at $O(\epsilon)$. This indicates that at $O(\epsilon)$, (3.7) provides the correct representation of the field's evolution.

To summarize, the formulation presented here considers a random, linear, and slowly varying wave field, which is concisely represented by the action variable, ψ . The definition of this action variable introduces convenient properties which will eventually lead to a derivation of a generalized action balance equation that accounts for the effect of wave interferences. As a first step in this path, the next subsection aims to demonstrate that the statistical information about wave interferences is naturally included in the representative second-order statistical functions (i.e., the correlation function and the Wigner distribution).

3.2.2. SECOND-ORDER STATISTICS

Following the statistical assumptions for the surface variables, η and ϕ , and following the linearity of the definition (3.3), the action variable $\psi(\mathbf{x}, t)$ is said to be a zero-mean, complex Gaussian and quasi-stationary field (e.g., Soong, 1973). The statistics of such a random field are defined completely by the following correlation function:

$$\Gamma(\mathbf{x}, \mathbf{x}', t) = \langle \psi(\mathbf{x} + \mathbf{x}'/2, t) \psi^*(\mathbf{x} - \mathbf{x}'/2, t) \rangle \quad (3.8)$$

The statistical information carried by the correlation function is better seen using its spectral form, written as,

$$\Gamma(\mathbf{x}, \mathbf{x}', t) = \int d\mathbf{k} \exp(i\mathbf{k} \cdot \mathbf{x}') \int \hat{\Gamma}(\mathbf{k}, \mathbf{k}', t) \exp(i\mathbf{k}' \cdot \mathbf{x}) d\mathbf{k}' \quad (3.9)$$

where, \mathbf{k} and \mathbf{k}' are defined as the average and difference of two interacting wavenumbers, namely, $\mathbf{k} = (\mathbf{k}_1 + \mathbf{k}_2)/2$ and $\mathbf{k}' = \mathbf{k}_1 - \mathbf{k}_2$. In addition $\hat{\Gamma}(\mathbf{k}, \mathbf{k}', t)$ is defined as,

$\hat{\Gamma}(\mathbf{k}, \mathbf{k}', t) = \langle \hat{\psi}(\mathbf{k} + \mathbf{k}'/2, t) \hat{\psi}^*(\mathbf{k} - \mathbf{k}'/2, t) \rangle$. The expression above reveals the spectral content of the correlation function. It shows that in general, Γ oscillates with a wavenumber difference \mathbf{k}' over the space \mathbf{x} . Such an oscillation occurs when wave components with two different wavenumber are statistically correlated, and thus, creating a spatial dependent pattern of wave interference.

The assumption that the wave field is quasi-homogeneous trims the spectral information provided by $\hat{\Gamma}$ with respect to \mathbf{k}' and accounts only for a narrow window around $\mathbf{k}' = 0$, which consists of the components that characterize the slow changes of the medium. Therefore, under this assumption, the spectrum obtained by the Fourier transform of Γ from \mathbf{x}' to \mathbf{k} only allows for slow variations of the variance terms of the field. This spectrum is the conventional action density spectrum, $N(\mathbf{x}, \mathbf{k}, t)$. In this study, however, statistical inhomogeneity of the wave field is taken into account by considering the full spectrum provided by $\hat{\Gamma}$ with respect to \mathbf{k}' . In this general case, the corresponding spectral representation of wave action follows the definition of the Wigner distribution, $\mathcal{W}(\mathbf{x}, \mathbf{k}, t)$:

$$\mathcal{W}(\mathbf{x}, \mathbf{k}, t) = \int \Gamma(\mathbf{x}, \mathbf{x}', t) \exp(-i\mathbf{k} \cdot \mathbf{x}') d\mathbf{x}' \quad (3.10)$$

Therefore, the Wigner distribution of ψ captures the same information as the correlation function and basically generalizes the concept of the action density spectrum by including the cross-correlation terms that correspond to wave interferences (also see, e.g., Hlawatsch and Flandrin, 1997). As such, the Wigner distribution provides a complete spectral description of the second order statistics of the field. Finally note that, as implied by (3.10), the zero-order moment of \mathcal{W} equals to the variance of ψ , and therefore, following (3.4) gives a leading order evaluation of the mean action density.

Practically speaking, one would eventually be interested in certain field parameters (e.g., characteristic wave height and period) for engineering applications. These parameters are commonly estimated based on the spectral moments of the energy density (Rice, 1945). Most importantly is the zero-order moment, m_0 , which is used to estimate ,e.g., the so-called "significant wave height", H_s (defined as the mean height of the highest one-third of the waves in the field) through the following formula:

$$H_s(\mathbf{x}, t) = 4\sqrt{m'_0} \quad (3.11)$$

where $m'_0 = m_0/(\rho g)$. Therefore, in order to estimate H_s using (3.11) one is required to calculate the transformation from the spectral representation of the action density to m_0 . Using the conventional spectrum of the action density, $N(\mathbf{x}, \mathbf{k}, t)$, m_0 is easily obtained as

$$m_0 = \rho \int \sigma(\mathbf{x}, \mathbf{k}) N(\mathbf{x}, \mathbf{k}, t) d\mathbf{k} \quad (3.12)$$

However, if cross-correlation terms are taken into account, (3.12) is no longer adequate since the cross terms at (\mathbf{x}, \mathbf{k}) should not be multiplied by $\sigma(\mathbf{x}, \mathbf{k})$. In order to multiply each term stored at (\mathbf{x}, \mathbf{k}) by the correct factor, one must distinguish between the variance term and the cross-correlation terms. Therefore, for cases where cross-correlation terms (e.g., interference terms) are important, a direct substitution of $\mathcal{W}(\mathbf{x}, \mathbf{k}, t)$ instead

of $N(\mathbf{x}, \mathbf{k}, t)$ in (3.12) would be inaccurate. A modified formula to calculate m_0 based on $\mathcal{W}(\mathbf{x}, \mathbf{k}, t)$ is given as follows:

$$m_0 = \rho \int \int \sqrt{\sigma(\mathbf{x}, \mathbf{k} + \mathbf{k}'/2)} \sqrt{\sigma(\mathbf{x}, \mathbf{k} - \mathbf{k}'/2)} \hat{\Gamma}(\mathbf{k}', \mathbf{k}, t) \exp(i\mathbf{k}' \cdot \mathbf{x}) d\mathbf{k}' d\mathbf{k} \quad (3.13)$$

where,

$$\hat{\Gamma}(\mathbf{k}, \mathbf{k}', t) = \int \mathcal{W}(\mathbf{x}, \mathbf{k}, t) \exp(-i\mathbf{k}' \cdot \mathbf{x}) d\mathbf{x} \quad (3.14)$$

Appendix C details on the derivation of (3.13) and also provides a simple example that explains why the cross-correlation terms should be scaled differently.

To conclude, the Wigner distribution, \mathcal{W} , of the action variable, ψ , generalizes the concept of the action density spectrum (i.e., N), by including the cross-correlation terms that correspond to wave interferences. Once \mathcal{W} is known, local field parameters (e.g., H_s) can be derived and used for practical applications. The last step of the formulation should therefore devoted to the derivation of a stochastic model for computing the evolution of \mathcal{W} .

3.2.3. EVOLUTION EQUATION FOR THE WIGNER DISTRIBUTION

The procedure to derive the evolution equation for \mathcal{W} is analogous to the procedure presented in Smit and Janssen (2013) and Smit et al. (2015a), and is briefly presented below. Starting with the governing equation of the action variable, (3.7), the evolution equation for the correlation function is derived (see e.g., Papoulis, 1965) by noting first that,

$$\partial_t \Gamma(\mathbf{x}_1, \mathbf{x}_2, t) = \langle \psi^*(\mathbf{x}_2, t) \partial_t \psi(\mathbf{x}_1, t) + \psi(\mathbf{x}_1, t) \partial_t \psi^*(\mathbf{x}_2, t) \rangle \quad (3.15)$$

then, by substituting the governing equation of ψ into the above equation, and using the variable transformation, $\mathbf{x}_1 = \mathbf{x} + \mathbf{x}'/2$ and $\mathbf{x}_2 = \mathbf{x} - \mathbf{x}'/2$, one obtains,

$$\partial_t \Gamma(\mathbf{x}, \mathbf{x}', t) = -i[\Omega(\mathbf{x} + \mathbf{x}'/2, -i\nabla_{\mathbf{x}'} - i\nabla_{\mathbf{x}}/2) - \Omega(\mathbf{x} - \mathbf{x}'/2, -i\nabla_{\mathbf{x}'} + i\nabla_{\mathbf{x}}/2)]\Gamma(\mathbf{x}, \mathbf{x}', t) \quad (3.16)$$

The corresponding evolution equation for the Wigner distribution is derived through the Fourier transformation, (3.10), and associating the factor \mathbf{x}' with $i\nabla_{\mathbf{k}}$ and the operator $-i\nabla_{\mathbf{x}}$ with \mathbf{k} , as,

$$\partial_t \mathcal{W}(\mathbf{x}, \mathbf{k}, t) = -i\Omega(\mathbf{x} + i\nabla_{\mathbf{k}}/2, \mathbf{k} - i\nabla_{\mathbf{x}}/2)\mathcal{W}(\mathbf{x}, \mathbf{k}, t) + c.c. \quad (3.17)$$

where $c.c.$ stands for complex conjugate. For the purpose of interpreting the operation Ω upon \mathcal{W} , (3.17) is written in the following, more explicit, form (see details in Appendix D):

$$\partial_t \mathcal{W}(\mathbf{x}, \mathbf{k}, t) = -i\omega(\mathbf{x}, \mathbf{k}) \exp[i\vec{\nabla}_{\mathbf{x}} \cdot \vec{\nabla}_{\mathbf{k}}/2 - i\vec{\nabla}_{\mathbf{k}} \cdot \vec{\nabla}_{\mathbf{x}}/2]\mathcal{W}(\mathbf{x}, \mathbf{k}, t) + c.c. \quad (3.18)$$

where the arrows indicate the function on which the differential operator should operate, i.e., ω or \mathcal{W} .

Formally, equation (3.18) defines the evolution of \mathcal{W} . Smit and Janssen (2013) showed that essentially two parameters, β and μ , governing the order of approximation introduced by a truncated version of the exponential operator in (3.18). The parameter β arises due to the operation of the first term in the exponential operator (i.e., $\nabla_{\mathbf{x}} \cdot \nabla_{\mathbf{k}}/2$), and it represents the ratio between the correlation length scale L_c and the medium variation scale L_m , namely, $\beta = L_c/L_m$. The parameter μ arises due to the operation of the second term in the exponential operator (i.e., $\nabla_{\mathbf{k}} \cdot \nabla_{\mathbf{x}}/2$) and it is equal to the ratio between the wave length L , that corresponds to \mathbf{k} and the characteristic length scale of the interference structures stored in \mathbf{k} , L_W , i.e., $\mu = L/L_W$. Accordingly, Taylor expansion may applied to define the operator in (3.17) by requiring that both, $\beta \ll 1$ and $\mu \ll 1$. Under these conditions, the general evolution equation, (3.17), can be approximated to $O(\beta, \mu)$ by:

$$\partial_t \mathcal{W} + \nabla_{\mathbf{k}} \omega \cdot \nabla_{\mathbf{x}} \mathcal{W} - \nabla_{\mathbf{x}} \omega \cdot \nabla_{\mathbf{k}} \mathcal{W} = 0 \quad (3.19)$$

which is exactly the transport equation being employed in most commonly used third-generation spectral wave models (e.g. SWAN). Therefore, the conventional transport equation, (3.19), is only valid for certain sea conditions for which β and μ are small.

Assuming that the incident wave field is statistically homogeneous, Smit and Janssen (2013) demonstrated that generated cross-correlations (and therefore, wave interferences) may have an important contribution for cases where the variation scale of the medium is at the same order or smaller than the scale of the correlation length, namely, for cases in which $\beta \geq O(1)$. Obviously, for such cases, the interpretation of the operator in (3.17) using a Taylor expansion is no longer valid. Alternatively, the operator can be partially defined using a Fourier integral (Smit and Janssen, 2013), leading to an integro-differential form, which remains valid also for cases in which $\beta \geq O(1)$, but retains the assumption of weak spatial variability of the field's statistics ($\mu \ll 1$). This form of the operator is defined as (see Appendix D for details),

$$\Omega(\mathbf{x} + i\nabla_{\mathbf{k}}/2, \mathbf{k} - i\nabla_{\mathbf{x}}/2) \mathcal{W}(\mathbf{x}, \mathbf{k}, t) = \int \hat{\omega}(\mathbf{q}, \mathbf{k}, \mathbf{x}) (1 - i\vec{\nabla}_{\mathbf{k}} \cdot \vec{\nabla}_{\mathbf{x}}/2) \mathcal{W}(\mathbf{x}, \mathbf{k} - \mathbf{q}/2, t) d\mathbf{q} \quad (3.20)$$

where, $\hat{\omega}(\mathbf{q}, \mathbf{k}, \mathbf{x})$ is the Fourier transform of the dispersion relation around the point \mathbf{x} . Additionally, the part of the operator that results in the common transport terms of (3.19), can be extracted out of the integral in (3.20) (see Smit et al., 2015a). However, for cases in which $\beta \geq O(1)$, it will be convenient to extract only the spatial transport term ($\nabla_{\mathbf{k}} \omega \cdot \nabla_{\mathbf{x}} \mathcal{W}$) and to leave the refraction term ($\nabla_{\mathbf{x}} \omega \cdot \nabla_{\mathbf{k}} \mathcal{W}$) inside the integral. This is because such cases involve relatively rapid variations in the medium and also narrow spectrum, and therefore, require not only high resolution in the spatial space, but also high resolution in the spectral space. Leaving the refraction term inside the integral eliminates the need to evaluate the derivative of \mathcal{W} with respect to \mathbf{k} , and thus, prevents excessive resolution in the spectral space. As a consequence, the integral of (3.20) can be computed much more efficiently. To this end, the local value of the dispersion relation at the point \mathbf{x} is subtracted from the original dispersion relation and the remainder is

defined as: $\Delta\omega(\mathbf{x} + \bar{\mathbf{x}}, \mathbf{k}) = \omega(\mathbf{x} + \bar{\mathbf{x}}, \mathbf{k}) - \omega(\mathbf{x}, \mathbf{k})$ (where, due to computational considerations, $\bar{\mathbf{x}}$ is defined as $\bar{\mathbf{x}} = \mathbf{x}'/2$, see details in Appendix E). With this decomposition, the evolution equation can be rewritten as,

$$\partial_t \mathcal{W} + \nabla_{\mathbf{k}} \omega \cdot \nabla_{\mathbf{x}} \mathcal{W} = S_{QC} \quad (3.21)$$

where, S_{QC} , is a scattering source term that takes into account the statistical effects of wave refraction and interference induced by medium variations. The expression that defines this source term is given by,

$$S_{QC} = -i \int \Delta\hat{\omega}(\mathbf{q}, \mathbf{k}, \mathbf{x}) (1 - i \bar{\nabla}_{\mathbf{k}} \cdot \bar{\nabla}_{\mathbf{x}/2}) \mathcal{W}(\mathbf{x}, \mathbf{k} - \mathbf{q}/2, t) d\mathbf{q} \\ + i \int \Delta\hat{\omega}(\mathbf{q}, \mathbf{k}, \mathbf{x}) (1 + i \bar{\nabla}_{\mathbf{k}} \cdot \bar{\nabla}_{\mathbf{x}/2}) \mathcal{W}(\mathbf{x}, \mathbf{k} + \mathbf{q}/2, t) d\mathbf{q} \quad (3.22)$$

Note that the letters QC , which indicate this source term, stand for "quasi-coherent" approximation (Smit and Janssen, 2013). The notion "quasi-coherent" refers to the assumption that $\mu \ll 1$. Assuming that μ is small, the model can accurately resolve only the interference patterns with spatial variation, L_W , larger than the length of the considered wave, L .

The transport equation of \mathcal{W} , (3.21), provides a generalization of the conventional transport model (3.19), by allowing statistical interferences to be generated due to the interaction of the wave field with variable bathymetry and currents. In that sense, (3.21) can be seen as a generalized action balance equation. In the following, the numerical implementation of (3.21) is discussed.

3.2.4. NUMERICAL IMPLEMENTATION

The numerical implementation of (3.21) is confined to steady-state solutions, for which spatial and spectral discretizations are required. A detailed explanation on the discretization process and how S_{QC} is implemented numerically is given in Appendix E. The discretization process results in a coupled system of algebraic equations that is characterized by a matrix of size $N_{x1} N_{x2} N_{k1} N_{k2} \times N_{x1} N_{x2} N_{k1} N_{k2}$, where N_j is the number of grid points in the direction j . As a consequence of the implicit approach adopted here, where the spatial derivatives and the terms that construct S_{QC} are evaluated at the same spatial point, the coupled system of algebraic equations must be solved iteratively. This is performed using the Gauss–Seidel method, where the rows of the matrix are arranged in accordance with the sweeping approach as detailed in Zijlema and van der Westhuisen (2005). Once a steady-state solution of \mathcal{W} is reached, the evaluation of m_0 which is required for the estimation of certain statistical field parameters, is computed through (3.52) (see Appendix C for details). The next subsection describes the numerical simulations which are considered in this study.

3.2.5. SETUP AND OVERVIEW OF THE CONSIDERED NUMERICAL SIMULATIONS

Two classical examples of wave-current interactions are considered. The first concerns the evolution of an incoming wave field over jet-like current. This example is used to

verify the model in Section 3.3. In the second example, the field interacts with a vortex-ring current. This example is used in Section 3.4 to study the statistical condition for the effect of wave interferences to appear. A visual description of the spatial variation of the considered current fields is presented by the arrows in Fig. 3.4 for the jet-like current and in Fig. 3.4 for the vortex-ring. Mathematically, these current fields are defined as follows. The jet is defined as,

$$\begin{cases} \mathbf{U}(x_1, x_2) = [U_{x_1}, 0] \\ U_{x_1} = C_1 f \left[\tanh[(x_2 + R)/(C_2 R)] - \tanh[(x_2 - R)/(C_2 R)] \right] \\ f = 1 + \tanh[(x_1 - R)/(C_2 R)] \end{cases} \quad (3.23)$$

where, $R = 200\text{m}$, $C_1 = -0.1\text{m/s}$ and $C_2 = 0.5$. In this case, the maximum opposing current value is $|U_{x_1}|_{max} = 0.38\text{m/s}$. Using cylindrical coordinates, the definition of the vortex-ring is given by (Mapp et al., 1985):

$$\begin{cases} \mathbf{U}(r, \theta) = [0, U_\theta] \\ U_\theta = \begin{cases} C_1 (r/R_1)^2, & r \leq R_1 \\ C_2 \exp[-(R_2 - r)^2/R_3^2], & r \geq R_1 \end{cases} \end{cases} \quad (3.24)$$

for which the values of R_1 , R_2 , R_3 , C_1 and C_2 , were chosen identical to those detailed in Belibassakis et al. (2011). In this case, the maximum current value is $|U_\theta|_{max} = 1.00\text{m/s}$.

Both of these examples are formulated over a spatial domain of $4000\text{m} \times 4000\text{m}$ and a constant depth of $h = 10\text{m}$. Waves entering the domain along the left boundary, on $x_1 = 0$. This is simulated by prescribing an incoming energy density, $E_0 = E(x_1 = 0, x_2, k_1, k_2)$. Note that, as the incoming wave field is assumed to be statistically homogeneous, the corresponding boundary condition of the Wigner distribution is readily obtained as follows: $W_0 = E_0/\sigma$. Finally, note that the lateral boundaries are treated as periodic.

Table 3.1: An overview of the considered simulations in terms of their physical, statistical and numerical parameters.

<i>Sim.</i>	H_{s0} (m)	T_0 (s)	θ_0 ($^\circ$)	$S_d^{(k)}$ (1/m)	$S_d^{(f)}$ (Hz)	$S_d^{(\theta)}$ ($^\circ$)	α	L_c (km)	β
Jet ₁	1	20	15	0.001	0.0015	1.78	1	4	$\beta \geq O(1)$
Jet ₂	1	20	15	0.005	0.0074	8.99	2	0.8	$\beta = O(1)$
Ring ₁	1	20	0	0.001	0.0015	1.78	1	4	$\beta \geq O(1)$
Ring ₂	1	20	0	0.002	0.003	3.56	1	2	$\beta = O(1)$
Ring ₃	1	20	0	0.005	0.0074	8.99	2	0.8	$\beta = O(1)$

An overview of the simulations considered in this study is given in Table 3.1. These simulations differ by the current type (indicated by the name of the simulation in the first column of the table), and by the parameters characterizing the incoming spectrum, E_0 . In all the simulations the incoming spectrum, E_0 , is defined as a 2d Gaussian centered around \mathbf{k}_0 . The incoming spectrum is therefore defined completely by the significant wave height, H_{s0} , the carrier wave period and direction, T_0 and θ_0 (which provide the center point \mathbf{k}_0 through the linear dispersion relation) and by the standard deviation, $S_d^{(k)}$, which are given in the second, third, fourth and fifth column of Table 3.1, respectively. In order to give a more intuitive physical interpretation of the width of the spec-

trum, the table also provides the corresponding standard deviations of the transformed spectrum written in terms of frequency and direction, $S_d^{(f)}$ and $S_d^{(\theta)}$, given in the sixth and seventh column. Numerically, E_0 is represented over the grid, N_k , with a resolution that is determined by $S_d^{(k)}$ and the resolution parameter, α (see Appendix E) given in the ninth column. The value of Δx , on the other hand, cannot be deduced from the table above. Appendix E guides how to choose a reasonable value for Δx . This value is fixed to $\Delta x = 25 \text{ m}$ for all the simulations. In addition, the table also provides the correlation length, L_c and the statistical parameter, β in the tenth and eleventh column. As outlined in Appendix E, L_c is evaluated using $S_d^{(k)}$. This can also be expected by the scaling property of the Fourier transform ($O(L_c) = O(2/S_d^{(k)})$). Throughout the analysis of the results in the following subsections, the value of L_c (as opposed to the value taken into account in the numerical model, see Appendix E) is defined as $L_c = 4/S_d^{(k)}$. For the considered Gaussian initial distribution, this value equals to the so-called $1/e^2$ width that provides the diameter connecting the two points with $1/e^2$ times the maximum value of the correlation function. Finally, the order of magnitude of β is obtained following its definition, $\beta = L_c/L_m$.

3.3. MODEL VERIFICATION

The main aim of this section is to verify the performance of the QCM. The model is verified through a comparison with REF/DIF 1 (Kirby and Dalrymple, 1986), which solves a parabolic approximation of the well-known mild-slope equation (e.g., Dingemans, 1997). Since REF/DIF 1 allows for monochromatic, uni-directional forcing at the incident boundary, statistics for multi-directional and irregular incident waves are constructed by superposition of variances, under the assumption that waves at the incident boundary are statistically independent (see details in Chawla et al., 1998). Additionally, to demonstrate the statistical contribution of the interference terms, the results of QCM are also compared to the results of the SWAN model (Booij et al., 1999). To this end, the first two simulations detailed in Table 3.1, namely Jet₁ and Jet₂, are considered.

The simulations Jet₁ and Jet₂ describe the evolution of waves over the jet-like current field. Ray tracing results (Fig. 3.1) show that for this jet-like current the waves refract and form a focal zone close to $x_1 = 2000 \text{ m}$ beyond which, interference structures may emerge.

The physical pattern described by the rays in Fig. 3.1 is also reflected statistically in the results of Fig. 3.2 and Fig. 3.3. While the results of QCM and of REF/DIF 1 agree well and share a similar evolution pattern before and after the crossing zone in both of the simulations, the SWAN results increasingly deviate beyond the crossing zone, where interference effects emerge (see upper panels in Fig. 3.2 and Fig. 3.3) (note that the small differences that arise at the lateral boundaries, as for instance appear in the results of Section B in Fig. 3.3, are due to different boundary conditions assumed in each of the models). The results also show that interference effects are not confined to caustic regions (where geometric optics break down) but rather, spread over much greater distances in the down-wave direction, beyond the crossing zone (e.g., upper panels of Fig. 3.2). The differences between the models are less pronounced in the results of simulation Jet₂ which is initiated using a broader spectrum (see lower panels in Fig. 3.2 and Fig.

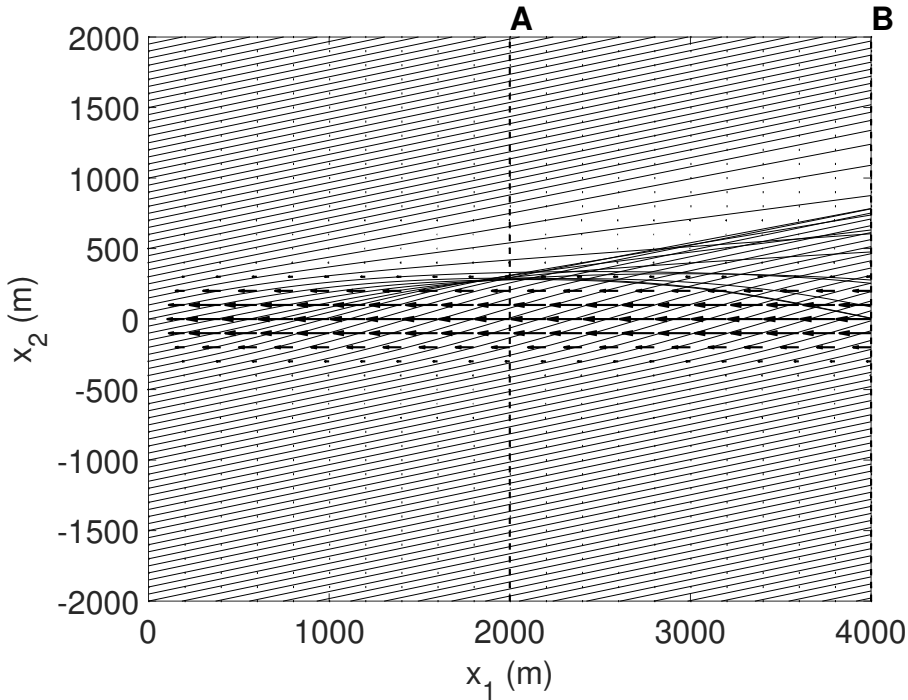


Figure 3.1: Wave rays due to \mathbf{k}_0 over a jet-like current field indicated by the solid lines. The rays at $x_1 = 0$ are obliquely incident with an angle of 15° . In addition, the ambient current is marked by arrows. Finally, the dashed vertical lines are sections along which the results of the significant wave height will be displayed.

3.3). In this case, all three models qualitatively predict a similar spatial structure of H_s throughout the domain.

Model differences are principally due to the statistical contribution of wave interferences. The transport equation employed by third-generation spectral models (e.g., SWAN), (3.19), disregards the contribution of cross-correlations (correlations of different wave components), which contain the information about wave interference. The QCM, on the other hand, does account for this information, and therefore, as the statistical contribution of wave interference becomes significant, the discrepancies between the results of QCM (or REF/DIF 1) and SWAN are more pronounced. Therefore, it is necessary to understand under which conditions the effect of wave interferences is important.

Generally speaking, the importance of the interference effects reduces as the spectrum of the incoming field becomes wider (e.g. Vincent and Briggs, 1989). Effectively, the multiple out-of-phase interference patterns generated by each wave component of the incoming field cancel each other out. Consequently, the superposition of the interference patterns becomes smoother as the incoming spectrum becomes wider. This is the reason why differences between QCM (and REF/DIF 1) and SWAN are larger for Jet_1 than Jet_2 . Whether or not interference effects can be expected may formally be related to the ratio β between the correlation length scale of the incident wave field, L_c , and a typ-

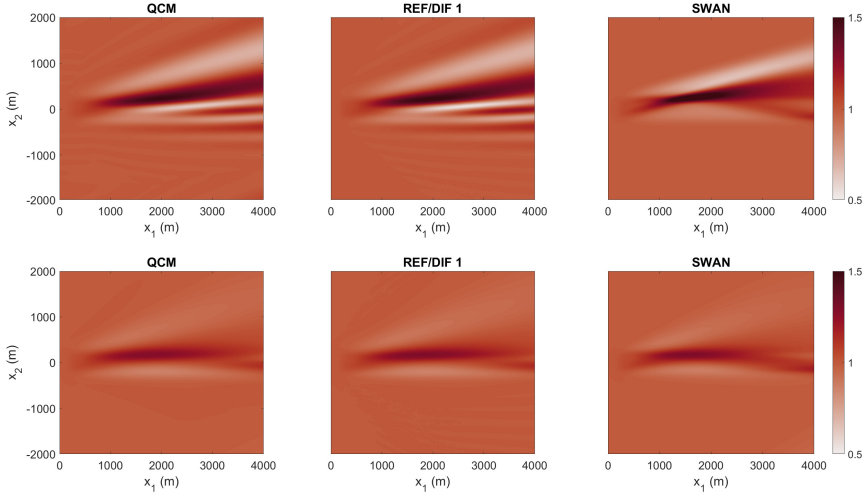


Figure 3.2: Comparison between QCM, REF/DIF 1 and SWAN in terms of the spatial distribution of the significant wave height. Upper panels show the results of the simulation Jet_1 , while the lower panels display the results due to Jet_2 .

ical length scale of the medium, L_m . Interference effects may become significant when $\beta \geq O(1)$ and are more pronounced for larger values of β (hence the difference between Jet_1 and Jet_2). This statistical condition is discussed in detail next.

3.4. DISCUSSION

The statistical contribution of wave interferences as a function of the parameter β can be analyzed conceptually as follows. Considering a certain point in space beyond the crossing zone, where interference effects are expected to play a role and assuming that the incoming field is monochromatic, for which $\beta \rightarrow \infty$. In this case, the correlation function at the considered point will extend over a very large spatial domain ($L_c \rightarrow \infty$), and will generally be composed of in-phase variance terms of the scattered field and out-of-phase cross-correlation terms between each pair of scattered waves. The cross-correlation terms include contributions that were generated due to correlation between the incoming field and the interference structures it forms. As the spectrum of the incoming field becomes wider (namely, $S_d^{(k)}$ becomes larger), the correlation function will extend over smaller domains and accordingly, β will take smaller values. The corresponding change in the interference effect can be analyzed from the physical point of view, by examining the correlation function, Γ , or from the spectral point of view, by considering the Wigner distribution, \mathcal{W} . From the physical point of view, when the incoming spectrum becomes wider and β reduces, the correlation value between the incoming field and the interference pattern it forms will become smaller, and consequently, the contribution of wave interference, at the considered point, reduces as well. In the limit, when $\beta \rightarrow 0$ (and therefore, $L_c \rightarrow 0$), this correlation value converges to zero and

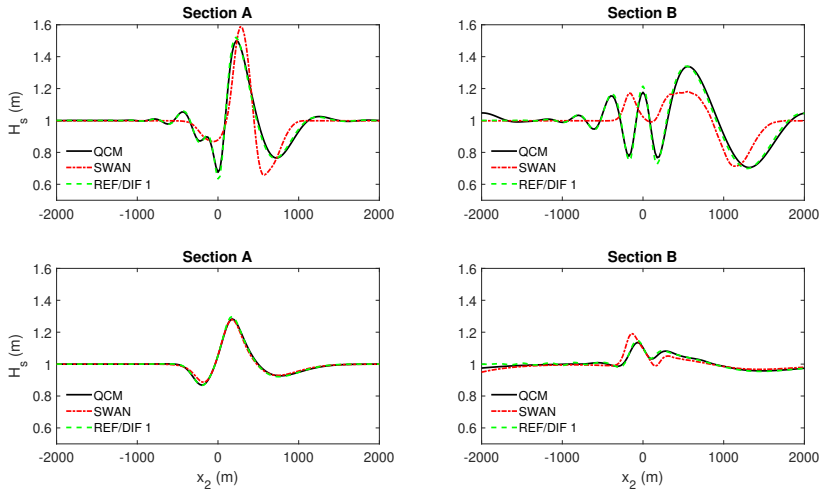


Figure 3.3: A comparison between QCM, REF/DIF 1 and SWAN in terms of the significant wave height along the sections that are indicated in Fig. 3.1. Upper panels show the results of the simulation Jet_1 , while the lower panels display the results due to Jet_2 .

the contribution of wave interference is eliminated.

The spectral point of view examines the representation of the cross-correlation terms in the Wigner distribution. Since the phases of the cross-correlation terms are not necessarily zero, their amplitudes may either be positive or negative, and therefore, tend to cancel each other and lose intensity. As a result, when the Wigner distribution at the considered point is integrated over the spectral space for the purpose of computing the total variance, and the corresponding value of, say H_s , the contribution of the cross-correlation terms will be less pronounced with the increasing of $S_d^{(k)}$, and therefore, less pronounced with the decreasing of β .

3.4.1. THE EVOLUTION OF THE CROSS-CORRELATION TERMS

This subsection provides a numerical demonstration of the above discussion on the statistical condition to the appearance of interference effects in the scattered field. The interaction problem between waves and a vortex-ring is a convenient example for this purpose. This is due to the fact that in this case, the domain essentially consists of two homogeneous regions separated by a scattering region, which are referred to as 'the incoming field', 'the scatterer' and 'the scattered field', respectively (see Fig. 3.4). Consequently, the statistical condition to wave interferences, which says that correlation should emerge between the incoming field and the interference structure it forms, is readily demonstrated through this interaction problem, as it can be replaced by the condition that the correlation function should extend over a larger domain than the effective domain of the vortex ring.

The statistical condition to the appearance of interference effects is examined by considering the evolution of the correlation function and the Wigner distribution for

simulations Ring₁ and Ring₃ (which differ by their initial spectrum width, see Table 3.1) over a specific spatial path. The spatial path was selected such that it would pass over an area where H_s is significantly affected by wave interferences (see Fig. 3.5). Finally, the contribution of the interference terms are emphasized by comparing the results of QCM to the corresponding results of SWAN.

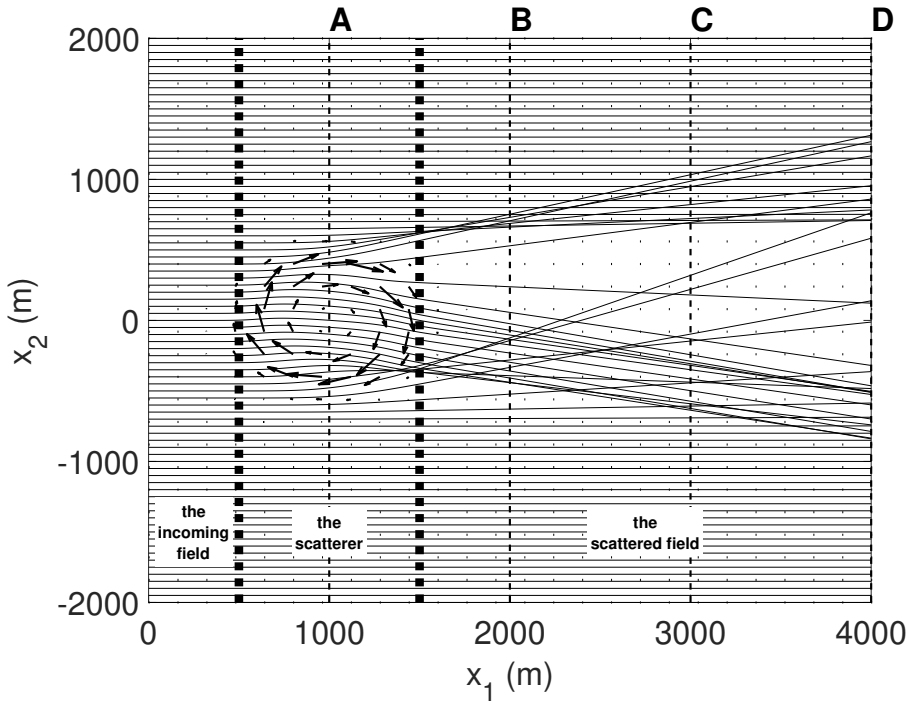


Figure 3.4: Wave rays due to \mathbf{k}_0 over a vortex-ring. The rays are indicated by the solid lines, and the ambient current is marked by arrows. Note that in this case, the rays at $x_1 = 0$ are normally incident. Additionally, the dashed vertical lines are sections along which the results of the significant wave height will be displayed. Finally, the dotted lines distinguish between different regions of the wave field.

In order to identify wave interference effects, the manner in which the cross-correlation terms (which represent the contribution of wave interferences) are represented is explained first (refer also to the definitions in (3.9) and (3.10)). Given two correlated wave components, their contribution in the correlation function results in two variance terms with wavenumbers \mathbf{k}_1 and \mathbf{k}_2 , and cross-correlation term (or interference term) with a wavenumber $(\mathbf{k}_1 + \mathbf{k}_2)/2$. The amplitude of the cross-correlation term depends on the amplitudes of the two wave components and their phase difference. If the point, around which the correlation function is considered, is located at the trough of the interference pattern generated by the two waves, then the amplitude of the cross-correlation term will be negative and vice versa. Also recall that the correlation function presented here follows the definition in (3.8). Consequently, $\Gamma(\mathbf{x}, \mathbf{x}')$ is the correlation between $\psi(\mathbf{x} + \mathbf{x}'/2)$ and $\psi^*(\mathbf{x} - \mathbf{x}'/2)$, which is different from the function that defines

the correlation between $\psi(\mathbf{x})$ and $\psi^*(\mathbf{x} + \mathbf{x}')$.

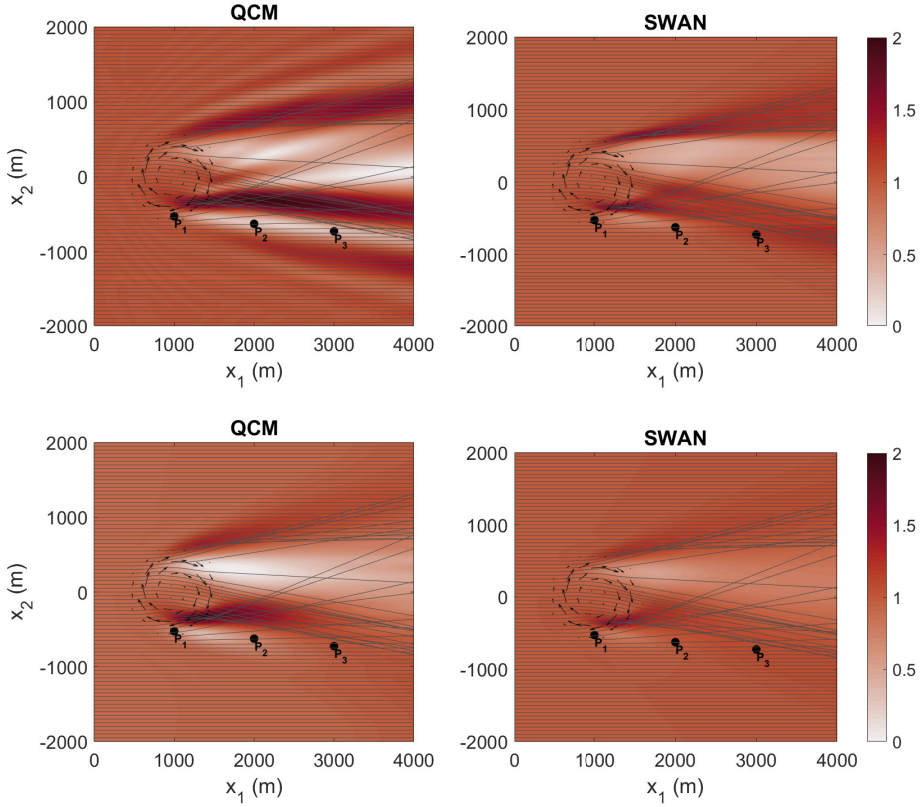


Figure 3.5: The distribution of the significant wave height due to the interaction between waves and a vortex-ring. The upper panels present the results of Ring₁ and the lower panels present the results due to Ring₃. Additionally, the solid lines represent the wave rays due to \mathbf{k}_0 . Finally, the three black points denoted by P_1 , P_2 and P_3 indicate the spatial path along which the evolution of the correlation function and the Wigner distribution is considered. P_1 , is located at $(1000m, -525m)$, P_2 , is at $(2000m, -625m)$ and P_3 , is at $(3000m, -725m)$.

The analysis starts by examining the evolution results of the correlation function and the Wigner distribution for the simulation Ring₁. In this case $\beta > 1$, and therefore, the effect of the cross-correlation terms on the structure of the correlation function and the Wigner distribution is likely to be significant. This is indeed evident by comparing the results of QCM (Fig. 3.6) to the results of SWAN (Fig. 3.7). Notable differences clearly appear in the results around P_2 and P_3 , in 'the scattered field', where interference effects are significant. Both of these points are located along the trough of the interference pattern (see Fig. 3.5). Indeed, the amplitudes of the cross-correlation terms, which are obtained at these points, are negative, as indicated by the blue areas in the Wigner distribution due to QCM. Note that these blue areas are located exactly between the red areas which

relate to the amplitudes of the variance terms. As expected, the blue areas do not appear in the action density spectrum due to SWAN, as it disregards the cross-correlation terms and only accounts for the variance terms. Moreover, in contrast to SWAN's results which only accounts for variance terms that are crossing close to the considered points, the QCM also includes contribution of variance terms and related cross-correlation terms that are crossing at some distance away from the considered points. This can be seen by comparing the Wigner distribution due to QCM and the action density spectrum due to SWAN and by referring to the wave rays in Fig. 3.4. Finally, note that the variance areas in the Wigner distribution are somewhat more spread than the corresponding variance areas appearing in the action density spectrum.

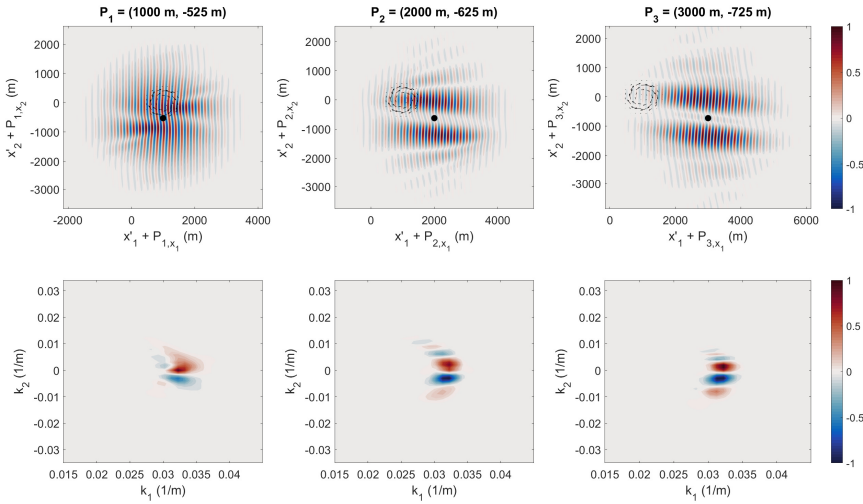


Figure 3.6: The evolution of the correlation function (shown by the upper panels) and the corresponding Wigner distribution (shown by the lower panels) as presented by the spatial points, P_1 , P_2 and P_3 . The values of the results are normalized by $|\Gamma(P_j, \mathbf{x}')|_{max}$ and $|\mathcal{W}(P_j, \mathbf{k})|_{max}$. These results were obtained for the simulation Ring₁ using QCM.

The negative values of the cross-correlation amplitudes in the results due to QCM lead to the fact that the correlation function at these points does not provide the maximum correlation value at its center (i.e., at $\mathbf{x}' = 0$). Conversely, since the SWAN model ignores the cross-correlation terms, the correlation function will always obtain the maximum value at $\mathbf{x}' = 0$. Therefore, the correlation function as defined in (3.8), does not necessarily show the maximum value at $\mathbf{x}' = 0$ for inhomogeneous fields.

Besides changing the correlation value at the central point, it is difficult to identify the cross-correlation terms directly through the correlation function. However, it is clear that these terms significantly change the structure of the correlation function, as reflected by the differences in the results due to QCM and SWAN (compare upper panels in Fig. 3.6 and Fig. 3.7).

The significant contribution of wave interferences appearing in the results around P_2 and P_3 implies that correlation emerges between the 'incoming field' and 'the scat-

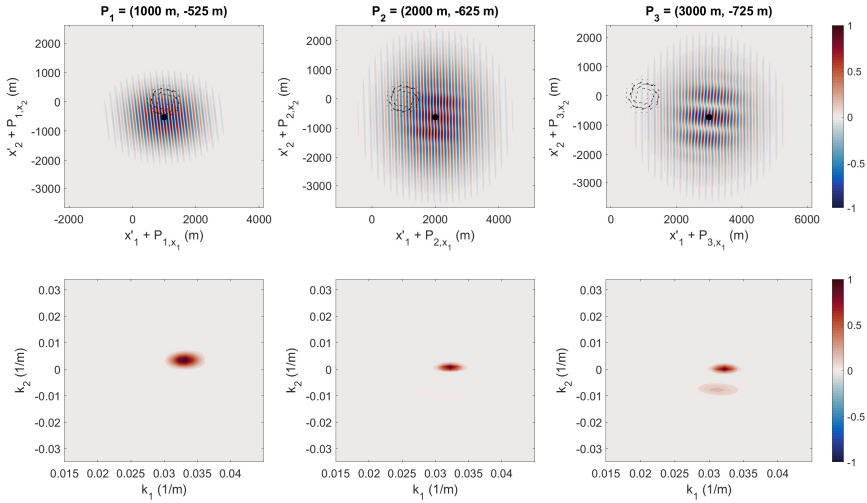


Figure 3.7: The evolution of the correlation function (shown by the upper panels) and the corresponding action density spectrum (shown by the lower panels) as presented by the spatial points, P_1 , P_2 and P_3 . The values of the results are normalized by $|\Gamma(P_j, \mathbf{x}')|_{max}$ and $|N(P_j, \mathbf{k})|_{max}$. These results were obtained for the simulation Ring₁ using SWAN.

tered field'. This is indeed shown by the results of the correlation function around P_1 in Fig. 3.6 (or in Fig. 3.7). The results show that the correlation function extends over a much larger domain than the effective domain of the vortex ring and that strong correlation values emerge between the incoming and the scattered field. Accordingly, the generated cross-correlation terms at P_1 have a clear signature on the structure of the correlation function and the Wigner distribution due to QCM (compare the results of P_1 in Fig. 3.6 and Fig. 3.7). These cross-correlation terms are transported along with the variance terms, altering dramatically the statistics of the scattered field, as shown by the significant differences between the results of QCM and SWAN around P_2 and P_3 .

The differences in the results between QCM and SWAN for the simulation Ring₃ are much less prominent (see Fig. 3.8 and Fig. 3.9). The reason for this is that at P_1 , the correlation function extends over a domain with about the same diameter as that of the vortex ring, and only small correlation value arises between the incoming field and the interference structure it forms in the vicinity of the crossing point at $(x_1, x_2) = (1365 \text{ m}, -355 \text{ m})$ (see Fig. 3.5). As a consequence, at P_1 , the amplitudes of the generated cross-correlation terms are quite low, as shown by the blue area in the Wigner distribution due to QCM in Fig. 3.8. Over the 'scattered field' region, at P_2 and P_3 , the influence of the cross-correlation terms is hardly detected through the correlation function, and indeed, at these points the correlation function due to QCM and SWAN are almost identical. However, the presence of the cross-correlation terms is visible in the Wigner distribution due to QCM by the blue area located between the variance areas. These cross-correlation terms eventually result in a limited contribution to the statistics of the scattered field, as for instance appears by the spatial distribution of H_s in Fig. 3.5.

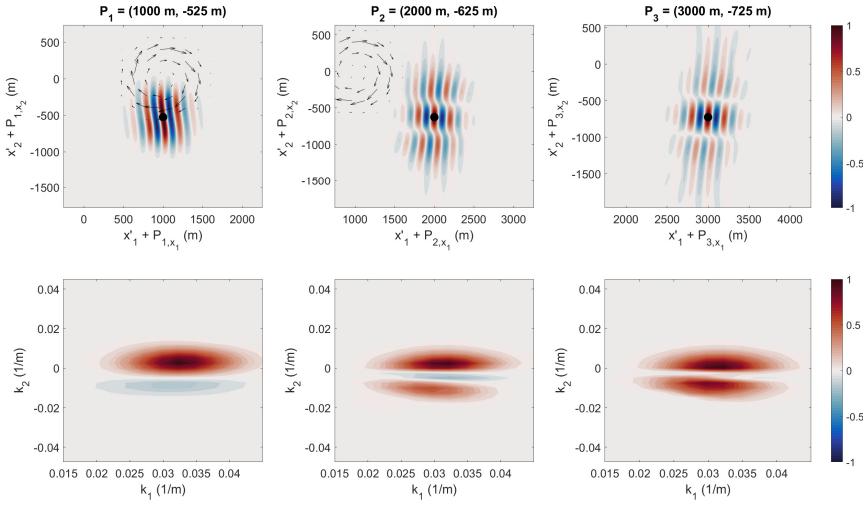


Figure 3.8: The evolution of the correlation function (shown by the upper panels) and the corresponding Wigner distribution (shown by the lower panels) as presented by the spatial points, P_1 , P_2 and P_3 . The values of the results are normalized by $|\Gamma(P_j, \mathbf{x}')|_{max}$ and $|\mathcal{W}(P_j, \mathbf{k})|_{max}$. These results were obtained for the simulation Ring₃ using QCM. Note that the scale over which the correlation function is plotted is much smaller than the corresponding scale used to present the results for Ring₁.

To conclude, the examination of the evolution of the correlation function and the Wigner distribution verifies the statistical condition for the generation of cross-correlation as was introduced conceptually in the beginning of this section. Moreover, the examination also demonstrates numerically, that the correlation value between the incoming field and the interference structure it forms determines the dominance of the interference patterns in the scattered field.

3.4.2. THE VALIDITY OF THE QCM

The final issue that is discussed here is the validity of the QCM versus the validity of SWAN over the parameter β . As was explained in the derivation of the QCM in Subsection 3.2.3 and following the presentation of the results so far, the QCM, in contrast to SWAN, seems to remain statistically valid for $\beta \geq O(1)$. The reason for this was extensively discussed in the previous subsection, and in short, is simply because the QCM accounts for statistical inhomogeneity of the wave field, generated due to interference effects.

The validity of QCM over β is presented by demonstrating the convergence of its results, obtained with an increasing value of β , to a single result of REF/DIF 1 obtained with a specific high value of β . To this end, QCM is used to compute H_s along the sections shown in Fig. 3.4 using simulations Ring₁, Ring₂ and Ring₃ which are defined with a decreasing value of β (i.e., Ring₁ is defined with the highest β value, whereas Ring₃ is defined with the lowest β value, see also Table 3.1). In addition, the result due to REF/DIF 1 is obtained through Ring₁. Finally, the convergence of QCM results to the result of

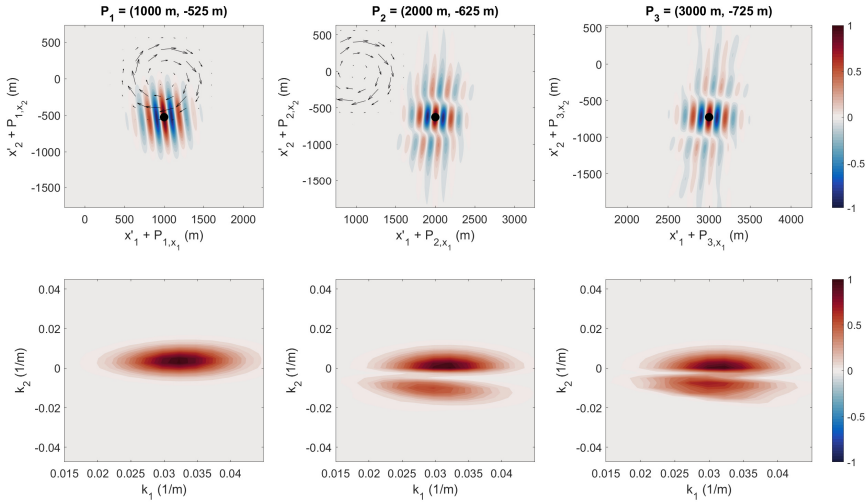


Figure 3.9: The evolution of the correlation function (shown by the upper panels) and the corresponding action density spectrum (shown by the lower panels) as presented by the spatial points, P_1 , P_2 and P_3 . The values of the results are normalized by $|\Gamma(P_j, \mathbf{x}')|_{max}$ and $|N(P_j, \mathbf{k})|_{max}$. These results were obtained for the simulation Ring₃ using SWAN. Note that the scale over which the correlation function is plotted is much smaller than the corresponding scale used to present the results for Ring₁.

REF/DIF 1 is shown by the upper panels in Fig. 3.10 and Fig. 3.11. The same procedure is performed using SWAN and is presented by the lower panels in Fig. 3.10 and Fig. 3.11.

Over 'the scatterer' region, before the focusing zones, SWAN seems to remain valid (see Fig. 3.10, section A) even for the highest β considered, that corresponds to the simulation Ring₁. However, over 'the scattered field' region, where interference effects emerge, SWAN does not converge to REF/DIF 1 when β increases. On the other hand, QCM does converge to REF/DIF 1, and seems to remain valid for the scattered field as well.

It is important to remember that the capabilities of QCM over β involve a constraint. This constraint is that $\epsilon \ll 1$, introduced by the deterministic model, (3.7), which underlies the development of QCM. Finally, recall that QCM is also limited to small values of μ , which basically limits its capabilities to accurately evolve interference terms with a wave length of $L_W \leq O(L)$, where L is the wave length of the considered point \mathbf{k} (see details in Smit and Janssen, 2013).

3.5. CONCLUSIONS

This study presents the development of a statistical model for problems of wave-current interaction, taking into account the effect of wave interferences. The theoretical basis of this model lies in the definition of the Wigner distribution \mathcal{W} , of the action variable, ψ . This distribution provides a complete spectral description of the second-order statistics of the wave field. It includes cross-correlation terms, which provide the statistical

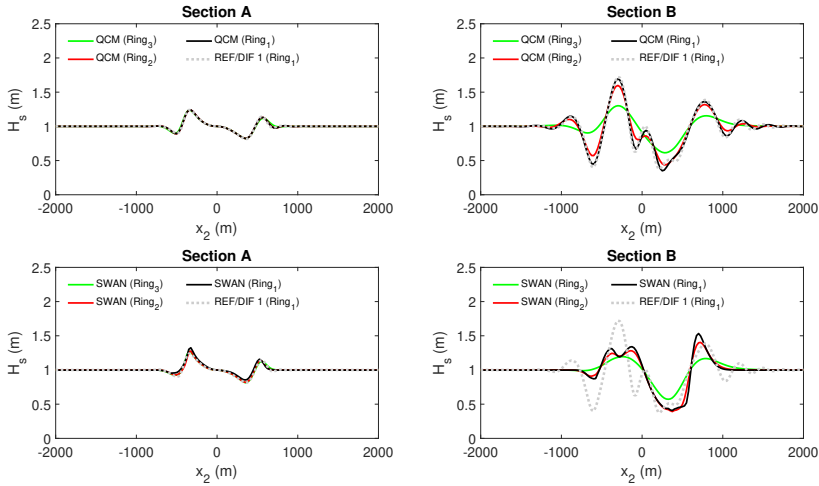


Figure 3.10: On the validity of QCM (upper panels) and SWAN (lower panels) over the parameter β , shown through the convergence of the significant wave height to the result of REF/DIF 1 with Ring₁. The results are given along sections *A* and *B* that are indicated in Fig. 3.4.

information about wave interferences. As such, \mathcal{W} generalizes the concept of the action density spectrum, N , which only accounts for the information of wave variances.

Using the procedure described in Smit and Janssen (2013) and Smit et al. (2015a), an evolution model for \mathcal{W} (the QCM) is developed. This model provides a generalization of the conventional action balance model (presently employed by third-generation spectral wave model, e.g., SWAN and WAVEWATCH III), by allowing the generation and transportation of statistical wave interferences.

The effect of wave interferences can contribute significantly for cases where the variation scale of the medium is at the same order or smaller than the scale of the correlation length, namely, for cases in which $\beta \geq O(1)$. This statistical condition is explicitly examined for scenarios where the incoming field is statistically homogeneous, but develops inhomogeneity while propagating over ambient currents. Specifically, in order to obtain a statistical signature of wave interferences, the incident and scattered fields should be correlated, with the dominance of the interference effect determined by the correlation value itself.

In cases where this correlation is strong, the interference patterns alter the statistics of the field significantly. The resulting effect on the significant wave height, H_s , is demonstrated through two examples of wave-current interaction and by a comparison to the SWAN model. It is demonstrated that in such cases, interference effects dramatically change the distribution of H_s , not only at the vicinity of wave focusing areas, but also in a significant distance away from the focusing points.

It is therefore concluded that for regions involving rapid variability in medium (e.g., coastal regions or oceanic regions which tend to contain submesoscale currents), consideration of the statistical information of wave interference might be crucial for many

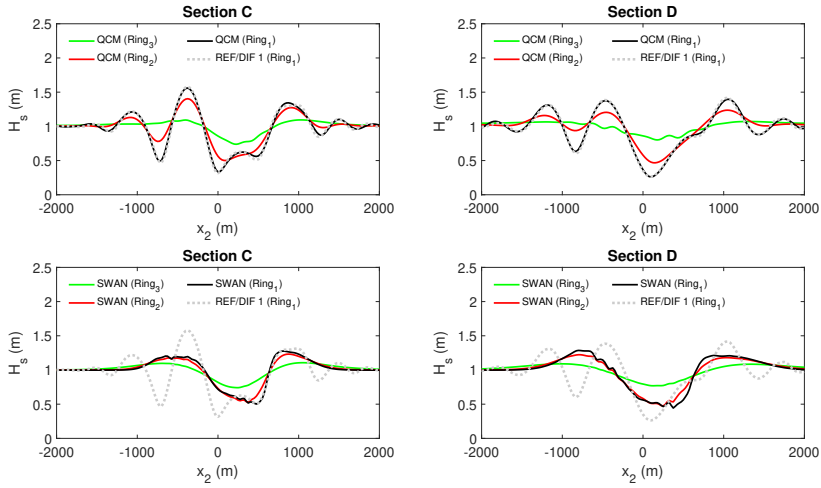


Figure 3.11: On the validity of QCM (upper panels) and SWAN (lower panels) over the parameter β , shown through the convergence of the significant wave height to the result of REF/DIF 1 with Ring₁. The results are given along sections C and D that are indicated in Fig. 3.4.

applications, such as, wave-induced circulation and transport processes in coastal regions or for prediction of extreme elevations in the open ocean.

ACKNOWLEDGEMENTS

This work is part of the research programme Earth and Life Sciences (ALW) with project number ALWOP.167, which is (partly) financed by the Dutch Research Council (NWO). Pieter Smit acknowledges support by the Office of Naval Research (N00014-16-1-2856).

APPENDICES

3.A. THE WEYL OPERATOR AND ITS ASYMPTOTIC FORM

The purpose of this appendix is to provide the definition of the pseudo-differential operators employed in this study. To this end, the operator $\Omega(\mathbf{x}, -i\nabla_{\mathbf{x}})$ will serve as a representative (the following also applies to the operators $\Sigma(\mathbf{x}, -i\nabla_{\mathbf{x}})$ and $\mathcal{A}(\mathbf{x}, -i\nabla_{\mathbf{x}})$ that were introduced in Section 3.2). Additionally, for convenience, the expressions in this appendix (and in Appendix B) are presented using the slow scale coordinates $\mathbf{x}_m = \epsilon \mathbf{x}$ and $t_m = \epsilon t$. However, in order to avoid cumbersome formulations, the subscript, m , indicating these slow scale coordinates will be removed, keeping in mind that for the purposes of this appendix (and Appendix B), \mathbf{x} and t are now serving as the slow scale coordinates. An additional notation is the letter D_j , which will be used here and in the following appendices to represent the operator $-i\nabla_j$.

The definition of the pseudo-differential $\Omega(\mathbf{x}, \epsilon D_{\mathbf{x}})$ is based on its association with a "phase-space" symbol (a function which is defined in (\mathbf{x}, \mathbf{k}) space). Here, it is assumed that such a "phase-space" symbol can be defined locally (in this case, it is the usual dispersion relation, (3.2)), which basically requires that the characteristic length scale of the medium variation is much larger than the considered wave length (e.g., Dingemans, 1997), i.e., that $\epsilon \ll 1$.

Given a "phase-space" symbol, the corresponding operator in the physical space can be defined through the association between \mathbf{k} and $D_{\mathbf{x}}$. However, because \mathbf{x} and $D_{\mathbf{x}}$ do not commute, one must follow an association rule for an arbitrary symbol. Here, the Weyl rule of association is adopted (see, e.g., Cohen, 2012), which is defined through the following Fourier transform of $\omega(\mathbf{x}, \mathbf{k})$:

$$\omega(\mathbf{x}, \mathbf{k}) = \int \hat{\omega}(\mathbf{q}, \mathbf{p}) \exp(i\mathbf{q} \cdot \mathbf{x} + i\mathbf{p} \cdot \mathbf{k}) d\mathbf{q} d\mathbf{p} \quad (3.25)$$

Then, the Weyl operator is obtained by substituting the operator $\epsilon D_{\mathbf{x}}$ instead of \mathbf{k} , which provides the following expression:

$$\Omega(\mathbf{x}, \epsilon D_{\mathbf{x}}) = \int \hat{\omega}(\mathbf{q}, \mathbf{p}) \exp(i\mathbf{q} \cdot \mathbf{x} + i\epsilon \mathbf{p} \cdot D_{\mathbf{x}}) d\mathbf{q} d\mathbf{p} \quad (3.26)$$

and which can be simplified using the commutator value, $[i\mathbf{q} \cdot \mathbf{x}, i\epsilon \mathbf{p} \cdot D_{\mathbf{x}}] = -i\epsilon \mathbf{q} \cdot \mathbf{p}$, to obtain,

$$\Omega(\mathbf{x}, \epsilon D_{\mathbf{x}}) = \int \hat{\omega}(\mathbf{q}, \mathbf{p}) \exp\left(\frac{i}{2}\epsilon \mathbf{q} \cdot \mathbf{p}\right) \exp(i\mathbf{q} \cdot \mathbf{x}) \exp(i\epsilon \mathbf{p} \cdot D_{\mathbf{x}}) d\mathbf{q} d\mathbf{p} \quad (3.27)$$

An important step is to define the asymptotic form of the Weyl operator, which will be used quite often to understand and interpret the leading orders results of its operation on a certain variable. As shown below, this asymptotic form depends on a Taylor expansion of the dispersion relation, and therefore (at least conceptually), should be defined

around $\mathbf{k}_0 \neq 0$, since derivatives of the dispersion relation at $\mathbf{k} = 0$ are singular. In order to obtain the asymptotic form of the Weyl operator, the Fourier transform of the dispersion relation around \mathbf{k}_0 is replaced by the Taylor expansion of the dispersion relation around that point,

$$\Omega(\mathbf{x}, \epsilon D_x) = \int [\exp(i\bar{\mathbf{k}} \cdot D_k) \hat{\omega}(\mathbf{q}, \mathbf{k})]_{\mathbf{k}=\mathbf{k}_0} \exp(-i\mathbf{p} \cdot \bar{\mathbf{k}}) \exp(\frac{i}{2}\epsilon \mathbf{q} \cdot \mathbf{p}) \exp(i\mathbf{q} \cdot \mathbf{x}) \exp(i\mathbf{p} \cdot (\epsilon D_x - \mathbf{k}_0)) d\bar{\mathbf{k}} d\mathbf{q} d\mathbf{p} \quad (3.28)$$

which, after Fourier transform with respect to $\bar{\mathbf{k}}$, reduces to,

$$\Omega(\mathbf{x}, \epsilon D_x) = \int \delta(\mathbf{p}) \left[\exp(i\mathbf{q} \cdot \mathbf{x}) \exp[i\mathbf{p} \cdot (\epsilon D_x - \mathbf{k}_0 + \frac{\mathbf{q}}{2})] \exp(i\bar{D}_p \cdot \bar{D}_k) \hat{\omega}(\mathbf{q}, \mathbf{k}) \right]_{\mathbf{k}=\mathbf{k}_0} d\mathbf{q} d\mathbf{p} \quad (3.29)$$

and eventually, leading to the following asymptotic form:

$$\Omega(\mathbf{x}, \epsilon D_x) = \left[\omega(\mathbf{x}, \mathbf{k}) \exp(\frac{i}{2}\epsilon \bar{D}_x \cdot \bar{D}_k) \exp[i\bar{D}_k \cdot (\epsilon D_x - \mathbf{k}_0)] \right]_{\mathbf{k}=\mathbf{k}_0} \quad (3.30)$$

In the following, the operation of Weyl operator, using its asymptotic form, (3.30), is examined for two examples: the case of a plane wave over homogeneous medium, and the case of a plane wave propagating over slowly varying medium. The operation of the Weyl operator in the first case is easily worked out, as in this case, the dispersion relation is not a function of \mathbf{x} , and also the spatial derivatives on the representative variable of the field can be resolved directly. This is demonstrated as follows. The plane wave is represented by the surface potential as, $\phi = A \exp[i(\mathbf{k}_0 \cdot \mathbf{x} - \omega_0 t)/\epsilon]$, and consequently, the operation, $\Omega\phi$, is obtained by the following:

$$\Omega(\epsilon D_x)\phi = \omega(\mathbf{k}_0)\phi \quad (3.31)$$

which is the desired result as detailed in the beginning of Appendix B.

In the second example, the considered wave component is represented by the surface potential as, $\phi = A(\mathbf{x}) \exp[(S - i\omega_0 t)/\epsilon]$. In this case, the operation of the Weyl operator is not immediately seen. The leading order ($O(1)$) term is obtained when the first exponent in (3.30) is taken to be equal one, and the spatial derivative of the second exponent, D_x , operates only on the exponent of ϕ . This term is the dispersion relation, (3.2). Terms of $O(\epsilon)$ are obtained for three different set of conditions. Two of these sets instruct to take the first exponent in (3.30) to be equal one, and at each expansion order of the second exponent the spatial derivative, D_x , should operate once on A for the one set or once on S , as instructed by the other set. The third term is obtained using the second term of the expansion of the first exponent of the operator and when the spatial derivative of the second exponent, D_x , operates only on the exponent of ϕ . This description is summarized as follows:

$$\Omega(\mathbf{x}, \epsilon D_{\mathbf{x}})\phi = \omega(\mathbf{x}, D_{\mathbf{x}}S)\phi + \epsilon i \left(D_{\mathbf{x}}A \cdot D_{\mathbf{k}}\omega + \frac{i}{2} AD_{\mathbf{x}}^2 SD_{\mathbf{k}}^2 \omega + \frac{1}{2} AD_{\mathbf{x}} \cdot D_{\mathbf{k}}\omega \right)_{\mathbf{k}=D_{\mathbf{x}}S} \exp[(S - i\omega_0 t)/\epsilon] + O(\epsilon^2) \quad (3.32)$$

This closes the formal definition of the Weyl operator, (3.27), and its asymptotic form, (3.30). The operation of the Weyl operator on representative variables in the homogeneous and weakly inhomogeneous case are used next to verify the evolution equation of the action variable, ψ .

3.B. ON THE EVOLUTION EQUATION OF THE ACTION VARIABLE

This appendix aims to demonstrate that the starting point equation (the evolution equation of the action variable), (3.7), is exact for the case of linear wave propagation over homogeneous medium, and reduces to the correct evolution equations for the weakly inhomogeneous case. In the latter, the correct evolution equations are the dispersion relation, (3.2), and the well-known action balance equation (e.g., Dingemans, 1997). For these purposes, the starting point equation, (3.7), is written once again, using the slow scale coordinates, as follows:

$$\epsilon \partial_t \psi = -i\Omega(\mathbf{x}, \epsilon D_{\mathbf{x}})\psi \quad (3.33)$$

where, as in the previous appendix, these slow scale coordinates are indicated using the same variable notation of the fast scale coordinates, \mathbf{x} , t , in order to avoid cumbersome formulations.

As introduced, the first aim here is to show that the starting point equation, (3.33), describes exactly the correct solution of an incoming plane wave over an homogeneous medium. To this end, the following example will be worked out. Considering a specific domain of interest, the example assumes that into one of the domain's boundaries enters a monochromatic wave field with an absolute frequency, ω_0 . In this case, the surface variables of the considered wave obey to the following form:

$$\begin{aligned} \phi &= A_0 \exp[(S - i\omega_0 t)/\epsilon] + c.c. \\ \eta &= B_0 \exp[(S - i\omega_0 t)/\epsilon] + c.c. \end{aligned} \quad (3.34)$$

where, $B_0 = iA_0(\omega_0 - \mathbf{U} \cdot (D_{\mathbf{x}}S))/g$, as follows from the linear relation between ϕ and η (see, e.g., Dingemans, 1997),

$$\eta = -\frac{1}{g}(\partial_t + \mathbf{U} \cdot \nabla_{\mathbf{x}})\phi \quad (3.35)$$

the wavenumber, $D_{\mathbf{x}}S$, is constant, and the constant amplitude, A_0 , assumed to be a "proper" (see, e.g., Lapidot, 2017) Gaussian random variable, namely, $\langle A_0^2 \rangle = 0$. The corresponding form of ψ is obtained following its definition, (3.3),

$$\psi = \frac{1}{\sqrt{2g}} \left[C_0 \exp[(S - i\omega_0 t)/\epsilon] + D_0 \exp[(-S + i\omega_0 t)/\epsilon] \right] \quad (3.36)$$

where, following (3.31), $a = \sqrt{\sigma(D_x S)}$, and the amplitudes, C_0 and D_0 are defined as, $C_0 = ga^{-1}B_0 + iaA_0$, and, $D_0 = ga^{-1}B_0^* + iaA_0^*$. Using these starting points, it is now aimed to show that (3.33) produces the correct magnitude of $D_x S$. By substituting (3.36) into (3.33), one obtains that the first solution (with the amplitude C_0), produces, as required, the equation: $\omega_0 = \omega(D_x S)$. Substituting this result into the definition of B_0 , which becomes $B_0 = iA_0\sigma(D_x S)/g$, provides the necessary result that $D_0 = 0$ (this is necessary, since the second term of ψ is not a solution of (3.33)), whereas, the value of C_0 is then given by: $C_0 = 2iA_0\sqrt{\sigma(D_x S)}$.

The second aim of this appendix is to show that the starting point equation (3.33) reduces to the correct evolution equations for the weakly inhomogeneous case. To do this, the same example as in the homogeneous case is considered. Following the WKB method (e.g., Holmes, 1995), and assuming that the bathymetry and the current are not time dependent, the surface velocity potential and elevation, ϕ and η , can be defined to leading order in ϵ by (3.34), where now, A_0 and S are functions of \mathbf{x} . The corresponding leading order definition of ψ is given by (3.36), but now, following (3.32), $a = \sqrt{\sigma(\mathbf{x}, D_x S)}$. By substituting this definition into (3.33) and using the result of (3.32), the $O(1)$ eikonal equation is obtained to be, $\omega_0 = \omega(\mathbf{x}, D_x S)$, which can be written as,

$$\omega_0 = \mathbf{U} \cdot D_x S + \sigma(\mathbf{x}, D_x S) \quad (3.37)$$

Using this result, B_0 , is obtained to be, $B_0 = iA_0\sigma(\mathbf{x}, D_x S)/g$, leading to the same necessary result as before, that $D_0 = 0$, whereas, C_0 , is given by: $C_0 = 2iA_0\sqrt{\sigma(\mathbf{x}, D_x S)}$. The remaining unknown, A_0 , is found through the following $O(\epsilon)$ transport equation:

$$\left(D_x C_0 \cdot D_k \omega + \frac{i}{2} C_0 D_x^2 S D_k^2 \omega + \frac{1}{2} C_0 D_x \cdot D_k \omega \right)_{k=D_x S} = 0 \quad (3.38)$$

which alternatively, can be written as,

$$D_x \cdot (\langle |C_0|^2 \rangle D_k \omega) = 0 \quad (3.39)$$

In order to verify that (3.39) is the well-known action balance equation (e.g., Dingemans (1997)), one should check that $\rho \langle |\psi|^2 \rangle = \rho \langle |C_0|^2 \rangle$ indeed defines the mean action density. To see this, one may calculate $\langle |\psi|^2 \rangle$ directly, using the definition of ψ , (3.3), which results in,

$$\rho \langle |\psi|^2 \rangle = \left[\frac{1}{2} \rho g \langle \eta_0^2 \rangle + \frac{1}{2g} \rho \langle (\Sigma \phi)_0^2 \rangle \right] / \Sigma + O(\epsilon) \quad (3.40)$$

where, the subscript, 0, indicates on $O(1)$ terms. The expression in the rectangular brackets is exactly the mean energy density, m_0 that was introduced in (3.6). Clearly, the first term of the expression represents the mean potential energy density, though the connection of the second term to the density of the kinetic energy might not be immediately obvious and should be clarified. Following (3.32), the first order operation, $(\Sigma \phi)_0$, is defined as $(\Sigma \phi)_0 = \sigma(\mathbf{x}, D_x S)\phi$. Substituting this result into (3.40), the second term becomes equal to the mean kinetic energy density for homogeneous medium that is defined by the local values, $h(\mathbf{x})$ and $\mathbf{U}(\mathbf{x})$ (e.g., Section 6.3 in Van Groesen and Molenaar, 2007). Similarly, the first order operation due to Σ^{-1} is equivalent to the division of the

expression in the rectangular brackets by the local intrinsic frequency, σ . The result is the definition of the mean action density (Bretherton and Garrett (1968)).

3.C. FROM WIGNER DISTRIBUTION TO LOCAL ENERGY

To motivate the necessity for an alternative formula that links between the energy density, m_0 , and the Wigner distribution, $\mathcal{W}(\mathbf{x}, \mathbf{k}, t)$, the following example is discussed (note that here, the formulation returns to be written in terms of the original spatial coordinates, \mathbf{x} and t). The example assumes an idealized sea state composed of three coherent and forward-propagating wave components in a 1d and homogeneous medium. The waves are defined with the following wavenumbers: k_1 , k_2 , and $k_3 = (k_1 + k_2)/2$. Accordingly, at a certain moment in time t_0 , the wave field may be represented as follows:

$$\begin{aligned}\phi &= \sum_{n=1}^3 A_n \exp(ik_n x) + c.c. \\ \eta &= \sum_{n=1}^3 B_n \exp(ik_n x) + c.c.\end{aligned}\tag{3.41}$$

where, A_n and B_n are complex random amplitudes. The amplitude, B_n , is given by, $B_n = iA_n\sigma_n/g$, as follows from the linear relation between ϕ and η , (see, (3.35) in Appendix B). The mean energy density, m_0 in this example, is derived using the expression in (3.6), and can be written as follows:

$$m_0 = \frac{2}{g} \sum_{n=1}^3 \sum_{m=1}^3 \sigma_n \sigma_m \langle A_n A_m^* \rangle \exp[i(k_n - k_m)x]\tag{3.42}$$

The approach employed in this study to get to (3.42) is via the Wigner distribution of the action variable, ψ , which for this example is given by,

$$\mathcal{W}(x, k, t_0) = \frac{2}{g} \sum_{n=1}^3 \sum_{m=1}^3 \sqrt{\sigma_n} \sqrt{\sigma_m} \langle A_n A_m^* \rangle \exp[i(k_n - k_m)x] \delta[k - \frac{k_n + k_m}{2}]\tag{3.43}$$

where $\delta(k)$ is now serving as the usual delta function. Now it can be seen explicitly that a simple substitution of (3.43) into (3.12) will not provide the result described in (3.42). As an example, consider the components in \mathcal{W} that multiply the function $\delta[k - (k_1 + k_2)/2]$. Following the definition of k_3 , there are two such components: $2\sigma_3 \langle |A_3|^2 \rangle / g$ and $2\sqrt{\sigma_1} \sqrt{\sigma_2} \langle A_1 A_2^* \rangle \exp[i(k_1 - k_2)x] + c.c. / g$, which related to the variance of the third wave component and to the correlation between the first and the second wave components, respectively. If \mathcal{W} is substituted into (3.12), both of these components will be factored by σ_3 , which by referring to (3.42), will not lead to the correct interference term between the first and the second wave components. It is concluded that in order to calculate the mean energy density correctly, one must distinguish between the variance term and the interference terms for each k , and only then multiply by the correct factor. The derivation of an alternative formula to obtain m_0 based on \mathcal{W} is detailed below.

The starting point of the following derivation is the relation between the action variable, ψ , and the mean energy density, m_0 , as given in (3.5), recalling that $a(\mathbf{x}, D_{\mathbf{x}})$ is a Weyl

operator associated with the square root of the intrinsic angular frequency, $\sigma^{1/2}(\mathbf{x}, \mathbf{k})$. Following the definition of Weyl's operator, the expression in (3.5) can be written as,

$$\langle |\mathcal{A}(\mathbf{x}, D_{\mathbf{x}})\psi|^2 \rangle = \int \hat{a}(\mathbf{q}_1, \mathbf{p}_1) \hat{a}^*(\mathbf{q}_2, \mathbf{p}_2) \exp\left(\frac{i}{2}\mathbf{q}_1 \cdot \mathbf{p}_1 + \frac{i}{2}\mathbf{q}_2 \cdot \mathbf{p}_2\right) \exp[i\mathbf{x} \cdot (\mathbf{q}_1 - \mathbf{q}_2)] \langle \psi(\mathbf{x} + \mathbf{p}_1, t) \psi^*(\mathbf{x} - \mathbf{p}_2, t) \rangle d\mathbf{q}_1 d\mathbf{q}_2 d\mathbf{p}_1 d\mathbf{p}_2 \quad (3.44)$$

By substituting the Fourier transform of the correlation function, $\Gamma = \langle \psi(\mathbf{x} + \mathbf{p}_1, t) \psi^*(\mathbf{x} - \mathbf{p}_2, t) \rangle$, the following expression is obtained:

$$\langle |\mathcal{A}(\mathbf{x}, D_{\mathbf{x}})\psi|^2 \rangle = \int \hat{a}(\mathbf{q}_1, \mathbf{p}_1) \hat{a}^*(\mathbf{q}_2, \mathbf{p}_2) \exp[i\mathbf{q}_1 \cdot (\mathbf{x} + \mathbf{p}_1/2) - i\mathbf{q}_2 \cdot (\mathbf{x} - \mathbf{p}_2/2)] \exp(i\mathbf{k}_1 \cdot \mathbf{p}_1 + i\mathbf{k}_2 \cdot \mathbf{p}_2) \hat{\Gamma}(\mathbf{k}_1, \mathbf{k}_2, t) \exp[i\mathbf{x} \cdot (\mathbf{k}_1 - \mathbf{k}_2)] d\mathbf{k}_1 d\mathbf{k}_2 d\mathbf{q}_1 d\mathbf{q}_2 d\mathbf{p}_1 d\mathbf{p}_2 \quad (3.45)$$

Integrating the above expression with respect to \mathbf{q}_1 and \mathbf{q}_2 leads to,

$$\langle |\mathcal{A}(\mathbf{x}, D_{\mathbf{x}})\psi|^2 \rangle = \int \hat{a}(\mathbf{x} + \mathbf{p}_1/2, \mathbf{p}_1) \hat{a}^*(\mathbf{x} - \mathbf{p}_2/2, \mathbf{p}_2) \exp(i\mathbf{k}_1 \cdot \mathbf{p}_1 + i\mathbf{k}_2 \cdot \mathbf{p}_2) \hat{\Gamma}(\mathbf{k}_1, \mathbf{k}_2, t) \exp[i\mathbf{x} \cdot (\mathbf{k}_1 - \mathbf{k}_2)] d\mathbf{k}_1 d\mathbf{k}_2 d\mathbf{p}_1 d\mathbf{p}_2 \quad (3.46)$$

By assuming that σ is independent of \mathbf{x} , (3.46) reduces to the following expression:

$$\langle |\mathcal{A}(\mathbf{x}, D_{\mathbf{x}})\psi|^2 \rangle = \int \sqrt{\sigma(\mathbf{k} + \mathbf{k}'/2)} \sqrt{\sigma(\mathbf{k} - \mathbf{k}'/2)} \hat{\Gamma}(\mathbf{k}', \mathbf{k}, t) \exp(i\mathbf{k}' \cdot \mathbf{x}) d\mathbf{k}' d\mathbf{k} \quad (3.47)$$

where, the change of variables, $\mathbf{k}_1 = \mathbf{k} + \mathbf{k}'/2$ and $\mathbf{k}_2 = \mathbf{k} - \mathbf{k}'/2$, was applied.

Otherwise, (3.46) can be integrated once more. Now the integration is performed with respect to \mathbf{p}_1 and \mathbf{p}_2 , leading to the following result:

$$\langle |\mathcal{A}(\mathbf{x}, D_{\mathbf{x}})\psi|^2 \rangle = \int \left[\exp\left(\frac{i}{2}D_{\mathbf{x}} \cdot D_{\mathbf{k}_1}\right) a(\mathbf{x}, \mathbf{k}_1) \right] \left[\exp\left(-\frac{i}{2}D_{\mathbf{x}} \cdot D_{\mathbf{k}_2}\right) a^*(\mathbf{x}, -\mathbf{k}_2) \right] \hat{\Gamma}(\mathbf{k}_1, \mathbf{k}_2, t) \exp[i\mathbf{x} \cdot (\mathbf{k}_1 - \mathbf{k}_2)] d\mathbf{k}_1 d\mathbf{k}_2 \quad (3.48)$$

Ultimately, if terms of $O(\epsilon)$ are omitted, and by applying the same change of variables over the wavenumber space (as indicated above), the following approximation for the zero order moment of the energy density spectrum, m_0 , is derived,

$$m_0 \sim \rho \int \sqrt{\sigma(\mathbf{x}, \mathbf{k} + \mathbf{k}'/2)} \sqrt{\sigma(\mathbf{x}, \mathbf{k} - \mathbf{k}'/2)} \hat{\Gamma}(\mathbf{k}', \mathbf{k}, t) \exp(i\mathbf{k}' \cdot \mathbf{x}) d\mathbf{k}' d\mathbf{k} \quad (3.49)$$

which generalizes (3.47) for case with a slowly varying medium.

The numerical implementation of (3.49) is not straightforward. It requires performing Fourier transform of the Wigner distribution for each wavenumber, \mathbf{k} , and around

each spatial location, \mathbf{x} . In addition, one should distinguish, at each location \mathbf{x} , between the Fourier components that relates to the slow variation of the variances and the Fourier components of the cross-correlation terms.

A different direction to obtain an evaluation of m_0 stems from an alternative formulation of (3.49). This formulation is detailed as follows. At first, the Fourier components, $\hat{\Gamma}(\mathbf{k}', \mathbf{k}, t) \exp(i\mathbf{k}' \cdot \mathbf{x})$, are replaced by the Fourier transform of the Wigner distribution around \mathbf{x} :

$$m_0 \sim \rho \int f(\mathbf{x}, \mathbf{k}', \mathbf{k}) \mathcal{W}(\mathbf{x} + \bar{\mathbf{x}}, \mathbf{k}, t) \exp(-i\mathbf{k}' \cdot \bar{\mathbf{x}}) d\bar{\mathbf{x}} d\mathbf{k}' d\mathbf{k} \quad (3.50)$$

where, $f(\mathbf{x}, \mathbf{k}', \mathbf{k}) = \sqrt{\sigma(\mathbf{x}, \mathbf{k} + \mathbf{k}'/2)} \sqrt{\sigma(\mathbf{x}, \mathbf{k} - \mathbf{k}'/2)}$. Then, assuming that the Wigner distribution around \mathbf{x} can be expressed as a Taylor expansion, and after integrating over $\bar{\mathbf{x}}$, the following approximation of m_0 is obtained:

$$m_0 \sim \rho \int \delta(\mathbf{k}') [f(\mathbf{x}, \mathbf{k}', \mathbf{k}) \exp(i\vec{D}_{\mathbf{k}'} \cdot \vec{D}_{\mathbf{x}}) \mathcal{W}(\mathbf{x}, \mathbf{k}, t)] d\mathbf{k}' d\mathbf{k} \quad (3.51)$$

where, due to the symmetry of f around $\mathbf{k}' = 0$, the exponent in the integral of the last expression can be replaced by a cosine. As opposed to the numerical implementation of (3.49), the implementation of (3.51) is straightforward. The first term in the expansion of (3.51) is exactly the formula used in SWAN, as given by (3.12). The high-order terms provide corrections (of $O(\mu)$, see the definition of μ in Subsection 3.2.3) to the cross-correlation components that are stored in \mathbf{k} . Ultimately, in the numerical examples, m_0 is evaluated up to second order using the following expression:

$$m_0 \sim \rho \int \sigma(\mathbf{x}, \mathbf{k}) \mathcal{W}(\mathbf{x}, \mathbf{k}, t) d\mathbf{k} + \frac{1}{2} \int [f(\mathbf{x}, \mathbf{k}', \mathbf{k}) (\vec{D}_{\mathbf{k}'} \cdot \vec{D}_{\mathbf{x}})^2 \mathcal{W}(\mathbf{x}, \mathbf{k}, t)]_{\mathbf{k}'=0} d\mathbf{k} \quad (3.52)$$

3.D. THE EVOLUTION EQUATION FOR THE WIGNER DISTRIBUTION

This appendix presents a more detailed derivation of the transport equation for the Wigner distribution, (3.21), based on Weyl's rule of association. The starting point of the derivation is the definition of the Weyl operator, (3.27). As a first step, the definition of the Weyl operator, (3.27), is used to define the operator that operates on the correlation function in (3.16) as,

$$\Omega(\mathbf{x} + \mathbf{x}'/2, D_{\mathbf{x}'} + D_{\mathbf{x}}/2) = \int \hat{\omega}(\mathbf{q}, \mathbf{p}) \exp[i\mathbf{q} \cdot (\mathbf{x} + \mathbf{x}'/2) + i\mathbf{p} \cdot (D_{\mathbf{x}'} + D_{\mathbf{x}}/2)] d\mathbf{q} d\mathbf{p} \quad (3.53)$$

Then, the operator can be organized such that the exponential functions being generated due to the disentanglement of the exponential operators (for details, see Section 2.4 in Cohen, 2012) will cancel each other, leading to the following expression:

$$\Omega(\mathbf{x} + \mathbf{x}'/2, D_{\mathbf{x}'} + D_{\mathbf{x}}/2) = \int \hat{\omega}(\mathbf{q}, \mathbf{p}) \exp(i\mathbf{q} \cdot \mathbf{x}) \exp(i\mathbf{p} \cdot D_{\mathbf{x}'}) \exp(i\mathbf{q} \cdot \mathbf{x}'/2) \exp(i\mathbf{p} \cdot D_{\mathbf{x}}/2) d\mathbf{q} d\mathbf{p} \quad (3.54)$$

Following the above expression and the operator correspondences, $f(\mathbf{x}') \leftrightarrow f(D_{\mathbf{k}})$ and $f(D_{\mathbf{x}'}) \leftrightarrow f(\mathbf{k})$, the corresponding operator that operates on the Wigner distribution in (3.17) is defined as,

$$\Omega(\mathbf{x}-D_{\mathbf{k}}/2, \mathbf{k}+D_{\mathbf{x}}/2) = \int \hat{\omega}(\mathbf{q}, \mathbf{p}) \exp(i\mathbf{q} \cdot \mathbf{x}) \exp(i\mathbf{p} \cdot \mathbf{k}) \exp(-i\mathbf{q} \cdot D_{\mathbf{k}}/2) \exp(i\mathbf{p} \cdot D_{\mathbf{x}}/2) d\mathbf{q} d\mathbf{p} \quad (3.55)$$

where the exponential operators that depend on $D_{\mathbf{k}}$ and $D_{\mathbf{x}}$ (the third exponential and the fourth exponential in the integral on the right hand side of (3.55)) can be written as an external operators outside of the integral, resulting in the following formulation:

$$\Omega(\mathbf{x}-D_{\mathbf{k}}/2, \mathbf{k}+D_{\mathbf{x}}/2) = \int \hat{\omega}(\mathbf{q}, \mathbf{p}) \exp(i\mathbf{q} \cdot \mathbf{x}) \exp(i\mathbf{p} \cdot \mathbf{k}) d\mathbf{q} d\mathbf{p} \exp(-i\overleftarrow{D}_{\mathbf{x}} \cdot \overrightarrow{D}_{\mathbf{k}}/2 + i\overleftarrow{D}_{\mathbf{k}} \cdot \overrightarrow{D}_{\mathbf{x}}/2) \quad (3.56)$$

which is exactly the exponential form of the operator as presented in (3.18). For the next steps, it will be convenient to write (3.56) as,

$$\Omega(\mathbf{x}-D_{\mathbf{k}}/2, \mathbf{k}+D_{\mathbf{x}}/2) = \int \hat{\omega}(\mathbf{q}, \mathbf{k}) \exp(i\mathbf{q} \cdot \mathbf{x}) \exp(i\overleftarrow{D}_{\mathbf{k}} \cdot \overrightarrow{D}_{\mathbf{x}}/2) \exp(-i\mathbf{q} \cdot \overrightarrow{D}_{\mathbf{k}}/2) d\mathbf{q} \quad (3.57)$$

which when operates on the Wigner distribution, leads to the following equation:

$$\Omega(\mathbf{x}-D_{\mathbf{k}}/2, \mathbf{k}+D_{\mathbf{x}}/2) \mathcal{W}(\mathbf{x}, \mathbf{k}, t) = \int \hat{\omega}(\mathbf{q}, \mathbf{k}) \exp(i\mathbf{q} \cdot \mathbf{x}) \exp(i\overleftarrow{D}_{\mathbf{k}} \cdot \overrightarrow{D}_{\mathbf{x}}/2) \mathcal{W}(\mathbf{x}, \mathbf{k}-\mathbf{q}/2, t) d\mathbf{q} \quad (3.58)$$

Finally, according to the assumption of small μ (see details in Subsection 3.2.3), the exponential operator is defined through Taylor series. By approximating the exponential operator to first order in μ , (3.58) becomes,

$$\Omega(\mathbf{x}-D_{\mathbf{k}}/2, \mathbf{k}+D_{\mathbf{x}}/2) \mathcal{W}(\mathbf{x}, \mathbf{k}, t) = \int \hat{\omega}(\mathbf{q}, \mathbf{k}) \exp(i\mathbf{q} \cdot \mathbf{x}) (1 + i\overleftarrow{D}_{\mathbf{k}} \cdot \overrightarrow{D}_{\mathbf{x}}/2) \mathcal{W}(\mathbf{x}, \mathbf{k}-\mathbf{q}/2, t) d\mathbf{q} \quad (3.59)$$

which is exactly the operator shown in (3.20).

A last an important step that is discussed here, which is necessary to the numerical implementation of (3.21), is the representation of the left hand side of (3.59) in terms of the correlation function, $\Gamma(\mathbf{x}, \mathbf{x}', t)$. One way to get to this representation involves a few algebraic steps. The other way is to see it directly through the convolution theorem. In order to present the second way, the multiplication term, $\hat{\omega}(\mathbf{q}, \mathbf{k}) \exp(i\mathbf{q} \cdot \mathbf{x})$, is replaced by the Fourier transform of ω around \mathbf{x} , represented by: $\hat{\omega}(\mathbf{q}, \mathbf{k}, \mathbf{x})$. Then, using the convolution theorem, the following equation is obtained:

$$\begin{aligned} & \int \hat{\omega}(\mathbf{q}, \mathbf{k}, \mathbf{x}) (1 + i\overleftarrow{D}_{\mathbf{k}} \cdot \overrightarrow{D}_{\mathbf{x}}/2) \mathcal{W}(\mathbf{x}, \mathbf{k}-\mathbf{q}/2, t) d\mathbf{q} \\ &= \int \omega(\mathbf{x} + \mathbf{x}'/2, \mathbf{k}) (1 + i\overleftarrow{D}_{\mathbf{k}} \cdot \overrightarrow{D}_{\mathbf{x}}/2) \Gamma(\mathbf{x}, \mathbf{x}', t) \exp(-i\mathbf{k} \cdot \mathbf{x}') d\mathbf{x}' \quad (3.60) \end{aligned}$$

3.E. ON THE NUMERICAL MODEL

The steady-state numerical solution of (3.21) uses the following two-dimensional and equispaced grids: $N_x, N_k, N_{\bar{x}}, N_q$ (where $\bar{x} = \mathbf{x}'/2$). These grids are constructed using the following spatial and spectral steps: $\Delta x, \Delta k, \Delta \bar{x}, \Delta q$. The value of Δk is chosen according to the standard-deviation, $S_d^{(k)}$, of the incoming wave spectrum as, $\Delta k = S_d^{(k)}/\alpha$, where $\alpha \geq 1$ serves as a resolution factor. Additionally, to ease the computation of the source term S_{QC} , the value of Δk is selected such that $\Delta k = \Delta q/2$ (this selection prevents the need to perform interpolation in the calculation of the integral in (3.22)).

Next, the choice of Δq is explained. This choice stems from the fact that for any realistic sea state, the correlation function around a certain point, \mathbf{x} , will effectively have a compact support in $|\mathbf{x}'| < L_c/2$, where L_c is the correlation length. Consequently, and as implied by (3.60), instead of an integral operation, the source term in (3.21), S_{QC} , can be calculated as a discrete convolution between $\Delta \hat{\omega}$ and \mathcal{W} (and their derivatives) over the grid N_q . This is done without introducing any discretization error if $\Delta q \leq 4\pi/L_c$ (for details which also include the additional treatment required to compute the discrete version of $\Delta \hat{\omega}$, see Smit et al., 2015a). If Δq is chosen such that $\Delta q = 4\pi/L_c$, then the applied value of L_c , which is taken into account in the numerical model, can be found from the definition of Δk as, $L_c = 2\pi\alpha/S_d^{(k)}$, which is consistent with the expected order that should characterize the standard-deviation of the envelope of the correlation function ($O(1/S_d^{(k)})$).

The choice of $\Delta \bar{x}$ is argued in a similar way to the selection of Δq , but now knowledge about the boundaries of \mathcal{W} over N_k at a certain point, \mathbf{x} (beyond which \mathcal{W} equals zero), is required. As for the correlation function, also here, the boundaries are not easily predicted in advance, because the support of \mathcal{W} over N_k can change significantly over N_x . For accuracy, the necessary $\Delta \bar{x}$ is evaluated in accordance with the boundaries introduced by N_k . A more economical selection of $\Delta \bar{x}$, which also introduces an acceptable error, is described by Smit et al. (2015b). Note that by introducing $\Delta \bar{x}$, the summation in S_{QC} becomes limited to the region $[-q_{max}, q_{max}]$, where $q_{max} = \pi/\Delta \bar{x}$.

Finally, the derivation of Δx is considered. Its value should be selected according to the characteristic variation length of \mathcal{W} over \mathbf{x} , and according to the adopted scheme for treating the spatial derivatives. Here, the second order upwind scheme (see Hirsch, 2007) is used. The local error introduced by this scheme is of $O[(\Delta x \mu/L)^3]$, where L is the characteristic wave length (L/μ represents the characteristic length of wave interference at the considered location). Therefore, Δx should be chosen to be small enough, so that the global error due to such a magnitude of local error would be acceptable.

4

SPECTRAL FORECASTING OF COASTAL SEA-SWELL AND INFRAGRAVITY WAVES USING QUADRATIC MODELS

Coastal wave forecasting over large spatial scales is essential for many applications (e.g., coastal safety assessments, coastal management and developments, etc.). This demand explains the necessity for accurate yet effective models. A well-known efficient modelling approach is the quadratic approach (members of this approach are often referred to as frequency-domain models, weakly nonlinear mild-slope models, amplitude models, etc.). The efficiency of this approach stems from a significant modelling reduction of the original governing equations (e.g., Euler equations). The outcome is a model that describes the evolution of wave fields based on the slowly varying amplitudes of the progressive components only. Most significantly, the description of wave nonlinearity essentially collapses into a single mode coupling term determined by the quadratic interaction coefficients. Consequently, it is expected that together with efficiency, this significant modelling reduction will also involve a decrease in prediction accuracy. In order to gain further insight into the predictive capabilities of this modelling approach, this study examines six different quadratic formulations, three of which are of the Boussinesq type (i.e., Freilich and Guza, 1984, Madsen and Sørensen, 1993 and Nwogu, 1993) and the other three are referred to as fully dispersive formulations (i.e., Whitham, 1967, Kaihatu and Kirby, 1995 and Bredmose et al., 2005). It is found that while Boussinesq formulations reliably predict the evolution of coastal waves, the predictions by the fully dispersive formulations tend to be affected by false developments of modulational instability. As a consequence, the predicted fields by the fully dispersive formulations are characterized by unexpectedly strong modulations of the sea-swell part and associated unexpected infragravity response. As an alternative to existing formulations, this study suggests a new modulationally stable and

fully dispersive formulation. This formulation is an attempt to push the limit of the prediction capabilities of coastal waves through the quadratic approach. To this end, a parametric process is proposed, striving to find the optimal quadratic interaction coefficients under the constraint of full linear dispersion. Based on a wide set of examples (including monochromatic, bichromatic and irregular wave conditions), it is found that the new formulation presents superior forecasting capabilities of both the swell-sea components and the infragravity field.

4.1. INTRODUCTION

Over coastal waters, incoming ocean waves undergo a dramatic transformation due to the interaction with the bathymetry and due to nonlinear wave-wave interactions. Quasi-linear sinusoidal waves in deep water transform into skewed and asymmetric saw-tooth like shape over shallower water. Ultimately, the waves break and dissipate their energy close to shore.

These complex wave dynamics in coastal waters gives rise to many important phenomena nearshore. Examples are, wave setup (e.g. Longuet-Higgins and Stewart, 1964), alongshore currents (e.g. Bowen, 1969, Longuet-Higgins, 1970, Reniers and Battjes, 1997, Ruessink et al., 2001), return flow (e.g. Dyhr-Nielsen and Sørensen, 1970, Stive and De Vriend, 1994) and associated sediment transport processes (e.g. Fredsoe and Deigaard, 1992, Van Rijn, 1993) and the generation of freely propagating infragravity waves which may significantly influence wave run-up and overtopping on dikes and dunes (e.g. Van Gent, 2001), dune erosion and sediment transport (e.g. Roelvink and Stive, 1989, Roelvink et al., 2009), and harbour oscillations (e.g. Bowers, 1977).

In practice, engineers and governmental agencies require accurate wave parameters over large spatial scales to correctly predict these processes. A well-known modelling approach that allows efficient wave prediction over large coastal scales is provided by the so-called quadratic formulation (other names are frequency-domain formulation, nonlinear mild-slope models, amplitude models, etc.). This approach is referred here as the quadratic approach to indicate its underlying weakly nonlinear assumption (terms of third-order and higher are neglected). Apart from the weakly nonlinear assumption, the efficiency of this approach is achieved by its formulation in terms of the slowly spatial scale that characterizes the slow bathymetric variations and the variation due to wave nonlinearity. Additionally, the quadratic modelling also neglects the effect of wave reflection and assumes that the wave field is composed of propagating modes only (the so-called evanescent modes are ignored). As a result, this modelling approach essentially solves the evolution of the field's amplitudes assuming slowly varying bathymetry and weakly nonlinear mode coupling. Obviously, such a simplified modelling approach constitutes a significant reduction of the original incompressible and inviscid Euler equations. Therefore, a central question that this study aims to answer is, how reliable would be the forecasting of coastal waves as provided by the quadratic formulation?

The earliest quadratic formulation was suggested by Freilich and Guza (1984) based on the classical Boussinesq formulation of Peregrine (1967). Over relatively shallow waters, this model agrees well with observations (Freilich and Guza, 1984). However, due to its weak dispersion assumption and the associated simplified shoaling description, its prediction of propagating wave fields over shoaling regions from intermediate to shallower waters may deviate significantly (e.g., Agnon et al., 1993). As a consequence of the limitations posed by the classical Boussinesq formulation, efforts were set forward to improve its dispersive behaviour and the associated linear shoaling. These efforts led to the development of the so-called weakly nonlinear Boussinesq models with improved dispersion (e.g., Witting, 1984, Madsen et al., 1991, Madsen and Sørensen, 1992, Nwogu, 1993). Based on this modelling paradigm, the quadratic model by Madsen and Sørensen (1993) was developed. This quadratic model, which serves as the starting point for the development of the nonlinear quadratic source term in the SWAN model (see Eldeberky,

1997), indeed demonstrated good agreement for different examples of nonlinear wave evolution from intermediate waters and over the shoaling and surf zones (e.g., Eldeberky and Battjes, 1996). The success of the weakly nonlinear Boussinesq models with improved dispersion has motivated further development in this direction. The goal was to develop fully dispersive and weakly nonlinear models which were expected to improve wave predictions without additional computational costs. Quadratic models with such properties were proposed by Agnon et al. (1993) and Kaihatu and Kirby (1995) and later generalized and further developed by numerous following studies (e.g., Eldeberky and Madsen, 1999, Bredmose et al., 2005, Janssen, 2006, Sheremet et al., 2016, Ardani and Kaihatu, 2019, Kim and Kaihatu, 2021).

4 There is no doubt that these developments have improved the linear characteristics of the quadratic modelling (i.e., dispersion and shoaling), however doubt arises concerning the improvement in the prediction of nonlinear evolution. This doubt stems from the fact that the improvement of the linear properties of the quadratic model is accompanied by a change in the quadratic coefficients, and therefore, also by a change in the truncation error obtained due to the modelling reduction associated with the formulation of the quadratic model. An indication for that is presented by the study of Bredmose et al. (2005), which proposes a fully dispersive quadratic model with exact second-order transfer. In other words, bound wave solutions obtained by this model exactly match the second-order bound wave predictions of Stokes theory (expressions of which are given by, e.g., Hasselmann, 1962, Sharma and Dean, 1981, Dalzell, 1999). Although it seems promising, Bredmose et al. (2005) observed phase errors of the model predictions by comparing to laboratory experiments. These phase errors were explained by the significant over prediction of the amplitude dispersion embedded in this model. However, apart from cumulative phase errors, errors in amplitude dispersion may lead to much more dramatic consequences. In specific, it is well known that the amplitude dispersion has a decisive impact on the evolution of narrow-banded fields (e.g., Lighthill, 2001, Whitham, 1974), controlling energy exchanges through the modulational instability mechanism (Benjamin and Feir, 1967). A well-known example that clearly highlights the effect of improving the linear dispersion relation on the stability characteristics in the context of weak nonlinear modeling is given by the Whitham equation. The Whitham equation was proposed by Whitham (1967) as a generalized Korteweg–de Vries (KdV) equation that incorporates the full linear dispersion relation. Such a generalization is expected to provide a more faithful description of wave field evolution which may also composed of shorter wave components. However, it is now known that this generalization is accompanied by a dramatic change in the characteristics of the modulational instability occurring in shallower water than expected (the threshold is $\mu > 1.146$, which is lower than the usual threshold of $\mu > 1.363$, see, e.g., Van Groesen, 1998, Hur and Johnson, 2015, where $\mu = k_p h$ and k_p is the characteristic wavenumber of a considered wave field and h represents the water depth). Thus, Whitham's generalization turns the modulationally stable KdV equation into a modulationally unstable Whitham equation which will predict faulty focusing/defocusing recurrence of narrow-banded fields over regions of relatively small μ . This erroneous effect may not only lead to false energy exchanges and thus incorrect evolution of the peak frequency components, but may also contaminate the associated development of the infragravity components as a result of incorrect

modulations of the wave field.

This study aims to reveal in further detail the nonlinear properties of the quadratic modelling approach and to gain insight into the prediction capabilities of different quadratic formulations to spectrally describe the nonlinear evolution of coastal wave fields, including the development of the sea-swell components (i.e., the primary harmonics and the secondary super-harmonics) and the generation and evolution of the infragravity components (i.e., the secondary sub-harmonics). In total six different formulations are examined and compared. These formulations consist of three Boussinesq formulations and three fully dispersive formulations. The leading order nonlinear properties of these formulations, including their second-order bound wave solutions, amplitude dispersion and stability characteristics are explored and compared in Section 4.2. The study also proposes a new fully dispersive formulation referred to as QuadWave1D. The main aim of QuadWave1D is to improve the prediction of coastal wave evolution based on the quadratic modelling paradigm. This is achieved by combining accurate linear properties and adequate nonlinear balance provided by the quadratic coefficients. The derivation of QuadWave1D is detailed in Section 4.3. The performances of QuadWave1D and the other six different quadratic formulations are compared to laboratory observations for monochromatic, bichromatic and irregular wave fields in Section 4.4. Finally, conclusions are drawn in Section 4.5.

4.2. MODEL ANALYSIS OVER FINITE DEPTH

This section aims to gain further insight into the leading order contributions of the nonlinear evolution of a considered wave field as obtained by different quadratic formulations. As in the rest of this study, the considered wave field is assumed to be composed of long-crested waves (i.e., this study is confined to one-dimensional wave propagation). For the purpose of the following analysis, the one-dimensional formulation (ignoring for now the effect of bathymetry changes) of the quadratic model is given as follows:

$$\partial_x a_n - i k_n a_n = -i \sum_r V_{r,n-r} a_r a_{n-r} \quad (4.1)$$

where $V_{l,m}$ are the quadratic interaction coefficients which stand at the center of interest of this study. Moreover, a_n and k_n are the n^{th} complex-amplitude and wavenumber of a time-periodic wave field, represented through the surface elevation function, η , as,

$$\eta = \sum_n a_n \exp(-i\omega_n t) \quad (4.2)$$

where ω_n is the n^{th} wave angular-frequency and x , t represent the spatial and temporal coordinates. Further details on the derivation of the quadratic model (4.1) are provided in Appendix 4.A.

The analysis here focuses on the bound wave solutions and the parameters which control the evolution of narrow-banded seas. To this end, it is assumed here that nonlinear effects are relatively weak, such that Stokes theory can be applied to predict the physical parameters of the wave field (e.g., surface elevation, fluid velocities, etc.). A well-known parameter which provides an indication regarding the validity of Stokes expansion is the so-called Ursell parameter (or Stokes parameter), defined as

$$U_r = \frac{H_p L_p^2}{h^3} \quad (4.3)$$

where H_p and L_p are the characteristic wave height and length of the considered wave field. Based on this definition, weak nonlinearity corresponds to $U_r < 26$, for which Stokes theory applies (see Le Méhauté, 1976). This parameter provides a convenient non-dimensional limit for the present analysis.

In total, six models are examined. The first three are the Boussinesq models proposed by Freilich and Guza (1984) (the "consistent shoaling model"), Madsen and Sørensen (1993) and Nwogu (1993). The other three are the fully-dispersive models proposed by Whitham (1967), Kaihatu and Kirby (1995) and Bredmose et al. (2005). Note that Nwogu (1993) and Whitham (1967) actually present time-domain model formulations. However, here those references are used to refer to the corresponding quadratic formulations which are derived based on these original time-domain models. The nonlinear interaction coefficients and also the linear parameters (for the linear dispersion and wave shoaling) of these six quadratic models are summarized in Appendix 4.A.

4.2.1. SECOND-ORDER BOUND WAVES

The leading nonlinear contributions to the evolution of wave fields, as provided by the quadratic model (4.1), are extracted here under the conditions of unidirectional propagation over constant and finite depth. Based on the assumption of weak nonlinearity (i.e., $U_r < 26$), the following multiple-scale expansion is being employed (e.g., Holmes, 1995). It is assumed that the waves evolve over two spatial scales. The fast scale is denoted by $x_1 = x$ and the slow scale is represented by $x_2 = \epsilon^2 x$, where the small parameter ϵ represents the ratio between the typical wave amplitude and wave length in deep/intermediate water or the ratio between the amplitude and water depth in shallow water. Note that x_2 is defined as $O(\epsilon^2)$ variable since resonance condition can only be satisfied between four-waves as dictated by the dispersion relation (this statement contradicts the so-called near-resonance assumption that underlies the development of the quadratic model, see discussion in Appendix 4.A).

In addition to the definition of the two new spatial variables, it is also assumed that the n^{th} complex-amplitude, a_n , can be written as follows:

$$a_n = \epsilon a_n^{(1)} + \epsilon^2 a_n^{(2)} + \epsilon^3 a_n^{(3)} + \dots \quad (4.4)$$

By substituting these assumptions into the quadratic model, (4.1), one obtains a set of equations, each balances terms of mutual order. The first three equations are given as follows:

$$\partial_{x_1} a_n^{(1)} - i k_n a_n^{(1)} = 0 \quad (4.5)$$

$$\partial_{x_1} a_n^{(2)} - i k_n a_n^{(2)} = -i \sum_r V_{r,n-r} a_r^{(1)} a_{n-r}^{(1)} \quad (4.6)$$

$$\partial_{x_1} a_n^{(3)} - i k_n a_n^{(3)} = -\partial_{x_2} a_n^{(1)} - i \sum_r V_{r,n-r} (a_r^{(1)} a_{n-r}^{(2)} + a_r^{(2)} a_{n-r}^{(1)}) \quad (4.7)$$

The interest here focuses on the bound wave solutions which can be obtained through the solution of (4.6). To this end, knowledge of $a_n^{(1)}$ is required. This knowledge is achieved through the solution of (4.5), given by

$$a_n^{(1)} = A_n \exp(ik_n x_1) \quad (4.8)$$

where A_n is a complex amplitude that depends on the boundary condition, say at $x = 0$, and the variable x_2 . In addition, the wavenumber, k_n , is obtained through the dispersion relation, $D(\omega_n, k_n) = 0$, as defined by the different model formulations (see details in Appendix 4.A). Returning now to the solutions of the bound waves which are obtained through (4.6). These bound wave solutions are considered for each possible bichromatic pair. To this end, a pair of two incoming primary wave component which are represented by A_l and A_m , are assumed. Using the linear solution, (4.8), and assuming that the homogeneous solution of $a_n^{(2)}$ equals zero, the following expression is obtained:

$$a_n^{(2)} = \begin{cases} 2G_{l,m} a_l a_m, & l \neq m \\ G_{l,m} a_l a_m, & l = m \\ 0, & m = -l \end{cases} \quad (4.9)$$

where $n = l + m$, and the so-called quadratic transfer function, $G_{l,m}$, is given by

$$G_{l,m} = V_{l,m} / (k_n - k_{lm}) \quad (4.10)$$

As in the rest of the text, notations like f_{lm} (e.g., k_{lm}) are interpreted as $f_{lm} = f_l + f_m$. Note that for the case where $m = -l$, $a_n^{(2)}$ is zero since $V_{l,-l}$ is zero (see Subsection 4.3.1 for introduction on the general properties of $V_{l,m}$). However, in the limit for which m approaches to l , the value of $G_{l,-m}$ does not converges to zero, but it converges to the coefficient that corresponds to the set-down associated with a monochromatic wave.

A computed demonstration of the bound solutions is presented in Fig. 4.1. The figure compares the solutions according to each of the models, where the values are normalized by the values of the solutions according to the second-order Stokes theory (expressions of which are given by, e.g., Hasselmann, 1962, Sharma and Dean, 1981, Dalzell, 1999).

Following these results, the model of Bredmose et al. (2005) is clearly preferable over the others with regard to the prediction of the bound waves. In fact, the solutions following Bredmose et al. (2005) match exactly to the solutions according to Stokes theory. The deviation of the other models arises as a result of two factors. The first relates to the nonlinear terms of the underlying time-domain models which construct the quadratic coefficients, $V_{l,m}$. These terms are subjected to some a priori assumed relation between the depth parameter μ and the parameter for nonlinearity ϵ . For example, a well-known relation is $\epsilon = O(\mu^2)$, which leads to the classical Boussinesq formulation (e.g., Peregrine, 1967). Therefore, under the classical Boussinesq regime, nonlinear terms involving corrections of the dispersion relation are neglected (refer also to Madsen and Schäffer, 1998 for detailed discussion on the impact of the relation between μ and ϵ on the second-order bound wave solutions). The second factor that leads to deviations in the bound wave predictions, which is also embedded in $V_{l,m}$, is the near-resonance assumption, that is usually taken to derive the quadratic formulation (see details in Appendix 4.A).

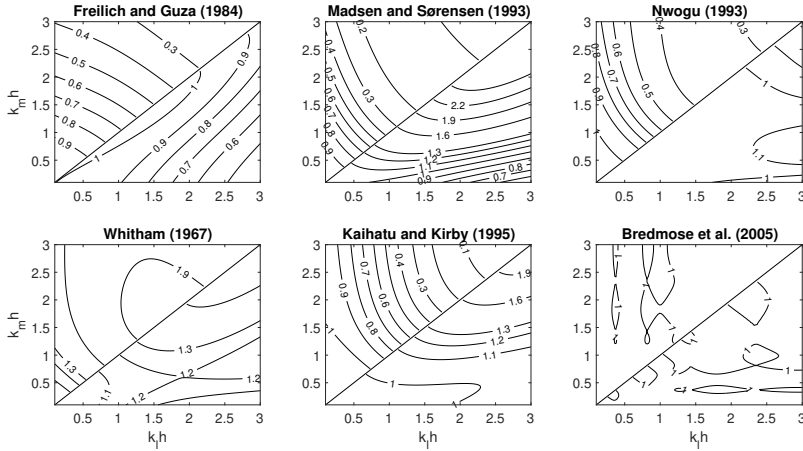


Figure 4.1: Second-order bound wave solutions normalized by the solutions of Stokes theory (or simply $G_{l,m}/Gs_{l,m}$ where $Gs_{l,m}$ is the quadratic transfer function according to Stokes theory). Solutions due to sum interactions are given for $k_m \geq k_l$ (upper triangular of each panel), while solutions of sub interactions are provided for $k_m < k_l$ (lower triangular of each panel).

The exception in this regard is the model by Bredmose et al. (2005), being formulated through an operator splitting idea suggested by Agnon (1999). The operator splitting idea bypasses the necessity to rely on the near-resonance assumption, and therefore, avoids an additional error in the bound wave solutions (see further discussion in Bredmose et al., 2005 and in Appendix 4.A).

The exceptional performance of the model by Bredmose et al. (2005) in predicting the bound waves, raises the anticipation of its preferable wave prediction capabilities in general. However, account should also be paid to the fact that the different definitions of the quadratic coefficients and dispersion relation are also accompanied by different definitions for the truncation error (arising as a result of the modelling reduction associated with the formulation of the quadratic model), which may significantly influence the evolution of the waves, and thus, the model forecast.

4.2.2. AMPLITUDE DISPERSION

An important nonlinear property that is deteriorated as a result of the modelling reduction, introduced by the quadratic model, is the amplitude dispersion. As stated by Whitham (1974), the dependence of the dispersion relation on the wave amplitudes does not merely provide quantitative corrections, but in fact leads to significant qualitative changes in the behaviour and introduces new phenomena. Here though, the focus is on the direct quantitative contributions of the amplitudes to the dispersion relation and how these contributions differ from one model to another.

The most general case that allows complete representation of the amplitude dispersion is the bichromatic case, which was introduced by Longuet-Higgins and Phillips (1962) for deep water and later generalized for waves over finite depth (e.g., Madsen and Fuhrman, 2006). Here, the amplitude dispersion is obtained based on (4.7). Gener-

ally speaking, the solutions for $a_n^{(3)}$, as also found for $a_n^{(2)}$, consist of bound components which provide high-order corrections to the primary solutions, $a_n^{(1)}$. However, the products of $a_i^{(1)}$ and $a_j^{(2)}$ can also result in resonance interactions as would be clearly understood for the product $a_{2l}^{(2)} a_{-l}^{(1)}$ which would lead to an unbounded growth of $a_l^{(3)}$. The multiple-scale method allows to keep the solution bounded by balancing such forcing terms with the derivatives of the primary solutions with respect to x_2 (as given by the right-hand-side of (4.7)). Namely, by requiring the following:

$$\partial_{x_2} a_n^{(1)} = -i \sum_r V_{r,n-r} (a_r^{(1)} a_{n-r}^{(2)} + a_r^{(2)} a_{n-r}^{(1)}) \quad (4.11)$$

which for the considered bichromatic case leads to

$$\begin{cases} i \partial_{x_2} a_l^{(1)} = L_{l,l} |a_l^{(1)}|^2 a_l^{(1)} + 2L_{l,m} |a_m^{(1)}|^2 a_l^{(1)} \\ i \partial_{x_2} a_m^{(1)} = L_{m,m} |a_m^{(1)}|^2 a_m^{(1)} + 2L_{m,l} |a_l^{(1)}|^2 a_m^{(1)} \end{cases} \quad (4.12)$$

where $L_{l,l}$ and $L_{l,m}$ are the cubic interaction coefficients which arise due to the trivial resonant quartets (see further details on the definition of the cubic interaction coefficients for trivial and non-trivial resonant quartets in Appendix 4.B).

The solution for (4.12) can be obtained explicitly, since the magnitudes square of $a_l^{(1)}$ and $a_m^{(1)}$ are constant in x_2 (as can be found from the corresponding evolution equations for $|a_l^{(1)}|^2$ and $|a_m^{(1)}|^2$). This solution can be written as

$$\begin{cases} a_l^{(1)} = A_l^0 \exp \left(i k_l x_1 - i (L_{l,l} |a_l^{(1)}|^2 + 2L_{l,m} |a_m^{(1)}|^2) x_2 \right) \\ a_m^{(1)} = A_m^0 \exp \left(i k_m x_1 - i (L_{m,m} |a_m^{(1)}|^2 + 2L_{m,l} |a_l^{(1)}|^2) x_2 \right) \end{cases} \quad (4.13)$$

and it clearly shows the effect of the amplitudes on the dispersion relation through modifications of the wavenumbers. As an example, if the coefficients $L_{i,j}$ are positive, then a particular wave component of a given wave field would not only travel faster due to self interaction but also due to the presence of other waves.

The values of the amplitude dispersion as given by the different model formulations are compared with those of the third-order Stokes theory over finite depth (Madsen and Fuhrman, 2006) in Fig. 4.2 and Fig. 4.3. The computed values are not the corrections for the wavenumbers, but the corrections for the angular frequencies. The latter are obtained based on the following transformation:

$$\omega_l^{(2)} = C_{g,l} k_l^{(2)} \quad (4.14)$$

where the correction for the wavenumber k_l is defined as

$$k_l^{(2)} = L_{l,l} |a_l^{(1)}|^2 + 2 \sum_m L_{l,m} |a_m^{(1)}|^2 \quad (4.15)$$

Note that the correction, $k_l^{(2)}$, is subtracted from the linear wavenumber, while $\omega_l^{(2)}$ is added to the linear angular frequency, and therefore, these modifications change the wave velocity in the same manner. Also note that the above transformation can be explained through a more general formulation which allows modulation in both space and time. The assumption of periodicity in time or in space can then be applied to obtain the

corresponding $\omega_l^{(2)}$ or $k_l^{(2)}$ which differ by the factor $C_{g,l}$ (also see Appendix 4.C and the alternative explanation in Bredmose et al., 2005).

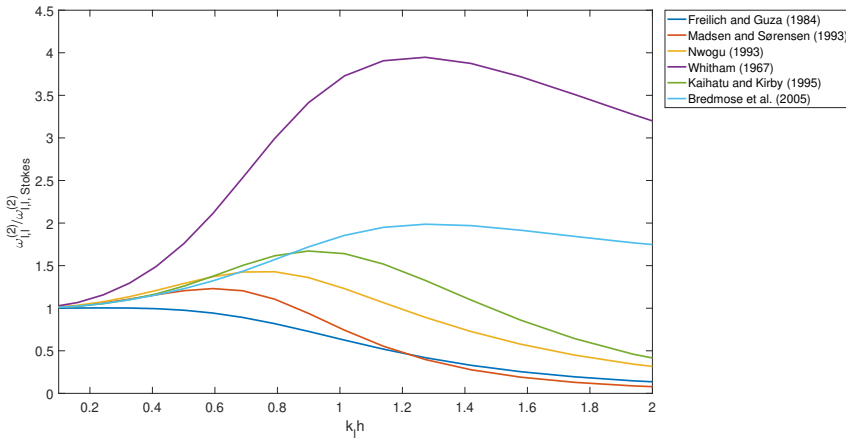


Figure 4.2: Model prediction of the amplitude dispersion contributions due to self interactions, $\omega_{l,l}^{(2)} = C_{g,l}L_{l,l}|a_l^{(1)}|^2$. The results are normalized by third-order Stokes theory as given by Madsen and Fuhrman (2006).

The results demonstrated in Fig. 4.2 show a clear over prediction of the contribution due to the self interaction, $\omega_{l,l}^{(2)} = C_{g,l}L_{l,l}|a_l^{(1)}|^2$, by most of the models. This over prediction is reduced for increasing values of μ . The one exception here is the formulation by Freilich and Guza (1984), which under-predicts the self interaction contribution. Consequently, most of the models will typically predict faster traveling waves in coastal waters, leading to cumulative phase errors as demonstrated by Bredmose et al. (2004) and Bredmose et al. (2005). Ultimately, these results provide further evidence for the implications of the modelling reduction associated with the formulation of the quadratic model and how different assumptions (e.g., different relation between μ and ϵ) affect the corresponding modelling errors.

The prediction of the mutual interactions' contributions to the amplitude dispersion due to the different model formulations is presented in Fig. 4.3. Over prediction is also revealed here by comparing to Stokes theory. The over prediction is again stronger by the formulation of Whitham (1967) and Bredmose et al. (2005). Nevertheless, the values due to the fully-dispersive models are consistent with the expected physics implied by the values of Stokes theory. Apart from being positive, which leads to faster traveling waves, the values of the fully-dispersive models also correctly predict the fact that the influence of a longer wave on the propagation of a shorter wave is stronger than the influence arising by the presence of a shorter wave on the propagation of a longer wave (this is made clear by the two black points included in each of the panels in Fig. 4.3). The Boussinesq models, on the other hand, do not appear to completely adhere to these physical properties as demonstrated by their negative values. However, at least for small μ values, the over prediction of the Boussinesq models is much weaker. Finally, note that the

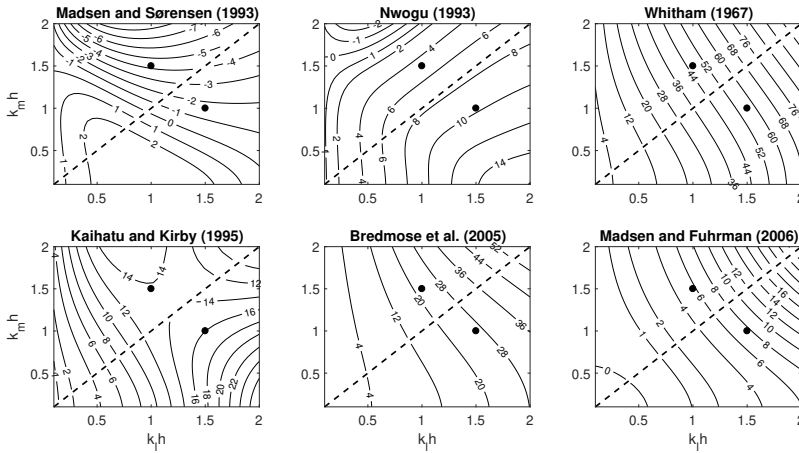


Figure 4.3: Model prediction of the amplitude dispersion contributions due to mutual interactions, $\omega_{l,m}^{(2)} = C g_l L_{l,m} |a_m^{(1)}|^2$. The results are normalized by $|a_m^{(1)}|^2$ and are compared to the results of third-order Stokes theory as given by Madsen and Fuhrman (2006) (see lower-right corner panel). The contributions due to a shorter wave in the presence of a longer wave and due to the opposite situation are compared using the two black points at each panel.

results due to Freilich and Guza (1984) are excluded, since they are simply equal to zero, as can be found by substituting the corresponding definitions for $V_{l,m}$ and k_n (see (4.69) and (4.66)) into the definition of $L_{l,m}$. On the one hand, the results of Freilich and Guza (1984) completely eliminates the physical contributions due to mutual interactions. On the other hand, at least for $\mu < 1$ these results show the smallest deviation with respect to Stokes results.

The bichromatic case considered here provides a complete quantitative determination of the amplitude dispersion and emphasises its direct physical consequences. Concisely, these refer to the change in wave velocity due to self and mutual interactions. Inaccuracy in the prediction of the amplitude dispersion will obviously result in phase errors with respect to, e.g., field/laboratory observations. However, beyond phase errors, inaccurate prediction of the amplitude dispersion may lead to much more dramatic deviations. These deviations are related to the formation of instability mechanism known as modulational instability, discussed next.

4.2.3. MODULATIONAL INSTABILITY

Narrowbanded wave fields which propagate over relatively deep water tend to develop modulational instability. Such an instability leads to a relatively rapid grow of a field's modulation at the expense of the carrier wave energy. Coastal waters though are typically shallow, and therefore, coastal wave fields are commonly not affected by modulational instability. However, model forecasting of coastal waves may be affected by such a mechanism if it wrongly predicts the amplitude dispersion.

The role of the amplitude dispersion in the development of the modulational insta-

bility is qualitatively described by Lighthill (2001) (page 462). Briefly speaking, the amplitude dispersion restructures the form of the carrier wave such that it becomes shorter in front of the amplitude of the modulation and longer behind, leading to a decreasing rate of energy transport across the modulation, and thus, to the accumulation of energy at the modulation peak. Mathematically, the evolution of the modulational instability can be analyzed by considering the interaction of three waves, namely, by considering the trichromatic case. To this end, the $O(\epsilon)$ solution is now considered to be composed of three components, indicated by the carrier component, $a_p^{(1)}$, and the two side-bands, $a_l^{(1)}$ and $a_m^{(1)}$. The corresponding angular-frequencies are defined as $\omega_l = \omega_p(1 - \delta_{\omega_p})$ and $\omega_m = \omega_p(1 + \delta_{\omega_p})$, where $\delta_{\omega_p} = \Delta\omega/\omega_p$. Accordingly, the solvability condition (4.11) for this case results in the following system of equations:

$$\begin{cases} i\partial_{x_2} a_l = \left(L_{l,l}|a_l|^2 + 2L_{l,p}|a_p|^2 + 2L_{l,m}|a_m|^2 \right) a_l + L_{l,m,p,p} a_p^2 a_{-m} \\ i\partial_{x_2} a_p = \left(L_{p,p}|a_p|^2 + 2L_{p,l}|a_l|^2 + 2L_{p,m}|a_m|^2 \right) a_p + 2L_{p,p,l,m} a_l a_m a_{-p} \\ i\partial_{x_2} a_m = \left(L_{m,m}|a_m|^2 + 2L_{m,l}|a_l|^2 + 2L_{m,p}|a_p|^2 \right) a_m + L_{m,l,p,p} a_p^2 a_{-l} \end{cases} \quad (4.16)$$

where the magnitude notation $()^{(1)}$ that accompanies the amplitudes is removed here to ease the presentation of the equations. Additionally, the formulation of each of the cubic coefficients, e.g. $L_{l,m,p,p}$, is defined in Appendix 4.B. The terms in the parenthesis on the right-hand-side of these equations are the amplitude dispersion components due to self and mutual interactions. These terms are real, and consequently, only result in phase corrections. In contrast, the last terms on the right allow exchange of energy among the components (e.g., Phillips, 1967). These last terms arise due to the interactions that satisfies the equality $2\omega_p - \omega_l - \omega_m = 0$. It could be argued that these last terms should not be included to satisfy the solvability condition, since they correspond to a wavenumber mismatch, i.e., $2k_p - k_l - k_m \neq 0$. However, if the wavenumber mismatch is close enough to zero, that is to say, if $2k_p - k_l - k_m = O(\epsilon^2)$, its contribution is absorbed as part of the slow spatial variation. Therefore, for such conditions, these terms should be included as well.

MODULATIONAL INSTABILITY OF STOKES WAVES

Modulational instability concerns with the evolution of weakly modulated wave fields. Accordingly, it is assumed that the side-band amplitudes are small compared to the amplitude of the carrier component. This allows to reduce the above coupled system (4.16) to the following linear system (the so-called 'pump-wave' approximation, e.g., Craik, 1985):

$$\begin{cases} i\partial_{x_2} a_l = 2L_{l,p}|a_p|^2 a_l + L_{l,m,p,p} a_p^2 a_{-m} \\ i\partial_{x_2} a_p = L_{p,p}|a_p|^2 \\ i\partial_{x_2} a_m = 2L_{m,p}|a_p|^2 a_m + L_{m,l,p,p} a_p^2 a_{-l} \end{cases} \quad (4.17)$$

The solution for a_p corresponds to a monochromatic Stokes wave, while the solution of either a_l or a_m is obtained through

$$\partial_x^2 \tilde{A}_{l/m} + i(\Delta^{(1)} - 2\Delta^{(2)}|A_p|^2)\partial_x \tilde{A}_{l/m} - L_{l,m,p,p}L_{m,l,p,p}|A_p|^4 \tilde{A}_{l/m} = 0 \quad (4.18)$$

which is derived by combining the first and last equations of (4.17), through substitution for a_l or for a_m , where

$$\begin{cases} A_l = \tilde{A}_l \exp(-i2L_{l,p}|A_p|^2 x) \\ A_m = \tilde{A}_m \exp(-i2L_{m,p}|A_p|^2 x) \\ \Delta^{(1)} = k_l + k_m - 2k_p \\ \Delta^{(2)} = L_{l,p} + L_{m,p} - L_{p,p} \end{cases} \quad (4.19)$$

and recall that the definition of the j^{th} complex-amplitude, A_j , is given by (4.8). The solution of (4.18) obeys to the following eigenvalues:

$$\sigma = -\frac{i}{2}(\Delta^{(1)} - 2\Delta^{(2)}|A_p|^2) \pm i\sqrt{R} \quad (4.20)$$

where R is defined as

$$R = \frac{1}{4}(\Delta^{(1)} - 2\Delta^{(2)}|A_p|^2)^2 - L_{l,m,p,p}L_{m,l,p,p}|A_p|^4 \quad (4.21)$$

Therefore, the side-bands are expected to grow when $R < 0$, where the growth rate value is provided by $\text{Im}\{\sqrt{R}\}$ ($\text{Im}\{\}$ =the imaginary part). In order to gain some insight into the conditions for which modulational instability is expected to emerge, the assumption of small modulation frequency is being employed. More specifically, it is assumed that $\delta_{\omega_p} = O(\epsilon)$ (i.e., $\Delta\omega \ll \omega_p$). Accordingly, the following asymptotic relations are assumed as well:

$$L_{l,m,p,p} \sim L_{m,l,p,p} \sim \Delta^{(2)} \quad (4.22)$$

which can be understood by letting $L_{l,m,p,p}$ and $L_{m,l,p,p}$ to be defined through the continuous definition (instead of the discontinuous definition applied so far) of $L_{i,j,k,l}$ (see details in Appendix 4.B). Furthermore, the assumption that $\delta_{\omega_p} \ll 1$ also allows to obtain the relation

$$\Delta^{(1)} \sim \partial_{\omega_p}^2 k_p \Delta\omega^2 \quad (4.23)$$

Using these relations, R can be approximated to fourth order (in ϵ or δ_{ω_p}) as follows:

$$R \sim \frac{1}{4}(\partial_{\omega_p}^2 k_p \Delta\omega^2)^2 - \Delta^{(2)}|A_p|^2 \partial_{\omega_p}^2 k_p \Delta\omega^2 \quad (4.24)$$

Accordingly, the requirement that $R < 0$ leads to the following instability condition:

$$1 < \Delta^{(2)}|A_p|^2 \frac{2v^3}{\alpha k_p \delta_{\omega_p}^2} \quad (4.25)$$

This formulation is obtained using the relation $\partial_{\omega_p}^2 k_p = -\partial_{k_p}^2 \omega_p / C_{g,p}^3$, and transforming to the notation described in Appendix 4.C, for which the expressions for $C_{g,p}$ and $\partial_{k_p}^2 \omega_p$

are given in term of the non-dimensional parameters ν and α . An equivalent stability condition is formulated in Appendix 4.C starting with the nonlinear Schrödinger equation (NLSE). A comparison of the two formulations (based on the NLSE and the one formulated here) suggests the relation between the wavenumber correction, $k_p^{(2)}$, defined in (4.96) and the term $\Delta^{(2)}|A_p|^2$. To further explore this relation, the latter is written more explicitly as follows:

$$\Delta^{(2)}|A_p|^2 = (2G_{m,p}V_{m+p,-p} + 2G_{l,p}V_{l+p,-p} - 2G_{p,p}V_{2p,-p})|A_p|^2 + (2G_{m,-p}V_{m-p,p} + 2G_{p,-l}V_{l-p,p})|A_p|^2 \quad (4.26)$$

Under the assumption of small modulation frequency and that each of the terms above are smooth enough around $\Delta\omega = 0$ (see details in Appendix 4.B), the first group of terms on the right-hand side of (4.26) converges to the definition of the wavenumber correction due to self interaction, while the second converges to a correction due to interaction between the primary component and the component that represents the wave-induced current. Therefore, at least qualitatively, the term arises through the analysis of NLSE, $k_p^{(2)}$, and the one found here, $\Delta^{(2)}|A_p|^2$, seem to provide the same physical representation. Additionally, these terms also determine the condition for modulational instability. Such that, stability is guaranteed only if the values of these terms are negative. This condition is clearly seen based on the fact that the parameters ν and α are always positive. This condition also highlights the opposite roles of the wavenumber correction due to self interaction and the correction due to the interaction of the primary component with the wave-induced current. As given by the definition of (4.26), the former is positive, and thus, triggers energy focusing (as qualitatively explained in Lighthill, 2001, page 462), whereas the latter is negative, and therefore, provides effect of stabilization (as discussed by Whitham, 1974 and Janssen and Onorato, 2007). Finally, quantitative comparison of $k_p^{(2)}$ as given by NLSE and $k_p^{(2)} = \Delta^{(2)}|A_p|^2$ as obtained through the different quadratic formulations is demonstrate in Fig. 4.4.

The results above are compared with the corresponding result of the NLSE (Appendix 4.C). The latter demonstrates the well-known modulational instability threshold of $\mu > 1.363$. As expected, the Boussinesq models are not exposed to this instability mechanism. Surprisingly though, this determination does not apply to the formulation by Nwogu (1993), demonstrating relatively weak positive values of $k_p^{(2)}/|A_p|^2$. On the other hand, the fully dispersive models are strongly affected by modulational instability. The important result revealed here is that these models obey to a much lower instability threshold. Consequently, using these formulation, predictions of narrow-banded fields over coastal waters may be affected significantly by false unstable evolution. This finding raises questions concerning the growth rate of the modulation and the ranges of δ_{ω_p} for which this mechanism is expected to emerge. Answers to these questions are discussed through Fig. 4.5.

Fig. 4.5 presents the growth rate of modulational instability as a function of the modulation frequency, Δf (recall that $\delta_{\omega_p} = \Delta f / f_p = \Delta\omega / \omega_p$), for three $k_p h$ values. For two of which ($k_p h = 1.07$ and $k_p h = 1.33$), instability is unexpected, and for the third ($k_p h = 2.10$), instability is expected to be relatively weak. The growth rate is calculated

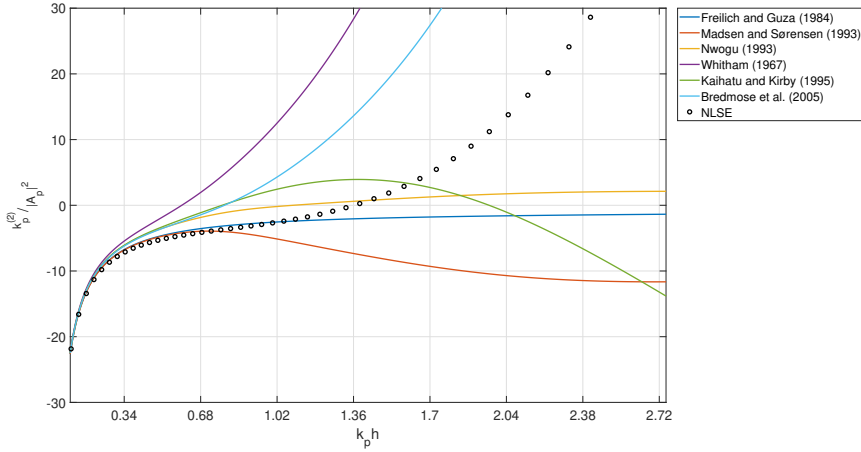


Figure 4.4: Modulational stability and unstable regions as predicted by the different quadratic formulations. Instability is expected over $k_p h$ values for which $k_p^{(2)} > 0$.

based on (4.21), which is not subjected to the small modulation frequency approximation. Note that the growth rate results based on (4.21) are expected to be somewhat weaker than those that would have been obtained through the approximated expression (4.24) (see Liu et al., 2022). Also note that the values presented are normalized by the expressions of the growth rate and modulation frequency that are obtained for the maximum growth rate (according to NLSE) over infinitely deep water (see expressions (4.104) and (4.105) in Appendix 4.C).

The results presented by the right panel of Fig. 4.5 (corresponding to $k_p h = 2.10$) were calculated using the following parameters: $f_p = 0.65$ Hz, $a = 0.1$ m and $h = 1.2$ m. These results show that the fully dispersive formulations of Bredmose et al. (2005) and Whitham (1967) are subjected to much stronger growth rates than the expected growth rate based on NLSE. The maximum growth rates and modulation frequencies presented by these model are even greater than the ones which are expected for infinitely deep water (which correspond to the values of 1 and $\sqrt{2}$, respectively). Note that the model by Kaihatu and Kirby (1995) predicts zero growth rate for $k_p h = 2.10$, a result that is consistent with the stability ranges shown in Fig. 4.4.

The results for $k_p h = 1.07$ and $k_p h = 1.33$ were obtained using $f_p = 0.65$ Hz, $a = 0.06$ m, $h = 0.5$ m and $f_p = 0.60$ Hz, $a = 0.08$ m, $h = 0.8$ m, respectively. It is remarkable to see that even for these cases, for which modulational instability is not expected to emerge at all (as emphasized by the zero values of NLSE), the growth rates and modulation frequencies demonstrated using the fully dispersive formulations are significant.

THE IMPACT OF MODULATIONAL INSTABILITY ON THE EVOLUTION OF IRREGULAR WAVES

The stability analysis presented so far allows to explain unstable evolution for the three wave interaction case (i.e., monochromatic cases subjected to small side-bands). However, the significance of modulational instability is not obviously determined for the

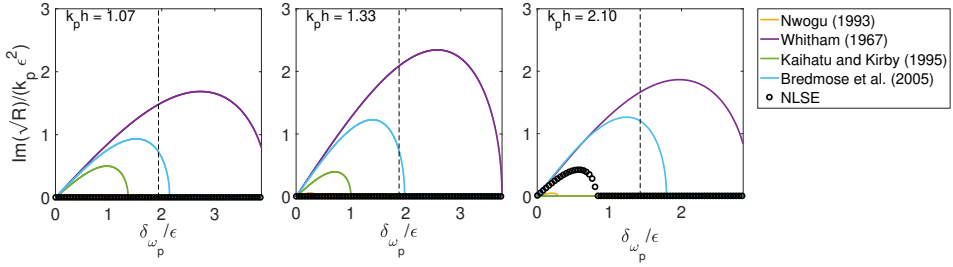


Figure 4.5: Normalized growth rate of modulational instability as a function of normalized modulation frequency as obtained by the different model formulations for three different values of μ (recall that $\epsilon = 2|A_p|k_p$). The maximum modulation frequency considered is $\Delta f = 0.5f_p$. The vertical dashed line crosses in the middle of each panel, thus indicates the value equal to a quarter of the peak frequency.

4

more general irregular cases. Two different perspectives were proposed to give an indication for the expected impact of modulational instability on the evolution of irregular wave fields. The first, due to Alber (1978), relies on statistical arguments which result in the ratio between the expected modulation scale (a representative scale over which coherent structures due to modulational instability are formed) and the correlation scale (a representative scale over which the field is still correlated). The second, due to Onorato et al. (2001), relies on physical arguments which concern the ratio between nonlinear and dispersion effects (equivalent arguments underlying the Ursell parameter). Ultimately, these two perspectives share the same parameter, commonly referred to as the Benjamin-Feir Index (BFI) (Janssen, 2003). An expression for this parameter is given by (4.106) based on the parameter β (see Appendix 4.C). Here though, the BFI parameter is written in terms of $k_p^{(2)}$ as follows:

$$\text{BFI} = \sqrt{k_p^{(2)} \frac{c\nu^3}{\alpha k_p \delta_{\omega_p}^2}} \quad (4.27)$$

This expression is merely the square root of the right-hand-side of (4.25). Small modification though is introduced by the parameter c . The value of this parameter is $c = 3.2$, selected such that the BFI value according to NLSE equals 1 for typical wave conditions offshore (see details in Appendix 4.C). Furthermore, δ_{ω_p} should be interpreted now as the bandwidth parameters, which defines the ratio between a representative of the spectral bandwidth and the peak frequency, ω_p (see specific definition in Appendix 4.C). Additionally, the wave steepness should now be interpreted as a typical steepness value, which commonly taken as $2k_p|A_p| = k_p H_s/2$, where H_s is the significant wave height.

The BFI values as obtained by the NLSE and the different quadratic formulations are examined and compared through the following example. The example considers a shoaling wave field that is characterized by a JONSWAP spectrum with $T_p = 2.25$ sec and $H_s = 0.2$ m (similar to the wave conditions of experiment A2 by Ruessink et al., 2013). The water depth is assumed to increase linearly from a value of $h = 0.2$ m and up to $h = 4$ m. It is assumed that over this shoaling region H_s stays constant (see, e.g., Ruessink et al., 2013). However, k_p does change and is determined by the linear dispersion relation

according to the mild slope assumption. These wave conditions result in a steepness value of $2k_p|A_p| \sim 0.2$ at the shallowest point and a value of $2k_p|A_p| \sim 0.08$ at the deepest point. The results of BFI as a function of $k_p h$ are presented in Fig. 4.6 for three different values of the peak-enhancement factor: $\gamma = 1, 3.3, 10$.

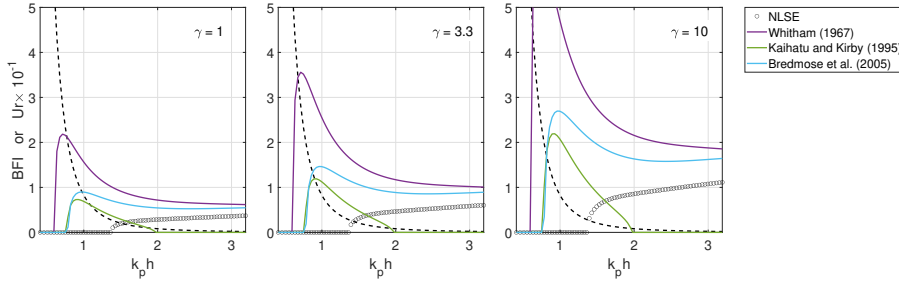


Figure 4.6: The BFI versus $k_p h$ as obtained by NLSE and the different quadratic formulations. The results are based on a shoaling wave field characterized by JONSWAP spectrum with $T_p = 2.25$ sec, $H_s = 0.2$ m and for three different peak-enhancement factor: $\gamma = 1, 3.3, 10$. The black dashed line provides the corresponding U_r number (factored by 10^{-1}).

The results shown in Fig. 4.6 provide further evidence for the expected effect of modulational instability on the predictions according to the fully dispersive quadratic formulations. The discrepancies are particularly significant over $0.5 < k_p h < 2$, a region where the effect of modulational instability is expected to be weak or absent (as confirmed by the NLSE, and see also additional support provided by results of Akrish et al., 2016, Fig. 5). The results also demonstrate the effect of increasing γ . Higher γ values correspond to narrower spectra, and thus also to weaker dispersion effects (or larger correlation scale). Consequently, as γ increases, modulational instability becomes more dominant. Finally, the inclusion of the U_r number highlights the significance of the results shown by the fully dispersive quadratic formulations. The U_r number suggests that over $0.5 < k_p h < 2$ the expected wave evolution can be characterized as quasi-linear. However, the BFI due to the fully dispersive formulations suggests that over this region of $k_p h$, the evolution may be significantly affected by the nonlinear modulational instability mechanism. This point is further demonstrated and discussed through the following numerical example.

BICHROMATIC GROUP EVOLUTION OVER CONSTANT DEPTH

The example considered here concerns the evolution of a bichromatic wave group in a 60 m long flume with constant depth of $h = 0.8$ m. The group is assumed to be composed of a primary frequency, $f_3 = 0.60$ Hz, that is subjected to a side-band frequency of $f_2 = 0.45$ Hz, and a forced subharmonic frequency of $f_1 = 0.15$ Hz ($f_1 = f_3 - f_2$). The corresponding incoming amplitudes are assumed to be $amp_3 = 0.08$ m and $amp_2 = 0.008$ m, where the amplitude of the forced subharmonic is obtained based on (4.9). These specifications result in the following primary wave parameters:

$$\begin{cases} k_3 h = 1.33 \\ \delta_{\omega_3} = 0.25 \end{cases} \quad (4.28)$$

Therefore, as suggested by Fig. 4.5 (middle panel), the modulation of the group is expected to grow along the flume following the predictions by Whitham (1967) and Bredmose et al. (2005). Modulational growth indeed occur in both of these model formulations as implied by the subharmonic growth shown in Fig. 4.7.

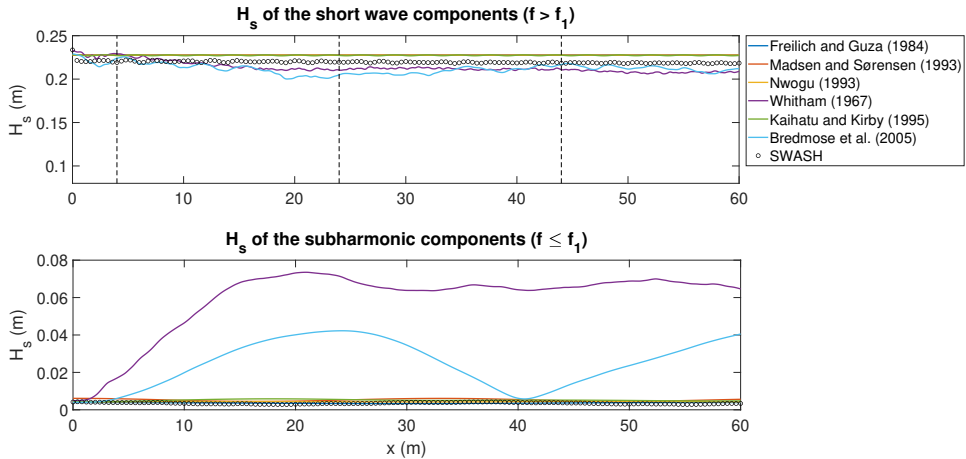


Figure 4.7: Bichromatic group evolution in a flume of constant depth (shown in terms of the significant wave heights, H_s), as predicted by the different model formulations and the SWASH model. The vertical dashed lines shown in the upper panel (located at $x = 4$ m, 24 m, 44 m) approximately indicate the spatial recurrence of the group's focusing/defocusing as obtained by the prediction following Bredmose et al. (2005).

The results shown in Fig. 4.7 are obtained numerically using a spatial step of $\Delta x = 0.05$ m and a spectral step of $\Delta f = 0.05$ Hz, where the highest frequency considered is $f_{max} = 4f_3$. Based on these parameters, the spatial-dependent solution of the quadratic system, (4.1), is achieved through the classical fourth-order Runge–Kutta (RK4) method. Also note that the solutions shown here are phase-averaged over ten different realisations (assuming random phases for a_3 and a_2 at the flume's boundary for each realization). Finally, the results of the quadratic models are compared with the highly accurate SWASH model (Zijlema et al., 2011), which is implemented here using two vertical layers, spatial step of $\Delta x = 0.02$ m, time step of $\Delta t = 0.005$ sec and simulation time of 10 min, where the results shown here are time-averaged over the last 5 min.

The significance of the results shown in Fig. 4.7 can be explained using the Ursell parameter, (4.3). The parameter value of the present example is estimated as $U_r \sim 4.4$, indicating that the amplitude spectrum, and accordingly also the significant wave heights, are expected to stay approximately constant along the flume. The results show that most of the quadratic formulations and SWASH indeed describe this permanent behaviour, demonstrating roughly constant H_s values of the shorter and longer waves (the small oscillation of the short wave prediction according to SWASH arises since it excludes the bound superharmonics at the incoming boundary). In contrast, the predictions of Whitham (1967) and Bredmose et al. (2005) present significant deviations from the prediction of SWASH and the expected outcome based on Ursell parameter. These deviations are the result of modulational instability, giving rise to significant energy transfers

between the carrier and the side-band components. Accordingly, the initial weak modulation, which forces relatively small subharmonic response, develops into a strong modulation and an abnormal subharmonic growth. As demonstrated by the lower panel of Fig. 4.7, the prediction of the subharmonic H_s following Whitham (1967) and Bredmose et al. (2005) is an order of magnitude higher than expected. Additionally, note that the amplified side-bands also force a significant subharmonic response at $f = 2f_1$. Eventually, the significant growth of the side-bands and the corresponding modulations is restricted by energy conservation. This leads to back and forth transfers of energy and to the well-known long distance behavior of focusing/defocusing recurrence (e.g., Lake et al., 1977), which is demonstrated through the prediction of Bredmose et al. (2005) in Fig. 4.8. The energy spectra shown in Fig. 4.8 clearly demonstrate the impact of the modulational instability mechanism. The initial weakly modulated monochromatic field evolves into an almost fully modulated bichromatic field due to intensive energy exchanges between the carrier and the side-band components. Close to the end of the flume, the initial energy spectrum is almost recovered (see lower-right panel Fig. 4.8).

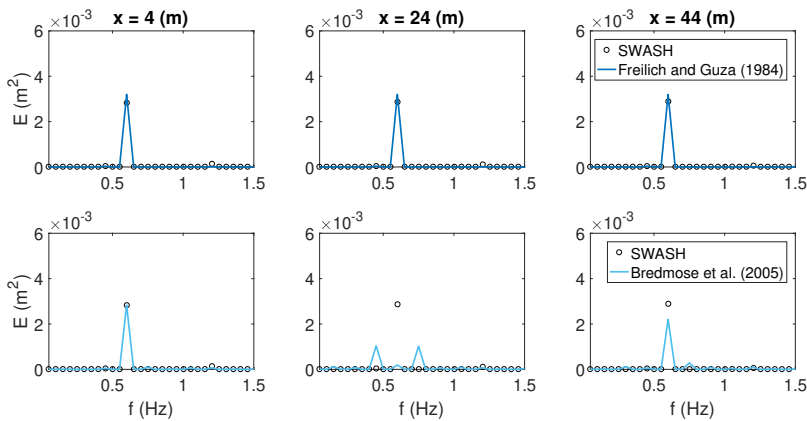


Figure 4.8: Energy spectra demonstrating the stable group's evolution according to Freilich and Guza (1984) and the spatial recurrence of the group's focusing/defocusing as obtained by the prediction following Bredmose et al. (2005).

To summarize, the analysis presented in this section shows that the positive effect of improving the dispersion on the linear behaviour of wave fields also involves an unfavorable effect on the nonlinear evolution. Nonlinear effects are governed by the quadratic interaction coefficients, $V_{l,m}$, and generally, also by higher-order factors which are neglected based on the quadratic modelling approach. As a consequence, a change of $V_{l,m}$ due to improvement of the linear dispersion relation also involves a change of the neglected higher-order residual. It turns out that this residual becomes significant for the fully dispersive models, leading to over prediction of the amplitude dispersion, and as a consequence, to changes in the modulational instability mechanism, including the instability threshold, the growth rate and the modulation ranges over which this mechanism is expected. Hence, fully dispersive quadratic formulations not only tend to develop significant phase errors, but are also exposed to intensive energy exchanges trig-

gered by false modulational instability, which may even take place over relatively shallow waters, where this mechanism is known to be weak or absent. These errors can lead to significant deviations in predicting the evolution of the primary components, the development of the secondary superharmonics (and therefore the development of the field's skewness and asymmetry) and the generation of subharmonics (the infragravity field).

4.3. QUADWAVE1D: A FULLY DISPERSIVE QUADRATIC MODEL FOR COASTAL WAVE PREDICTION IN ONE DIMENSION

The aim of this section is to develop a new fully dispersive quadratic model for coastal wave predictions which is not exposed to modulational instability. Moreover, it is aimed that this new formulation will adequately describe energy exchanges due to super and sub wave interactions, and thus, will adequately predict nonlinear wave development. Instead of a rigorous physical-based formulation, the formulation proposed here is based on a parameterization which relies on available data. This formulation aims to find the quadratic coefficients that will lead to the most adequate prediction capabilities, while using the full dispersion relation as a constraint. The search for the optimal $V_{l,m}$ is subjected to additional constraints which are provided by general properties required for any candidate of $V_{l,m}$. These general properties are detailed next.

4.3.1. GENERAL PROPERTIES FOR THE QUADRATIC INTERACTION COEFFICIENTS

The properties required to be satisfied by the quadratic interaction coefficients are explained in the following. The starting point is the definition of η based on the Fourier series in (4.2). Following this starting point, the reality of η yields the condition

$$(a_n)^* = a_{-n} \quad (4.29)$$

Based on this condition and assuming that k_n and $V_{l,m}$ are defined as real functions, the general quadratic formulation (4.1) leads to the following properties:

$$\begin{cases} k_{-n} = -k_n \\ V_{-l,-m} = -V_{l,m} \end{cases} \quad (4.30)$$

Without loss of generality, it will be convenient to assume the following symmetry:

$$V_{l,m} = V_{m,l} \quad (4.31)$$

This symmetry indeed holds for all the quadratic formulations presented so far. As a consequence of the properties defined by (4.30) and (4.31), the following result is obtained:

$$V_{l,-l} = -V_{l,-l} = 0 \quad (4.32)$$

An additional property is obtained through the analysis of the dynamical behavior of a typical triad interaction of the quadratic system. To this end, consider the following triad model:

$$\begin{cases} \partial_x a_1 - i k_1 a_1 = -i 2 V_{3,-2} a_3 a_{-2} \\ \partial_x a_2 - i k_2 a_2 = -i 2 V_{3,-1} a_3 a_{-1} \\ \partial_x a_3 - i k_3 a_3 = -i 2 V_{1,2} a_1 a_2 \end{cases} \quad (4.33)$$

This model is derived based on the quadratic model (4.1), by restricting the dynamics to three frequencies which satisfy the relation $\omega_1 + \omega_2 = \omega_3$. The corresponding coupled equations for the variance spectrum, $E_j = a_j a_{-j}$, are given by

$$\begin{cases} \partial_x E_1 = 4 V_{3,-2} \text{Im}\{a_3 a_{-2} a_{-1}\} \\ \partial_x E_2 = 4 V_{3,-1} \text{Im}\{a_3 a_{-2} a_{-1}\} \\ \partial_x E_3 = -4 V_{1,2} \text{Im}\{a_3 a_{-2} a_{-1}\} \end{cases} \quad (4.34)$$

This system leads to the following Manley-Rowe relations (e.g., Craik, 1985):

$$\partial_x \left(\frac{E_1}{V_{3,-2}} + \frac{E_3}{V_{1,2}} \right) = 0, \quad \partial_x \left(\frac{E_2}{V_{3,-1}} + \frac{E_3}{V_{1,2}} \right) = 0, \quad \partial_x \left(\frac{E_2}{V_{3,-1}} - \frac{E_1}{V_{3,-2}} \right) = 0 \quad (4.35)$$

As is clearly described by these relations, the evolution of the variance spectrum is bounded if the quadratic coefficients $V_{1,2}$, $V_{3,-1}$ and $V_{3,-2}$ have the same sign. In that case, the wave components are periodically exchanging energy (energy loss by a_1 and a_2 is gained by a_3 and vice versa). Therefore, each variance component, E_j , is spatially oscillating, which implies on a conservative interaction (see further details by Craik, 1985 and Vanneste, 2005). This leads to the general conclusion that in order to obtain a quadratic formulation that is characterized by conservative and bounded triad interactions, its super and sub interaction coefficients should have the same sign, namely,

$$\text{sgn}\{V_{l,m}\} = \text{sgn}\{V_{l,-m}\} \quad (4.36)$$

for which

$$\text{sgn}\{l+m\} = \text{sgn}\{l-m\} \quad (4.37)$$

Finally, the last property considered here is derived from the solutions of the bound super and sub harmonics. Specifically, it is required that $V_{l,m} > 0$ for $l+m > 0$. Referring back to (4.10), and following the linear dispersion relation, this property means that

$$\begin{cases} G_{l,m} > 0, \quad \text{sgn}\{l\} = \text{sgn}\{m\} \\ G_{l,m} < 0, \quad \text{sgn}\{l\} = -\text{sgn}\{m\} \end{cases} \quad (4.38)$$

Namely, secondary bound superharmonics are in phase with respect to the primary forcing components, whereas secondary bound subharmonics are 180° out of phase with respect to the primary forcing.

4.3.2. A PARAMETRIC DERIVATION OF IMPROVED FULLY DISPERSIVE QUADRATIC COEFFICIENTS

Generally speaking, there are infinitely fully dispersive formulations that can be defined, which satisfy the general properties of $V_{l,m}$ as defined above. Nevertheless, it is attempted here to find the $V_{l,m}$ that optimizes prediction capabilities of nonlinear wave

evolution. Since the interest here is devoted to the dynamics of coastal waves, the search is for $V_{l,m}$ with optimal performance over water depths that roughly satisfy $\mu \leq 2$.

In contrast to the conventional rigorous formulation approach, the search for the optimal $V_{l,m}$ is performed here through an alternative approach using data of laboratory experiments and the well-validated time-domain model SWASH. Such an approach requires an ensemble of wave simulations which were conducted under the desired depth conditions and which describe spatially evolving and stationary (time-periodic) wave fields. For each such simulation, it is required to extract the corresponding complex-amplitude vector and its spatial derivative at several different locations in order to construct an algebraic system which can be solved for $V_{l,m}$ (alternatively, it is also possible to construct similar system based on the energy-flux gradients and the bispectrum). This complex process requires large data sets with different conditions and requires to correctly evaluate numerical derivatives which pose difficulties due to the presence of noise. An additional difficulty arises as a result of the dependence of the extracted $V_{l,m}$ values on the amplitudes themselves, suggesting different values of $V_{l,m}$ for simulations of different Ursell numbers. Given the complexity of this direct method, an alternative procedure is proposed here. This procedure would not lead to the ambitious goal of finding the optimal values of $V_{l,m}$, but may allow formulating a satisfying and robust solution for $V_{l,m}$, which avoids the dependence on the amplitudes.

The alternative procedure proposed here relies on a weight function, $W_{l,m}$, that is defined through a basic parameter χ and through three additional parameters, α_1 , α_2 and α_3 as follows:

$$W_{l,m} = \exp \left[- \left(\frac{\chi}{\alpha_3} \right)^{\alpha_2} \right] \quad (4.39)$$

where χ is defined as

$$\chi = |k_{lm}| h \left(\frac{|k_{lm}|}{|k_n|} \right)^{\alpha_1} \quad (4.40)$$

and where α_1 , α_2 and α_3 define ranges of positive numbers over which the optimization is performed. This weight function together with the quadratic coefficients suggested by Bredmose et al. (2005) are used to define the following weighed coefficients:

$$V_{l,m}^{WQC} = W_{l,m} V_{l,m}^{BC} \quad (4.41)$$

where the superscripts *WQC* and *BC* stand for 'Weighted Quadratic Coefficients' and 'Bredmose Coefficients', respectively. Thus, instead of finding many discrete optimal values of $V_{l,m}$ directly, the optimization problem proposed here amounts to finding only three values of α_1 , α_2 and α_3 which minimize the prediction errors with respect to data of laboratory experiments and SWASH. It remains to explain the selected functional structure of the weight function (which is also defined by χ) and the choice to use $V_{l,m}^{BC}$.

The chosen definition of $W_{l,m}$ is based on the following requirements. First, it should be defined such that $V_{l,m}^{WQC}$ complies with the general properties detailed in Subsection 4.3.1. Second, since in deeper waters triad interactions are far from being resonant and for fully dispersive formulation tend to contaminate the predicted evolution due to over

prediction of the amplitude dispersion, $W_{l,m}$ should converge to zero as μ increases, a requirement that also complies with the assumption that deep water waves may be regarded as quasi-linear over coastal scales. The definition of $W_{l,m}$ as given by (4.39) satisfies the first requirement due to its symmetry with respect to the indices l and m and since it is positive. The second requirement is satisfied as well under the condition that χ is positive and represents in a certain way the parameter μ . The selected exponential structure of $W_{l,m}$ indeed preserves weighted regions that correspond to interactions of waves over relatively shallow waters and weakens weighted regions that correspond to interactions in deep water.

The specific definition of χ , as given by (4.40), is intimately related to the quadratic interaction coefficients of Freilich and Guza (1984) (see Eqs. (4.67)-(4.68)). The implementation of this definition in $W_{l,m}$ generates a structure which roughly describes straight contour lines with a 45° decreasing slope for the superharmonic interactions and a -45° decreasing slope for the subharmonic interactions (see Fig. 4.9). This is more or less the structure of the normalized coefficients and transfer function of Freilich and Guza (1984) (see Janssen, 2006, Fig. 3.6 and Fig. 4.1). Thus, the weighted coefficients, $V_{l,m}^{WQC}$, defined through the functional structure of $W_{l,m}$, the definition of χ and the coefficients of Bredmose et al. (2005) presents a structure similar to that of Freilich and Guza (1984). This choice is motivated by the success of the quadratic coefficients of Freilich and Guza (1984) to accurately describe energy exchanges over shallow waters (e.g., Herbers et al., 2000, De Bakker et al., 2015, Rijnsdorp et al., 2022). Based on this motivation one may argue that the quadratic coefficients of Freilich and Guza (1984) could be used directly. However, following the experience of the present investigation, direct use of the coefficients of Freilich and Guza (1984) under fully dispersive conditions would not yield satisfying results.

At this stage, the roles of α_1 , α_2 and α_3 are introduced. The parameter α_1 allows for some structural deviations of the contour lines including their rotation (see the different contour pattern obtained for different values of α_1 in Fig. 4.9). The parameters α_2 and α_3 determine the dispersion (similar to the definition of the standard deviation) and the steepness (namely, how fast is the transition from 1 to 0) of the contours, respectively. Different values of α_1 , α_2 and α_3 generate different contour patterns of $V_{l,m}^{WQC}$, resulting in different dynamical balance of superharmonics and subharmonics energy transfers. Finally, note that the allowable ranges for α_1 , α_2 and α_3 are limited, so that only reasonable candidates of $V_{l,m}^{WQC}$ are included as part of the optimization. For example, to guarantee the convergence of $V_{l,m}^{WQC}$ to zero for deep water interactions, it is required that $\alpha_1 > 0$ (see Fig. 4.9). Additionally, to allow for a reliable subharmonic bound wave forcing, α_1 should also be subjected to an upper bound limit of around 2 (refer again to Fig. 4.9). Similarly, the values for α_2 and α_3 are limited as well to exclude exceptional and undesirable candidates of $V_{l,m}^{WQC}$.

THE OPTIMIZATION PROCESS

The optimization process is summarized by the following. In total, data of three examples of monochromatic wave propagation along a flume of constant depth are considered. These examples are referred to as E1, E2, and E3. The physical parameters that define each of the examples are summarized in Table 4.1. These include the length of

the flume L , the water depth h , the wave period T , the depth parameter μ , the incoming wave amplitude amp_I and the Ursell parameter U_r .

Table 4.1: Physical parameters of the examples considered for the optimization process.

Example	L (m)	h (m)	T (s)	μ	amp_I (m)	U_r
E1	40	0.4	3.3	0.39	0.03	38
E2	25	0.4	2.5	0.53	0.042	29
E3	10	0.4	2	0.68	0.06	26

These examples were chosen such that the nonlinearity of the generated monochromatic wave is relatively weak (all the examples assigned to similar small U_r values to avoid wave breaking). Additionally, the depth parameters of the examples were selected such that a wide range sample of $V_{l,m}^{WQC}$ values is generated. Specifically, the sample should be concentrated over $(k_l h, k_m h)$ region that corresponds to coastal water depths. The effective sample of $V_{l,m}^{WQC}$ values over $(k_l h, k_m h)$ (including points that correspond to interactions of up to $O(\epsilon^4)$) is described in Fig. 4.9. These points include $V_{l,m}^{WQC}$ values that correspond to the $O(\epsilon^2)$ self interaction of the first harmonic, the $O(\epsilon^3)$ super and sub interactions between the first and the second harmonics, the $O(\epsilon^4)$ self interaction of the second harmonic and the $O(\epsilon^4)$ super and sub interactions between the first and the third harmonics.

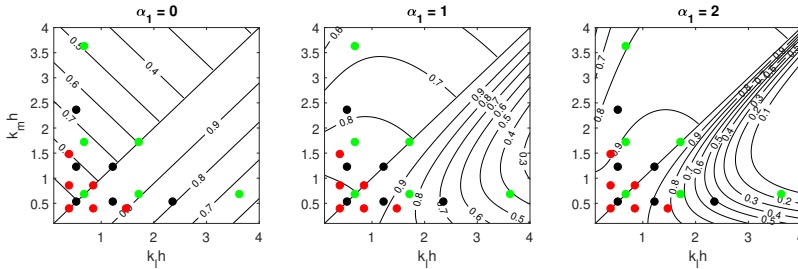


Figure 4.9: The weighted quadratic coefficients, $V_{l,m}^{WQC}$, normalized by the quadratic coefficients of Bredmose et al. (2005) (or simply the weight function $W_{l,m}$) for three values of α_1 and using the parameter values $\alpha_2 = 1.4$ and $\alpha_3 = 5.5$. The dots represent the sampled interaction coefficients that correspond to interactions of up to $O(\epsilon^4)$ due to the different considered examples. Red, black and green dots correspond to E1, E2, and E3 respectively.

Based on the above described examples (E1, E2, and E3), the optimization process strives to find the weighted quadratic formulation (using the full linear dispersion relation and $V_{l,m}^{WQC}$) which minimizes the prediction errors (defined by (4.43)) with respect to given data. The search is performed over the following domain:

$$\begin{cases} \alpha_1 = [0.5, 2] \\ \alpha_2 = [1, 2] \\ \alpha_3 = [2, 10] \end{cases} \quad (4.42)$$

The accuracy of the results at each point $(\alpha_1, \alpha_2, \alpha_3)$ is examined with respect to experimental data and results of simulation using SWASH. To this end, the following normalized error is defined:

$$e(\alpha_1, \alpha_2, \alpha_3) = \sum_j \sum_i |amp_{i,j} - amp_{R,i,j}| / amp_I \quad (4.43)$$

where j runs over the first three harmonics and i runs over the data locations. The reference amplitudes, $amp_{R,i,j}$, are based on SWASH results for E1 and E3, and on the experimental results of Chapalain et al. (1992) for E2. The results through SWASH are obtained using two vertical layers, spatial step of $\Delta x = 0.01$ m, time step of $\Delta t = 0.0025$ sec and simulation time of 10 min. The results of the quadratic model are computed based on the RK4 method, using the first six harmonics only (the first harmonic also serves as the frequency step and the maximum frequency is the sixth harmonic) and a spatial step of $\Delta x = 0.05$ m. Finally, the normalized errors obtained through each of the examples are summed together, providing the point which scores the minimum total normalized error with respect to the reference data. This point is given by $(\alpha_1 = 1, \alpha_2 = 1.4, \alpha_3 = 5.5)$, as partially described (over (α_2, α_3) only) by Fig. 4.10.

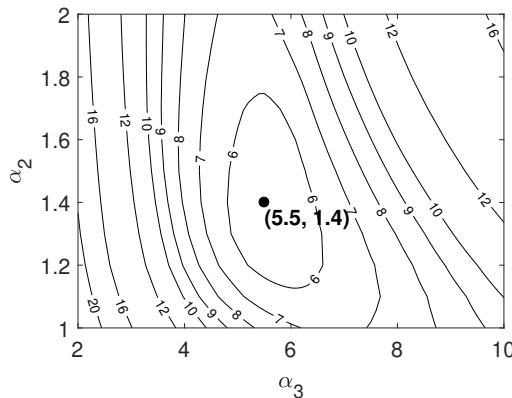


Figure 4.10: Normalized total amplitude error with respect to experimental data following Chapalain et al. (1992) and results of simulation using SWASH for $\alpha_1 = 1$.

The quadratic model with the optimized weighed quadratic coefficients is referred here as the QuadWave1D model. The quadratic interaction coefficients of QuadWave1D are described by the middle panel of Fig. 4.9 (the result of Fig. 4.9 were already computed using the optimal values for α_2 and α_3). Note that, since QuadWave1D is fully dispersive, the middle panel of Fig. 4.9 also describes the normalized second-order bound wave solutions due to QuadWave1D (as is described due to the other considered formulations in Fig. 4.1). Finally, the amplitude dispersion and the modulational instability threshold which are obtained based on QuadWave1D are demonstrated in Fig. 4.11.

The nonlinear properties of QuadWave1D, as presented by Fig. 4.11, describe relatively small overprediction of amplitude dispersion contributions for $\mu < 1$. In contrast, considerable underprediction is observed for deeper water depths. These observations

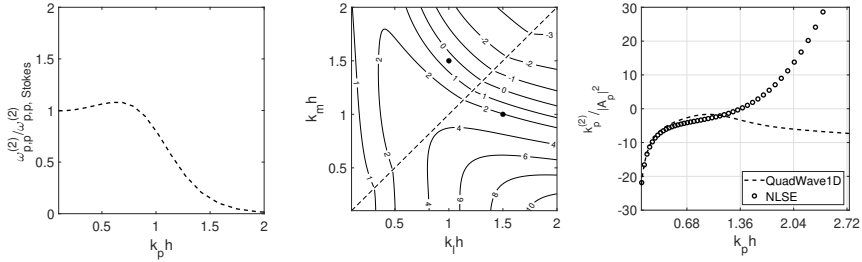


Figure 4.11: Normalized amplitude dispersion due self interactions (left panel), amplitude dispersion contributions due to mutual interactions (middle panel) and modulationally stable/unstable regions (right panel) obtained for QuadWave1D.

4

suggest that for cases for which third-order Stokes theory applies, prediction with QuadWave1D is expected to involve cumulative phase errors. The results of Fig. 4.11 also indicate that predictions using QuadWave1D are not exposed to modulational instability, since QuadWave1D is shown to be modulationally stable.

Ultimately, the satisfying performance of QuadWave1D for the examples E1, E2, and E3 has only been announced so far, but has not been shown. An explicit presentation of this performance is provided by Figs. 4.12-4.14.

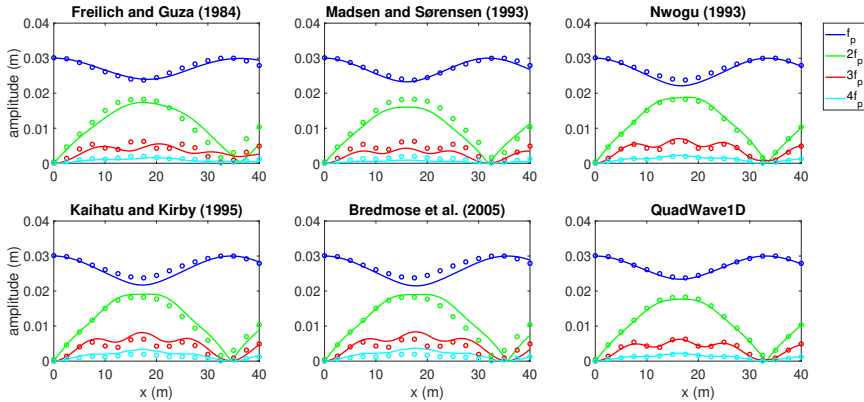


Figure 4.12: Amplitude evolution of the first four harmonics as obtained by the different quadratic formulations (lines) and the SWASH model (circles) for example E1.

The results presented by Figs. 4.12-4.14 suggest that QuadWave1D adequately predicts the wave evolution in all of the three monochromatic examples considered. The adequate prediction is measured here on the basis of the magnitude of the amplitudes and the recurrence length, given by the beating pattern of the harmonics. The comparison between the quadratic formulations shows that QuadWave1D and the model by Nwogu (1993) present the most satisfying agreement with the data. Additionally, exceptional unfavorable results are demonstrated by Kaihatu and Kirby (1995) and Bredmose

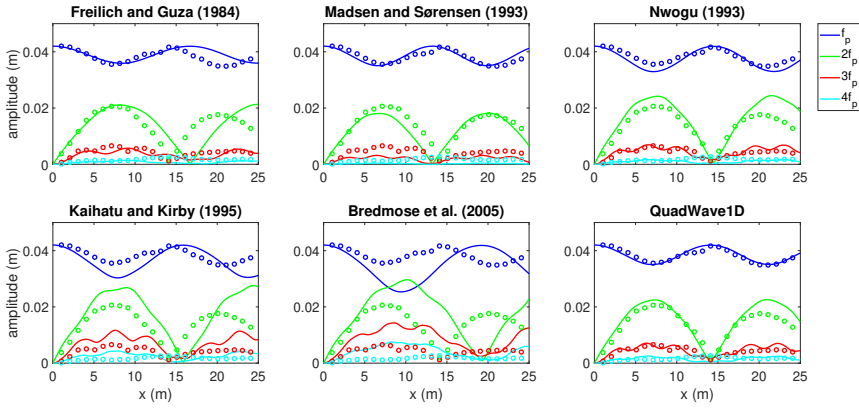


Figure 4.13: Amplitude evolution of the first four harmonics as obtained by the different quadratic formulations (lines) and the laboratory results measured by Chapalain et al. (1992) (circles) for example E2.

et al. (2005). These unfavorable results are attributed to inadequate dynamical balance between the super and sub interactions which is controlled by the structure of $V_{l,m}$ and especially by its dissipation pattern for increasing values of μ . This implies a dependence of the prediction of these models on the maximum considered frequency. To demonstrate this dependence, Fig. 4.15 shows model predictions for the case E2 due to Kaihatu and Kirby (1995), Bredmose et al. (2005) and QuadWave1D, and for two maximum frequency values. Besides the unfavorable maximum frequency dependence of the models by Kaihatu and Kirby (1995) and Bredmose et al. (2005), the results of Fig. 4.15 also suggests the insensitivity of QuadWave1D to the maximum frequency. Note that the results at the upper row of Fig. 4.15 given by the model of Kaihatu and Kirby (1995) can be also compared with equivalent result performed with the same maximum frequency which were considered by Kim and Kaihatu (2021), Fig. 6. This comparison verifies the computation conducted here. In summary, the observed dependence of model prediction on the maximum considered frequency (which satisfies the frequency limit due to numerical stability), constitutes a serious modelling problem. Such a problem requires further analysis which is beyond the scope of the present study.

Finally, the satisfying agreements presented by QuadWave1D should not provide a firm conclusion regarding its overall performance. The judgment concerning the predictive capabilities of QuadWave1D should rather be determined on the basis of independent cases, which are considered next.

4.4. MODEL VERIFICATION

The prediction capabilities of QuadWave1D and the other quadratic formulations considered here are studied through comparisons with different laboratory experiments. For some examples, results due to the SWASH model are included as an additional reference. The presented verification considers first two basic monochromatic cases, and later on, also more general cases where the incoming wave field is either bichromatic or

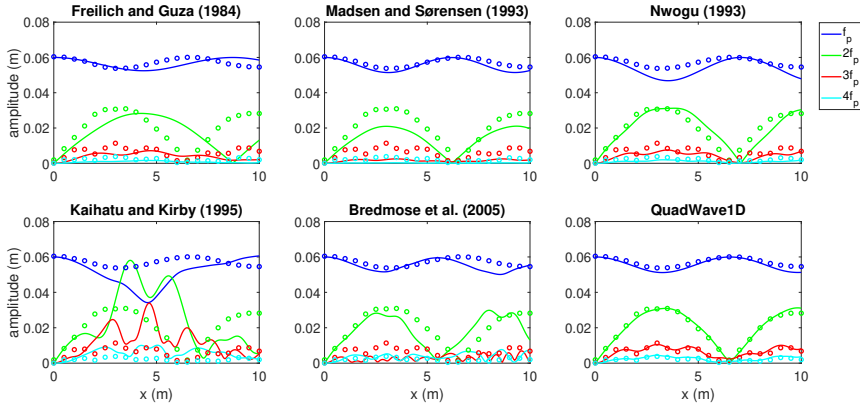


Figure 4.14: Amplitude evolution of the first four harmonics as obtained by the different quadratic formulations (lines) and the SWASH model (circles) for example E3.

described through a continuous spectrum.

Since most of the examples presented here involve bathymetry changes, the quadratic formulation (4.1) discussed so far should be modified to include the effect of wave shoaling (see discussion in Appendix 4.A). This can be readily implemented by using the energy-flux related amplitude, $b_n = a_n \sqrt{C_{g,n}}$, which for the linear case, stays constant over mild slopes (see (4.76)). Therefore, the modified quadratic formulation reads

$$\partial_x b_n - i k_n b_n = -i \sum_r \sqrt{\frac{C_{g,n}}{C_{g,r} C_{g,n-r}}} V_{r,n-r} b_r b_{n-r} \quad (4.44)$$

The quadratic model (4.44) is solved numerically using the RK4 method. For most of the considered examples, the spatial step being used is $\Delta x = 0.05$ m (the exception is the monochromatic case in Subsection 4.4.1 for which $\Delta x = 0.025$ m), while the spectral resolution and thus also the number of realizations are determined for each example specifically. Similarly, all the computations with SWASH are performed here using two vertical layers, a spatial step of $\Delta x = 0.02$ m and a time step of $\Delta t = 0.005$ sec, while the simulation time is determined separately for each example.

4.4.1. MONOCHROMATIC WAVE EVOLUTION

The predictive capabilities of the different quadratic formulations are first tested through two monochromatic examples. The first example is given by the 'Trial D' experiment conducted by Chapalain et al. (1992). This experiment describes the evolution of a progressive monochromatic wave in a flume of constant depth (see schematic illustration in Fig. 4.16). The incoming wave generated by the wavemaker is characterized by a relatively large U_r (see Table 4.2), implying strong nonlinear effects. Such incoming wave conditions provide a challenging case for prediction, especially when the prediction is based on the quadratic formulation which neglects third and higher order terms.

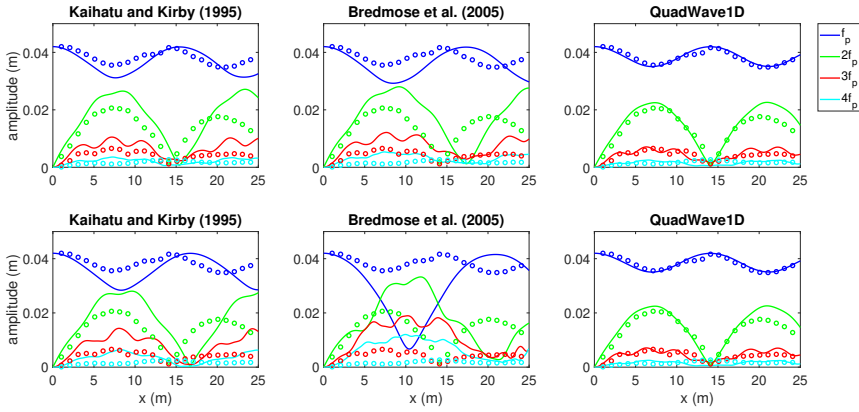


Figure 4.15: Model sensitivity to the maximum considered frequency as obtained for example E2. Results shown at the upper row are based on the maximum frequency $f_{max} = 5f_p$ where f_p is the incoming frequency. Results shown at the lower row are based on $f_{max} = 8f_p$. These results can be also compared with the results shown in Fig. 4.13 for which $f_{max} = 6f_p$.

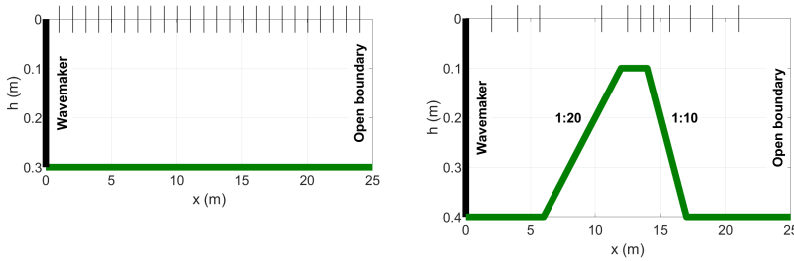


Figure 4.16: Schematic illustration of the experiments conducted by Chapalain et al. (1992) (left panel) and Dingemans (1994) (right panel). The structures of the bathymetries are described by the thick green lines. The thin vertical lines, plotted along the still water level ($h = 0$), indicating measurement locations.

The second example is an experiment conducted first by Beji and Battjes (1993) and later by Dingemans (1994), which describes monochromatic wave propagation over a submerged bar (see illustration in Fig. 4.16). Specifically, 'measuring condition A' (as referred to by Dingemans, 1994) are considered and detailed in Table 4.2. The evolution of the wave field being generated in this example involves several interesting phenomena, which are briefly described as follows. The wave adjacent to the wavemaker can be characterized as a permanent second-order Stokes wave. Over the front slope of the bar the wave steepens, suggesting the development of higher harmonics. This process is accelerated over the head of the bar, where resonance due to triad interactions is nearly met. Ultimately, behind the bar, the increasing water depth decreases the effect of nonlinearity, and therefore, decouples the mutual forcing between the harmonics. As a consequence, this de-shoaling process results with totally differed wave conditions than the incoming conditions (compare the incoming and outgoing amplitudes presented by the panels in Fig. 4.18). This combination of phenomena results from the interplay of

nonlinearity and dispersion. The fact that in this example the roles of both of these wave properties are important makes this example a standard test case for wave model verification.

Table 4.2: Incoming wave parameters (indicated by the subscript ' I ') and maximum Ursell number ($U_{r,max}$) of the considered monochromatic examples.

Example	T (sec)	μ_I	amp_I (m)	$U_{r,I}$	$U_{r,max}$
Chapalain et al. (1992) (Trial D)	2.5	0.454	0.0354	45.2	45.2
Dingemans (1994) (Condition A)	2.02	0.67	0.01	4.5	101.5

The parameters detailed in Table 4.2 indicate that both of the examples describe wave evolution in relatively shallow water depth. Note the distinction between the Ursell number of the incoming wave and the maximum Ursell number. The latter is estimated based on linear shoaling of the incoming monochromatic component. The relatively high U_r value that characterizes the case of Chapalain et al. (1992) indicates on significant energy exchanges between wave harmonics along the entire flume. The second case of Dingemans (1994) also presents high values of U_r , but these are limited only to short segment of the domain. Specifically, U_r of the second case is higher than the validity limit of the second-order Stokes expansion ($U_r = 26$) over the region $10.5 \leq x \leq 14.8$, reaching to a very high value ($U_{r,max}$) at the top of the bar.

These examples are computed with the different quadratic formulations using the first six harmonics for the case of Chapalain et al. (1992) and using the first eight harmonics for the case of Dingemans (1994) (the first harmonic serves as the frequency step and the maximum frequency is the sixth or the eighth harmonic). The comparison between the different quadratic models and the measurements is discussed in the following.

MONOCHROMATIC WAVE EVOLUTION OVER CONSTANT DEPTH

The predictions of the different quadratic formulations for the case of Chapalain et al. (1992) are compared to laboratory observations in Fig. 4.17. As expected, the high value of U_r leads to significant energy exchanges between the harmonics, such that the amplitudes of the first and the second harmonics become approximately equal to each other at certain locations. The predictive capabilities of the models are measured here with respect to the magnitude of the amplitudes and the beat lengths. Generally speaking, the Boussinesq models tend to underestimate the magnitude of the amplitudes, while the fully dispersive models tend to overestimate those magnitudes. Additionally, most of the predictions show some discrepancies of the beat lengths with respect to the measurements. Clearly, the deviations in the predictions are much more pronounced by the model results of the fully dispersive formulations. In part, these pronounced deviations are also attributed to the unfavorable behaviour of these models in the presence of very high frequencies (as briefly discussed in Subsection 4.3.2). The exceptional results are those of Nwogu (1993) and QuadWave1D. These model predictions show good agreement with the laboratory observations in terms of both amplitude values and beat lengths. Note however that the results due to Nwogu (1993) slightly overpredicts the energy transfer between the harmonics, leading to more obvious deviations than those obtained through QuadWave1D.

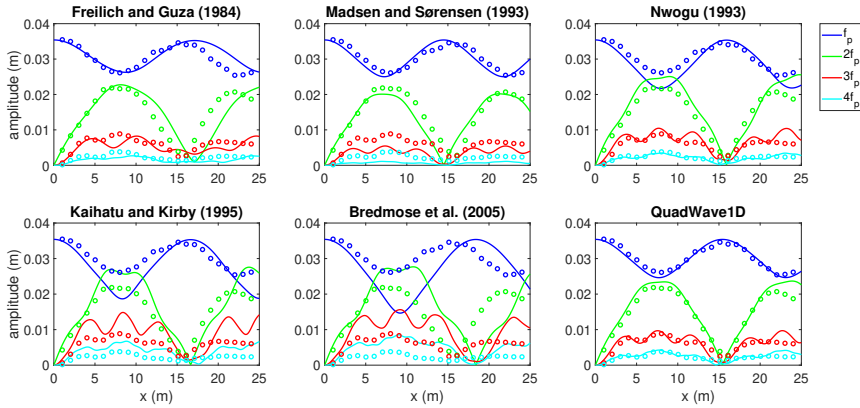


Figure 4.17: Amplitude evolution of the first four harmonics as obtained by the different quadratic formulations (lines) and the laboratory results measured by Chapalain et al. (1992) (circles).

MONOCHROMATIC WAVE EVOLUTION OVER A BAR

The evolution of monochromatic wave over a bar is described by the different quadratic formulations in Fig. 4.18. Generally speaking, the comparison of the computed and measured results suggests that all the formulations capture the expected physical phenomena emerging in this example. Namely, the permanent Stokes behaviour over the incoming zone, the harmonics' growth over the bar and the decoupling of the harmonics in deeper water beyond the bar where they are essentially propagate as linear waves (this process effectively decomposes the initial wave into its harmonics, as nicely described by Beji and Battjes, 1993). However, the main modelling challenge of this example is to correctly describe the development of the harmonics outside the validity range of second-order Stokes theory, i.e., over the region $10.5 \leq x \leq 14.8$. As shown in Fig. 4.18, the fully dispersive models describe excessive energy exchanges between the harmonics and thus inaccurately describe the development of the different amplitudes. As a result, these models mispredict the output spectrum. In addition, these models also describe rapid oscillations attributed to the sensitivity of these models to the presence of very high frequencies (here $f_{max} = 8f_p$ is used, while slightly better predictions of these models are obtained when using $f_{max} = 6f_p$). The predictions of the Boussinesq models, on the other hand, seem much more adequate and show better agreement with the measurements. Nevertheless, some deviations are demonstrated by these predictions as well, given by the under-prediction of Freilich and Guza (1984) and Madsen and Sørensen (1993) and over prediction of Nwogu (1993). Finally, QuadWave1D demonstrates the most adequate results and accurately agrees with the measurements.

To summarize, the two examples considered here provide satisfying verification for the modelling capabilities of QuadWave1D to describe the development of a monochromatic wave under significant nonlinear conditions and under conditions that combine nonlinearity, dispersion and bathymetry changes. The Boussinesq models presented satisfying predictions as well, demonstrating only limited deviations in comparison with the measurements. However, the deviations observed through the fully dispersive mod-

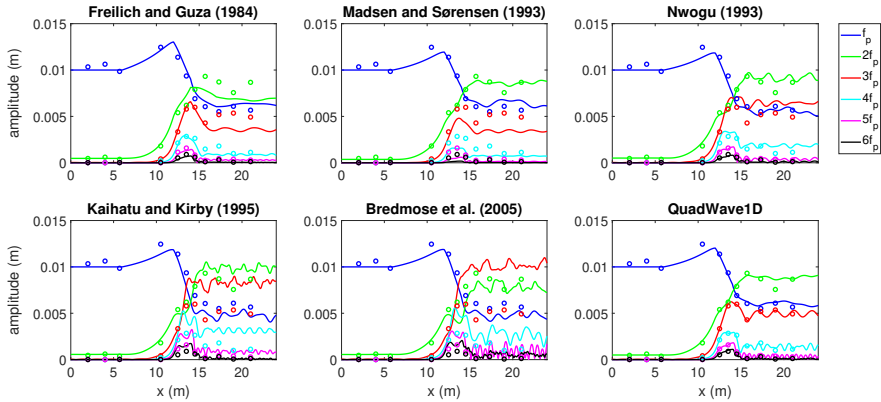


Figure 4.18: Amplitude evolution of the first six harmonics as obtained by the different quadratic formulations (lines) and the laboratory results measured by Dingemans (1994) (circles).

els are significant. The unfavorable behaviour of these models requires further investigation which is beyond the scope of the present study. It seems though that these formulations are sensitivity to the presence of very high frequencies, which creates uncertainty regarding the choice of the maximum frequency considered, and thus, limiting the capabilities of these models to provide reliable predictions. In the following, the predictive capabilities of the different quadratic formulations are further investigated for more general cases involving multi-component wave fields.

4.4.2. EVOLUTION OF BICHROMATIC GROUPS AND IRREGULAR WAVES OVER A SLOPE

The predictions of the different quadratic formulations for more general cases are studied here using two sets of laboratory experiments conducted by Van Noorloos (2003) and Ruessink et al. (2013). Generally speaking, these experiments describe one-dimensional, nonlinear shoaling of wave fields over a mild slope. The settings of these experiments are described schematically in Fig. 4.19 and the parameters of the incoming wave fields are detailed in Table 4.3 and Table 4.4. Model capabilities are examined by comparisons to measured results and to the predictions of SWASH up to the breaking points beyond which the quadratic formulations become invalid. The comparison focuses on the evolution of the primary components and the generation and development of the secondary components (the super and sub harmonics). Special attention is devoted to the modelling performance of the different quadratic formulations to predict the generation and growth of the sub-harmonics (the infragravity components). Finally, recall that the quadratic formulations only account for the incoming wave components. Therefore, the examined cases considered here are such that the effect of wave reflection on the evolution of the primary and secondary components is negligible (Rijnsdorp et al., 2014, De Bakker et al., 2015). Accordingly, the measured data is not separated into incoming and reflected wave components. Nevertheless, the simulations conducted with SWASH attempt to avoid the contribution of the reflected part. This is performed by applying

a radiation condition on the downwave side of the domain at a depth of $h \sim 0.057$ m accompanied by a sponge layer of 5 m in front of it. The combination of these measures allows an effective absorption of both the long and the short wave components, as verified in Fig. 4.20 and Fig. 4.24.

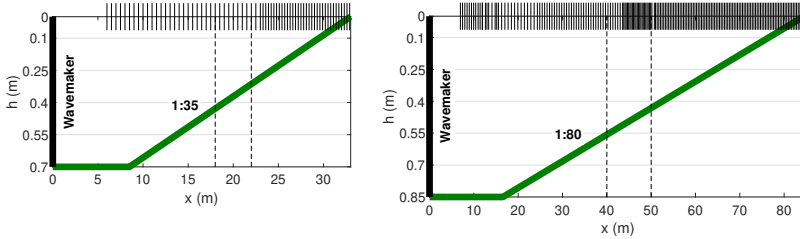


Figure 4.19: Schematic illustration of the experiments conducted by Van Noorloos (2003) (left panel) and Ruessink et al. (2013) (right panel). The structures of the bathymetries are described by the thick green lines. The thin vertical lines, plotted along the still water level ($h = 0$), indicating measurement locations. The vertical dashed lines indicate the locations where computed and measured wave spectra are compared.

BICHROMATIC GROUPS OVER A SLOPE

Three bichromatic examples introduced by Van Noorloos (2003) (i.e., A1, B3 and B5) are considered. Wave predictions for these examples as obtained by the different quadratic formulations are compared to measured and SWASH results in Fig. 4.20. The comparison is presented in terms of the H_s of the primary and super harmonics (defined by $f > f_{ig,max}$ and referred to as the sea-swell components) and the H_s of the sub harmonics (defined by $f \leq f_{ig,max}$ and referred to as the infragravity (IG) components), where the separating frequency takes the following value: $f_{ig,max} = 0.3$ Hz. Additionally, the results of the quadratic formulation are computed using spectral resolution of $\Delta f = 0.025$ Hz and maximum frequency of $f_{max} = 4f_p$ (recall that f_p is the peak frequency). Furthermore, these results define ensemble average of 10 realizations. Finally, the results according to SWASH define time average of the last 6 min, where the total simulation time is chosen to be 10 min.

Table 4.3: Incoming wave parameters for the bichromatic examples of Van Noorloos (2003). The incoming forced amplitude amp_1 of the sub harmonic indicated by f_1 is calculated based on second-order Stokes theory. Additionally, $U_{r,max}$ estimates the Ursell number at the breaking point and $x_{s,max}$ estimates the maximum location for which $U_r < 26$.

Exp.	f_3 (Hz)	f_2 (Hz)	f_1 (Hz)	amp_3 (m)	amp_2 (m)	μ_I	$U_{r,I}$	$U_{r,max}$	$x_{s,max}$ (m)
A1	0.6714	0.4761	0.1953	0.06	0.012	1.43	4.7	41.8	21
B3	0.6470	0.5005	0.1465	0.06	0.024	1.35	5.6	39.2	20
B5	0.6470	0.5005	0.1465	0.06	0.036	1.35	6.0	38.6	19

The values given in Table 4.3 indicate that the considered examples describe incoming wave groups over intermediate water depth. Additionally, these groups are characterized by relatively small incoming U_r value (see $U_{r,I}$ in Table 4.3). Therefore, it is expected that wave evolution up to $x \sim 10$ would agree with the second-order permanent Stokes solution. In fact, the Ursell number only becomes significant around the breaking

area. Thus, the evolution is expected to be quasi-linear, namely, dominated by linear dispersion and shoaling along most of the domain (up to $x \sim x_{s,max}$) for all the considered examples. Based on these expectations, the predictions presented by the fully dispersive models are surprising. These predictions describe significant energy transfers from the primary component (i.e., the component with frequency f_3) to secondary components, as implied by the decrease of the sea-swell H_s and the relatively rapid H_s growth of the IG components. The mechanism which triggers these energy exchanges is attributed to modulational instability.

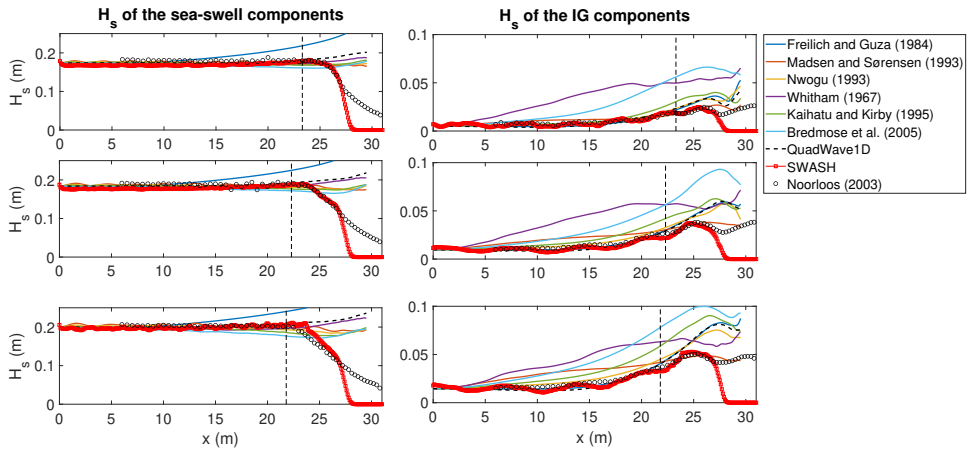


Figure 4.20: A comparison of computed and measured H_s for the bichromatic examples A1 (upper row), B3 (middle row) and B5 (lower row) of Van Noorloos (2003). The vertical dashed lines provide estimation for the wave breaking locations.

The impact of modulational instability on the group evolution may be explained through the data detailed in Table 4.3. The depth parameter of the primary component (given by μ_I) provides an indication whether modulation instability can emerge. Following Fig. 4.4, it is clear that all the three fully dispersive formulations (i.e., the formulations by Whitham, 1967, Kaihatu and Kirby, 1995 and Bredmose et al., 2005) are subjected to modulational instability for all the considered examples. However, the significance of the energy transformation due to modulational instability is determined by the steepness parameter (i.e., ϵ) and the normalized modulation frequency (i.e., δ_{ω_3}). As an example, the wave conditions, based on which the growth rate shown in Fig. 4.5 (left panel) is calculated, approximately describe the wave conditions of example B3 and B5 at $x \sim 15$. Consequently, it is expected that the predictions for these examples following the formulations by Whitham (1967) and Bredmose et al. (2005) will be strongly affected by the modulational instability mechanism. These models indeed describe rapid H_s growth of the IG components, indicating significant modulational growth. On the other hand, the Boussinesq formulations agree better with the measured and SWASH results and with the expectation of quasi-linear evolution. However, exceptional Boussinesq results are still described by the sea-swell H_s prediction due to Freilich and Guza (1984) and by the H_s prediction of the infragravity response due to Madsen and Sørensen (1993). The for-

mer develops due to over prediction of linear shoaling (see the comparison presented in Fig. 4.28). Whereas the latter stems from the nonlinear balance generated by the quadratic coefficients, $V_{l,m}$, which is characterized by relatively strong tendency towards sub interactions (as also described by the $G_{l,m}$ of Madsen and Sørensen, 1993, as given in Fig. 4.1). In summary, it seems that the model by Nwogu (1993) and QuadWave1D describe most adequately the development of the wave groups for the considered examples. These adequate predictions are obtained due to a combination of accurate linear formulation (dispersion and shoaling) and adequate nonlinear balance provided by the quadratic coefficients.

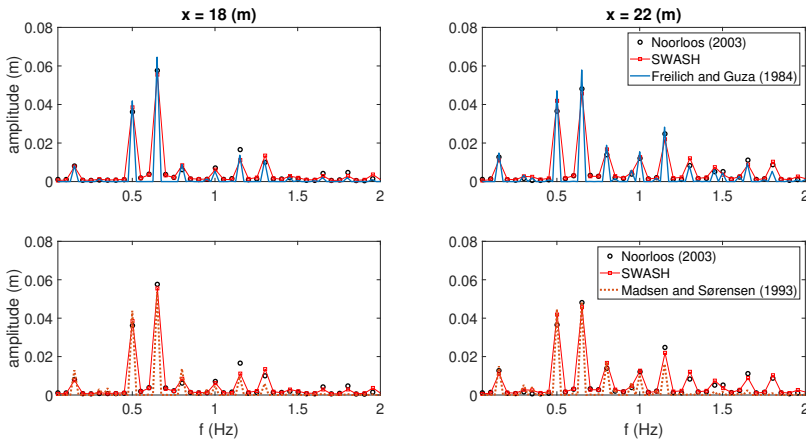


Figure 4.21: A comparison of amplitude spectra as obtained by the measurements, SWASH and the models of Freilich and Guza (1984) and Madsen and Sørensen (1993).

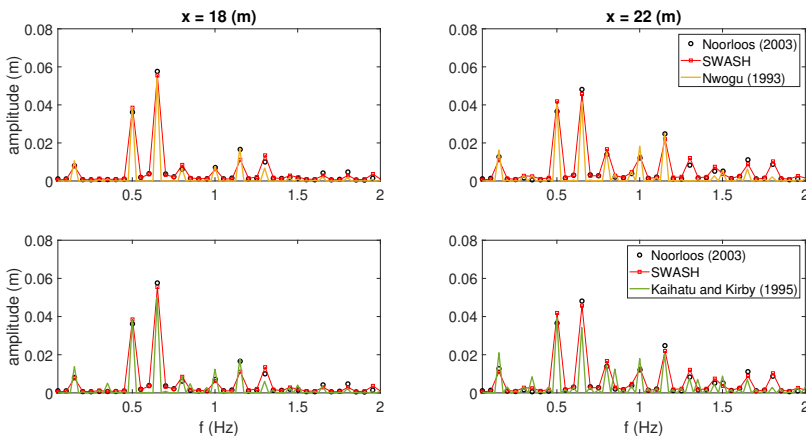


Figure 4.22: A comparison of amplitude spectra as obtained by the measurements, SWASH and the models of Nwogu (1993) and Kaihatu and Kirby (1995).

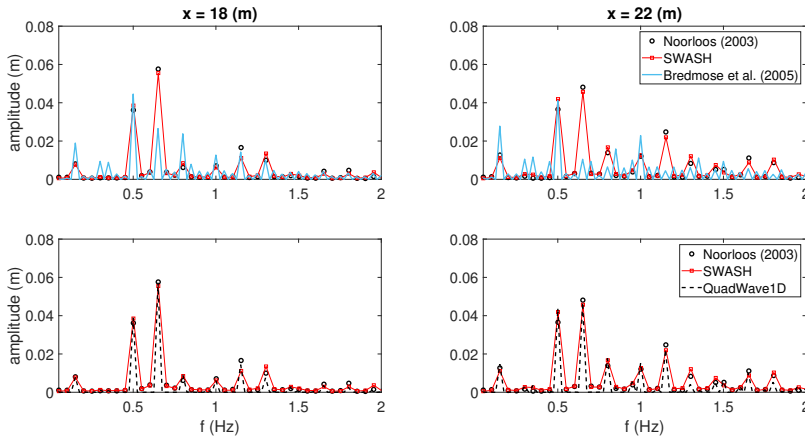


Figure 4.23: A comparison of amplitude spectra as obtained by the measurements, SWASH, QuadWave1D and the model of Bredmose et al. (2005).

The prediction capabilities of the different quadratic formulations is further investigated using example B5, which describes the most significant incoming wave conditions in terms of nonlinearity. Further insight is gained by considering the predicted spectral development of the group along the flume. To this end, Figs. 4.21-4.23 present the amplitude spectra at two different locations in the vicinity of the breaking point. This spectral point of view provides further evidence to the impact of modulational instability on the evolution of the wave group. Especially, the results of Bredmose et al. (2005), but also less prominently the results of Kaihatu and Kirby (1995), show significant energy transfer from the primary component to the side-bands, providing explanation to the amplitude increase of the modulation frequency (as apparent at $x = 18$ m). This initial stage is followed by a significant spectrum broadening towards sub and super harmonics (as presented at $x = 22$ m). The predictions of the rest of the models agree well with the measured and SWASH results. Especially, the results of Freilich and Guza (1984), Nwogu (1993) and QuadWave1D show accurate development of the complete spectrum. The prediction of Madsen and Sørensen (1993) though, tend to under-predict the development of the super harmonics (as also demonstrated earlier for the monochromatic cases).

IRREGULAR WAVES OVER A SLOPE

This part presents the last validation examples devoted to the evolution of irregular wave fields. The aim here is to study the prediction capabilities of the different quadratic formulations for these more general wave conditions. The considered examples are the irregular cases which were experimentally investigated by Ruessink et al. (2013). The generated wave fields are defined based on the JONSWAP spectrum using the parameters detailed in Table 4.4. The computations through the quadratic formulations are based on a spectral resolution of $\Delta f = 0.015$ Hz, maximum frequency of $f_{max} = 4f_p$ and averaging over 60 realizations. The computations through SWASH is based on a simula-

tion time of 60 min, where the results represent time-average of the last 54 min.

Table 4.4: Wave parameters for the irregular examples of Ruessink et al. (2013). The incoming wave fields are defined based on the JONSWAP spectrum requiring the values of f_p , H_s and γ (recall that γ stands for the peak-enhancement factor). Also here, $U_{r,max}$ represents the Ursell number at the breaking point and $x_{s,max}$ indicates the maximum location for which $U_r < 26$.

Exp.	f_p (Hz)	H_s (m)	γ	$f_{ig,max}$	μ_I	$U_{r,I}$	$U_{r,max}$	$x_{s,max}$ (m)
A1	0.6329	0.1	3.3	0.37	1.5	2.1	47.5	61
A2	0.4444	0.2	3.3	0.26	0.9	11.4	52.5	37
A3	0.4444	0.1	20	0.26	0.9	5.7	77.3	49

The computed and measured results are compared in Fig. 4.24 in terms of H_s . Here again, the values of H_s are presented separately for the shorter waves (denoted as the sea-swell components and satisfy $f > f_{ig,max}$) and for the longer waves (denoted as the infragravity (IG) components and satisfy $f \leq f_{ig,max}$), where the separation frequency, $f_{ig,max}$, is provided in Table 4.4 for each of the considered examples. For the intermediate to shallow water depth conditions that characterize these examples, the values of $x_{s,max}$ define the regions over which second-order Stokes theory is expected to be valid. Over these regions, wave evolution is expected to be dominated by linear dispersion and shoaling, while evidence of nonlinear exchanges of energy is expected to be weak. This highlights again the abnormal infragravity responses as presented by the fully dispersive formulations in Fig. 4.24. Here, the explanation for these results is based on the BFI parameter. As an example, refer to the middle panel of Fig. 4.6 which shows the BFI values due to the fully dispersive formulations under the same wave conditions as of example A2. These BFI values indeed suggest that for the considered μ values, wave prediction using the fully dispersive formulations (especially using the model by Whitham, 1967) would be strongly affected by the modulational instability mechanism. This may lead to unexpectedly strong prediction of wave field's modulations, and consequently, to the prediction of unexpectedly strong responses of the infragravity components as indeed suggested by Fig. 4.24. Furthermore, the results of Fig. 4.24 provides an additional evidence to the reliability of wave prediction using QuadWave1D and the Boussinesq models. These models agree well with the measured and SWASH results up until the breaking points. However, also here, the inaccurate shoaling prediction of Freilich and Guza (1984) and the inadequate nonlinear balance due to the quadratic coefficients of Madsen and Sørensen (1993) result in over prediction of the sea-swell H_s and the infragravity H_s , respectively.

Further details explaining the prediction capabilities of the different quadratic formulations are presented in Figs. 4.25-4.27. These results provide a limited view on the spectral evolution as obtained for example A2 close to the breaking point. In order to highlight the modelling capabilities of the infragravity components (which also provide possible indication to the significance of modulational instability), the spectra are plotted through logarithmic scales. The results provide another perspective on the effect of modulational instability, which induces much faster spectral broadening than predicted by the measurements (especially notable by the results of Bredmose et al., 2005 in Fig. 4.27, but also seen less obviously through the results of Kaihatu and Kirby, 1995 in Fig. 4.26). In addition, the tendency of the model by Madsen and Sørensen (1993) to over pre-

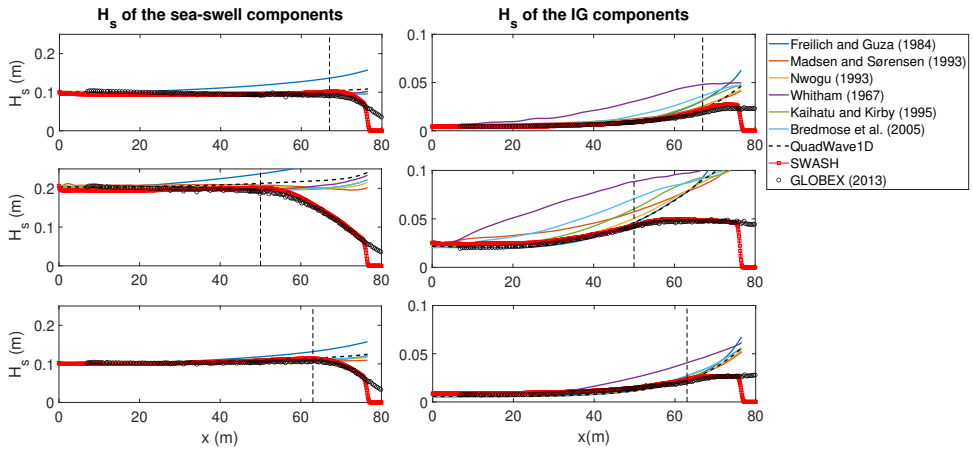


Figure 4.24: A comparison of computed and measured H_s for the irregular examples A1 (upper row), A2 (middle row) and A3 (lower row) of Ruessink et al. (2013). The vertical dashed lines provide estimation for the wave breaking locations.

dict the sub-harmonic responses and to under-predict the super-harmonic responses is revealed again through Fig. 4.25. In summary, QuadWave1D and the models by Freilich and Guza (1984) and Nwogu (1993) seems to generate the most accurate prediction for this example.

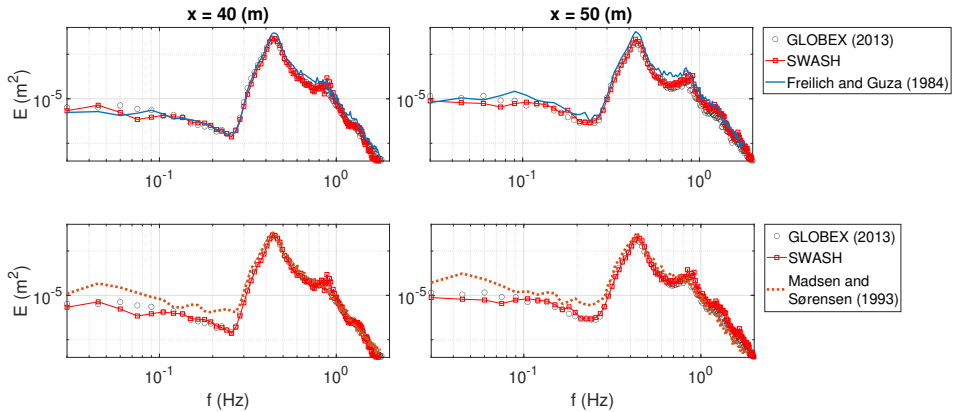


Figure 4.25: A comparison of variance spectra as obtained by the measurements, SWASH and the models of Freilich and Guza (1984) and Madsen and Sørensen (1993).

To summarize, the verification conducted for both bichromatic an irregular wave conditions shows the preferable prediction capabilities of QuadWave1D and the Boussinesq models. However, all the examples considered showed the tendency of Freilich and Guza (1984) to over predict the sea-swell components due to inaccurate formulation of linear shoaling and the tendency of Madsen and Sørensen (1993) to under-predict the

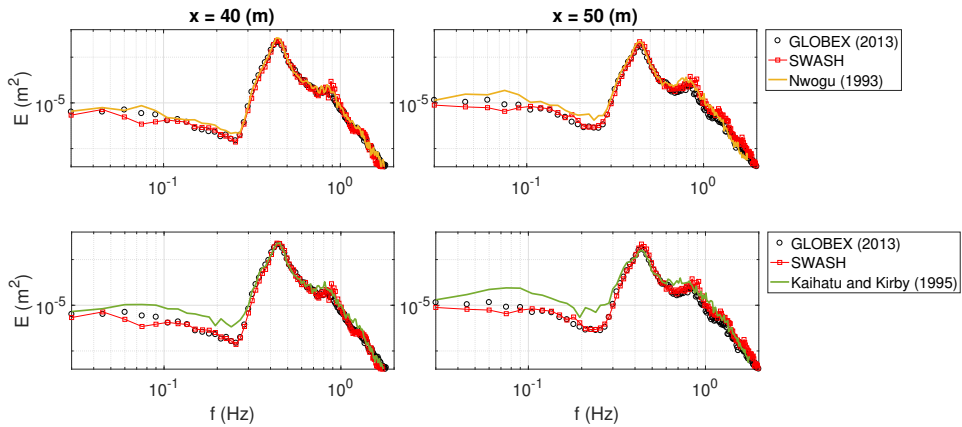


Figure 4.26: A comparison of variance spectra as obtained by the measurements, SWASH and the models of Nwogu (1993) and Kaihatu and Kirby (1995).

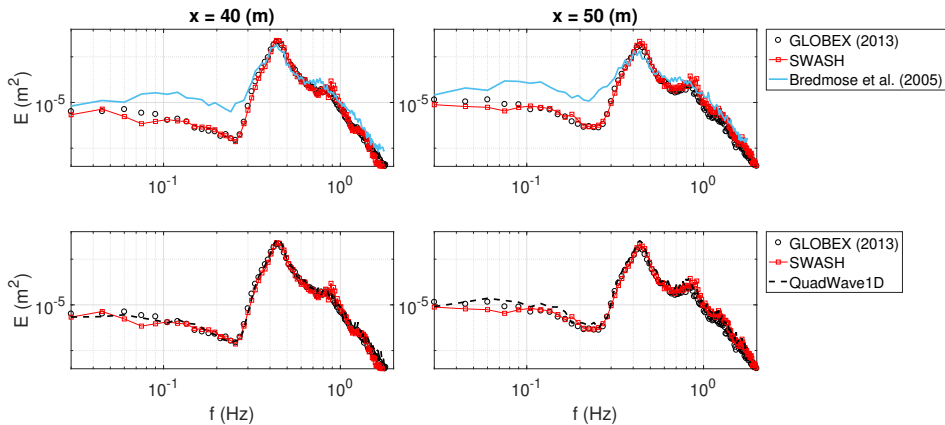


Figure 4.27: A comparison of variance spectra as obtained by the measurements, SWASH, QuadWave1D and the model of Bredmose et al. (2005).

sea-swell components and to over predict the IG components due to inadequate non-linear balance provided by the quadratic coefficients. QuadWave1D and the model of Nwogu (1993) present the most satisfying general agreement with the measured and SWASH results, and together with the model of Freilich and Guza (1984) showed the most accurate prediction of the infragravity response. Finally, as observed for the monochromatic cases, also here the predictions of the fully dispersive formulations deviated considerably from the measurement results. However here, the mechanism that leads to the observed deviations appears to be the modulational instability. This instability mechanism triggered rapid energy exchanges and accompanying growth of wave modulations over regions for which the waves are expected to develop (almost) linearly. As a result, an unexpectedly strong response of the infragravity field is presented by the predictions

of both these fully dispersive formulations.

4.5. DISCUSSION AND CONCLUDING REMARKS

The quadratic modelling approach proposes a significant modelling reduction of the original Euler equations. The description of wave nonlinearity essentially collapses into a single mode coupling term determined by the quadratic interaction coefficients. Therefore, doubt arises regarding the prediction capabilities of this modelling approach especially for coastal waves which are characterized by significant nonlinearity.

Since the first development of the quadratic formulation by Freilich and Guza (1984), efforts were mainly devoted to the improvement of the dispersion relation and the inclusion of highly dispersive and weakly nonlinear terms. Beyond the improvement of the linear wave properties, accounting for high-order dispersive terms also improves the representation of the second-order bound waves (see Madsen and Schäffer (1998)). As an example, the formulation by Bredmose et al. (2005) provides second-order bound wave solutions which exactly match those of Stokes theory. However, as demonstrated throughout this study, these added values also involve unfavourable consequences on the nonlinear evolution. This unexpected impact can be explained by considering the neglected residual (or truncation error) arising due to the modelling reduction of the quadratic modelling approach. It turns out that this residual may become significant for quadratic formulations with improved dispersion. Specifically, the residuals corresponding to the fully dispersive models of Whitham (1967), Kaihatu and Kirby (1995) and Bredmose et al. (2005) lead to considerable over predictions of the so-called modulational dispersion, and consequently, also to unfavourable modifications of the modulational instability mechanism. Therefore, beyond phase errors, errors related to nonlinear energy exchanges are expected to evolve as well using these models. Stability analysis showed that these models become modulationally unstable over much shallower water than expected and are subjected to much stronger growth rates and much larger modulation ranges. As a result, predictions using these models may be significantly affected by modulational instability even under conditions (e.g., water depth, spectral bandwidth) for which this mechanism is expected to be weak or absent. Specifically, this study shows the consequences of false development of modulational instability on the prediction of waves in coastal waters. As an example, the evolution of relatively linear waves (characterized by small Ursell number) over relatively shallow waters ($\mu < 1.36$) was examined several times along this study. The expected evolution for such conditions should be well described by linear theory. However, the fully dispersive formulations demonstrated entirely different results, which are characterized by rapid growth of wave modulations and associated growth of the infragravity field.

The fully dispersive formulations also showed significant deviations compared to experiments for monochromatic cases, for which the modulational instability mechanism is not expected to develop. In addition, it was found that for these cases the results depend on the choice of the maximum frequency (f_{max}), taking into account the frequency allowed to prevent numerical instability. Generally, it seemed that choosing relatively lower f_{max} (say $4f_p$, where f_p is the peak frequency) leads to more reliable predictions. This implies sensitivity of these models' predictions to the presence of relatively high frequencies, and thus, also to the choice of f_{max} . It is hypothesized that this sensitivity

is caused by an inadequate balance between the super and sub interactions obtained by the quadratic coefficients of these models, especially interactions involving high values of μ . However, understanding the mechanism leading to this unfavourable behaviour requires separated investigation which is beyond the scope of this study.

In contrast to the fully dispersive formulations, the predictions of the Boussinesq models (i.e., the models by Freilich and Guza, 1984, Madsen and Sørensen, 1993 and Nwogu (1993)) agreed well with the measured results for the examples considered. Specifically, the model by Freilich and Guza (1984) predicts accurately the infragravity field, but shows shoaling deviations of the shorter waves. Furthermore, the model by Madsen and Sørensen (1993) demonstrated deviations of both the sub and super harmonics. These deviations are explained by the inadequate nonlinear balance characterizing the quadratic coefficients of Madsen and Sørensen (1993). Finally, the model by Nwogu (1993) seems to predict well the evolution of both the sea-swell field and infragravity field. Nevertheless, this study presents an attempt to push the limits of the prediction capabilities of the quadratic approach. To this end, an optimization process was put forward in order to find the optimal quadratic coefficients under the constraint of full linear dispersion. The outcome is the model QuadWave1D: a fully dispersive quadratic model for coastal wave prediction in one dimension. Based on accurate linear properties and adequate nonlinear balance, QuadWave1D showed satisfying agreements with the measured results with respect to the evolution of both the sea-swell components and the infragravity components. However, the verification of QuadWave1D only considered long-crested wave conditions. Therefore, further development is required to generalize the predictive capabilities of QuadWave1D for directional spectra. Ultimately, QuadWave1D also serves as a reliable and accurate starting point for the implementation of a nonlinear source term in operational spectral models for coastal waters (e.g. the SWAN model, Booij et al., 1999).

ACKNOWLEDGEMENTS

This work is part of the research programme Earth and Life Sciences (ALW) with project number ALWOP.167, which is (partly) financed by the Dutch Research Council (NWO).

APPENDICES

4.A. DIFFERENT FORMULATIONS FOR THE QUADRATIC MODEL

Generally speaking, the derivation of the quadratic model starts with the underlying time-domain model. The latter is usually written as a set of two equations for the surface elevation, η , and for the fluid velocity variable (may be the depth-averaged horizontal velocity or the horizontal velocity at a certain elevation level or the surface potential velocity etc.). However, in order to simplify the discussion, it is assumed that the underlying time-domain model can be written through the following combined form:

$$\mathcal{D}(i\partial_t, -i\partial_x)\eta = \mathcal{N}(i\partial_{t^{(1)}}, i\partial_{t^{(2)}}, -i\partial_{x^{(1)}}, -i\partial_{x^{(2)}})\eta^{(1)}\eta^{(2)} \quad (4.45)$$

where \mathcal{D} is a linear differential operator and \mathcal{N} defines a nonlinear operator. The superscripts used on the right-hand-side of (4.45) (indicated by the numbers 1, 2) specify the partial derivatives with superscript (j) operates on $\eta^{(j)}$. Additionally, as implied by (4.45), the effect of slow bottom variations is ignored here (otherwise the differential operators were dependent on x). This is done based on the common assumption that this effect, which is manifested by the so-called linear shoaling term, is of the same order as of the quadratic nonlinear term. As such, the shoaling term can be simply added to the quadratic model separately at a later stage.

The usual procedure to derive the quadratic model, (4.1), is through the multiple-scale method. A detailed account for this derivation can be found for instance in Dingemans (1997), Chapter 7. Here, this derivation is briefly summarized based on the combined model form, (4.45). To start with, two spatial scales are defined, $x_1 = x$ and $x_2 = \epsilon x$, where recall that ϵ represents a small valued measure of the field's nonlinearity. In addition, η is expanded as $\eta = \epsilon\eta_1 + \epsilon^2\eta_2 + \dots$. By substituting these assumptions into (4.45), one obtains a set of equations, each balances terms of mutual order. Here, only the first two equations are required. These are given by,

$$\mathcal{D}_1\eta_1 = 0 \quad (4.46)$$

$$\mathcal{D}_1\eta_2 = i\mathcal{D}'_1\partial_{x_2}\eta_1 + \mathcal{N}_1\eta_1^{(1)}\eta_1^{(2)} \quad (4.47)$$

where the subscript in \mathcal{D}_1 and \mathcal{N}_1 indicates that these operators are functions of the spatial derivative ∂_{x_1} . In addition, the definition of the operator \mathcal{D}'_1 stems from the following symbolic Taylor expansion:

$$\mathcal{D}(i\partial_t, -i\partial_{x_1} - i\epsilon\partial_{x_2}) = \mathcal{D}_1 - i\epsilon\mathcal{D}'_1\partial_{x_2} - \frac{\epsilon^2}{2}\mathcal{D}''_1\partial_{x_2}^2 + \dots \quad (4.48)$$

where the tag notation defines derivative with respect to the factor $-i\partial_{x_1}$.

The non-trivial solution, η_1 , is assumed to be periodic in time and slowly modulated in space, and therefore, it is assumed to take the following form:

$$\eta_1 = \sum_n A_n(x_2) \exp(ik_n x_1 - i\omega_n t) \quad (4.49)$$

By substituting this solution into (4.46), the following linear dispersion relation is obtained

$$D(\omega_n, k_n) = 0 \quad (4.50)$$

and the substitution of η_1 into (4.47) provides

$$\mathcal{D}_1 \eta_2 = \sum_n \exp(-i\omega_n t) \left[iD'_n \partial_{x_2} A_n \exp(ik_n x_1) + \sum_r N_{r,n-r} A_r A_{n-r} \exp(i(k_r + k_{n-r})x_1) \right] \quad (4.51)$$

where now the tag of D'_n indicates derivative with respect to k_n and $D_n = D(\omega_n, k_n)$. Additionally, N is associated with the operator \mathcal{N}_1 , such that $N_{r,n-r} = N(\omega_r, \omega_{n-r}, k_r, k_{n-r})$.

It is well-known that the dispersion relation does not allow resonance to occur between three waves, and therefore, at this stage, only bound wave solutions are expected to exist. However, as the water depth becomes shallower, the wavenumber mismatch, $k_r + k_{n-r} - k_n$, becomes smaller, creating a weaker condition that is commonly referred to as "near resonance", which practically allows energy exchange to take place. Therefore, in order to keep the solution bounded over relatively shallow waters, it is required that the right-hand-side of (4.51) is set to zero. This condition is expressed as follows:

$$iD'_n \partial_{x_2} A_n \exp(ik_n x_1) + \sum_r N_{r,n-r} A_r A_{n-r} \exp(i(k_r + k_{n-r})x_1) = 0 \quad (4.52)$$

or, in terms of $a_n = A_n \exp(ik_n x_1)$

$$\partial_x a_n - ik_n a_n = -i \sum_r V_{r,n-r} a_r a_{n-r} \quad (4.53)$$

As can be observed, this is exactly the quadratic model which is introduced by (4.1), where since the scale separation has stopped to play a role at this stage, it is simply reduced. Additionally, the transition from (4.52) to (4.53) suggests the following relation:

$$V_{l,m} = -N_{l,m} / D'_n \quad (4.54)$$

where $n = l + m$. This relation can be conveniently used to derive the missing quadratic coefficients of Nwogu (1993) and Whitham (1967).

The quadratic coefficients of four out of the six formulations considered here are well reported. However, the quadratic coefficients of Nwogu (1993) and Whitham (1967) are absent since these studies were designed for time-domain formulations. In the following, the missing quadratic coefficients are derived based on the underlying time-domain formulations and the relation given by (4.54).

The quadratic coefficients of Nwogu (1993) can be derived by formulating first the combined equation with respect to η and then extracting the functions $N_{l,n-l}$ and D'_n .

Alternatively, these functions can be obtained based on the quadratic transfer function, $G_{l,m}$, which for time-domain models is defined as

$$G_{l,m} = N_{l,m}/D_{lm} \quad (4.55)$$

This relation for the quadratic transfer function is easily obtained based on (4.47) and the assumption that the forcing due to η_1 only leads to bound wave solutions.

Following Nwogu's transfer function (see Nwogu (1993), Eq. 40), the functions $N_{l,m}$ and D'_n are obtained as

$$N_{l,m} = -\frac{\omega_l m k_{lm} h^2 L_{1,lm} (\omega_l k_m L_{2,m} + \omega_m k_l L_{2,l}) + \omega_l \omega_m (k_{lm} h)^2 L_{2,lm}}{2k_l L_{2,l} k_m L_{2,m} h^3} \quad (4.56)$$

and

$$D'_n = 2 \left(g k_n h L_{2,n} + \alpha \omega_n^2 k_n h^2 - g(\alpha + 1/3)(k_n h)^3 \right) \quad (4.57)$$

where $L_1(k) = (1 - \alpha(kh)^2)$, $L_2(k) = (1 - (\alpha + 1/3)(kh)^2)$ and α is a constant chosen by Nwogu (1993) to be $\alpha = -0.39$ in order to optimize the dispersion behaviour of the model.

The corresponding functions of Whitham (1967) can be easily derived from the time-domain formulation directly and are given as

$$N_{l,m} = -i \frac{3}{4} \sqrt{\frac{g}{h}} k_{lm} \quad (4.58)$$

$$D'_n = i C_{g,n} \quad (4.59)$$

where C_g is the fully dispersive group velocity. This completes the derivation of the missing quadratic coefficients.

It is desired to stress a final point here that concerns the reason why quadratic formulations which are derived based on the above procedure provide different bound wave solutions from the ones obtained by the underlying time-domain formulations, and why the formulation of Bredmose et al. (2005) is exceptional in that sense. Recall that the bound wave solutions based on the quadratic model are governed by the quadratic transfer function through (4.10). Therefore, using (4.54), the following alternative expression of $G_{l,m}$ is obtained:

$$G_{l,m} = N_{l,m}/(D'_n(k_{lm} - k_n)) \quad (4.60)$$

On the other hand, time-domain formulations provide different expression for the quadratic transfer function as presented by (4.55). These two predictions would agree if $1/D'_n$ would equal to $(k_{lm} - k_n)/D_{lm}$. Yet this equality is obtained asymptotically at the shallow water limit as suggested by

$$\lim_{k_{lm} \rightarrow k_n} \frac{k_{lm} - k_n}{D_{lm}} = \lim_{k_{lm} \rightarrow k_n} \frac{1}{D'_{lm}} = \frac{1}{D'_n} \quad (4.61)$$

This observation is indeed consistent with the near-resonance assumption of the quadratic model derivation (see further discussion in Bredmose et al., 2005).

The exceptional derivation of the quadratic model by Bredmose et al. (2005) fixes the disagreement between the quadratic formulations and the underlying time-domain formulations with regard to the bound wave solutions. This is achieved due to an operator splitting idea suggested by Agnon (1999). The operator splitting idea bypasses the necessity to rely on the near-resonance assumption, resulting in the following modified quadratic coefficients:

$$V_{l,m} = -N_{l,m}/H_{lm} \quad (4.62)$$

where $H_{lm} = D_{lm}/(k_{lm} - k_n)$. By substituting this definition into (4.10), one obtains an exact match with the quadratic transfer function of the underlying time-domain model as given by (4.55).

A summary of the six different quadratic formulations which are considered in this study is given by the following subsections. These formulations include the models given by Freilich and Guza (1984), Madsen and Sørensen (1993), Kaihatu and Kirby (1995), Bredmose et al. (2005) and the two formulations which are derived here based on the time-domain models of Nwogu (1993) and Whitham (1967).

4.A.1. DISPERSION RELATION

The dispersion relation, (4.50), of the Boussinesq models, namely the models by Freilich and Guza (1984), Madsen and Sørensen (1993) and Nwogu (1993) can be summarized through (also see Eq. 30 by Nwogu, 1993)

$$\omega_n = k_n \sqrt{gh \frac{1 - (\alpha + 1/3)(k_n h)^2}{1 - \alpha(k_n h)^2}} \quad (4.63)$$

where

$$\alpha = \begin{cases} -1/3, & \text{Freilich and Guza (1984)} \\ -2/5, & \text{Madsen and Sørensen (1993)} \\ -0.39, & \text{Nwogu (1993)} \end{cases} \quad (4.64)$$

For the other fully dispersive models, the dispersion relation is defined as

$$\omega_n = k_n \sqrt{g \tanh(k_n h)/k_n} \quad (4.65)$$

For all but one model, the value of k_n is evaluated numerically. The exceptional model with this regard is the one by Freilich and Guza (1984) for which k_n is evaluated asymptotically using the following expression:

$$k_n = \frac{\omega_n}{\sqrt{gh}} + \frac{\sqrt{h}\omega_n^3}{6g^{3/2}} \quad (4.66)$$

4.A.2. QUADRATIC COEFFICIENTS

The quadratic coefficients for each of the models are summarized by the following. The expressions are presented using (4.54). For the model by Bredmose et al. (2005) though, the quadratic coefficients are presented through (4.62).

Freilich and Guza (1984):

The functions N_{lm} and D'_n which are used to calculate the quadratic coefficients by Freilich and Guza (1984) obey to an additional assumption. The additional assumption of Freilich and Guza (1984) dictates that the contribution to the dispersion relation (which corrects the non-dispersive relation in shallow water) is of $O(\epsilon)$, and therefore, should be ignored for the evaluation of N_{lm} and D'_n . Accordingly, the reduced N_{lm} and D'_n are given by

$$N_{l,m} = -\frac{3}{2} g k_{lm}^2 \quad (4.67)$$

$$D'_n = 2ghk_n \quad (4.68)$$

for which $k_n = \omega_n / \sqrt{gh}$. Therefore, using (4.54), the the quadratic coefficients by Freilich and Guza (1984) are obtained as

$$V_{l,m} = \frac{3}{4} \frac{\omega_n}{h\sqrt{gh}} \quad (4.69)$$

Madsen and Sørensen (1993):

The formulation of the quadratic coefficients by Madsen and Sørensen (1993) is completely consistent with the general derivation presented here, without any additional assumptions. The expression for the functions N_{lm} and D'_n are given by Madsen and Sørensen (1993), Eqs. (5.4a) and (5.4f).

Nwogu (1993):

The quadratic coefficients of Nwogu (1993) are obtained through (4.56) and (4.57).

Whitham (1967):

The quadratic coefficients of Whitham (1967) are obtained through (4.58) and (4.59).

Kaihatu and Kirby (1995):

The functions N_{lm} and D'_n which are used to calculate the quadratic coefficients of Kaihatu and Kirby (1995) are given by

$$N_{l,m} = -\frac{1}{2} \frac{g}{\omega_l \omega_m} \left(\omega_n^2 k_l k_m + \omega_n k_{lm} (k_l \omega_m + k_m \omega_l) \right) - \frac{1}{2} \frac{\omega_n^2}{g} (\omega_l \omega_m - \omega_n^2) \quad (4.70)$$

and

$$D'_n = 2\omega_n C_{g,n} \quad (4.71)$$

which can be deduced based on the expressions in Eqs. (26-27) and Eq. (36) of Kaihatu and Kirby (1995).

Bredmose et al. (2005):

The quadratic coefficients of Bredmose et al. (2005) are defined through (4.62), which requires the expressions for $N_{l,m}$ and H_{lm} . These are summarized by the following:

$$N_{l,m} = -\frac{1}{2} \frac{g}{\omega_l \omega_m} \left(\omega^2(k_{lm}) k_l k_m + \omega_n k_{lm} (k_l \omega_m + k_m \omega_l) \right) - \frac{1}{2} \frac{\omega_n^2}{g} \left(\frac{\omega^2(k_{lm})}{\omega_n^2} \omega_l \omega_m - \omega^2(k_{lm}) \right) \quad (4.72)$$

and

$$H_{lm} = \frac{\omega_n^2 - \omega^2(k_{lm})}{k_n - k_{lm}} \quad (4.73)$$

where $\omega^2(k_{lm})$ is given by $\omega^2(k_{lm}) = k_{lm} g \tanh(k_{lm} h)$. Note that even though the starting point equations of Kaihatu and Kirby (1995) and Bredmose et al. (2005) obey to similar properties, the resulting quadratic coefficients are different. Apart from the reason discussed above regarding the derivation methods, which result in the different denominators D'_n and H_{lm} , the differences in $N_{l,m}$ is explained by the different ways to obtain the combined form for η as discussed by Eldeberky and Madsen (1999).

4.A.3. SHOALING TERM

As mentioned earlier, the shoaling term can be added into the quadratic formulation separately by assuming it to be of the same order as the quadratic nonlinear term. The derivation of the shoaling term is based on the usual WKB assumption allowing the wavenumbers to be weakly dependent on x . Namely, the first order solution, η_1 , takes now the following form:

$$\eta_1 = \sum_n A_n \exp(iS_n(x) - i\omega_n t) \quad (4.74)$$

where $\partial_x S_n = k_n$. The linear operator, \mathcal{D} , is now weakly dependent on x as well. For model formulations which are based on the so-called free-surface velocity potential (see definition in, e.g., Zakharov, 1968), the slowly varying operator, \mathcal{D} , can be treated as a Weyl operator (Akrish et al. 2022). This is convenient since the Weyl operator provides the following general formula for the shoaling term (see, e.g., Akrish et al., 2020, Eq. (A8)):

$$\frac{\partial_x A_n}{A_n} = -\frac{\partial_x k_n D''_n + \partial_x D'_n}{2D'_n} \quad (4.75)$$

where D''_n indicates second derivative with respect to k_n . This equation leads to the following well-known linear shoaling definition (which corresponds to the well-known energy flux conservation):

$$\partial_x \left(A_n \sqrt{C_{g,n}} \right) = 0 \quad (4.76)$$

where $C_{g,n}$ is the fully dispersive group velocity if one of the fully dispersive models is considered, while for the model by Freilich and Guza (1984), the shallow water approximation, $C_{g,n} = \sqrt{gh}$, is used. Note that the shoaling term formula, (4.75) (or (4.76)), is applied here also for the model by Whitham (1967) which was developed for constant depth. This applicability is argued heuristically based on the derivations of the Whitham systems in Moldabayev et al. (2015) and Akrish et al. (2022). A more rigorous derivation is beyond the scope of this study. Finally, recall that the Weyl formula, (4.75), is valid for models which are formulated based on the free-surface velocity potential. Accordingly, this formula does not lead to the correct shoaling terms of Madsen and Sørensen (1993) and Nwogu (1993). Furthermore, the expression in (4.76), written in terms of $C_{g,n}$, is also not found to agree with the shoaling terms of Madsen and Sørensen (1993) and Nwogu (1993) (see discussions by Beji and Nadaoka, 1996 and Schäffer and Madsen, 1998). However, Fig. 3 in Schäffer and Madsen (1995) shows that the deviation of the shoaling terms of Madsen and Sørensen (1993) and Nwogu (1993) from the fully dispersive shoaling is practically negligible over depths that characterize coastal waters. Therefore, for the computations performed here, the fully dispersive shoaling term is applied for the models by Madsen and Sørensen (1993) and Nwogu (1993) as well.

A comparison between the fully dispersive shoaling term and the shoaling term of Freilich and Guza (1984) is shown in Fig. 4.28.

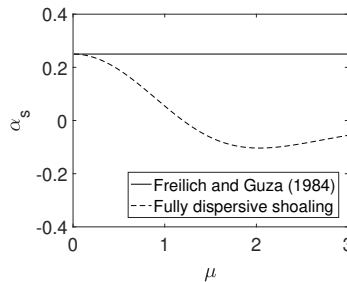


Figure 4.28: The shoaling coefficient of the fully dispersive formulations and of Freilich and Guza (1984) as a function of the depth parameter μ .

The comparison is presented in terms of the shoaling coefficient, α_s , that defines the following relation (see Madsen and Sørensen, 1992, Section 3):

$$\frac{\partial_x A_n}{A_n} = -\alpha_s \frac{\partial_x h}{h} \quad (4.77)$$

The comparison shown in Fig. 4.28 explains the tendency of the model by Freilich and Guza (1984) to exaggerate the effect of linear shoaling over coastal waters (say, for μ values satisfy $\mu \leq 2$).

4.B. CUBIC INTERACTION COEFFICIENTS OF THE QUADRATIC FORMULATION

The cubic interaction coefficients, $L_{i,j,k,l}$, are formulated through the solvability condition, (4.11), that is obtained at third order. This equation describes the interaction of resonant quartets, which satisfy the conditions

$$\begin{cases} \omega_i + \omega_j = \omega_k + \omega_l \\ k_i + k_j = k_k + k_l + O(\epsilon^2) \end{cases} \quad (4.78)$$

for non-trivial interactions, while exact resonance is obtained for the trivial interactions (the interactions which result in amplitude dispersion contributions). As implied by the formulation of the solvability condition, the cubic coefficients of the cubic terms (appearing implicitly on the right-hand-side of (4.11)) are constructed as sums of multiplications of the quadratic coefficients, V , and the quadratic transfer function, G . To demonstrate this explicitly, an example of a resonant quartet is considered. Consider first the more common resonant case which satisfies the following:

$$\begin{cases} \omega_i - \omega_k = \omega_l - \omega_j \\ \omega_j - \omega_i \neq \omega_i - \omega_k \end{cases} \quad (4.79)$$

In this case, any wave component participates in four trivial resonant interactions and one non-trivial interaction, as is demonstrated for the component corresponding to ω_i as follows:

$$\begin{cases} \omega_i = \omega_i + \omega_i - \omega_i \\ \omega_i = \omega_i + \omega_j - \omega_j \\ \omega_i = \omega_i + \omega_k - \omega_k \\ \omega_i = \omega_i + \omega_l - \omega_l \\ \omega_i = \omega_l + \omega_k - \omega_j \end{cases} \quad (4.80)$$

The cubic coefficient corresponding to each of these interactions consists of different products of G and V which are determined by the right-hand-side of the equations in (4.80). For example, consider the formulation for the cubic coefficient of the non-trivial interaction which is determined according to the last equation of (4.80). Each pair of frequencies on the right-hand-side of this equation forces a second-order bound solution which is in resonant with the third frequency and with ω_i . As a result, the following expression is obtained:

$$L_{i,j,k,l} = 2G_{l,k}V_{l+k,-j} + 2G_{l,-j}V_{l-j,k} + 2G_{k,-j}V_{k-j,l} \quad (4.81)$$

The formulation for the cubic coefficients of the trivial interactions can be derived in a similar fashion based on the other equations of (4.80). The resulted evolution equation for a_i is given by

$$i\partial_{x_2} a_i = \left(L_{i,i}|a_l|^2 + 2L_{i,k}|a_k|^2 + 2L_{i,j}|a_j|^2 + 2L_{i,l}|a_l|^2 \right) a_l + 2L_{i,j,k,l} a_l a_k a_{-j} \quad (4.82)$$

which is coupled with the corresponding equations for a_k , a_j and a_l . Note that the compact notations defined for the cubic coefficients of the trivial interactions $L_{n,n}$ and $L_{n,m}$ conveniently represent the notations $L_{n,n,n,n}$ and $L_{n,m,n,m}$, respectively. In addition, note that for the special case which also satisfies the condition $\omega_j - \omega_i = \omega_i - \omega_k$, two additional non-trivial interactions appears. These can be described as

$$\begin{cases} \omega_i = \omega_j + \omega_k - \omega_l \\ \omega_i = \omega_j + \omega_j - \omega_l \end{cases} \quad (4.83)$$

The above described formulation, when applied for cubic coefficients that correspond to the trivial resonant interactions, raises some doubt due to apparent singularity demonstrated by terms like $G_{n,-n}$. The quadratic model naturally bypasses this difficulty since it excludes the set-down terms due to self interactions as a results of the property given by (4.32) which states that $V_{n,-n} = 0$. The formulation of the cubic coefficients based on the quadratic model is referred here as the discontinuous definition. On the other hand, the continuous definition requires some assumptions regarding the limit of $G_{n,-n}$, which should be identical through the different convergence paths described by $G(\omega_n \pm \Delta\omega, -\omega_n \pm \Delta\omega)$ and by taking the limit $\Delta\omega \rightarrow 0$. Thus, consider for instance the cubic coefficient, $L_{i,i}$, defined by the right-hand-side of the first equation in (4.80). The discontinuous definition expresses this coefficient as

$$L_{i,i} = 2G_{i,i}V_{2i,-i} \quad (4.84)$$

whereas the formulation following the continuous definition gives

$$L_{i,i} = 2G_{i,i}V_{2i,-i} + 4G_{i,-i}V_{i,0} \quad (4.85)$$

The continuous definition is used in this study to relate between the different cubic coefficients for the case of three-wave interaction. An example of such case is defined by the condition (4.79) and assuming that $\omega_j = \omega_i$. The three cubic coefficients that correspond to the non-trivial interaction are given as follows:

$$\begin{cases} L_{k,l,i,i} = 2G_{i,i}V_{2i,-l} + 4G_{i,-l}V_{i-l,i} \\ L_{l,k,i,i} = 2G_{i,i}V_{2i,-k} + 4G_{i,-k}V_{i-k,i} \\ L_{i,i,k,l} = 2G_{l,k}V_{l+k,-i} + 2G_{l,-i}V_{l-i,k} + 2G_{k,-i}V_{k-i,l} \end{cases} \quad (4.86)$$

Under the assumption of small modulation frequency, namely, $\omega_i - \omega_k = \omega_l - \omega_i = \Delta\omega$, where $\Delta\omega \ll \omega_i$, one obtains the approximation

$$L_{k,l,i,i} \sim L_{l,k,i,i} \sim L_{i,i,k,l} \sim L_{i,i} \quad (4.87)$$

if the following conditions hold:

$$\begin{cases} G(\omega_i \pm \Delta\omega, -\omega_i \pm \Delta\omega) = G_{i,-i} + O(\Delta\omega) \\ G(\omega_i \pm \Delta\omega, \omega_i \pm \Delta\omega) = G_{i,i} + O(\Delta\omega) \\ V(2\omega_i \pm \Delta\omega, -\omega_i \pm \Delta\omega) = V_{2i,-i} + O(\Delta\omega) \\ V(\omega_i \pm \Delta\omega, \pm\Delta\omega) = V_{i,0} + O(\Delta\omega) \end{cases} \quad (4.88)$$

4.C. SPATIAL MODULATIONAL GROWTH OF NARROW-BANDED WAVE FIELDS

Modulational instability is conveniently studied through the well-known nonlinear Schrödinger equation (NLSE). This equation is derived under the assumption of a narrow-banded wave field represented by the complex envelope, A . Additionally, the waves are assumed to be weakly nonlinear. Nevertheless, the NLSE accurately captures third-order nonlinear effects, and thus, serves an adequate reference for comparison with relevant results obtained through the quadratic formulations. Specifically, this appendix briefly summarizes the derivation of modulational instability threshold and its spatial growth. For a one-dimensional settings, the NLSE can be formulated as follows (e.g., Mei et al., 2005):

$$\partial_{t_2} A + \frac{1}{2} \nu \frac{\omega_p}{k_p} \partial_{x_2} A + i \frac{1}{8} \alpha \frac{\omega_p}{k_p^2} \partial_{x_1}^2 A + i \frac{1}{2} \beta \omega_p k_p^2 A |A|^2 = 0 \quad (4.89)$$

where, as before, the subscripts introduce multiple scales with respect to the small parameter ϵ (e.g., $x_j = \epsilon^j x$). In addition, k_p and ω_p are defined as the carrier wavenumber and angular frequency, respectively. This formulation is easily adapted to deep water conditions by setting $\nu = \alpha = \beta = 1$. For finite depth, these parameters are defined as follows (e.g., Liu et al., 2022):

$$\left\{ \begin{array}{l} \nu = 1 + \frac{2k_p h}{\sinh(2k_p h)} \\ \alpha = 2 - \nu^2 + 8(k_p h)^2 \frac{\cosh(2k_p h)}{\sinh^2(2k_p h)} \\ \beta = \frac{8 + \cosh(4k_p h) - 2 \tanh^2(k_p h)}{8 \sinh^4(k_p h)} - \frac{(2 \cosh^2(k_p h) + \nu/2)^2}{\sinh^2(2k_p h) (k_p h / \tanh(k_p h) - \nu^2/4)} \end{array} \right. \quad (4.90)$$

To study the spatial development of modulational instability, it is convenient to introduce the following variable transformation (Djordjević and Redekopp, 1978):

$$\left\{ \begin{array}{l} \bar{x} = x_2 \\ \tau = \frac{x_1}{C_{g,0}} - t_1 \end{array} \right. \quad (4.91)$$

Based on these new variables, the NLSE (4.89) transforms into,

$$\partial_{\bar{x}} A + i \frac{\alpha}{\nu^3} \frac{k_p}{\omega_p^2} \partial_{\tau}^2 A + i \frac{\beta}{\nu} k_p^3 A |A|^2 = 0 \quad (4.92)$$

which provides the starting point to the following linear stability analysis.

4.C.1. STABILITY CONDITION

In order to analyze the stability due to side-band perturbation of otherwise permanent monochromatic Stokes wave, the complex envelop, A , is assumed to be defined as

$$A = A_p(1 + \delta_{A_p}) \quad (4.93)$$

where A_p defines the complex amplitude of the unmodulated field, namely, it satisfies the reduced equation

$$\partial_{\bar{x}} A_p + i \frac{\beta}{\nu} k_p^3 A_p |A_p|^2 = 0 \quad (4.94)$$

and therefore, it obeys to the solution

$$A_p = C \exp(-i k_p^{(2)} \bar{x}) \quad (4.95)$$

where C is some constant and $k_p^{(2)}$ is the wavenumber correction due to self interaction, which is defined as

$$k_p^{(2)} = \frac{\beta}{\nu} k_p^3 |A_p|^2 \quad (4.96)$$

Note that through the definition of β , this wavenumber correction includes the effect of wave-induced current. Also note that through the usual analysis in time, one would obtain the equivalent frequency correction $\omega_p^{(2)}$. The relation between these two corrections is readily verified to be

$$\omega_p^{(2)} = C_{g,p} k_p^{(2)} \quad (4.97)$$

By substituting the assumed structure (4.93) into (4.92) and linearizing in terms of the disturbance δ_{A_p} , one obtains the following equation (see details in Mei et al., 2005, Section 13.4):

$$\partial_{\bar{x}}^2 \delta_{A_p} + \frac{\alpha^2 k_p^2}{\nu^6 \omega_p^4} \partial_{\bar{t}}^4 \delta_{A_p} + 2 \frac{\alpha \beta k_p^4}{\nu^4 \omega_p^2} |A_p|^2 \partial_{\bar{t}}^2 \delta_{A_p} = 0 \quad (4.98)$$

Assuming that the disturbance can be written as $\delta_{A_p} = \delta_{A_p}^0 \exp(i \Delta \omega \tau - i \sqrt{R} \bar{x})$, where $\delta_{A_p}^0$ is some constant (see physical interpretation in Mei et al., 2005, Section 13.4), the following dispersion relation is obtained:

$$R = \frac{\alpha^2 k_p^2}{\nu^6} \left(\delta_{\omega_p}^4 - \frac{2\nu^2 \beta}{\alpha} (k_p |A_p|)^2 \delta_{\omega_p}^2 \right) \quad (4.99)$$

where $\delta_{\omega_p} = \Delta \omega / \omega_p$. Therefore, instability emerges when $R < 0$ requiring that

$$1 < \frac{2\nu^2 \beta}{\alpha} \left(\frac{k_p |A_p|}{\delta_{\omega_p}} \right)^2 \quad (4.100)$$

Since ν and α are defined positive (over μ), this condition can only be satisfied when $\beta > 0$. Accordingly, when $\beta \leq 0$ the wave field is modulationally stable. Alternatively, the condition for instability can be written in terms of the wavenumber correction, $k_p^{(2)}$, as follows:

$$1 < k_p^{(2)} \frac{2\nu^3}{\alpha k_p \delta_{\omega_p}^2} \quad (4.101)$$

where now, stability is guaranteed when $k_p^{(2)} \leq 0$.

4.C.2. SPATIAL MODULATIONAL GROWTH

As implicitly described by the condition for modulational instability, (4.100), modulational growth emerges only over limited range of δ_{ω_p} given by

$$\delta_{\omega_p} \in \left(0, \sqrt{\frac{2\nu^2\beta}{\alpha}} (k_p |A_p|) \right) \quad (4.102)$$

Therefore, the range of instability is essentially determined by $\delta_{\omega_p, max} = \sqrt{2\nu^2\beta/\alpha} (k_p |A_p|)$. Over the unstable range, the spatial growth is determined by $\text{Im}\{\sqrt{R}\}$, defined as

$$\text{Im}\{\sqrt{R}\} = \frac{\alpha k_p}{\nu^3} \sqrt{\left(\frac{2\nu^2\beta}{\alpha} (k_p |A_p|)^2 \delta_{\omega_p}^2 - \delta_{\omega_p}^4 \right)} \quad (4.103)$$

Accordingly, the maximum growth rate is equal to

$$\text{Im}\{\sqrt{R}\}_{max} = k_p (\beta/\nu) (k_p |A_p|)^2 \quad (4.104)$$

for which

$$\delta_{\omega_p} = \sqrt{\frac{\nu^2\beta}{\alpha}} (k_p |A_p|) \quad (4.105)$$

The two non-dimensional parameters $p_1 = \nu^2\beta/\alpha$ and $p_2 = \beta/\nu$ seem to play an important role in determining the growth rate values and the range of instability. These parameters are described in Fig. 4.29 as functions of the depth parameter μ .

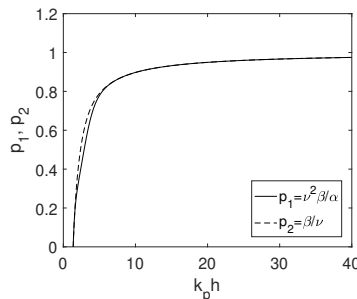


Figure 4.29: The parameters $p_1 = \nu^2\beta/\alpha$ and $p_2 = \beta/\nu$ described as functions of μ .

This clearly shows that the maximum growth rate value and the maximum range of instability are obtained for the infinite water depth limit, for which $p_1 = p_2 = 1$.

4.C.3. BENJAMIN-FEIR INDEX (BFI)

The linear stability analysis described above may provide clear indication for the impact of the modulational instability mechanism on monochromatic (weakly modulated) cases. However, the determination of the importance of this mechanism for more general irregular cases is less obvious. The need for a parameter that indicates whether the evolution of a given field would be affected by modulational instability led to the formulation of a statistical parameter by Alber (1978), which was later called the Benjamin-Feir Index (BFI) (Janssen, 2003). The definition of BFI is given by the square root of the right-hand-side of (4.100), written as

$$\text{BFI} = \sqrt{\frac{cv^2|\beta| k_p|A_p|}{\alpha \delta_{\omega_p}}} \quad (4.106)$$

However now, the normalized modulation frequency, δ_{ω_p} , should be interpreted as the bandwidth parameters, which defines the ratio between the spectral bandwidth (usually defined as the standard deviation of the spectrum) and the peak frequency, ω_p . Additionally, the wave steepness should now be interpreted as a typical steepness value, which commonly taken as $k_p|A_p| = k_p H_s/2$, where k_p is the wavenumber that corresponds to ω_p and H_s is the significant wave height. Similarly to the definition of Ursell number, also BFI defines qualitatively the typical ratio of the competing effects of dispersion, which tend to restrict the development of nonlinear coherent structures, and nonlinearity, which generates them (also see discussion by Onorato et al., 2006, Section 2).

The BFI is computed here based on the definition of δ_{ω_p} as given by Liu et al. (2022), Eq. (31). This definition provides lower values than the definition of the standard deviation (as it is less affected by the high frequencies tail). Furthermore, the value of the parameter c is given by $c = 3.2$. This value is selected such that BFI equals 1 for the typical deep water wave conditions characterized by a JONSWAP spectrum with peak-enhancement factor of $\gamma = 3.3$ and peak steepness of $k_p H_s/2 = 0.1$.

5

CONCLUSIONS AND OUTLOOK

This study was set forward with the aim of advancing the statistical forecasting capabilities of coastal waves. Present operational forecasting models for coastal waves (e.g. the SWAN model) rely on developments which are designed to the dynamics of waves in the open ocean. However, over coastal waters, waves evolve much faster due to medium inhomogeneities of smaller scales (e.g., submerged shoals and channels and small scale eddies and jets) and since nonlinear interactions between wave triads become nearly resonant. Consequently, the statistical assumptions of quasi-homogeneity and quasi-Gaussianity valid in the open ocean become invalid over coastal waters. This clearly calls for a fundamental improvement of the present statistical formulation for the forecasting of coastal waves. Specifically, the statistical formulation presently implemented by operational forecasting models for coastal waves (e.g. the SWAN model) should be modified to allow for inhomogeneous and non-Gaussian contributions. The developments achieved and the conclusions drawn along the journey of this study towards this goal are discussed in the following.

5.1. CONCLUSIONS

To leading order, statistical inhomogeneity of wave fields is induced by linear interaction of waves and a variable medium. Traditionally, linear inhomogeneity is formulated based on the WKB approximation and the assumption that different wave components are statistically independent (e.g. Hasselmann, 1963, Dewar, 1970, Willebrand, 1975, Hertzog et al., 2002). This formulation results in the well-known energy balance equation that is presently implemented in operational forecasting models for coastal waves (e.g. the SWAN model, Booij et al., 1999). Based on the energy balance equation, statistical inhomogeneity is described by the variance-related energy density radiation in phase space, while the cross correlation contributions are totally ignored. However, coastal waters are characterized by rather rapid medium variations which often induce wave crossing and associated wave interference patterns. Such scenarios may result in a significant statistical inhomogeneity if crossing waves are statistically correlated (e.g.,

the emergence of lateral oscillations of the significant wave height behind a submerged shoal, demonstrated experimentally by Vincent and Briggs, 1989). To account for cross correlation contributions, Smit and Janssen (2013) developed a more general statistical formulation known as the Wigner-Weyl formulation. This formulation accounts for the generation and transformation of the complete second-order statistics, and effectively reduces to the conventional energy balance equation when the statistical correlations between crossing waves are superimposed to a negligible contribution. The formulation proposed by Smit and Janssen (2013) rely on an assumed Schrödinger-type deterministic equation that is written in terms of the Weyl operator of the linear dispersion relation. This starting point equation provides a direct and formal derivation of the Wigner-Weyl kinetic equation for water waves. The detailed derivation, starting with a similar Schrödinger-type equation, is provided by numerous studies in other fields of physics (e.g., Leaf, 1968, Bremmer, 1973, Besieris and Tappert, 1976, McDonald and Kaufman, 1985, Zhu and Dodin, 2021). Therefore, the remaining gap to establish the statistical development proposed by Smit and Janssen (2013) on solid foundations is the theoretical justification of their starting point deterministic equation. The results of Chapter 2 close this gap by showing the necessary equivalence between a formal definition of the Dirichlet-to-Neumann operator of waves over variable bathymetry and the Weyl operator of the dispersion relation. This equivalence eventually leads to the formal derivation of the Schrödinger-type deterministic equation used as the starting point for the Wigner-Weyl formulation of Smit and Janssen (2013). As a consequence, this derivation establishes the desired formal link between the deterministic formulation (e.g. Euler equations) and the stochastic formulation of the Wigner-Weyl formalism, which includes the energy balance equation as a statistically well-defined limiting case.

Except for the presence of bathymetry, the coastal environment is also characterized by the presence of ambient currents, the effect of which is excluded in the statistical model of Smit and Janssen (2013). To include the effect of currents, Chapter 3 proposes a statistical model for the evolution of wave fields over non-uniform currents and bathymetry. The model formulation is based on a Schrödinger-type deterministic equation for the so-called action variable (a variable definition that is closely related to the definition of the wave action). This equation is found to be exact for linear wave interaction with homogeneous media and is found to reduce to the local dispersion relation and to the transport equation for the mean action density under weakly inhomogeneous conditions and using the usual WKB ansatz. Through similar steps presented by Smit and Janssen (2013), the proposed Schrödinger equation is readily transformed into a kinetic equation for the Wigner distribution of the action variable. This distribution provides a complete spectral description of the second-order statistics of a given wave field. It includes cross-correlation terms, which provide the statistical information about wave interferences. As such, the Wigner distribution of the action variable generalizes the concept of the action density spectrum, which only accounts for the information of wave variances. Consequently, the principle result presented in Chapter 3 is a generalized action balance equation which accounts for the generation and propagation of statistical wave interference contributions. For cases where interference effects are negligible, namely for cases where the ratio between the correlation length scale and the medium variation scale is small, model verification showed the agreement of the

present model predictions with the predictions of the SWAN model. However, it is also demonstrated that for cases where this ratio is relatively large, interference effects alter the statistics of the wave field significantly and lead to significant deviations from SWAN predictions which are not confined to the vicinity of the wave-focusing areas, but also persist over significant distances away from the focusing points. These findings are supported by the well-verified REF/DIF 1 model (Kirby and Dalrymple, 1986). It is therefore concluded that for regions involving rapid variability in medium (as often described by the coastal environment), consideration of the statistical information of wave interferences might be crucial for correct wave forecasting.

Beyond statistical inhomogeneity, wave fields in coastal environment tend to develop significant non-Gaussian contributions which are triggered by shallow water non-linearity. The derivation of a statistical model that is able to properly describe the development of non-Gaussian statistics is a challenging task. A principle difficulty relates to the necessity to preserve computational efficiency for coastal applications of large-scales. Consequently, statistical modelling of shallow water nonlinearity inevitably relies on model reductions. Nonlinear statistical models for coastal applications are usually formulated based on two separated approximations. The first is the quadratic approximation, which is obtained based on a reduction of a more detailed modelling approach (e.g., the Euler equations). The second approximation relates to the stochastic closure problem which requires a truncation of the hierarchical dependence between the statistical moments. Chapter 4 examines in detail the first approximation. Specifically, the analysis carried out in Chapter 4 provides insight into the nonlinear properties of different quadratic formulations in terms of the second-order bound wave solutions, amplitude dispersion and stability characteristics. In agreement with the analysis of Madsen and Schäffer (1998), it is demonstrated that the second-order bound solutions tend to converge to the solutions of Stokes theory through the improvement in the dispersion relation (i.e., by taking into account high-order linear and nonlinear dispersive terms). As an example, the fully dispersive formulation proposed by Bredmose et al. (2005) provides second-order bound wave solutions which exactly match those of Stokes theory. However, the analysis of Chapter 4 shows that the improvement in the dispersion property and the associated improvement of the bound wave solutions may also involve unfavourable impact on the nonlinear wave evolution. This is explained by the fact that the modification of the dispersion property is accompanied by a change in the quadratic coefficients, and therefore, also by a change in the truncation error obtained due to the modelling reduction associated with the formulation of the quadratic model. In particular, the amplitude dispersion may be altered dramatically due to the enhancement in dispersive effects. This may not only lead to phase errors, but also to unfavourable modifications of the modulational instability mechanism. To demonstrate this, the stability analysis given in Chapter 4 shows that the fully dispersive models of Whitham (1967), Kaihatu and Kirby (1995) and Bredmose et al. (2005) become modulationally unstable over much shallower water than expected and are subjected to much stronger growth rates and much larger modulation ranges. As a result, these models present unexpected energy exchanges in several bichromatic and irregular examples considered throughout this study. In some cases, these models even demonstrated significant energy exchanges under conditions for which linear theory is expected to be valid (i.e., conditions char-

acterized by an intermediate depth and a small Ursell number). These excessive energy transfers not only lead to significant deviations in the sea-swell forecast, but also to unexpectedly strong field modulations and associated unexpected infragravity responses. In contrast to the fully dispersive formulations, the examined Boussinesq models, namely the models of Freilich and Guza (1984), Madsen and Sørensen (1993) and Nwogu (1993) are found to predict well the nonlinear evolution of coastal wave fields, including the development of the sea-swell components and the generation and evolution of the infragravity components. This conclusion is based on comparisons to measured results of a wide set of examples (including monochromatic, bichromatic and irregular wave conditions). Finally, the study of Chapter 4 also presents an attempt to push the limits of the prediction capabilities of the quadratic approach. To this end, an optimization process was carried out in order to find the optimal quadratic coefficients under the constraint of full linear dispersion. The outcome is the model QuadWave1D: a fully dispersive quadratic model for coastal wave prediction in one dimension. Based on accurate linear properties and adequate nonlinear balance, QuadWave1D showed satisfying agreements with the measured results with respect to the evolution of both the sea-swell components and the infragravity components. This new formulation provides a reliable starting point to further developments of the deterministic modelling capabilities of the quadratic approach (e.g., modelling directional spectra over two dimensional bathymetric patterns, modelling of wave breaking, etc.), and in addition, this model provides a well-behaved starting point for the development of a nonlinear source term for the phase-averaged approach.

5.2. OUTLOOK

This study is part of a general effort to develop and improve the predictive capabilities of the phase-averaged approach over coastal waters. The phase-averaged approach strives to preserve computational efficiency for large-scale coastal applications. Accordingly, this modelling approach is based on rather simplified formulations to describe the complex wave processes that characterize the coastal environment (e.g., the interaction of waves with inhomogeneous media, shallow water nonlinearity and depth-induced wave breaking). Despite the success of existing formulations in the prediction of coastal waves, there are still aspects that require further development (e.g. Gorrell et al., 2011). These refer to the improvement in the prediction of complex wave processes (e.g. nonlinear wave evolution, wind generation, wave breaking, etc.) and even to the inclusion of missing information (e.g. the generation and transformation of infragravity waves). This study concerns with the improvement of wave interaction with variable media (i.e. variable bathymetry and ambient currents) and takes part in the general effort to statistically model shallow water nonlinearity.

In order to improve the statistical description of wave-medium interaction, the present study extends upon the work of Smit and Janssen (2013). This extension includes the theoretical foundations derived in Chapter 2 and the generalization of the statistical framework suggested by Smit and Janssen (2013) to allow for wave-current interactions as detailed in Chapter 3. The theoretical development discussed in Chapter 2 essentially provides a formal connection between the deterministic formulation (e.g. Euler equations) and the energy balance equation and its generalization (the Wigner-Weyl formal-

ism). However, this theoretical foundation excludes the effect of wave-current interaction which is required for similar connection to the action balance equation. The inclusion of the effects due to ambient currents can be achieved through a formal derivation of the starting point equation of Chapter 3. To this end, similar steps as detailed in Chapter 2 can be considered. These steps include the formulation of a generalized mild-slope equation written in terms of the Weyl operator of the dispersion relation and the subsequent transformation to a Schrödinger system that is written in terms of the action variable and its complex-conjugate. If successful, this derivation would provide a formal connection to the Wigner-Weyl formulation of Chapter 3, which includes the action balance equation as a statistically well-defined limiting case. Preliminary results indicate that the derivation of the generalized mild-slope equation which accounts for the effect of ambient current is obtained straightforwardly. The results also verify the reduction of this generalized mild-slope formulation to the classical mild-slope model of Kirby (1984) under the assumption of quasi-periodicity. However, the transformation of this mild-slope formulation to the system consisting of the desired Schrödinger equation and its complex-conjugate may not obviously be derived. One may either be required to deal with an additional reflection-like term, which requires further assumptions to characterize the current field (e.g. Dingemans, 1997) or one may propose an alternative (and closely related) definition to the action variable. This discussion highlights the need for further investigation of the transformation between those two systems.

Even though the statistical model of Chapter 3 presently relies on a starting point equation which is only verified for idealized cases (evolution of wave field over homogeneous media, or evolution of a single wave component over weakly inhomogeneous media), its performance for more general cases is extensively demonstrated through comparisons with the SWAN model and the REF/DIF 1 model. Based on its satisfying performance, this generalized action balance model is nowadays available for operational use as part of the open source SWAN model using a source term known as the quasi-coherent (QC) term (indicated by 'SCAT' in SWAN, also see the SWAN manual that is available in the SWAN website: <https://swanmodel.sourceforge.io/>). However, its improved predictive capabilities come with rather expensive computational costs. Additionally, the present formulation cannot cope with discontinuities (e.g., breakwaters and coastline patterns) which create partially enclosed water areas dominated by wave diffraction. These issues call for further model development to extend the utility of the QC source term for application of larger scales (e.g., by somehow extracting the main wave interference contribution which may allow to approximate the costly convolution integral required for the computation of this source term) and for applications involving discontinuities (e.g., by somehow extending the obstacle formulation in SWAN to allow radiation of the coherent information between incoming waves in the vicinity of obstacles).

The final part of this study, described in Chapter 4, attempts to contribute to the more general effort of formulating statistically the nonlinear evolution of waves in shallow water. Specifically, Chapter 4 concerns with the quadratic formulation that is used as the starting point for the present phase-averaged nonlinear formulations (e.g. Eldeberky, 1996, Herbers and Burton, 1997), but also provides an independent deterministic tool for wave prediction over coastal waters (e.g., the model by Kaihatu and Kirby, 1995 and the TRIADS model by Sheremet et al., 2016). Generally speaking, Chapter 4 is

divided into two parts. The first deals with the investigation of existing quadratic formulations, including fully dispersive and Boussinesq formulations. The second part focuses on a heuristic derivation of a new fully dispersive quadratic formulation with optimized nonlinear performance (i.e. QuadWave1D). In the first part, the tendency of the fully dispersive formulations to over predict the amplitude dispersion and the associated unfavourable modifications of the modulational instability mechanism are discussed. However, beyond these findings, the fully dispersive formulations also seem to suffer from an additional unfavourable effect in the absence of modulational instability. In particular, simple monochromatic cases suggest that the prediction results using these formulations are sensitive to the presence of relatively high frequencies. This sensitivity is demonstrated through significant deviations in the amplitude evolution of the various harmonics characterized by rapid oscillations and by excessive energy exchanges. The consequence of this sensitivity is that the predictions using these formulations become dependent on the choice of the maximum frequency. It is assumed that this sensitivity is related to an inadequate nonlinear balance created by excessive values of the interaction coefficients involving high frequencies. However, in-depth investigation is required to clarify the mechanism that leads to this unfavourable model sensitivity. Additional issue that requires further investigation relates to the generalization of QuadWave1D (a new quadratic formulation derived in the second part of Chapter 4) for the prediction of directional spectra. Based on comparisons to other quadratic formulations and to measured results, QuadWave1D indeed seems to provide superior forecasting capabilities in one dimensional settings. However, its predictive capabilities were not verified for non-collinear wave interactions. In principle, the parameterization based on which QuadWave1D is formulated can also be applied for directional spectra since it is written in terms of wavenumber magnitudes. However, whether this parameterization actually leads to adequate energy exchanges between non-collinear waves remains an open question. Finally, the path toward an adequate phase-averaged formulation of shallow water nonlinearity should also be noted. To this end, QuadWave1D provides a convenient starting point (the nonlinearity is described by a single simple term) and enables a computationally efficient investigation for the needs of gaining additional insights and developing different prediction tools with minimal accompanying errors.

ACKNOWLEDGEMENTS

I would like to express my acknowledgements to the people who directly and indirectly supported and helped me to complete this study. First and foremost, I am indebted to my supervisors for their help, support, guidance, and ideas during the years of working together. Pieter, I have learned from you enormously, about water waves, about mathematical and statistical methods and through your guidance and smart ideas, thank you very much for all of that. Marcel, thank you very much for your support along the way, for helping me with every question and problem I referred to you and for the chance to learn from your immense knowledge about numerical methods. Thank you also for turning Chapter 3 from a theoretical work into an actual prediction tool! Finally, Ad, I am sincerely grateful for the opportunity you gave me (quite a few years ago) to take part in the research proposal that Pieter initiated, which luckily received the grant and led to this study. Since then, you have supported and helped me to develop as a researcher. I would like to thank you for the ideas, knowledge and experience from which I learned a lot. Thank you also for the many hours of guidance which helped me to focus on the important things, to gain confidence in the directions I chose and ultimately led me to the completion of this work. Finally, I thank all of you for your trust and patience along this journey.

I would also like to thank my colleagues from the Environmental Fluid Mechanics section, especially my colleagues from office 2.95, for the friendly atmosphere and the pleasant working environment. Thank you also Otti for helping me with any matter I referred to you along the way and for your insistence on teaching me Dutch.

Finally, I would like to thank my family. To the love of my life Ronni, to my wonderful children, Daphna, Noam and Yonatan, to my parents and Ronni's parents and to the rest of the family members for supporting me along this long way of research. A special thanks is dedicated to Micky (my mother-in-law) for the endless help with the kids. Without this help, it would have been possible for me to retire as a PhD student. Last but not least is Sjalène (the partner of my brother-in-law). Without your help with the kids I wouldn't have any chance to participate in Coastal Dynamics 2021! So, thank you for that.

BIBLIOGRAPHY

- Aceves-Sánchez, P., Minzoni, A., & Panayotaros, P. (2013). Numerical study of a nonlocal model for water-waves with variable depth. *Wave Motion*, 50(1), 80–93.
- Agnon, Y. (1999). Linear and nonlinear refraction and Bragg scattering of water waves. *Physical Review E*, 59(2), R1319.
- Agnon, Y., Madsen, P. A., & Schäffer, H. A. (1999). A new approach to high-order Boussinesq models. *Journal of Fluid Mechanics*, 399, 319–333.
- Agnon, Y., & Sheremet, A. (1997). Stochastic nonlinear shoaling of directional spectra. *Journal of Fluid Mechanics*, 345, 79–99.
- Agnon, Y., Sheremet, A., Gonsalves, J., & Stiassnie, M. (1993). Nonlinear evolution of a unidirectional shoaling wave field. *Coastal Engineering*, 20(1-2), 29–58.
- Akrish, G., Rabinovitch, O., & Agnon, Y. (2016). Extreme run-up events on a vertical wall due to nonlinear evolution of incident wave groups. *Journal of Fluid Mechanics*, 797, 644–664.
- Akrish, G., Smit, P., Zijlema, M., & Reniers, A. (2020). Modelling statistical wave interferences over shear currents. *Journal of Fluid Mechanics*, 891.
- Alber, I. (1978). The effects of randomness on the stability of two-dimensional surface wavetrains. *Proceedings of the Royal Society of London. A. Mathematical and Physical Sciences*, 363(1715), 525–546.
- Ardani, S., & Kaihatu, J. M. (2019). Evolution of high frequency waves in shoaling and breaking wave spectra. *Physics of Fluids*, 31(8), 087102.
- Ardhuin, F., Gille, S. T., Menemenlis, D., Rocha, C. B., Rascle, N., Chapron, B., Gula, J., & Molemaker, J. (2017). Small-scale open ocean currents have large effects on wind wave heights. *Journal of Geophysical Research: Oceans*, 122(6), 4500–4517.
- Ardhuin, F., O'reilly, W., Herbers, T., & Jessen, P. (2003). Swell transformation across the continental shelf. part i: Attenuation and directional broadening. *Journal of Physical Oceanography*, 33(9), 1921–1939.
- Bateman, W. J., Swan, C., & Taylor, P. H. (2001). On the efficient numerical simulation of directionally spread surface water waves. *Journal of Computational Physics*, 174(1), 277–305.
- Battjes, J., Bakkenes, H., Janssen, T., & van Dongeren, A. R. (2004). Shoaling of subharmonic gravity waves. *Journal of Geophysical Research: Oceans*, 109(C2).
- Becq-Girard, F., Forget, P., & Benoit, M. (1999). Non-linear propagation of unidirectional wave fields over varying topography. *Coastal Engineering*, 38(2), 91–113.
- Beji, S., & Battjes, J. (1993). Experimental investigation of wave propagation over a bar. *Coastal Engineering*, 19(1-2), 151–162.
- Beji, S., & Nadaoka, K. (1996). A formal derivation and numerical modelling of the improved Boussinesq equations for varying depth. *Ocean Engineering*, 23(8), 691–704.

- Belibassakis, K., Gerostathis, T. P., & Athanassoulis, G. (2011). A coupled-mode model for water wave scattering by horizontal, non-homogeneous current in general bottom topography. *Applied Ocean Research*, 33(4), 384–397.
- Benjamin, T. B., & Feir, J. E. (1967). The disintegration of wave trains on deep water part 1. theory. *Journal of Fluid Mechanics*, 27(3), 417–430.
- Benney, D., & Saffman, P. G. (1966). Nonlinear interactions of random waves in a dispersive medium. *Proceedings of the Royal Society of London. Series A. Mathematical and Physical Sciences*, 289(1418), 301–320.
- Benoit, M., Marcos, F., & Becq, F. (1996). Development of a third generation shallow-water wave model with unstructured spatial meshing. *Coastal Engineering Proceedings*, (25), 465–478.
- Berkhoff, J. (1972). Computation of combined refraction—diffraction. *Coastal Engineering Proceedings*, (13), 471–490.
- Besieris, I. M. (1985). Wave-kinetic method, phase-space path integrals, and stochastic wave propagation. *JOSA A*, 2(12), 2092–2099.
- Besieris, I. M., & Tappert, F. D. (1976). Stochastic wave-kinetic theory in the Liouville approximation. *Journal of Mathematical Physics*, 17(5), 734–743.
- Bonneton, P., Barthélemy, E., Chazel, F., Cienfuegos, R., Lannes, D., Marche, F., & Tissier, M. (2011). Recent advances in Serre–Green Naghdi modelling for wave transformation, breaking and runup processes. *European Journal of Mechanics-B/Fluids*, 30(6), 589–597.
- Booij, N., Ris, R. C., & Holthuijsen, L. H. (1999). A third-generation wave model for coastal regions: 1. model description and validation. *Journal of Geophysical Research: Oceans*, 104(C4), 7649–7666.
- Bowen, A. J. (1969). Rip currents: 1. Theoretical investigations. *Journal of Geophysical Research*, 74(23), 5467–5478.
- Bowers, E. (1977). Harbour resonance due to set-down beneath wave groups. *Journal of Fluid Mechanics*, 79(1), 71–92.
- Bredmose, H., Agnon, Y., Madsen, P. A., & Schäffer, H. A. (2005). Wave transformation models with exact second-order transfer. *European Journal of Mechanics-B/Fluids*, 24(6), 659–682.
- Bredmose, H., Schäffer, H. A., & Madsen, P. A. (2004). Boussinesq evolution equations: Numerical efficiency, breaking and amplitude dispersion. *Coastal Engineering*, 51(11-12), 1117–1142.
- Bremmer, H. (1973). General remarks concerning theories dealing with scattering and diffraction in random media. *Radio Science*, 8(6), 511–534.
- Bretherton, F., & Garrett, C. J. R. (1968). Wavetrains in inhomogeneous moving media. *Proceedings of the Royal Society of London. Series A. Mathematical and Physical Sciences*, 302(1471), 529–554.
- Bryant, P. J. (1973). Periodic waves in shallow water. *Journal of Fluid Mechanics*, 59(4), 625–644.
- Carter, J. D., Dinvey, E., & Kalisch, H. (2021). Fully dispersive Boussinesq models with uneven bathymetry. *Journal of Engineering Mathematics*, 127(1), 1–14.
- Chapalain, G., Cointe, R., & Temperville, A. (1992). Observed and modeled resonantly interacting progressive water-waves. *Coastal Engineering*, 16(3), 267–300.

- Chawla, A., Özkan-Haller, H. T., & Kirby, J. T. (1998). Spectral model for wave transformation and breaking over irregular bathymetry. *Journal of Waterway, Port, Coastal, and Ocean Engineering*, 124(4), 189–198.
- Chen, Q., Dalrymple, R. A., Kirby, J. T., Kennedy, A. B., & Haller, M. C. (1999). Boussinesq modeling of a rip current system. *Journal of Geophysical Research: Oceans*, 104(C9), 20617–20637.
- Chen, X. (2016). Impacts of overtopping waves on buildings on coastal dikes. *PhD thesis, Delft University of Technology*.
- Cohen, L. (2012). *The Weyl Operator and its Generalization*. Springer Science & Business Media.
- Craig, W., Guyenne, P., Nicholls, D. P., & Sulem, C. (2005). Hamiltonian long-wave expansions for water waves over a rough bottom. *Proceedings of the Royal Society A: Mathematical, Physical and Engineering Sciences*, 461(2055), 839–873.
- Craig, W., & Sulem, C. (1993). Numerical simulation of gravity waves. *Journal of Computational Physics*, 108(1), 73–83.
- Craik, A. D. D. (1985). *Wave Interactions and Fluid Flows*. Cambridge University Press.
- Craik, A. D. D., & Leibovich, S. (1976). A rational model for langmuir circulations. *Journal of Fluid Mechanics*, 73(3), 401–426.
- Dalrymple, R. A., & Rogers, B. (2006). Numerical modeling of water waves with the SPH method. *Coastal Engineering*, 53(2-3), 141–147.
- Dalzell, J. (1999). A note on finite depth second-order wave-wave interactions. *Applied Ocean Research*, 21(3), 105–111.
- De Bakker, A., Herbers, T., Smit, P., Tissier, M., & Ruessink, B. G. (2015). Nonlinear infragravity-wave interactions on a gently sloping laboratory beach. *Journal of Physical Oceanography*, 45(2), 589–605.
- Dewar, R. (1970). Interaction between hydromagnetic waves and a time-dependent, inhomogeneous medium. *The Physics of Fluids*, 13(11), 2710–2720.
- Dingemans, M. W. (1994). Comparison of computations with Boussinesq-like models and laboratory measurements. *Memo in framework of MAST project (G8-M), Delft Hydraulics memo H1684. 12*.
- Dingemans, M. W. (1997). *Water Wave Propagation over Uneven Bottoms* (Vol. 13). World Scientific.
- Djordjević, V. D., & Redekopp, L. G. (1978). On the development of packets of surface gravity waves moving over an uneven bottom. *Zeitschrift für Angewandte Mathematik und Physik ZAMP*, 29(6), 950–962.
- Dommermuth, D. G., & Yue, D. K. (1987). A high-order spectral method for the study of nonlinear gravity waves. *Journal of Fluid Mechanics*, 184, 267–288.
- Dyhr-Nielsen, M., & Sørensen, T. (1970). Some sand transport phenomena on coasts with bars. *Coastal Engineering Proceedings*, (12), 855–865.
- Dysthe, K., Krogstad, H. E., & Müller, P. (2008). Oceanic rogue waves. *Annual Review of Fluid Mechanics*, 40, 287–310.
- Eldeberky, Y. (1996). Nonlinear transformation of wave spectra in the near-shore zone. *PhD thesis, Delft University of Technology*.
- Eldeberky, Y. (1997). Nonlinear transformation of wave spectra in the nearshore zone. *Oceanographic Literature Review*, 4(44), 297.

- Eldeberky, Y., & Battjes, J. A. (1996). Spectral modeling of wave breaking: Application to Boussinesq equations. *Journal of Geophysical Research: Oceans*, 101(C1), 1253–1264.
- Eldeberky, Y., & Madsen, P. A. (1999). Deterministic and stochastic evolution equations for fully dispersive and weakly nonlinear waves. *Coastal Engineering*, 38(1), 1–24.
- Elgar, S., & Guza, R. (1985). Observations of bispectra of shoaling surface gravity waves. *Journal of Fluid Mechanics*, 161, 425–448.
- Fedele, F., Brennan, J., Ponce de León, S., Dudley, J., & Dias, F. (2016). Real world ocean rogue waves explained without the modulational instability. *Scientific Reports*, 6(1), 1–11.
- Fredsoe, J., & Deigaard, R. (1992). *Mechanics of Coastal Sediment Transport* (Vol. 3). World Scientific Publishing Company.
- Freilich, M., & Guza, R. (1984). Nonlinear effects on shoaling surface gravity waves. *Philosophical Transactions of the Royal Society of London. Series A, Mathematical and Physical Sciences*, 311(1515), 1–41.
- Goodman, J. W. (1985). *Statistical optics*. John Wiley & Sons.
- Gorrell, L., Raubenheimer, B., Elgar, S., & Guza, R. (2011). SWAN predictions of waves observed in shallow water onshore of complex bathymetry. *Coastal Engineering*, 58(6), 510–516.
- Gouin, M., Ducrozet, G., & Ferrant, P. (2016). Development and validation of a nonlinear spectral model for water waves over variable depth. *European Journal of Mechanics-B/Fluids*, 57, 115–128.
- Guyenne, P., & Nicholls, D. P. (2008). A high-order spectral method for nonlinear water waves over moving bottom topography. *SIAM Journal on Scientific Computing*, 30(1), 81–101.
- Hasselmann, K. (1962). On the non-linear energy transfer in a gravity-wave spectrum Part 1. General theory. *Journal of Fluid Mechanics*, 12(4), 481–500.
- Hasselmann, K. (1963). On the non-linear energy transfer in a gravity wave spectrum Part 2. Conservation theorems; wave-particle analogy; irreversibility. *Journal of Fluid Mechanics*, 15(2), 273–281.
- Hasselmann, K. (1974). On the spectral dissipation of ocean waves due to white capping. *Boundary-Layer Meteorology*, 6(1), 107–127.
- Herbers, T., & Burton, M. (1997). Nonlinear shoaling of directionally spread waves on a beach. *Journal of Geophysical Research: Oceans*, 102(C9), 21101–21114.
- Herbers, T., Orzech, M., Elgar, S., & Guza, R. (2003). Shoaling transformation of wave frequency-directional spectra. *Journal of Geophysical Research: Oceans*, 108(C1).
- Herbers, T., Russnogle, N., & Elgar, S. (2000). Spectral energy balance of breaking waves within the surf zone. *Journal of Physical Oceanography*, 30(11), 2723–2737.
- Hertzog, A., Souprayen, C., & Hauchecorne, A. (2002). Eikonal simulations for the formation and the maintenance of atmospheric gravity wave spectra. *Journal of Geophysical Research: Atmospheres*, 107(D12), ACL–4.
- Hirsch, C. (2007). *Numerical Computation of Internal and External Flows: The Fundamentals of Computational Fluid Dynamics*. Elsevier.

- Hlawatsch, E., & Flandrin, P. (1997). The interference structure of the Wigner distribution and related time-frequency signal representations. *The Wigner Distribution—Theory and Applications in Signal Processing*, 59–133.
- Hoeke, R. K., McInnes, K. L., Kruger, J. C., McNaught, R. J., Hunter, J. R., & Smithers, S. G. (2013). Widespread inundation of pacific islands triggered by distant-source wind-waves. *Global and Planetary Change*, 108, 128–138.
- Holloway, G., & Hendershott, M. C. (1977). Stochastic closure for nonlinear rossby waves. *Journal of Fluid Mechanics*, 82(4), 747–765.
- Holmes, M. H. (1995). *Introduction to Perturbation Methods*. Springer Science & Business Media.
- Holthuijsen, L. H. (2007). *Waves in Oceanic and Coastal Waters*. Cambridge University Press.
- Hur, V. M., & Johnson, M. A. (2015). Modulational instability in the Whitham equation for water waves. *Studies in Applied Mathematics*, 134(1), 120–143.
- Janssen, P. (2003). Nonlinear four-wave interactions and freak waves. *Journal of Physical Oceanography*, 33(4), 863–884.
- Janssen, P., Hansen, B., & Bidlot, J.-R. (1997). Verification of the ECMWF wave forecasting system against buoy and altimeter data. *Weather and Forecasting*, 12(4), 763–784.
- Janssen, P., & Onorato, M. (2007). The intermediate water depth limit of the Zakharov equation and consequences for wave prediction. *Journal of Physical Oceanography*, 37(10), 2389–2400.
- Janssen, T. (2006). Nonlinear surface waves over topography. *PhD thesis, Delft University of Technology*.
- Janssen, T., Battjes, J., & Van Dongeren, A. (2003). Long waves induced by short-wave groups over a sloping bottom. *Journal of Geophysical Research: Oceans*, 108(C8).
- Janssen, T., & Herbers, T. (2009). Nonlinear wave statistics in a focal zone. *Journal of Physical Oceanography*, 39(8), 1948–1964.
- Janssen, T., Herbers, T., & Battjes, J. (2008). Evolution of ocean wave statistics in shallow water: Refraction and diffraction over seafloor topography. *Journal of Geophysical Research: Oceans*, 113(C3).
- Kaihatu, J. M., & Kirby, J. T. (1995). Nonlinear transformation of waves in finite water depth. *Physics of Fluids*, 7(8), 1903–1914.
- Kharif, C., & Pelinovsky, E. (2003). Physical mechanisms of the rogue wave phenomenon. *European Journal of Mechanics-B/Fluids*, 22(6), 603–634.
- Kim, I.-C., & Kaihatu, J. M. (2021). A consistent nonlinear mild-slope equation model. *Coastal Engineering*, 170, 104006.
- Kirby, J. T. (1984). A note on linear surface wave-current interaction over slowly varying topography. *Journal of Geophysical Research: Oceans*, 89(C1), 745–747.
- Kirby, J. T., & Dalrymple, R. A. (1986). An approximate model for nonlinear dispersion in monochromatic wave propagation models. *Coastal Engineering*, 9(6), 545–561.
- Komen, G. J., Cavaleri, L., Donelan, M., Hasselmann, K., Hasselmann, S., & Janssen, P. (1994). *Dynamics and Modelling of Ocean Waves*. Cambridge University Press.
- Krasitskii, V. P. (1994). On reduced equations in the hamiltonian theory of weakly nonlinear surface waves. *Journal of Fluid Mechanics*, 272, 1–20.

- Lake, B. M., Yuen, H. C., Rungaldier, H., & Ferguson, W. E. (1977). Nonlinear deep-water waves: Theory and experiment. Part 2. Evolution of a continuous wave train. *Journal of Fluid Mechanics*, 83(1), 49–74.
- Lapidoth, A. (2017). *A Foundation in Digital Communication*. Cambridge University Press.
- Le Méhauté, B. (1976). *An Introduction to Hydrodynamics and Water Waves*. Springer Science & Business Media.
- Leaf, B. (1968). Weyl transformation and the classical limit of quantum mechanics. *Journal of Mathematical Physics*, 9(1), 65–72.
- Lighthill, J. (2001). *Waves in Fluids*. Cambridge University Press.
- Liu, S., Zhang, X., Yang, J., & Yao, J. (2022). Modulational instability and statistical properties of irregular waves in finite water depth. *Applied Ocean Research*, 120, 103031.
- Liu, Y., & Yue, D. K. (1998). On generalized Bragg scattering of surface waves by bottom ripples. *Journal of Fluid Mechanics*, 356, 297–326.
- Longuet-Higgins, M. S. (1962). Resonant interactions between two trains of gravity waves. *Journal of Fluid Mechanics*, 12(3), 321–332.
- Longuet-Higgins, M. S. (1970). Longshore currents generated by obliquely incident sea waves: 1. *Journal of Geophysical Research*, 75(33), 6778–6789.
- Longuet-Higgins, M. S., & Phillips, O. M. (1962). Phase velocity effects in tertiary wave interactions. *Journal of Fluid Mechanics*, 12(3), 333–336.
- Longuet-Higgins, M. S., & Stewart, R. (1964). Radiation stresses in water waves; a physical discussion, with applications. *Deep Sea Research and Oceanographic Abstracts*, 11(4), 529–562.
- Longuet-Higgins, M. S., & Stewart, R. (1961). The changes in amplitude of short gravity waves on steady non-uniform currents. *Journal of Fluid Mechanics*, 10(4), 529–549.
- Madsen, P. A., & Schäffer, H. A. (1998). Higher-order Boussinesq-type equations for surface gravity waves: Derivation and analysis. *Philosophical Transactions of the Royal Society of London. Series A: Mathematical, Physical and Engineering Sciences*, 356(1749), 3123–3181.
- Madsen, P. A., & Sørensen, O. R. (1993). Bound waves and triad interactions in shallow water. *Ocean Engineering*, 20(4), 359–388.
- Madsen, P. A., & Fuhrman, D. R. (2006). Third-order theory for bichromatic bi-directional water waves. *Journal of Fluid Mechanics*, 557, 369–397.
- Madsen, P. A., Murray, R., & Sørensen, O. R. (1991). A new form of the Boussinesq equations with improved linear dispersion characteristics. *Coastal Engineering*, 15(4), 371–388.
- Madsen, P. A., & Sørensen, O. R. (1992). A new form of the Boussinesq equations with improved linear dispersion characteristics. Part 2. A slowly-varying bathymetry. *Coastal Engineering*, 18(3-4), 183–204.
- Mapp, G. R., Welch, C. S., & Munday, J. C. (1985). Wave refraction by warm core rings. *Journal of Geophysical Research: Oceans*, 90(C4), 7153–7162.
- McDonald, S. W., & Kaufman, A. N. (1985). Weyl representation for electromagnetic waves: The wave kinetic equation. *Physical Review A*, 32(3), 1708.

- McWilliams, J. C. (2016). Submesoscale currents in the ocean. *Proceedings of the Royal Society A: Mathematical, Physical and Engineering Sciences*, 472(2189), 20160117.
- McWilliams, J. C. (2018). Surface wave effects on submesoscale fronts and filaments. *Journal of Fluid Mechanics*, 843, 479–517.
- Mei, C. C. (1989). *The Applied Dynamics of Ocean Surface Waves*. World scientific.
- Mei, C. C., Stiassnie, M. A., & Yue, D. K.-P. (2005). *Theory and Applications of Ocean Surface Waves*. World Scientific.
- Mei, C. C., & Ünlüata, Ü. (1972). Harmonic generation in shallow water waves. In *Waves on Beaches and Resulting Sediment Transport* (pp. 181–202). Academic Press.
- Metzger, J. J., Fleischmann, R., & Geisel, T. (2014). Statistics of extreme waves in random media. *Physical Review Letters*, 112(20), 203903.
- Milder, D. M. (1990). The effects of truncation on surface-wave hamiltonians. *Journal of Fluid Mechanics*, 217, 249–262.
- Miles, J. (1957). On the generation of surface waves by shear flows. *Journal of Fluid Mechanics*, 3(2), 185–204.
- Miles, J. (1985). Surface waves in basins of variable depth. *Journal of Fluid Mechanics*, 152, 379–389.
- Milewski, P. A. (1998). A formulation for water waves over topography. *Studies in Applied Mathematics*, 100(1), 95–106.
- Moldabayev, D., Kalisch, H., & Dutykh, D. (2015). The Whitham equation as a model for surface water waves. *Physica D: Nonlinear Phenomena*, 309, 99–107.
- Moyal, J. E. (1949). Quantum mechanics as a statistical theory. *Mathematical Proceedings of the Cambridge Philosophical Society*, 45(1), 99–124.
- Muraschko, J., Fruman, M., Achatz, U., Hickel, S., & Toledo, Y. (2015). On the application of Wentzel–Kramer–Brillouin theory for the simulation of the weakly nonlinear dynamics of gravity waves. *Quarterly Journal of the Royal Meteorological Society*, 141(688), 676–697.
- Newell, A. C. (1968). The closure problem in a system of random gravity waves. *Reviews of Geophysics*, 6(1), 1–31.
- Nikolkina, I., & Didenkulova, I. (2011). Rogue waves in 2006–2010. *Natural Hazards and Earth System Sciences*, 11(11), 2913–2924.
- Nwogu, O. (1993). Alternative form of Boussinesq equations for nearshore wave propagation. *Journal of Waterway, Port, Coastal, and Ocean Engineering*, 119(6), 618–638.
- Onorato, M., Waseda, T., Toffoli, A., Cavaleri, L., Gramstad, O., Janssen, P., Kinoshita, T., Monbaliu, J., Mori, N., Osborne, A. R., Serio, M., Stansberg, C. T., Tamura, H., & Trulsen, K. (2009). Statistical properties of directional ocean waves: The role of the modulational instability in the formation of extreme events. *Physical Review Letters*, 102(11), 114502.
- Onorato, M., Osborne, A. R., Serio, M., & Bertone, S. (2001). Freak waves in random oceanic sea states. *Physical Review Letters*, 86(25), 5831.
- Onorato, M., Osborne, A. R., Serio, M., Cavaleri, L., Brandini, C., & Stansberg, C. T. (2006). Extreme waves, modulational instability and second order theory: Wave flume

- experiments on irregular waves. *European Journal of Mechanics-B/Fluids*, 25(5), 586–601.
- O'Reilly, W., & Guza, R. (1991). A comparison of spectral refraction and refraction-diffraction wave models. *Journal of Waterway Port, Coastal and Ocean Engineering*, 117(3), 199–215.
- Orszag, S. A. (1970). Analytical theories of turbulence. *Journal of Fluid Mechanics*, 41(2), 363–386.
- Papoulis, A. (1965). *Probability, random variables, and stochastic processes*. McGraw-Hill.
- Peregrine, D. H. (1967). Long waves on a beach. *Journal of Fluid Mechanics*, 27(4), 815–827.
- Phillips, O. M. (1960). On the dynamics of unsteady gravity waves of finite amplitude Part 1. The elementary interactions. *Journal of Fluid Mechanics*, 9(2), 193–217.
- Phillips, O. M. (1967). Theoretical and experimental studies of gravity wave interactions. *Proceedings of the Royal Society of London. Series A. Mathematical and Physical Sciences*, 299(1456), 104–119.
- Poje, A. C., Özgökmen, T. M., Lipphardt Jr., B. L., Haus, B. K., Ryan, E. H., Haza, A. C., Jacobs, G. A., Reniers, A., Olascoaga, M. J., Novelli, G., Griffa, A., Beron-Vera, F. J., Chen, S. S., Coelho, E., Hogan, P. J., Kirwan Jr., A. D., Huntley, H. S., & Mariano, A. J. (2014). Submesoscale dispersion in the vicinity of the deepwater horizon spill. *Proceedings of the National Academy of Sciences of the United States of America*, 111(35), 12693–12698.
- Radder, A. (1999). Hamiltonian dynamics of water waves. In *Advances in Coastal and Ocean Engineering* (pp. 21–59). World Scientific.
- Reniers, A., & Battjes, J. (1997). A laboratory study of longshore currents over barred and non-barred beaches. *Coastal Engineering*, 30(1-2), 1–21.
- Rice, S. O. (1945). Mathematical analysis of random noise. *The Bell System Technical Journal*, 24(1), 46–156.
- Rijnsdorp, D. P., Smit, P. B., & Guza, R. (2022). A nonlinear, non-dispersive energy balance for surfzone waves: Infragravity wave dynamics on a sloping beach. *Journal of Fluid Mechanics*, 944.
- Rijnsdorp, D. P., Smit, P. B., & Zijlema, M. (2014). Non-hydrostatic modelling of infragravity waves under laboratory conditions. *Coastal Engineering*, 85, 30–42.
- Roeber, V., & Bricker, J. D. (2015). Destructive tsunami-like wave generated by surf beat over a coral reef during typhoon haiyan. *Nature Communications*, 6(1), 1–9.
- Roelvink, D., Reniers, A., Van Dongeren, A., de Vries, J. v. T., McCall, R., & Lescinski, J. (2009). Modelling storm impacts on beaches, dunes and barrier islands. *Coastal Engineering*, 56(11-12), 1133–1152.
- Roelvink, J. A., & Stive, M. J. F. (1989). Bar-generating cross-shore flow mechanisms on a beach. *Journal of Geophysical Research: Oceans*, 94(C4), 4785–4800.
- Ruessink, B. G., Michallet, H., Bonneton, P., Mouazé, D., Lara, J., Silva, P. A., & Wellens, P. (2013). Globex: Wave dynamics on a gently sloping laboratory beach. *Proceedings Coastal Dynamics*, 1351–1362.
- Ruessink, B. G., Miles, J., Feddersen, F., Guza, R., & Elgar, S. (2001). Modeling the along-shore current on barred beaches. *Journal of Geophysical Research: Oceans*, 106(C10), 22451–22463.

- Ruggiero, P., Komar, P. D., McDougal, W. G., Marra, J. J., & Beach, R. A. (2001). Wave runup, extreme water levels and the erosion of properties backing beaches. *Journal of Coastal Research*, 407–419.
- Salmon, J., Smit, P., Janssen, T., & Holthuijsen, L. (2016). A consistent collinear triad approximation for operational wave models. *Ocean Modelling*, 104, 203–212.
- Schäffer, H. A. (2008). Comparison of Dirichlet–Neumann operator expansions for nonlinear surface gravity waves. *Coastal Engineering*, 55(4), 288–294.
- Schäffer, H. A., & Madsen, P. A. (1995). Further enhancements of Boussinesq-type equations. *Coastal Engineering*, 26(1-2), 1–14.
- Schäffer, H. A., & Madsen, P. A. (1998). Discussion of a formal derivation and numerical modelling of the improved Boussinesq equations for varying depth. *Ocean Engineering*, 25(6), 497.
- Sen, B. (1927). Waves in canals and basins. *Proceedings of the London Mathematical Society*, 2(1), 363–376.
- Sharma, J., & Dean, R. (1981). Second-order directional seas and associated wave forces. *Society of Petroleum Engineers Journal*, 21(01), 129–140.
- Sheremet, A., Davis, J. R., Tian, M., Hanson, J. L., & Hathaway, K. K. (2016). Triads: A phase-resolving model for nonlinear shoaling of directional wave spectra. *Ocean Modelling*, 99, 60–74.
- Smit, P., & Janssen, T. (2013). The evolution of inhomogeneous wave statistics through a variable medium. *Journal of Physical Oceanography*, 43(8), 1741–1758.
- Smit, P., Janssen, T., & Herbers, T. (2015a). Stochastic modeling of coherent wave fields over variable depth. *Journal of Physical Oceanography*, 45(4), 1139–1154.
- Smit, P., Janssen, T., & Herbers, T. (2015b). Stochastic modeling of inhomogeneous ocean waves. *Ocean Modelling*, 96, 26–35.
- Smith, R. A. (1998). An operator expansion formalism for nonlinear surface waves over variable depth. *Journal of Fluid Mechanics*, 363, 333–347.
- Smith, R., & Sprinks, T. (1975). Scattering of surface waves by a conical island. *Journal of Fluid Mechanics*, 72(2), 373–384.
- Soong, T. T. (1973). *Random Differential Equations in Science and Engineering*. Elsevier.
- Stive, M. J., & De Vriend, H. J. (1994). Shear stresses and mean flow in shoaling and breaking waves. *Coastal Engineering Proceedings*, (24), 594–608.
- Toffoli, A., Proment, D., Salman, H., Monbaliu, J., Frascoli, F., Dafilis, M., Stramignoni, E., Forza, R., Manfrin, M., & Onorato, M. (2017). Wind generated rogue waves in an annular wave flume. *Physical Review Letters*, 118(14), 144503.
- Toledo, Y., & Agnon, Y. (2012). Stochastic evolution equations with localized nonlinear shoaling coefficients. *European Journal of Mechanics-B/Fluids*, 34, 13–18.
- Tolman, H. L. (1991). A third-generation model for wind waves on slowly varying, unsteady, and inhomogeneous depths and currents. *Journal of Physical Oceanography*, 21(6), 782–797.
- Van Gent, M. R. (2001). Wave runup on dikes with shallow foreshores. *Journal of Waterway, Port, Coastal, and Ocean Engineering*, 127(5), 254–262.
- Van Groesen, E. (1998). Wave groups in uni-directional surface-wave models. *Journal of Engineering Mathematics*, 34(1), 215–226.

- Van Groesen, E., & Molenaar, J. (2007). *Continuum Modeling in the Physical Sciences*. SIAM.
- Van Noorloos, J. C. (2003). Energy transfer between short wave groups and bound long waves on a plane slope. *MSc thesis, Delft University of Technology*.
- Van Rijn, L. C. (1993). *Principles of Sediment Transport in Rivers, Estuaries and Coastal Seas* (Vol. 1006). Aqua Publications Amsterdam.
- Vanneste, J. (2005). Wave interactions. In *Nonlinear Waves in Fluids: Recent Advances and Modern Applications* (pp. 69–94). Springer.
- Vargas-Magana, R., & Panayotaros, P. (2016). A Whitham–Boussinesq long-wave model for variable topography. *Wave Motion*, 65, 156–174.
- Vellinga, P. (1982). Beach and dune erosion during storm surges. *Coastal Engineering*, 6(4), 361–387.
- Vincent, C. L., & Briggs, M. J. (1989). Refraction-diffraction of irregular waves over a mound. *Journal of Waterway, Port, Coastal and Ocean Engineering*, 115(2), 269–284.
- Vrecica, T., & Toledo, Y. (2016). Consistent nonlinear stochastic evolution equations for deep to shallow water wave shoaling. *Journal of Fluid Mechanics*, 794, 310–342.
- WAMDI Group. (1988). The WAM model—a third generation ocean wave prediction model. *Journal of Physical Oceanography*, 18(12), 1775–1810.
- Watson, K. M., & West, B. J. (1975). A transport-equation description of nonlinear ocean surface wave interactions. *Journal of Fluid Mechanics*, 70(4), 815–826.
- Wei, G., Kirby, J. T., Grilli, S. T., & Subramanya, R. (1995). A fully nonlinear Boussinesq model for surface waves. Part 1. Highly nonlinear unsteady waves. *Journal of Fluid Mechanics*, 294, 71–92.
- West, B. J., Brueckner, K. A., Janda, R. S., Milder, D. M., & Milton, R. L. (1987). A new numerical method for surface hydrodynamics. *Journal of Geophysical Research: Oceans*, 92(C11), 11803–11824.
- Weyl, H. (1931). *The Theory of Groups and Quantum Mechanics*. Dover, New York.
- Whitham, G. B. (1967). Variational methods and applications to water waves. *Proceedings of the Royal Society of London. Series A. Mathematical and Physical Sciences*, 299(1456), 6–25.
- Whitham, G. B. (1974). *Linear and Nonlinear Waves*. John Wiley & Sons.
- Willebrand, J. (1975). Energy transport in a nonlinear and inhomogeneous random gravity wave field. *Journal of Fluid Mechanics*, 70(1), 113–126.
- Witting, J. M. (1984). A unified model for the evolution nonlinear water waves. *Journal of Computational Physics*, 56(2), 203–236.
- Wu, W.-C., Wang, T., Yang, Z., & Garcia-Medina, G. (2020). Development and validation of a high-resolution regional wave hindcast model for us west coast wave resource characterization. *Renewable Energy*, 152, 736–753.
- Yoon, S. B., & Liu, P. L.-F. (1989). Interactions of currents and weakly nonlinear water waves in shallow water. *Journal of Fluid Mechanics*, 205, 397–419.
- Zakharov, V. E. (1968). Stability of periodic waves of finite amplitude on the surface of a deep fluid. *Journal of Applied Mechanics and Technical Physics*, 9(2), 190–194.
- Zhu, H., & Dodin, I. (2021). Wave-kinetic approach to zonal-flow dynamics: Recent advances. *Physics of Plasmas*, 28(3), 032303.

- Zijlema, M., Stelling, G., & Smit, P. (2011). SWASH: An operational public domain code for simulating wave fields and rapidly varied flows in coastal waters. *Coastal Engineering*, 58(10), 992–1012.
- Zijlema, M., & van der Westhuysen, A. J. (2005). On convergence behaviour and numerical accuracy in stationary SWAN simulations of nearshore wind wave spectra. *Coastal Engineering*, 52(3), 237–256.

LIST OF PUBLICATIONS

JOURNAL ARTICLES

FIRST AUTHOR

Akrish, G., Smit, P., Zijlema, M., & Reniers, A. (2020). Modelling statistical wave interferences over shear currents. *Journal of Fluid Mechanics*, 891.

CO-AUTHOR

Reniers, A., Naporowski, R., Tissier, M. F., de Schipper, M. A., Akrish, G., & Rijnsdorp, D. P. (2021). North sea infragravity wave observations. *Journal of Marine Science and Engineering*, 9(2), 141.

CONFERENCES AND WORKSHOPS

Akrish, G., Smit, P., Zijlema, M., & Reniers, A. (2018). Inhomogeneous wave statistics over shear currents. *Waves in Shallow Environments (WISE) Conference*, Tel-Aviv.

Akrish, G., Smit, P., Zijlema, M., & Reniers, A. (2018). Modelling wave interference patterns using the SWAN model. *Coastal Engineering Proceedings*, (36).

Akrish, G., Reniers, A., Zijlema, M., & Smit, P. (2021). Spectral modelling of infragravity waves. *Coastal Dynamics Conference*, Delft.

Akrish, G., Reniers, A., Zijlema, M., & Smit, P. (2022). Coastal wave forecasting using quadratic models. *Water Waves - Mathematical Theory and Applications*, Plymouth.

SCIENTIFIC REPORTS

Akrish, G., Smit, P., Zijlema, M., & Reniers, A. (2019). Modelling statistical wave interference over variable bathymetry and currents. *Annual Report 2019 JMBC – Research Highlight*.

CURRICULUM VITAE

- September 29, 1983 Born in Tveria, Israel
- 2008–2012 Bachelor of Science in Civil Engineering (Summa cum Laude)
Technion - Israel Institute of Technology
Haifa, Israel
- 2012–2015 Master of Science in Civil Engineering (Summa cum Laude)
Technion - Israel Institute of Technology
Haifa, Israel
- Thesis: '*Interaction between a Deformable Wall and Water Waves*'
Supervisors: Prof. Oded Rabinovitch & Prof. Yehuda Agnon
- 2014–2016 Civil Engineer at Witteveen+Bos – Engineering and Consulting
Department of Ports and Waterways
Deventer, the Netherlands
- 2016–Present PhD candidate
Faculty of Civil Engineering and Geosciences
Delft University of Technology
The Netherlands
- 2022–Present Post Doctoral Researcher
Faculty of Civil Engineering and Geosciences
Delft University of Technology
The Netherlands